Energy Harvesting Wireless Sensor Networks Leveraging Wake-up Receivers: Energy Managers and MAC Protocols

Fayçal Ait Aoudia

ANNÉE 2017

UNIVERSITÉ DE RENNES 1

UNIVERSITE BRETAGNE LOIRE

THÈSE / UNIVERSITÉ DE RENNES 1
sous le sceau de l'Université Bretagne Loire

pour le grade de

DOCTEUR DE L'UNIVERSITÉ DE RENNES 1

Mention : Traitement du Signal et Télécommunications

Ecole doctorale Matisse

présentée par

Fayçal Aït Aoudia

préparée à l'unité de recherche **GRANIT/IRISA-UMR 6074**
Institut de Recherche en Informatique et Systèmes Aléatoires de Rennes (MATISSE)

Energy Harvesting Wireless Sensor Networks Leveraging Wake-up Receivers: Energy Managers and MAC Protocols

Thèse soutenue à l'ENSSAT Lannion le 28 Septembre 2017
devant le jury composé de :

Alain PEGATOQUET, Rapporteur
Maître de Conférence (HDR), Université de Nice

Jean-Marie GORCE, Rapporteur
Professeur, INSA Lyon

Mérouane DEBBAH, Examinateur
Professeur, CentraleSupelec

Nathalie MITTON, Examinatrice
Chargée de Recherche, INRIA Lille

Dominique MORCHE, Invité
Ingénieur de Recherche, CEA-LETI

Michele MAGNO, Invité
Chercheur, ETH Zürich

Olivier BERDER, Directeur
Professeur, Université de Rennes 1

Matthieu GAUTIER, Co-Directeur
Maître de Conférence, Université de Rennes 1

Abstract

Wireless Sensor Networks (WSNs) are made of multiple sensor devices which measure physical value (e.g. temperature, pressure...) and communicate wirelessly. These networks form a key enabling technology of many Internet of Things (IoT) applications such as smart building and precision farming. The bottleneck of long-term WSN applications is typically the energy. Indeed, traditional WSNs are powered by individual batteries and a significant effort was devoted to maximizing the lifetime of these devices. However, as the batteries can only store a finite amount of energy, the network is still doomed to die, and changing the batteries is not always possible if the network is dense or if the nodes are deployed in a harsh environment.

A promising solution is to enable each node to harvest energy directly in its environment, using individual energy harvesters. As most of the energy sources are dynamic and uncontrolled, avoiding power failures of the nodes is critical to enable reliable networks. Increasing the quality of service typically requires increasing the power consumption, and a simple solution is to set the quality of service of the nodes to a constant value low enough to avoid power failures. However, this solution does not fully exploits the available energy and therefore leads to high energy waste and poor quality of service regarding the available environmental energy.

A more efficient solution is online adaptation of the node power consumption, which is performed by an energy manager on each node. In this thesis, two new approaches for online adaptation of the nodes energy consumption were proposed, relying on fuzzy control theory and reinforcement learning. Moreover, as communications are typically the most energy consuming task of a WSN node, emerging wake-up receivers were leveraged to reduce the energy cost of communications. A generic analytical framework for evaluating Medium Access Control (MAC) protocols was proposed, and it was combined to experiments to evaluate emerging wake-up receivers. A new opportunistic MAC protocol was also introduced for "on-the-fly" relay selection. Finally wake-up receivers and energy harvesting were combined and experimentally evaluated in a practical use case.

Résumé

Les Réseaux de Capteurs Sans Fils (RCSFs) sont composés d'une multitude de nœuds, chacun étant capable de réaliser des mesures (température, pression, etc) et de communiquer par radio fréquence. Ces réseaux forment une pierre angulaire de l'Internet des Objets, en étant au cœur de nombreuses applications, par exemple de domotique ou d'agriculture de précision. La limite d'utilisation des RCSFs provient souvent de leurs durées de vie restreintes, les rendant peut intéressants pour des applications nécessitants de longues périodes de fonctionnement en autonomie. En effet, les RCSFs traditionnels sont alimentés par des piles individuelles équipant chaque nœud, et les nœuds sont ainsi condamnés à une durée de vie finie et courte par rapport aux besoins de certaines applications. De plus, changer les piles n'est pas toujours réalisable si le réseau est dense, ou si les nœuds sont déployés dans des environnements les rendant difficile d'accès.

Une solution plus prometteuse est d'équiper chaque nœud d'un ou de plusieurs récolteur(s) d'énergie individuel(s), et ainsi de le rendre capable de s'alimenter exclusivement à partir de l'énergie récoltée dans son environnent. Plusieurs sources d'énergie sont possibles, telles que le vent ou le solaire. Étant donné que les sources d'énergie sont typiquement dynamiques et non contrôlées, ne pas tomber en panne d'alimentation et nécessaire pour garantir un fonctionnement fiable. Comme l'augmentation de la qualité de service engendre souvent une augmentation de la puissance consommée, une solution simple est de configurer la qualité de service au déploiement à une valeur constante suffisamment faible pour éviter la panne d'alimentation. Cependant, cette solution ne permet pas d'exploiter pleinement l'énergie récoltée, et mène ainsi à un gaspillage d'énergie important ainsi qu'à de faibles qualités de service au vu de l'énergie récoltée.

Une solution plus efficace est d'adapter dynamiquement la puissance consommée, et donc la qualité de service. Cette adaptation est faite par un composant logiciel appelé *gestionnaire d'énergie*. Dans cette thèse, deux nouvelles approches pour l'adaptation en ligne sont proposées, l'une s'appuyant sur la théorie du contrôle floue, et l'autre sur l'apprentissage par renforcement. De plus, comme la communication est souvent la tâche la plus énergivore dans les RCSFs, les *wake-up receivers* sont utilisées dans cette thèse pour pour réduire le coût des communications. Un modèle analytique générique a été proposé pour étudier différents protocoles de contrôle d'accès au support (*Medium Access Control* – MAC), et combiné à des résultats expérimentaux pour évaluer les *wake-up receivers*. Aussi, un nouveau protocole MAC permettant la sélection opportuniste de relais a été proposé. Enfin, la combinaison des *wake-up receivers* et de la récolte d'énergie a été étudiée expérimentalement avec un cas pratique.

Contents

Abbreviations

ACK Acknowledgment.

ADMM Alternating Direction Method of Multipliers.

AMC Absorbing Markov Chain.

CCA Clear Channel Assessment.

CTS Clear To Send.

EH Energy Harvesting.

EM Energy Manager.

ENO Energy Neutral Operation.

EWMA Exponentially Weighted Moving-Average.

IoT Internet of Things.

MAC Medium Access Control.

MC Markov Chain.

MCU Microcontroller Unit.

MDP Markov Decision Process.

OOK On-Off Keying.

PDR Packet Delivery Ratio.

RF Radio Frequency.

RL Reinforcement Learning.

RTS Ready To Send.

TD Temporal-Difference.

ULP Ultra Low Power.

WBAN Wireless Body Area Network.

WSN Wireless Sensor Network.

WuC Wake up Command.

WuRx Wake up receiver.

Nomenclature

Common

χ_g	Packet generation rate (in packets per second)
χ_r	Packet reception rate (in packet per second)
ξ	Energy efficiency
$e_b[k]$	Energy budget for the time slot k (in Joule)
E_b^{min}	Minimal energy budget (in Joule)
$e_h[k]$	Energy harvested during the time slot k (in Joule)
$e_r[k]$	Residual energy at the beginning of the time slot k (in Joule)
E_r^{fail}	Energy buffer failure threshold (in Joule)
E_r^{max}	Capacity of the energy buffer (in Joule)
$e_w[k]$	Energy wasted during the time slot k (in Joule)
K	Length of the harvested energy time window in time slots
N_A	Number of attempts
N_N	Number of nodes
T_s	Duration of a time slot (in seconds)
T_{WI}	Wake-up interval duration (in seconds)
X^{max}	Maximum packet generation rate (in packet per second)
X^{min}	Minimum packet generation rate (in packet per second)

Energy Management

α_{R^i}	Firing strength which measures the contribution of the i^{th} fuzzy rule
δ	Temporal difference error
η	Power conversion efficiency
γ	Discount factor in reinforcement learning
κ	Fuzzyman membership function parameter
λ	Decay parameter of the temporal-difference learning method with eligibility traces
$\mathcal{A}$	Action space in reinforcement learning theory
$\mathcal{R}$	Reward function in reinforcement learning theory
$\mathcal{S}$	State space in reinforcement learning theory

$\mathcal{T}$ State transition probability density function in reinforcement learning theory

μ_S Membership function of the fuzzy set S

ν Eligibility trace

ϕ Feature in reinforcement learning

π Policy in reinforcement learning theory

ψ Policy parameter

θ State value function approximator parameter

E_h^{strong} Threshold above which the harvested energy is considered completely strong in Fuzzyman (in Joule)

E_h^{weak} Threshold under which the harvested energy is considered completely weak in Fuzzyman (in Joule)

E_r^{empty} Threshold under which the energy storage device is considered completely empty in Fuzzyman (in Joule)

E_r^{full} Threshold above which the energy storage device is considered completely full in Fuzzyman (in Joule)

J Objective function in reinforcement learning

P_L Leakage power (in Watt)

Q^* Optimal state-action value function in reinforcement learning

Q^π State-action value function in reinforcement learning

$R[k]$ Reward received at time step k in reinforcement learning theory

V^* Optimal state value function in reinforcement learning

V^π State value function in reinforcement learning

MAC protocols and Wake-up Receivers

χ_u Receive wake-up rate (in frames per second)

Δe_b Energy budget correction in REM (in Joule)

$\kappa_C, \kappa'_C, \kappa_D, \kappa'_D$ REM parameters

$\mathbf{B}$. Absorption probability matrix

$\mathbf{c}$. Energy cost vector

$\mathbf{l}$. Latency cost vector

$\mathbf{N}$. Fundamental matrix

$\mathbf{n}$. Vector corresponding to the initial state row of $\mathbf{N}$.

$\mathbf{P}$. Absorbing Markov chain transition matrix

$\bar{a}$ Average number of transmission attempts

$\bar{c}$. Average energy cost of a packet transmission/reception (in Joule)

$\bar{l_t}$ Expected latency of a packet transmission (in seconds)

$\overline{P_C}$ Average power consumption of the node (in Watt)

ζ	Energy utilization coefficient (in packet/(second and Joule))
$b_{\bullet,\mathfrak{s}}$	Probability of a successful transmission/reception
$C_\bullet$	Absorbing Markov chain modeling a MAC protocol
D_c	Contention window duration of OPWUM (in seconds)
e_u	Energy cost of a receive wake-up operation (in Joule)
E_{ENI}^{down}	Lower bound of the energy neutral interval in REM (in Joule)
E_{ENI}^{up}	Upper bound of the energy neutral interval in REM (in Joule)
l_u	Duration of a receive wake-up operation (in seconds)
p_f	Frame transmission failure probability
P_{SBY}	Power consumption of the node in STDBY mode (in Watt)
R_u	Bitrate at which wake-up commands are transmitted (in bits per second)

List of Figures

List of Tables

Chapter 1

Introduction

Wireless Sensor Networks (WSNs) are composed of multiple wireless sensor nodes that monitor an environment and gather data to one or more locations called sinks. These networks form a key enabling technology of the Internet of Things (IoT), and are critical in many applications such as smart cities, smart factories, precision farming... Unlike cellular networks or IEEE 802.11, WSNs do not rely on any fixed infrastructure, and therefore the nodes typically self-organize in an ad-hoc manner. Multiple network topologies are possible for nodes organization, the simplest one being *star networks* in which nodes are organized around the sink. In this topology, all nodes are at a one-hop distance from the sink, and therefore directly send their data to it. In situations were the monitoring area is large and where part of the sensor nodes are too far from the sink(s) for one-hop communication, a *multi-hop network* is used. In this topology, each node both generates new data by sensing and sends the so-obtained data to the sink, but also relays data for the networks. The rate at which a node senses and sends packets is referred to as the *packet generation rate*, while the rate at which it relays packets from other nodes is referred to as the *packet relaying rate*. This latter is only defined in multi-hop networks.

A wireless sensor node is made of several components: a Microcontroller Unit (MCU), memory, sensors, a transceiver, and a power source. The MCU controls the other components and processes the data. The sensors are used to capture the data from the environment. The transceiver enables communication with the other nodes. Finally, the power source provides the energy required to power the system. In order to be able to deploy large WSNs, an important consideration is the cost of the nodes which must be kept low. Also, in order for some applications to be interesting, WSNs must be able to operate for long period of times. Typically, the bottleneck of long-term WSNs applications is the energy. Indeed, traditional wireless nodes are powered by individual batteries, which can store only a finite amount of energy. Therefore, when a node consumes all the energy initially stored in its battery, it turns off, and replacing the batteries is not always possible if the network is dense or deployed in harsh environment. Therefore, energy efficiency is critical in WSNs as it is closely related to network lifetime.

In the last decades, important efforts were devoted to develop low power consumption devices and energy efficient communication schemes to maximize the lifetime of WSNs. Indeed, it is well-known that communications are one of the most, if not the most, energy consuming tasks in WSNs [10]. Typically, a node power consumption, which is closely related to the quality of service (sensing rate, throughput...) is set at deployment to a value that guarantees the required lifetime. However, as batteries can only store a finite amount of energy, the network is doomed to die. A promising solution to increase the lifetime of WSNs is to enable each node to harvest energy in its environment. In this scenario, each node is equipped with one or more energy harvesters, as well as an energy buffer (battery or capacitor) to allow storing part of the harvested energy for future use during periods of energy scarcity. Various energy sources are possible, such as light, wind, motion, fuel cells... [9, 11]. As the energy sources are typically dynamic and uncontrolled, it is required to dynamically adapt the power consumption of the nodes, by adjusting their quality of service in order to avoid power failure while maximizing the energy efficiency and ensuring the fulfillment of application requirements. This task is done by a software module called Energy Manager (EM), which is in charge of dynamically adapting the power consumption of the nodes, and therefore their quality of service.

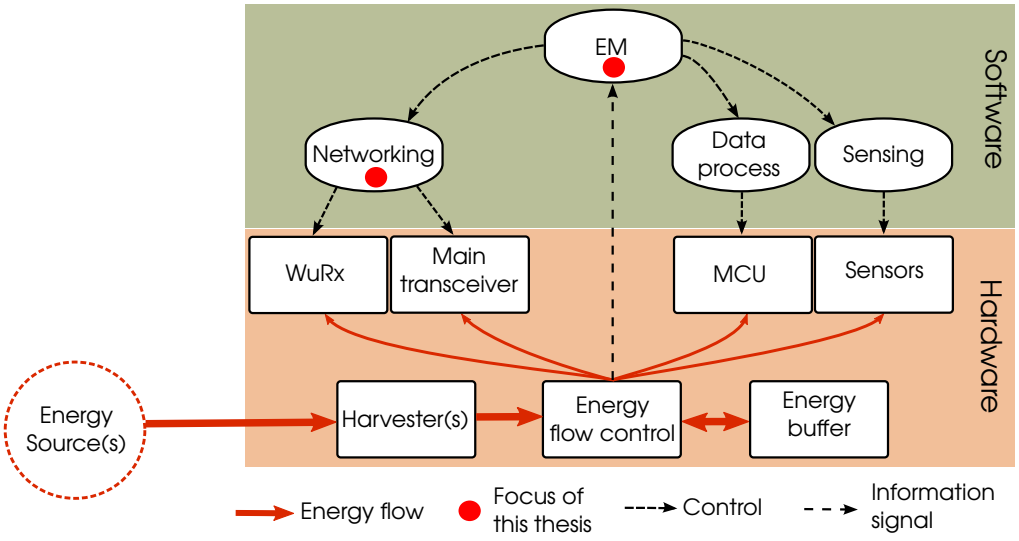

Figure 1.1 – Architecture of an energy harvesting sensor node equipped with a WuRx.

In order to achieve sustainable EH-WSNs, the power consumption of the nodes should be minimized. Many schemes were proposed to improve the energy efficiency of communication protocols for WSNs. Especially, a great emphasis was put on Medium Access Control (MAC) protocols, which are responsible for point-to-point communication and control the transceiver and therefore strongly impact the energy efficiency of communications [12]. An efficient way to reduce the power consumption of the nodes is *duty-cycling*, which idea is simply to turn off the transceivers when they are not needed. However, to avoid deafness, the nodes need to periodically listen to the channel for incoming packets. Recent circuit-level advances have made possible the realization of ultra low power Wake up receiver (WuRx) circuits that can efficiently "wake up" a node when a specific signal, called Wake up Command (WuC), is sent by a neighboring node [2, 5, 13–15]. Moreover, many WuRx embed address matching features, which allow nodes to wake up only a specific node and not all their neighbors [16, 17]. The main feature of WuRx is the continuous listening of the wireless medium while keeping the main transceiver in sleep state. The cost of ultra low power consumption is low sensitivity and low bitrates, which makes sending WuCs energetically costly. Therefore, the WuRx does not replace the main receiver, but is an extra device in addition to a traditional transceiver. However, in order to efficiently take advantage of WuRx, the design of ad-hoc protocols leveraging these emerging devices is required.

The typical architecture of Energy Harvesting (EH) sensor nodes considered in this thesis is shown in Figure 1.1. The EM reads information from the energy flow controller about the currently amount of energy stored in the energy buffer and possibly the the amount of harvested energy, and uses this information to control various tasks of the node (e.g. sensing, processing and networking). Therefore, the EM indirectly controls the energy consumption. This thesis focuses on the design of energy management algorithms and MAC protocols leveraging WuRx. An important consideration when designing algorithms for WSNs is to make them able to run on the highly constraint systems that are wireless sensor nodes in terms of computational power, memory, storage and energy.

1.1 Energy Management in Energy Harvesting Wireless Sensor Networks

In EH-WSNs, each node is equipped with one or more energy harvesting devices, enabling the nodes to be entirely powered by the energy harvested in their environments. To be able to store part of the harvested energy for future use, e.g. periods of energy scarcity, each node also embeds an energy storage device, which can be a supercapacitor or a battery. The energy buffer has a finite capacity denoted by E_r^{max} and a failure threshold denoted by E_r^{fail}, as illustrated in Figure 1.2. The failure threshold corresponds to the minimum amount of energy required for the node to

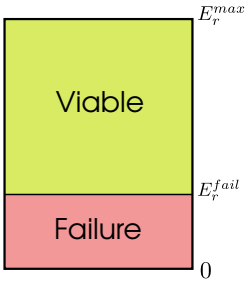

Figure 1.2 – Energy Buffer thresholds.

Source	Source Power	Harvested Power
Ambient light		
Indoor	0.1mW/cm^2	$10\mu\text{W/cm}^2$
Outdoor	100mW/cm^2	10mW/cm^2
Vibration/Motion		
Human	0.5 m at 1 Hz	
	$1\ \text{m/s}^2$ at 50 Hz	$4\ \mu\text{W/cm}^2$
Industrial	1 m at 5 Hz	
	$10\ \text{m/s}^2$ at 1 kHz	$100\ \mu\text{W/cm}^2$
Thermal Energy		
Human	20mW/cm^2	$30\mu\text{W/cm}^2$
Industrial	100mW/cm^2	$1-10\text{mW/cm}^2$
RF		
GSM Base Station	$0.3\mu\text{W/cm}^2$	$0.1\mu\text{W/cm}^2$

Table 1.1 – Characteristics of various energy sources (from [9]).

operate, and a power failure arises if the residual energy drops below this threshold. The capacity E_r^{max} is the maximum amount of energy that the energy buffer can store, and the finite capacity of the energy buffer is the origin of energy waste. Indeed, if the harvested energy is not immediately used after it has been harvested, it will be stored in the energy buffer by the energy flow controller shown in Figure 1.1. However, if the energy buffer is full, then the harvested energy will not be stored, and therefore it will be wasted leading to energy inefficiencies.

A handful of energy sources can be considered, according to the environment in which the nodes are deployed, and the energy required by the application. The harvested power strongly depends on the energy source type, as well as on the efficiency of the harvester, *i.e.* the ratio between the power extracted from the source by the harvester and the source power. Table 1.1 shows some characteristics of various energy sources (from [9]). As one may see, the power harvested from outdoor ambient light is 10^5 higher than the power available from Radio Frequency (RF) harvesting, showing the strong variation in the available energy from one source to the other. Moreover, typical sources present strong time variations. This behavior motivates the need for online adaptation of the performance of nodes forming an EH-WSN. Indeed, increasing the quality of service of a WSN application (e.g. sensing rate, throughput...), requires higher power consumption. A naive solution to achieve sustainable EH-WSN is to set the nodes to deliver a constant poor quality of service, that incurs a low enough power consumption to avoid power failure. This solution has two main drawbacks: (i) it leads to poor performance as a significant amount of energy is wasted and (ii) precise knowledge of the energy source is required to guarantee that no power failure will happen. Another solution is to perform online adaptation of the performance, which enables quality of service maximization while avoiding power failure.

Formally, if we denote by $P_h(t)$ the harvested power at time $t \in \mathbb{R}^+$, and by $P_c(t)$ the consumed

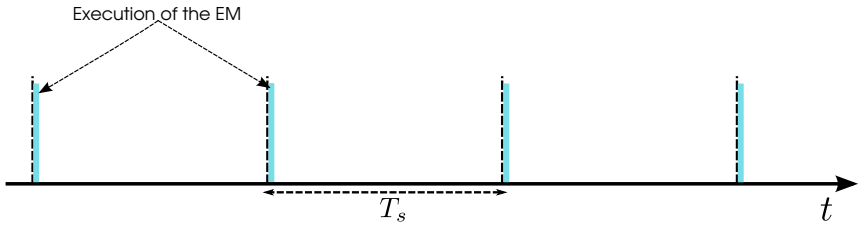

Figure 1.3 – Periodic execution of the EM.

power at time t, the residual energy at time t is defined by:

$$e_r(t) = e_r(0) + \int_0^t P_h(\tau)d\tau - \int_0^t P_c(\tau)d\tau - \int_0^t P_w(\tau)d\tau, \tag{1.1}$$

where $e_r(0) \in [0, E_r^{max}]$ is the initial residual energy, and P_w is the wasted power, *i.e.* the power wasted because of the saturated energy buffer. The finite size of the energy buffer constrains the residual energy:

$$\forall t,\ e_r(t) \leqslant E_r^{max}. \tag{1.2}$$

Assuming that the application performance can be measured by a utility metric $\mathcal{U}(P_c)$, which is a function of the power consumption (e.g. packet rate, energy efficiency...), the energy management problem can be expressed as follows:

$$\begin{aligned} &\underset{P_c}{\text{maximize}}\ \mathcal{U}(P_c) \\ &\text{subject to: } e_r(t) \leqslant E_r^{max},\ \forall t \\ &\qquad\qquad e_r(t) \geqslant E_r^{fail},\ \forall t \end{aligned} \tag{1.3}$$

In this problem, the last constraint corresponds to power failure avoidance, and satisfying this last constraint is sometimes referred to as achieving Energy Neutral Operation (ENO) [18] in the literature. In order to maximize the energy efficiency, P_c should be chosen such that no energy is wasted, or formally:

$$\forall t,\ P_w(t) = 0. \tag{1.4}$$

Satisfying this constraint is sometimes referred to as achieving ENO-MAX [19].

In practice, the EM is a software component that is part of the program embedded on each node as shown in Figure 1.1, and that is periodically executed, as illustrated in Figure 1.3. The duration between two executions of the EM is denoted by T_s. Therefore, (1.1) is discretized as follows:

$$e_r[k] = e_r[0] + \sum_{i=0}^{k-1} e_h[i] - \sum_{i=0}^{k-1} e_c[i] - \sum_{i=0}^{k-1} e_w[i],\ k = 1, 2, \dots \tag{1.5}$$

where $e_r[k]$ is the residual energy at time step k, and $e_h[k]$, $e_c[k]$ and $e_w[k]$ are respectively the harvested energy, consumed energy and wasted energy during time step k. The energy management problem in discrete form is:

$$\begin{aligned} &\underset{e_c[0], e_c[1], \dots}{\text{maximize}}\ \mathcal{U}(e_c[0], e_c[1], \dots) \\ &\text{subject to: } e_r[k] \leqslant E_r^{max},\ k = 1, 2, \dots \\ &\qquad\qquad e_r[k] \geqslant E_r^{fail},\ k = 1, 2, \dots \end{aligned} \tag{1.6}$$

and ENO-MAX is achieved if:

$$e_w[k] = 0,\ k = 1, 2, \dots \tag{1.7}$$

However, in some applications, achieving ENO-MAX is not an appropriate objective. In multi-hop networks for example, in which each node both generates packets and relays packets from other nodes, a node can have its packet generation rate limited because its relays cannot forward the packets it generates, and not by the amount of energy it harvests. In such a scenario, wasting

energy may be necessary if the energy buffer is not large enough to store the harvested energy in excess. In this thesis, the focus is put on star networks, and in such scenarios the *energy efficiency*, *i.e.* the ability of an EM to minimize the wasted energy, is relevant to evaluate the EM. Therefore, the energy efficiency, formally defined by:

$$\xi = 1.0 - \frac{\sum_k e_w[k]}{\sum_k e_h[k] + e_r[0]}, \tag{1.8}$$

is used as a metric to evaluate energy management strategies. In addition to the energy efficiency, the *dead ratio* D_R is also considered, which is defined as the ratio of time spent in power failure state over the total application duration. The multi-hop scenario is however considered in the Appendix A.

A challenge of energy management in EH-WSNs is due to the lack of knowledge of the harvested energy e_h. As we will see in the related work on EMs (Chapter 2), some approaches tackle this problem by using predictors which aim to guess the future harvested energy over a finite time window. However, using predictors requires measurements of the amount of harvested energy in the previous time slots $e_h[k-1], e_h[k-2], \ldots$, which is difficult to get in practice. Therefore, some approaches, such as the one proposed in Chapter 4, rely only on the residual energy to take decision about energy management. Another difficulty of energy management in EH-WSNs is the accurate control of the node power consumption. Indeed, some tasks executed by a WSN node do not have deterministic energy costs. Communication tasks for example have energy cost that strongly depends on the channel quality, as error in packet transmissions generally leads to retransmissions. Some EMs do not consider this problem as they compute an *energy budget* $e_b[k]$, which corresponds to the amount of energy that the node should spend during the time slot k, and do not focus on how this energy budget is allocated among the different tasks executed by the node. These EMs therefore do not directly set the quality of service, but indirectly control it via the energy budget. Another software component is in charge of setting the quality of service (e.g. sensing rate) from the energy budget. Other approaches directly set some quality of service parameter, and therefore indirectly control the energy consumption of the node. Another challenge of energy management in EH-WSNs comes from the highly constrained systems that are WSN nodes. Indeed, such devices usually provide only very few computational power (frequency typically less than 16 MHz), memory (typically 2 KB) and storage (typically less than 100 KB), and the proposed algorithms should therefore be suited to these kinds of platforms.

1.2 MAC Protocols in Wireless Sensor Networks

Communication is usually one of the most energy consuming task in WSNs due to the high power consumption of radio transceivers [10]. Therefore, significant efforts were devoted to the design of energy efficient communication protocols, and especially MAC protocols [12]. MAC protocols play a critical role in the energy efficiency of communications as they control the transceiver. The aim of MAC protocols is to allow point-to-point communication between two neighboring nodes. *Pseudo-asynchronous* approaches are based on the idea of duty-cycling, and common in low packet rate networks such as EH-WSNs. In these schemes, each node periodically wakes up to check for incoming packets. If no packet is pending, the node goes back to the sleep state. Otherwise, it stays active to receive the incoming packet. Pseudo-asynchronous protocols require a *rendez-vous* scheme to ensure that two nodes can meet to exchange packets, and designing energy efficient rendez-vous schemes is critical to achieve energy efficient communications. Pseudo-asynchronous protocols can be classified in two types according to their rendez-vous approach: transmitter-initiated or receiver-initiated.

In transmitter-initiated protocols, a packet transmission is initiated by the transmitter (obviously), as illustrated in Figure 1.4a. This figure shows a packet transmission using the TICER protocol [1], a representative protocol of this category. Using TICER, the receiver periodically wakes up to listen the channel, in order to check for incoming packets. The time between two periodical wake-ups is called the *wake-up interval*, and denoted by T_{WI}. When a node needs to send a packet, it starts by sending Ready To Send (RTS) frames to express the willingness to communicate. Each RTS frame is followed by a channel listening. The periodic listening of the receiver

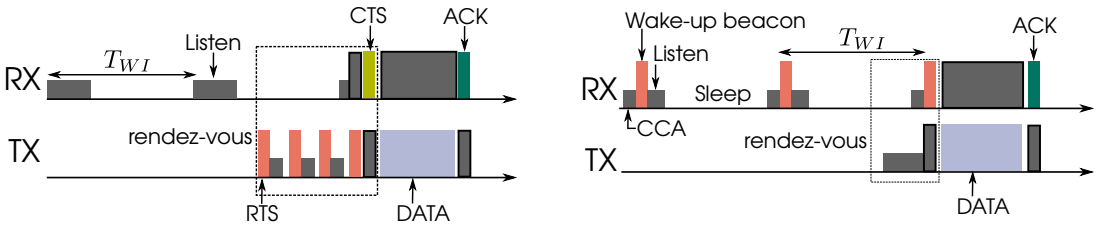

(a) TICER. (b) RICER.

Figure 1.4 – TICER and RICER illustration.

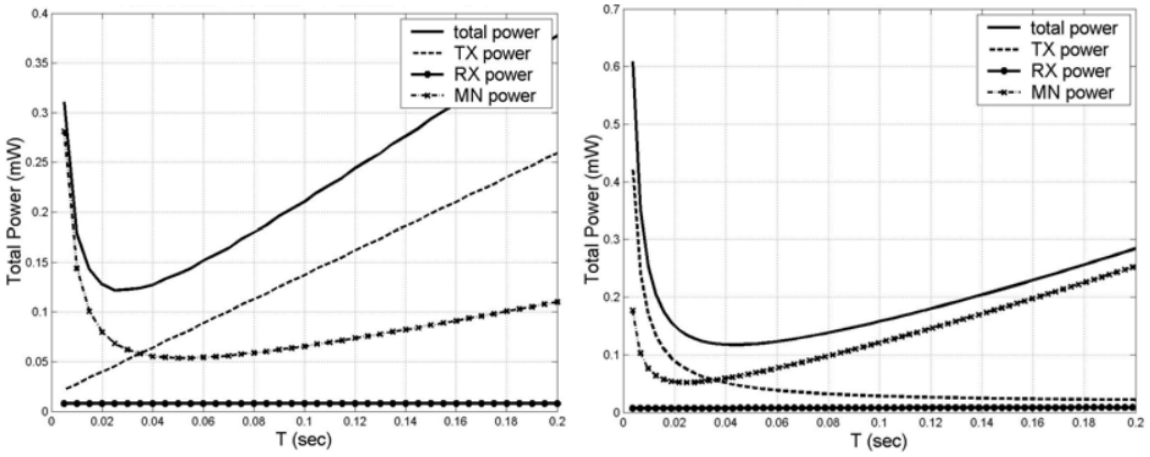

(a) TICER power breakdown. (b) RICER power breakdown.

Figure 1.5 – TICER and RICER power breakdown, from [1]. TX: transceiver transmitting, RX: transceiver receiving, MN: transceiver sensing, T is the wake-up interval, denoted by T_{WI} in this thesis.

must be long enough to ensure that RTS frames will be detected. If the receiver detects an RTS frame, it sends a Clear To Send (CTS) frame to inform the transmitter that it is ready to receive a packet. Finally the data packet exchange takes place, which is followed by an Acknowledgment (ACK) to ensure that the data packet is correctly received.

In receiver-initiated protocols, a packet transmission is initiated by the receiver as illustrated in Figure 1.4b with the RICER protocol [1]. Using RICER, each node periodically wakes up and sends a wake-up beacon to inform its neighbors that it is ready to receive a packet. Each wake-up beacon sending is preceded by a Clear Channel Assessment (CCA) to avoid collisions, and is followed by a channel listening to check for incoming packets. When a node needs to transmit a packet, it starts by listening the channel until a wake-up beacon is received. Once the beacon is received, it sends its data packet. The transmission ends with the transmission of an ACK, to ensure that the data packet is correctly received.

While pseudo-asynchronous approaches enable significant power consumption reduction in low packet rate networks, the rendez-vous scheme incurs significant overhead. Moreover, these approaches do not eliminate idle listening, *i.e.* useless channel listening during which no data is received. Figure 1.5 (from [1]) shows TICER and RICER power breakdown, in which TX corresponds to the transceiver being transmitting, RX to the transceiver being receiving, and MN (MoNitor) to idle listening. These results show that there exists an optimal wake-up interval T_{WI} (denoted by T in Figure 1.5) for which the power consumption is minimal. However, this optimal wake-up interval depends on the hardware and the traffic load, and the authors showed that by adjust the wake-up interval to the traffic load, most power saving can be obtained. In practice, this requires predicting the traffic load, which is not trivial in WSNs.

Recently, ultra low power WuRx circuit have emerged. These devices enable continuous monitoring of the wireless channel, while achieving power consumption orders of magnitude lower than traditional WSN transceivers. Moreover, these devices are able to wake up the rest of the node using interrupts. However, ultra low power consumption comes at the cost of significantly lower

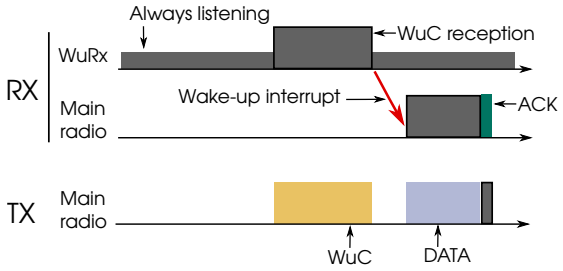

Figure 1.6 – Packet transmission using WuRx.

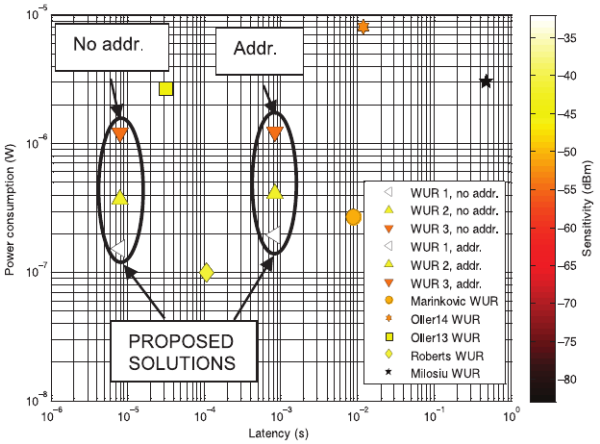

Figure 1.7 – Comparison of some WuRx in terms of power consumption, latency and sensitivity (from [2]). WUR 1, WUR 2 and WUR 3 correspond to various designs proposed in [2]. Marinkovic WUR corresponds to [3]. Oller14 and Oller13 respectively correspond to [4] and [5]. Roberts WUR corresponds to [6]. Milosiu WUR corresponds to [7].

bit-rate and lower sensitivity (and therefore range) compared to traditional transceivers, which make these devices inefficient to transmit long frames. Therefore, WuRx typically does not replace traditional WSN radio receivers, but comes as an extra device used to reduce the power consumption of communications.

Using these devices, no rendez-vous is required to perform a packet transmission, as illustrated in Figure 1.6. Indeed, when a node needs to transmit a packet, it first transmits a specific signal, called WuC, intended to the receiver node WuRx. Some WuRx have address matching capabilities, which makes possible to wake up only the addressed node and not all the neighboring nodes. When the receiver WuRx detects the WuC, it generates a hardware interrupt to wake up the main microcontroller, which can then put the main transceiver in the receive mode to receive the data packet. As the data packet is typically large compared to the WuC, it is more efficient to send it using the main transceiver. Indeed, state of the art WuRx achieve lower sensitivity and bitrate than traditional transceivers. In this thesis, the WuRx from [2] was used for experimentations and simulations, and Figure 1.7 shows its performance compared to other state of the art WuRx. It can be seen that current WuRx achieves sensitivity around $-55\,\mathrm{dBm}$, which is significantly lower than usual WSN transceiver, that achieves sensitivity around $-115\,\mathrm{dBm}$ (e.g. of the Texas Instruments CC1120). Therefore, WuC are transmitted at higher transmission power than the other frames. Moreover, the bitrates of WuRx is typically of a few kbps (1 kbps for the WuRx used in this work), leading to higher latencies, especially when the address of the node to wake up is transmitted in the WuC, as shown in Figure 1.7. Therefore, WuC needs to be transmitted at higher transmission power and for longer time, which make their sending energetically expensive. As a consequence, the potential benefits brought by WuRx need to be studied, and communication protocols leveraging these emerging devices must be carefully designed.

WuRx have the potential of improving the efficiency of wireless communications, which is critical in WSNs. Moreover, WuRx remove the need for time synchronization between the node

MAC layers, or finding optimal wake-up intervals. This is especially important in EH-WSNs, as dynamic quality of service adaptation may lead to dynamic packet rates, unsuitable in networks in which the MAC layers need time-synchronization.

1.3 Contributions and Thesis Outline

This thesis is divided into two parts. The first part deals with energy management in EH-WSNs, while the second part is dedicated to MAC protocols and WuRx.

1.3.1 Contributions

The three main contributions of this thesis in the field of energy management in EH-WSNs are:

- A first EM, named Fuzzyman, and based on model-free fuzzy control theory, is proposed to deal with the variability of the energy sources. The strategy of Fuzzyman is implemented as a set of fuzzy inference rules, through which an intuitive energy management policy can be formally expressed. Fuzzyman requires as an input the current residual energy, as well as the amount of energy harvested in the last time slot.
- A second EM, named RLMan, and based on Reinforcement Learning (RL) theory, is introduced. RL is concerned with getting an agent to take actions in an environment so as to maximize a cumulative reward, which is a scalar feedback from the environment. Contrary to Fuzzyman, RLMan requires as an input the residual energy only. Indeed, RLMan was in part motivated by the difficulty of measuring the amount of harvested energy accurately in practice.
- A distributed algorithm was proposed to tackle the problem of packet generation rate assignment in multi-hop EH-WSNs. In multi-hop networks, each sensor node is also a relay for the network, and when setting the packet generation rate of a given node, the energy states of the nodes that serve as a relay for it must also be considered. Packet generation rate assignment is therefore a network-scale problem in multi-hop EH-WSNs.

In the field of MAC protocols and WuRx, the main contributions of this thesis are:

- A generic analytical framework for modeling MAC protocols was designed and used to evaluate the benefits of WuRx. Using the proposed framework, a simple MAC leveraging WuRx was compared to state of the art MAC. Experimentations were realized to support the obtained results.
- An opportunistic forwarding MAC scheme named OPWUM and leveraging WuRx was designed. It is based on timer-based contention, and was compared to other opportunistic forwarding schemes using network simulations.
- WuRx are combined with the recent LoRa^{TM} long-range communication scheme for the Internet of things in a new heterogeneous communication network architecture. The proposed network architecture enables low latency and low energy communication both from the sensor nodes to the sink and from the sink to the sensor nodes.

Energy harvesting and WuRx were combined experimentally in the context of star networks:

- An EM inspired by Fuzzyman but that is more practical to implement as it does not require the amount of energy harvested as an input was designed and implemented, as well as a MAC protocol leveraging WuRx that achieves energy efficient communications in the context of data gathering star networks.

I realized part of this thesis at the *Eidgenössische Technische Hochschule Zürich* (ETHZ - Swiss Federal Institute of Technology in Zurich), were I stayed from September 2015 to March 2016. I was hosted by the Integrated Systems Laboratory (IIS), working with Dr. Michele Magno and Prof. Luca Benini. The work presented in Chapters 5, 6, 8 and in the Appendix B were done in collaboration with ETHZ.

1.3.2 Thesis outline

Part I – Energy Harvesting for Wireless Sensor Networks

Chapter 2 – Related Work The Chapter 2 presents the related work on energy management in EH-WSNs. Energy management schemes can be organized as prediction-based or prediction-free. Prediction-based schemes require a predictor, which provides guesses of the harvested energy in the near future. At the opposite, prediction-free algorithms do not require predictions. This chapter provides the state of the art on energy prediction algorithms, prediction based EMs, and prediction-free EMs.

Chapter 3 – Fuzzyman: an Energy Manager Based on Fuzzy Control Theory The Chapter 3 introduces the first contribution of this thesis in the field of EH-WSNs, which is an EM based on fuzzy control theory. The chapter starts by giving the background on fuzzy sets, fuzzy logic and fuzzy control required to understand the design of the proposed EM. The proposed EM is called Fuzzyman and relies on model-free fuzzy control theory. Fuzzyman is compared to state of the art algorithms using simulations, and details on the tuning of Fuzzyman and comparison results are given in this chapter.

Chapter 4 – RLMan: an Energy Manager Based on Reinforcement Learning The Chapter 4 presents a new EM based on RL theory called RLMan. This chapter starts by giving the background on RL theory, before describing RLMan's algorithm. In order to achieve low computation and memory overhead, linear function approximators were used to deal with the continuous state and action spaces, and the required background on this kind of approximators is also introduced. RLMan is compared to state of the art EMs using simulations, and the results are presented in this chapter.

Part II – MAC Protocols leveraging Wake-up Receivers

Chapter 5 – A Generic Framework For Modeling MAC Protocols The Chapter 5 presents a generic analytical framework based on Absorbing Markov Chains (AMCs) for modeling MAC protocols. The proposed framework evaluates the average power consumption, the average latency, and the probability of a successful transmission. In order to illustrate how it can be used to model a protocol, the chapter shows in detail the modeling of PW-MAC [20], a state of the art receiver-initiated protocol. To achieve high accuracy, the parameters of the model are set using micro-benchmarks measurements. The accuracy of the model is validated by experimental measurements.

Chapter 6 – Benefits of Wake-up Receivers The Chapter 6 starts by introducing the state of the art on WuRx circuits and MAC protocols leveraging WuRx devices. The analytical framework introduced in Chapter 5 is then used to show the benefits enabled by WuRx by comparing simple MAC protocols leveraging WuRx devices to several state of the art pseudo-asynchronous MAC protocols. Experimental measurements are used to support the analytical comparison results.

Chapter 7 – OPWUM: OPportunistic Wake-Up Mac The Chapter 7 presents OPWUM, an opportunistic forwarding protocol leveraging WuRx. OPWUM relies on the timer-based contention method to enable "on-the-fly" selection of the next-hop relay node according to an arbitrary metric that is application dependent. OPWUM is evaluated using network simulations regarding energy consumption and Packet Delivery Ratio (PDR). Energy harvesting is studied as an application case of OPWUM, when the next-hop selection metric is calculated according to the energy state of each node.

Chapter 8 – Combining Wake-up Receivers and Energy Harvesting in Star Networks In Chapter 8, energy harvesting and WuRx are experimentally combined in the case of data gathering star networks. As it was found out that getting the amount of harvested energy is not easy

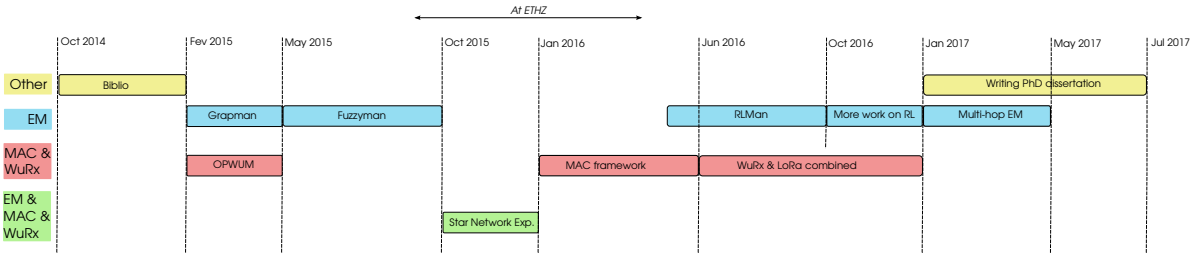

Figure 1.8 – Organization of the PhD.

in practice and incurs significant energy overhead, another EM (Rules Based EM – REM), inspired by Fuzzyman, was designed and implemented (RLMan was not yet designed when this work was done). Moreover, a protocol for data gathering star network was designed and implemented. Implementation details and experimentation results are available in this chapter.

Appendices

Appendix A – Packet Rate Assignment in Multi-hop Energy Harvesting Wireless Sensor Networks The problem of packet generation rate assignment in multi-hop EH-WSNs is tackled in this appendix in the case of network with a tree topology. Packet generation rate assignment is formulated as a convex optimization problem, with the objective to achieve proportionally fair assignment. A distributed algorithm was designed using the fast Alternating Direction Method of Multipliers (ADMM).

Appendix B – Long-Short Range Communication with LoRa^{TM}and Wake-up Receivers In Appendix B, WuRx were combined with LoRa^{TM}, an emerging long-range and low bitrate communication technology for the Internet of things. A new network architecture is proposed, as well as a MAC protocol to leverage it. In collaboration with ETHZ, a platform was designed and evaluated that includes a WuRx in addition to a transceiver that can handle both LoRa^{TM}and IEEE 802.15.4.

1.4 Timeline of the PhD

Figure 1.8 shows the organization of the PhD. After five months of full-time bibliography, the first two contributions were proposed: GRAPMAN [21], which was the first EM designed during this PhD, but which is not presented in this thesis, and OPWUM (Chapter 7), an opportunistic forwarding MAC protocol leveraging WuRx.

The next few months, the emphasis was put on the study of fuzzy control theory and on the design and evaluation of Fuzzyman (Chapter 3). The first half of the second year was carried out at ETHZ, in collaboration with Dr. Michele Magno and Prof. Luca Benini, who designed the WuRx used in this PhD. The first three months were devoted to the implementation of a Fuzzyman-based EM, on a node leveraging WuRx (Chapter 8). It was initially planned to implement Fuzzyman as it is presented in this thesis, but it was found out to be difficult to get precise measurements of the harvested energy. This observation motivated the latter design of RLMan (Chapter 4).

The experience of working with WuRx triggered the willingness to study in details the potential benefits enabled by WuRx, and in that aim to compare different MAC protocols based on different paradigms. The analytical framework presented in Chapter 5 was designed to fulfill this objective, and was used to evaluate simple protocols leveraging WuRx. As this framework was established after the design of OPWUM, it was not used to evaluate the latter even if it is introduced in this dissertation before OPWUM.

The next months, RLMan, an EM that requires only the residual energy to operate, was designed using RL theory. At the same time, a new network topology relying on the combination of recent long-range radio technologies for WSNs and WuRx was investigated, in collaboration with ETHZ (Appendix B). In the last six months of my PhD, while writing this dissertation, the problem of setting the packet generation rates in multi-hop EH-WSNs was addressed (Appendix A).

Part I

Energy Harvesting for Wireless Sensor Networks

Chapter 2

Related Work on Energy Managers

Many energy management schemes were proposed in the last years to address the non trivial challenge of designing efficient adaptation algorithms, suitable for the limited resources provided by sensor nodes in terms of memory, computation power, and energy storage. EM schemes can be classified based on their requirement of predicted information about the amount of energy that can be harvested in the future, *i.e.* *prediction-based* and *prediction-free*. This chapter exposes a comprehensive overview of the state of the art in EMs for EH-WSNs. First, prediction-based schemes are presented. Then, we show how energy management can be achieved without any predictions of the harvested energy.

2.1 Prediction-Based Energy Management

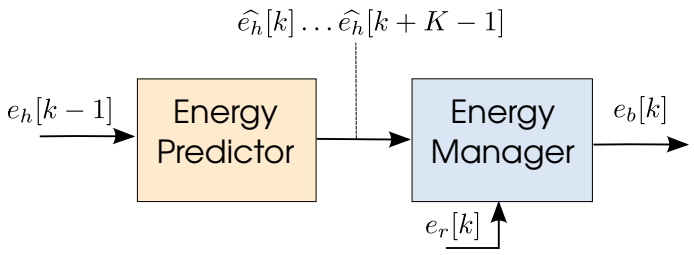

Figure 2.1 – Prediction-based energy management scheme architecture. A predictor supplies the energy management algorithm with forecasts of the harvested energy.

As the name implies, prediction-based schemes require that an energy predictor supplies the EM with predictions of the energy that can be harvested in the future. The general architecture of a prediction-based EM is shown in Figure 2.1. The time is divided into equal length time slots of duration T_s, and the EM is executed at the beginning of every time slot. It is assumed that the residual energy at the beginning of any time slot k, *i.e.* the amount of energy stored in the energy buffer, can be measured, as well as the amount of energy harvested during the $(k-1)^{th}$ slot. These quantities are respectively denoted $e_r[k]$ and $e_h[k-1]$. The energy predictor is fed with $e_h[k-1]$ at the beginning of every slot k, and uses these values to compute predictions of the harvested energy $\widehat{e}_h[k] \dots \widehat{e}_h[k+K-1]$ over a window of K time slots. The EM then uses these predictions, as well as the current residual energy, to take decision about the energy budget $e_b[k]$, *i.e.* the amount of energy that the node can use at the next time slot. Thus, the EM indirectly sets the quality of service of the node, as the quality of service depends on the energy budget. In this section, we first present an overview of energy prediction algorithms, before exposing prediction-based energy management schemes.

2.1.1 Energy Prediction Algorithms

Energy harvesting modeling and prediction is a hot topic, and great efforts were devoted over the last decade to the design of energy forecasting models [22]. Typically, the energy source is assumed

to be dynamic, non-controllable, and predictable. Most of the proposed forecasting schemes are specific to a type of source, such as RF, solar, wind...

Regarding RF harvesting, performing prediction is similar to predicting the link quality. In [23], the authors modeled the link as a Markov chain, with parameters discovered on-the-fly, and combined this model with a classifier system. Genetic algorithms were used to dynamically adapt the classifiers according to rewards computed from the quality of predictions. In [24], the authors proposed the *Oriented Birth-Death* model, a modified version of the Birth-Death prediction scheme in which the notion of orientation was added to represent a tendency in the link future state, *i.e.* if the link tends to increase or decrease the signal strength. *Liu et al.* proposed in [25] a data-driven approach to predict link features, named 4C, suited for static networks. The algorithm consists of three steps: data collection, offline modeling and online predictions. The data collection phase involves gathering link quality data, such as Received Signal Strength Indication (RSSI), Link Quality Indicator (LQI) and Signal to Noise Ratio (SNR). The modeling step consists of training prediction models. Three methods were evaluated by the authors: Bayes classifiers, logistic regression and neural networks, and they concluded that logistic regression works well among the three models with small computational cost. The last step involves the implementation of the proposed scheme of the trained predictor for online prediction.

In their seminal work on EH-WSN [18], *Kansal et al.* proposed a forecasting scheme based on Exponentially Weighted Moving-Average (EWMA) targeting solar energy. It was assumed that the amount of harvested energy at a particular time slot is similar to the amount of harvested energy the previous days at the same time slot. The prediction is done for each time slot by averaging the energy observed the previous day at the same time slot, with an exponential decrease of the old data. A drawback of the EWMA predictor is that it does not suit well to environment in which the weather frequently changes. To overcome this deficiency, *Piorno et al.* proposed in [26] the Weather-Conditioned Moving Average (WCMA) predictor, which considers both the current and past-day weather conditions for computing predictions, as opposite to EWMA which only considers past-day conditions. The authors introduced the GAP factor, which measures the solar conditions in the present day relative to the previous days, and makes the predictor more reactive in frequently changing weather conditions. *Moser et al.* further enhanced the WCMA algorithm in [27], by using a phase displacement regulator. The so obtained algorithm, called WCMA-PDR, reduces the average error. In [28], the authors used a method similar to EWMA but that considers both the energy available in the past time slots and the energy available in the current time slot. Moreover, a scaling factor was introduced by the authors to overcome short-term varying weather conditions.

Different solar energy prediction algorithms were compared in [29], that incur a small memory footprint and computational overhead, and are thus well-suited for implementation of WSNs. The authors also introduced a prediction scheme based on neural networks with two hidden layers, and which was trained using supervised learning and error back propagation. Results show that WCMA outperforms in term of prediction error EWMA, the scheme from [28] as well as the neural network solution, however at the cost of higher memory and computational overhead than EWMA and [28]. Still focusing on solar energy prediction, *Lu et al.* proposed SunCast in [30]. SunCast uses a three-stage process. First, it calculates the similarity of the current sunlight level with all historical data traces previously observed. This step involves computing the squared error between the real-time data stream and the historical data stream for a given time window, and then ranking all the historical traces by normalizing the different values. The second step applies regression analysis to all the historical traces to map the trends in historical data to match pattern of the current day. The last stage applies the regression model to the future time window to produce predictions.

In [31], *Petrioli et al.* proposed Pro-Energy, which targets both solar and wind energy. Pro-Energy keeps a pool of "typical" energy profiles observed in the past as well as the current day profile. At every time slot, Pro-Energy chooses the typical profile which is the most similar to the current day stream, and uses it to make forecast about the harvested energy. Pro-Energy is made up of three components: i) the profile analyzer, which selects among the stored profiles the most similar one to the current-day stream, ii) the prediction module, which delivers predictions, and iii) the profile pool refresh, which updates the typical profile pool, according to their age and similarity. Pro-Energy with Variable-Length Time slots (Pro-Energy-VLT), an enhancement of Pro-Energy, was proposed in [32], which fine-tune the time slots duration to achieve better accuracy while

reducing the memory overhead compared to the original algorithm. In contrast with previous schemes, *Renner* proposed to consider global knowledge in terms of fractional sky cloudiness in addition to local knowledge to achieve accurate prediction of solar energy intake [33]. The general idea is to compute the harvested energy under clear sky, and then to scale this value using cloud cover forecast. The scaling is done using well-studied meteorological models, and prediction relies on the EWMA algorithm. More recently, *Kosunalp* proposed to combine EWMA Q-Learning for Solar Energy Prediction [34] with QL-SEP. Q-Learning is a reinforcement learning approach, which aims to maximize the discounted cumulative rewards defined according to the prediction error in the case of QL-SEP. Using simulations, the author showed that QL-SEP can outperform EWMA and Pro-Energy.

Focusing on energy harvesting from wind sources, *Porcarelli et al.* proposed in [35] to use linear regression to forecast the availability of the power source, and the expected energy intakes in near future. The prediction variable is the time and the response variable the estimated power at the given time, and the aim of the predictor is to find the equation of the straight line which would provide the best fit to the observed data points. In [36], the authors compared three different methods for predicting the harvested energy from wind sources. In the first one, harvested energy is considered to be almost constant for two consecutive time slots, and the predicted amount of harvested energy in a time slot is equal to the amount of energy harvested in the previous time slot. In the second approach, the Adaptive Response Rate Single Exponential Smoothing (ARRSES) method [37], a variation of EWMA, is used. ARRSES either increases the smoothing factor during periods of high fluctuations or decreases it during periods of low fluctuations. In the last approach, an extension of the ARRSES method is introduced, called ARRSES 2^{nd} order, in which longest periods are considered for forecasting. Results show that the ARRSES 2^{nd} order method enables better quality of service and lower power outages compared to the other approaches when used with the same EM. *Fan et al.* focused on modeling and predicting harvested energy for self-powered Wireless Body Area Network (WBAN) in [38], particularly on indoor light and thermoelectric sources. The proposed prediction scheme is a Kalman filter, and the state of the system, predicted by the Kalman filter, is defined by the amount of solar energy harvested at the current time slot, the amount of thermoelectric energy harvested, the light intensity, the temperature difference, and the amount of human motion. The authors show using measurements that their approach enables better precision than moving average, exponential smoothing and linear regression for various activities such as walking, working at desk...

2.1.2 Prediction-Based Energy Management

As shown in Figure 2.1, the task of the energy predictor is to feed the EM with forecasts of the harvested energy for time window of K slots. Prediction-based EMs then use these forecasts, as well as the residual energy e_r, to set an energy budget e_b, which corresponds to the amount of energy that the node can use in the next time slot, before the next execution of the EM routine.

The first EM using the prediction-based approach was introduced in 2007 by *Kansal et al.* [18]. In their approach, the energy source is assumed to be pseudo-periodic, and EWMA is used to predict the future amount of harvested energy. Then, the duty-cycle is computed by taking into account the difference between predicted and observed energy inputs. This scheme suffers from the poor performance of EWMA during high-fluctuations weather. Moreover, a drawback of this approach is that it aims to maximize the duty-cycle, without balancing it over a pseudo-period of the energy source, leading to high quality of service during periods of energy availability, and poor quality of service during periods of energy scarcity. A distinctive feature of this scheme is that it only considers the predicted harvested energy to take decision about the duty-cycle, without using the residual energy, which can lead to frequent power failures.

Moser et al. [28, 39] formulated the problem of energy management as a linear program which objective is to maximize the minimal execution rate of the sensor node task over the horizon window, which guarantees some balance of the quality of service with regard to time. The optimization problem is reformulated as a multi-parameter linear program, which is partially solved offline to reduce the computational power required by the EM, and the resulting control profile can be seen as a piecewise affine function of the state vector. Indeed, after having solved the optimization problem in advance, a set of polyhedrons with the associated control laws has to be stored and

evaluated at each time step, which can still lead to a large computational effort if the number of critical regions is big. In [40, 41], this approach was extended by decoupling the control problem into two independent subproblems. Each subproblem is solved by an independent subcontroller and energy predictor. The first subcontroller works at a daily time scale, and receives forecasts of the energy, with the aim to ensure long-term sustainability, *i.e.* with a horizon of several weeks. The second subcontroller works with hourly estimates of the harvested energy, and ensures short-term adaptation. The first subcontroller sets an energy allowance, *i.e.* the amount of energy that the system should use in the current day, and therefore the first subcontroller sets the energy budget of the second subcontroller. The authors of [39, 42, 43] formulated the EM problem as a reward maximization problem, in which the reward associated with a service increases with the amount of computation required to provide the service. The authors explored how to exploit energy harvested from the environment to maximize the system performance for applications with different concave reward functions, and derived a polynomial-time algorithm for optimal assignments to maximize an overall reward. A proof of the algorithm optimality is provided, and the algorithm was evaluated using simulations against an adversary scheme. Results show that the proposed algorithm achieves better balancing of the energy budget over time slots compared to the adversary scheme.

Castagnetti et al. introduced in [44] two EMs, the Open-Loop Power Manager (OL-PM) and the Closed-Loop Power Manager (CL-PM). It is assumed that a node embeds an energy harvesting sensor, which is used to estimate the current level of harvested energy. A recharge rate is estimated, based on the energy harvested sensor readings as well as on a battery recharge model. The OL-PM uses only the recharge rate to take decision about the duty-cycle, *i.e.* to set the wake-up interval, and aims to achieve ENO. CL-PM is more sophisticated and tries to predict the durations of energy scarcity periods, called Zero Energy Intervals (ZEIs), and defined as periods during which the recharge rate is below a fixed threshold. CL-PM uses two distinct energy management schemes: one for ZEIs, which aims to avoid power failures by using the ZEI duration estimation from a ZEI predictor, and one for non-ZEIs, which is the same as OL-PM. *Le et al.* proposed Wake up Variation Reduction Power Manager (WVR-PM) in [45, 46] which aims to achieve balanced quality of service with regard to time. Similarly to [44], WVR-PM uses two distinct energy management schemes, called Positive Energy Power Manager (PE-PM) and Negative Energy Power Manager (NE-PM), and one of this two schemes is used according to the current amount of harvested energy. Indeed, if the current energy intake is higher than a fixed threshold, then PE-PM is used, otherwise NE-PM is used. During ZEIs, the NE-PM uses ZEI duration predictions to compute the wake-up interval in the aim to avoid power failures. During non-ZEI periods, the PE-PM uses predictions of the harvested energy, calculated using an EWMA filter, to take decision about the duty-cycle. A distinctive feature of WVR-PM compared to CL-PM is that during non-ZEI periods, it aims to store enough energy to prevent power failures during non-ZEIs periods, instead of achieving neutrality. Moreover, a quantizer is used to reduce fluctuations of the wake-up interval, by filtering small variations.

Gorlatova et al. [47, 48] presented the results of a 16 month-long indoor radiant energy measurements campaign, and a mobile outdoor light energy study. The authors showed that in indoor environment, the energy models are mostly partially predictable. Also, the resource allocation problem for energy harvesting was formulated, and algorithms were proposed to solve this problem online for deterministic energy profile and stochastic environmental energy models. In the first case, lexicographic maximization and utility maximization framework were used. In the second case, the harvested energy was modeled by i.i.d random variables, and the problem was formulated as an MDP. In [49], the authors focused on kinetic (motion) energy harvesting. They presented a dataset of long-term human motion and a study of the corresponding energy generation process, as well as an energy allocation algorithm. The energy allocation problem was formulated as an NP-hard integer optimization problem, and proposed an offline dynamic programming algorithm for solving the energy allocation problem, an offline fully polynomial time approximation scheme for cases where the dynamic programming algorithm is unpractical, and an online greedy algorithm that is optimal in particular scenarios. In [50], *Yang et al.* introduced AutoSP-WSN framework, which combines a routing protocol (SP-BCP) and a rate control scheme (PEA-DLEX) for solar powered EH-WSNs. The algorithms use forecasts of the harvested energy computed using a predictor introduced by the authors called WC-EWMA, which is, as the name suggests, based on the EWMA scheme, and uses both long-term seasonal and short-term daily solar profiles, as well as a

predefined cloudiness degree threshold to filter the influence of bad weather days over the seasonal stable reference power. The problem of local power management is formulated as a linear problem, and solved locally by the nodes. Two adaptive network protocols are proposed, named SP-BCP and PEA-DLEX. The first one is an extension of the BCP protocol [51], and is an energy-aware back-pressure routing protocol. The second is an extension of the DLEX algorithm [52]. *Jushi et al.* focused on wind energy harvesting in [36] and proposed a wake-up interval adaptation scheme that uses harvested energy forecasts provided by various predictors type, as well as consumed energy predictions and the current residual energy.

2.2 Prediction-Free Energy Management

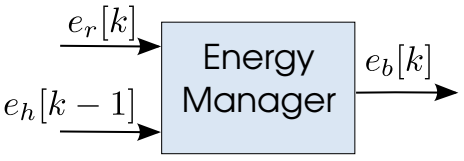

Figure 2.2 – Prediction-free energy management scheme architecture. No predictor is required.

In contrast with prediction-based energy management schemes, prediction-free approaches do not rely on forecasts of the harvested energy to take decision about the energy budget, as shown in Figure 2.2. The motivation of these approaches is the fact that the amount of energy that a sensor can harvest shows large fluctuations and is hard to predict. As a consequence, energy predictors can suffer from significant errors, which would incur overuse or underuse of the harvested energy.

The first prediction-free EM was LQ-Tracker [19], proposed in 2007 by *Vigorito et al.*. This scheme relies on linear quadratic tracking, a technique from control theory, to adapt the duty-cycle according the the current state of charge of the energy buffer. In this approach, the energy management problem is modeled as a first order discrete time linear dynamical system with colored noise, in which the system state is the state of charge of the energy buffer, the control is the duty-cycle and the colored noise the moving average of state of charge increments produced by the harvested energy. The objective is to minimize the average squared tracking error between the current state of charge and a target residual energy level. The authors used classical control theory results to get the optimal control, which does not depend on the colored noise, and the control law coefficients are learned online using gradient descent. Finally, the outputs of the control system are smoothed by an exponential weighting scheme to reduce the duty-cycle variance. Using simulations, the authors showed that the proposed algorithm can outperform the EM by *Kansal et al.* from [18]. *Hsu et al.* [53] considered energy harvesting WSNs with throughput requirement, and used Q-Learning, a well-known RL algorithm, to meet the throughput constraints. In this approach, states and actions are discretized, and a reward is defined according to the satisfaction of the throughput constraints. The aim of the algorithm is to maximize the overall rewards, by learning the Q-values, *i.e.* the accumulative reward associated with a given state-action pair. The proposed EM requires the tracking of the harvested energy and the energy consumed by the node in addition to the state of charge. Moreover it uses two dimensional look-up tables to store the Q-values, which incurs significant memory footprint. At each execution of the EM, the action is chosen according to the Q-values using soft-max function, and the Q-value of the last state-action pair observed is updated using the corresponding last observed reward.

In [54], the authors focus on energy harvesting nodes on which control is done by setting two actions: measurement and transmission action, and storage action. They used fuzzy rule based systems to generate two different controllers, one for each action. The state of the system was made of the energy buffer level and state of the data buffer, and the fuzzy rule based system covered each of the two dimensions with five triangular membership functions. The membership functions were related using twenty five automatically generated rules which were then weighted using one of the five membership function for each of the two possible action dimensions. The fuzzy rules were weighted by trial and error, specifically for a precise energy source. Indeed, the authors considered two different locations for solar light energy harvesting, and control surfaces were generated for each location and for each controller using energy traces of each location. The surfaces produced where

then discretized and stored as look-up tables in the device memory. Storing discretized version of the control surfaces in the device memory incurs a significant memory footprint. Moreover, as specific tuning was done for each energy source using recordings, the proposed scheme is hard to generalize.

With P-FREEN [55], *Peng et al.* proposed an EM that maximizes the duty-cycle of a sensor node in the presence of battery storage inefficiencies. The authors formulated the average duty-cycle maximization problem as a non-linear programming problem, and as solving this kind of problem directly is computationally intense, they proposed a set of *budget assigning principles* that maximizes the duty-cycle by only using the current observed energy harvesting rate and the residual energy. The proposed algorithm requires the current state of charge of the energy buffer as well as the harvested energy to take decision about the energy budget. If the state of charge of the energy buffer is below a fixed threshold or if the amount of energy harvested at the previous time slot is below the minimum required energy budget, then the node is operating with the minimum energy budget. Otherwise, the energy budget is set to a value that is a function of both the amount of energy harvested at the previous time slot and the energy storage efficiency.

2.3 Summary

EH-WSNs have received increasing attention in the last decade, and designing efficient and low overhead EMs for achieving energy neutrality is a hot topic. The EM task is to set the energy budget or, equivalently, the duty-cycle of the node, with the aim to maximize the quality of service while avoiding power failures. Therefore, it is a critical component. The majority of proposed algorithms assume the availability of forecasts of the harvested energy, and therefore designing accurate predictors is an active research field. Typically, predictors are specific to one type of energy source. Prediction-based EMs assume the presence of such a predictor and uses the energy harvesting forecasts to take decision about the energy budget. On the other hand, motivated by the difficulty of getting accurate forecasts of the harvested energy, prediction-free schemes do not require forecasts of the harvested energy.

Prediction-free approaches such as LQ-Tracker or P-FREEN proved that it is possible to achieve efficient energy management without requiring the overhead incurred by prediction mechanisms in terms of memory and computational power. Therefore, we focus on this thesis on prediction-free schemes. The recent EM P-FREEN is similar to a "all-or-nothing" policy, *i.e.* the energy budget is either the minimum energy budget, or an energy budget computed from the harvested energy to avoid energy waste. This approach leads to abrupt variations of the energy budgets, which is usually not suited for WSNs applications. In the next chapter, Fuzzyman, an EM based on fuzzy control theory, is presented and evaluated, which unlike P-FREEN achieves soft energy management.

However, Fuzzyman requires the amount of harvested energy at the previous time slots to take decisions about the energy budget. Even if it is assumed that this value is available in the majority of energy management schemes, this value is in practice hard to measure. Therefore, in Chapter 4, an EM based on reinforcement learning in continuous state and action spaces is introduced, which requires only the residual energy as an input. The proposed scheme was compared to LQ-Tracker, in addition to P-FREEN and Fuzzyman, as it is also a prediction-free scheme that requires only the residual energy as an input.

Chapter 3

Fuzzyman: an Energy Manager Based on Fuzzy Control Theory

Fuzzy control theory aims to extend the existing conventional control system techniques and methods for a class of ill-modeled systems, *i.e.* fuzzy systems [56]. Because of the unstable and hard to predict behavior of the harvested energy, EH-nodes are usually hard-to-model systems, and fuzzy control theory therefore constitutes an appropriate framework to design EMs for these systems. Accordingly, we introduce Fuzzyman [57], a new EM for EH-nodes that relies on fuzzy control theory. This chapter starts by presenting background on fuzzy control theory in Section 3.1, before introducing the design of Fuzzyman in Section 3.2. In Section 3.3, the parameterization of Fuzzyman is discussed in the case of EH-nodes powered by indoor ambient light using exhaustive trace-driven network simulations. Section 3.4 exposes the results of Fuzzyman evaluation, which was compared to P-FREEN [55] using exhaustive trace-driven simulations. Finally, Section 3.5 concludes this chapter.

3.1 Background on Fuzzy Control Theory

Fuzzy control relies on the concept of fuzzy logic for which truth values can be any real numbers between 0 and 1, as opposite to Boolean logic. Similarly, in fuzzy set theory, elements can have partial membership to a given set, as opposite to classical set theory in which an individual is either a member or not a member of a set. These concepts are detailed in Section 3.1.1. Next, in Section 3.1.2, the relevant background of fuzzy control theory required for understanding Fuzzyman design is exposed.

3.1.1 Fuzzy Set and Fuzzy Logic

Let A be a classical set, and let us define I_A its characteristic function defined by:

$$I_A(x) = \begin{cases} 0, & \text{if } x \notin A \\ 1, & \text{if } x \in A \end{cases} \tag{3.1}$$

which is an indication of membership to A. In fuzzy set theory, an element can be not fully in a set, but only partially. This can be formally expressed by extending the characteristic function. If we consider partial membership, the associated characteristic function needs to be generalized to describe the membership grade of a given element. The so-obtained generalized characteristic function maps any element x to a real in the range $[0, 1]$, where 0 can be interpreted "not a member at all" and 1 can be interpreted "full member". It can be seen that the characteristic function of a classical set is a particular case of this generalized characteristic function.

To motivate the concept of partial membership, let's consider the example of outdoor temperature and H be the set of temperatures for which the day is considered to be hot. As there is no precise threshold above which a day is considered as hot, the set H is not well-defined. For example, if the temperature is 25 °C, it is not clear if it is a hot day or not. A solution to make

H well-defined is to not classify a day as being absolutely hot or not hot at all, but to be *partially* hot depending on the temperature, which can be formally expressed as partial membership to the set H. An example of partial membership function is shown in Figure 3.1. On this example, the day is considered to be absolutely not hot for temperature of 10 °C or less, and absolutely hot for temperature of 50 °C or more. The day hotness is 0.5 if the temperature is 25 °C. The curve shown in Figure 3.1 is called the *membership function* of H.

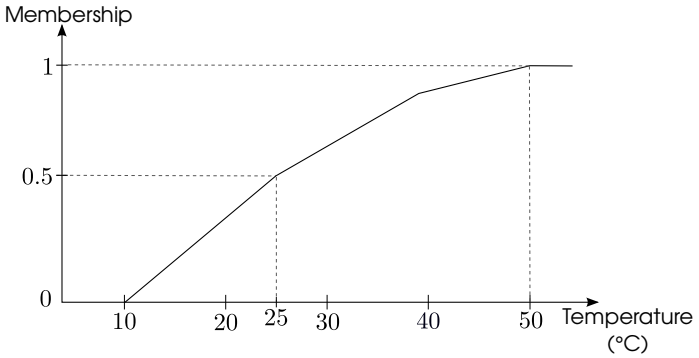

Figure 3.1 – An example of a membership function.

Once the membership function associated with a set has been chosen, the set along with the membership function associated to it is called a *fuzzy set*. A fuzzy set is thus made of two elements: a set and a membership function. If A is a fuzzy set, its membership function is denoted by μ_A.

The ultimate goal of fuzzy logic is to provide foundations for approximate reasoning using imprecise propositions based on fuzzy set theory, in the same way that the classical logic provides foundation for reasoning using precise propositions. In classical logic, every proposition is assumed to be either true or false. However, it is now well understood that many propositions are both partially true and partially false, and multi-valued logics were developed to generalize the classical two-valued logic. As a consequence, several three-valued logics are now well-established, and $n-$valued logics were further developed, and in particular the $n-$valued logic of Lukasiewicz allows $n = \infty$. Moreover, in the same way that there exists an isomorphism between the two-valued logic and the classical set theory, there is an isomorphism between Lukasiewicz logic and fuzzy set theory [56].

In order to work with fuzzy reasoning, we first need to introduce fuzzy logic operations, which are extensions of the classical logic operations, *i.e.* *and*, *or*, *not*, *implication* and *equivalence*, to the concepts of fuzzy reasoning. If A is a fuzzy set and if $\mu_A(x) \in [0,1]$ represents the truth value of proposition "x is a", we will denote $\mu_A(x \text{ is } a) = \mu(x)$. We have:

$$\begin{aligned}
\mu_A(\bar{x}) &= 1 - \mu_A(x) \\
\mu_A(x \wedge y) &= \min\left(\mu(x), \mu(y)\right) \\
\mu_A(x \vee y) &= \max\left(\mu(x), \mu(y)\right) \\
\mu_A(x \implies y) &= \min\left(1, 1 + \mu_A(y) - \mu_A(x)\right) \\
\mu_A(x \iff y) &= 1 - |\mu_A(x) - \mu_A(y)|
\end{aligned}$$

where $\bar{x}$ denotes "x is not a". We now focus on the implication relation $x \Rightarrow y$ as it plays an important role in fuzzy control. The fuzzy implication relation $x \Rightarrow y$ is defined in linguistic terms as:
"IF$x \in A$ with a truth value $\mu_A(x)$ THEN $y \in A$ with a truth value of $\mu_A(y)$"
has a truth value $\mu_A(x \Rightarrow y) = \min(1, 1 + \mu_A(y) - \mu_A(x))$, assuming that x and y take values in the same set A. In the general case, a fuzzy IF-THEN rule has the form:

$$\text{IF } (x_1 \text{ is } A_1) \ \wedge \ (x_2 \text{ is } A_2) \ldots (x_N \text{ is } A_N) \text{ THEN } y \text{ is } B,$$

and is implemented by the following evaluation formula: $\mu_{A_1}(x_1) \wedge \cdots \wedge \mu_{A_N}(x_N) \Rightarrow \mu_B(y)$, where:

$$\mu_{A_1}(x_1) \wedge \mu_{A_2}(x_2) \ldots \mu_{A_N}(x_N) = \min(\mu_{A_1}(x_1), \mu_{A_2}(x_2), \ldots, \mu_{A_N}(x_N)).$$

One may notice the absence of NOT or OR logical operations in this rule. The NOT operation can be easily incorporated as "IF x is not A" is equivalent to "IF $\bar{x}$ is A". Regarding the OR operation, any IF-THEN rule containing OR statements can be turned into a set of IF-THEN containing only AND statements. For example, the following rule:

$$\begin{aligned}&\text{IF } (x_1 \text{ is } A_1 \ \vee \ x_2 \text{ is } A_2) \wedge (x_3 \text{ is } A_3 \ \vee \ x_4 \text{ is } A_4)\\&\text{THEN} \dots\end{aligned}$$

is equivalent to:

$$\begin{aligned}&\text{IF } (x_1 \text{ is } A_1 \ \wedge \ x_3 \text{ is } A_3) \vee (x_1 \text{ is } A_1 \ \wedge \ x_4 \text{ is } A_4) \vee (x_2 \text{ is } A_2 \ \wedge \ x_3 \text{ is } A_3) \vee\\&(x_2 \text{ is } A_2 \ \wedge \ x_4 \text{ is } A_4)\\&\text{THEN} \dots\end{aligned}$$

which can be expressed as:

$$\begin{aligned}&\text{IF } (x_1 \text{ is } A_1 \ \wedge \ x_3 \text{ is } A_3)\\&\text{THEN} \dots\\&\text{IF } (x_1 \text{ is } A_1 \ \wedge \ x_4 \text{ is } A_4)\\&\text{THEN} \dots\\&\text{IF } (x_2 \text{ is } A_2 \ \wedge \ x_3 \text{ is } A_3)\\&\text{THEN} \dots\\&\text{IF } (x_2 \text{ is } A_2 \ \wedge \ x_4 \text{ is } A_4)\\&\text{THEN} \dots\end{aligned}$$

removing the need for explicit OR operators. Such a set of fuzzy IF-THEN rules is called a *fuzzy rules base*, and plays an essential role in fuzzy control.

An important practical consideration is how fuzzy IF-THEN rules are evaluated. A handful of options are available for evaluated the rule $\mu_{A \Rightarrow B}(x, y) = \mu_A(x) \Rightarrow \mu_B(y)$:

- $\mu_{A \Rightarrow B}(x, y) = \min(\mu_A(x), \mu_B(y))$
- $\mu_{A \Rightarrow B}(x, y) = \mu_A(x)\mu_B(y)$
- $\mu_{A \Rightarrow B}(x, y) = \min(1, 1 + \mu_B(y) - \mu_A(x))$
- $\mu_{A \Rightarrow B}(x, y) = \max\left(\min(\mu_A(x), \mu_B(y)), 1 - \mu_A(x)\right)$
- $\mu_{A \Rightarrow B}(x, y) = \max(1 - \mu_A(x), \mu_B(y))$
- Goguen's formula:

$$\mu_{A \Rightarrow B}(x, y) = \begin{cases} 1 & \text{if } \mu_A(x) \leqslant \mu_B(y) \\ \frac{\mu_B(y)}{\mu_A(x)} & \text{if } \mu_A(x) > \mu_B(y) \end{cases}$$

For the purpose of fuzzy logic inference, all these evaluation formulas are valid provided that the same formula for the implication relation is used. However, different formulas give different resulting values. In the next section, fuzzy control theory is introduced.

3.1.2 Fuzzy Control

In this section, the background on fuzzy control theory required to understand the design of Fuzzyman is exposed. This section focuses on the model-free approach of fuzzy control, which relies on the fuzzy set and fuzzy logic theories introduced in the previous section.

A significant part of fuzzy control systems are knowledge-based, in that their fuzzy controllers are described by fuzzy sets and fuzzy IF-THEN rules, which have been predefined from "expert" knowledge about the system. The basic architecture of a fuzzy logic controller consists of four

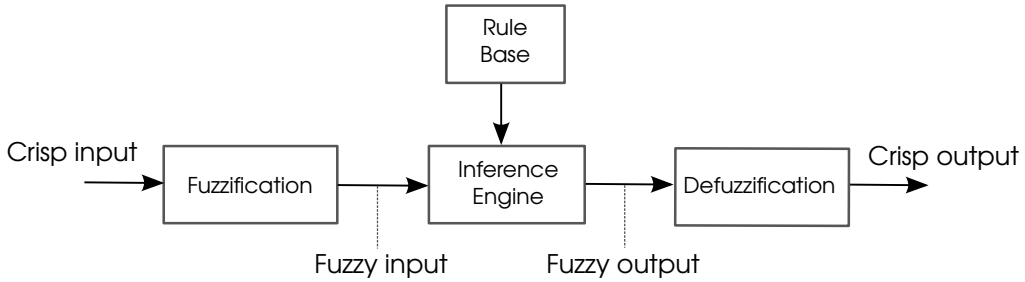

Figure 3.2 – Fuzzy logic controller architecture.

components: a fuzzification unit, an inference engine, a rule base and a defuzzification unit as shown in Figure 3.2. The crisp inputs of the controller are denoted by $e_1, \ldots, e_N$ where N is the number of inputs. The task of the fuzzification unit is to convert the "crisp" input signals into a normalized fuzzy set consisting of a set for the range of the input values, and an associated membership function. The aim of the fuzzification unit is to make the controller input signals compatible with the fuzzy inference engine. The rule base is made of a set of fuzzy IF-THEN rules, where the i^{th} rule is of the form:

$$\begin{aligned}&\text{IF controller input } e_1 \text{ is } E_{i,1} \wedge \cdots \wedge \text{ controller input } e_N \text{ is } E_{i,N}\\ &\text{THEN controller output } u_i \text{ is } U_i\end{aligned}$$

where $E_{i,j}$ is a fuzzy set associated to the i^{th} rule and j^{th} input. The fuzzy inference engine is responsible for applying these fuzzy rules to the controller inputs, and implements the fuzzy logic operators. The outputs of the inference engine are the controller outputs expressed in fuzzy terms, and are therefore incompatible with the system to control. The aim of the defuzzification unit is to convert those fuzzy outputs into crisp outputs, that the system can use.

Takagi and Sugeno proposed a modified version of IF-THEN rules in [58], in which the consequence of a rule is a function of the input variables. In this mode of reasoning, the i^{th} controller rule is of the form:

$$\begin{aligned}&\text{IF controller input } e_1 \text{ is } E_{i,1} \wedge \cdots \wedge \text{ controller input } e_N \text{ is } E_{i,N}\\ &\text{THEN controller output } u_i = f_i(e_1, \ldots, e_N)\end{aligned}$$

The defuzzification process calculates the crisp output by performing a weighted average on the output of each rule:

$$u = \frac{\sum_i \alpha_{R^i} f_i(e_1, \ldots, e_N)}{\sum_i \alpha_{R^i}}, \tag{3.2}$$

where the weight α_{R^i} associated to the i^{th} rule is the firing strength which measures the contribution of the rule:

$$\alpha_{R^i} = \min\left(\mu_{E_{i,1}}(e_1), \ldots, \mu_{E_{i,N}}(e_N)\right). \tag{3.3}$$

Fuzzyman is a Takagi-Sugeno controller type, and is introduced in the next section. Details on each unit (fuzzification, rule base/inference engine, defuzzification) will be given while describing the design of Fuzzyman.

3.2 Design of Fuzzyman

The task of Fuzzyman is to compute the energy budget $e_b[k]$ that the node should use during the slot k regarding the residual energy $e_r[k]$ and the energy harvested during the previous time slot $e_h[k-1]$. Therefore, Fuzzyman is executed at the beginning of every time slot. As a fuzzy logic controller, Fuzzyman is made of four units as shown in Figure 3.2. The inputs of the controller at the time slot k are $e_h[k-1]$ and $e_r[k]$, while the output is $e_b[k]$. We next describe in details the design of each unit.

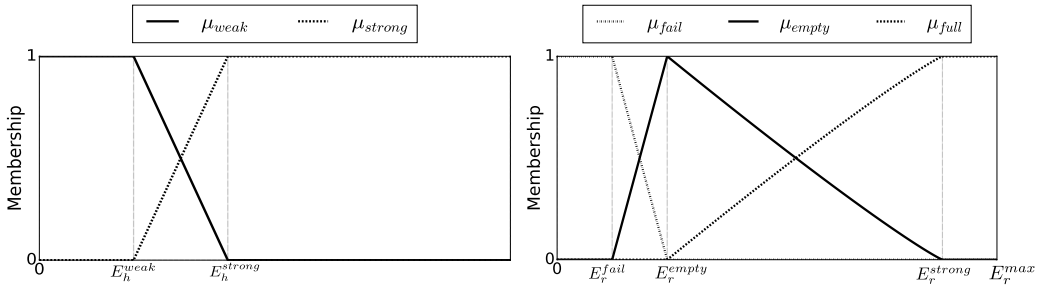

(a) Membership functions for the harvested energy.

(b) Membership functions for the residual energy.

Figure 3.3 – Membership functions used by the fuzzification module.

3.2.1 Fuzzification of the Controller Inputs

The first module of Fuzzyman is the fuzzification unit, which converts each crisp input value, *i.e.* $e_r[k]$ and $e_h[k-1]$, into fuzzy sets.

Harvested Energy Fuzzification

To describe the harvested energy physical value $e_h \geqslant 0$, two fuzzy sets named "WEAK" and "STRONG" are considered. They are associated to the following normalized membership functions, shown in Figure 3.3a:

$$\mu_{weak}(x) = \begin{cases} 1, & \text{if } x \leqslant E_h^{weak} \\ \frac{-x+E_h^{strong}}{E_h^{strong}-E_h^{weak}}, & \text{if } E_h^{weak} < x < E_h^{strong} \\ 0, & \text{if } x \geqslant E_h^{strong} \end{cases} \tag{3.4}$$

$$\mu_{strong}(x) = \begin{cases} 0, & \text{if } x \leqslant E_h^{weak} \\ \frac{x-E_h^{weak}}{E_h^{strong}-E_h^{weak}}, & \text{if } E_h^{weak} < x < E_h^{strong} \\ 1, & \text{if } x \geqslant E_h^{strong} \end{cases} \tag{3.5}$$

where E_h^{weak} is equal to the amount of energy required to ensure the minimum quality of service for one time slot, when the power conversion efficiency and the leakage are taken into account, *i.e.*:

$$E_h^{weak} = \frac{E_b^{min}}{\eta} + P_L T_s, \tag{3.6}$$

where P_L is the leakage power, and T_s is a time slot duration. Thus, if the source is fully "WEAK", then the amount of harvested energy is not enough to provide the minimum energy budget E_b^{min}. E_h^{strong} is the threshold at which the harvested energy is considered to be fully "STRONG".

Residual Energy Fuzzification

Three fuzzy sets are used to describe the residual energy e_r, which is within the range $[0, E_r^{max}]$. These fuzzy sets, named "FAIL", "EMPTY" and "FULL", are associated to the following membership functions:

$$\mu_{fail}(x) = \begin{cases} 1, & \text{if } x \leqslant E_r^{fail} \\ \frac{-x+E_r^{empty}}{E_r^{empty}-E_r^{fail}}, & \text{if } E_r^{fail} < x < E_r^{empty} \\ 0, & \text{if } x \geqslant E_r^{empty} \end{cases} \tag{3.7}$$

$$\mu_{empty}(x) = \begin{cases} 0, & \text{if } x \leqslant E_r^{fail} \\ \frac{x-E_r^{fail}}{E_r^{empty}-E_r^{fail}}, & \text{if } E_r^{fail} < x \leqslant E_r^{empty} \\ f_\kappa(x), & \text{if } E_r^{empty} < x < E_r^{full} \\ 0, & \text{if } x \geqslant E_r^{full} \end{cases} \tag{3.8}$$

$$\mu_{full}(x) = \begin{cases} 0, & \text{if } x \leqslant E_r^{empty} \\ 1 - f_\kappa(x), & \text{if } E_r^{empty} < x < E_r^{full} \\ 1, & \text{if } x \geqslant E_r^{full} \end{cases} \tag{3.9}$$

where

$$f_\kappa(x) = \left(\frac{-x + E_r^{full}}{E_r^{full} - E_r^{empty}} \right)^\kappa, \tag{3.10}$$

where $\kappa \geqslant 0$. The membership functions are shown in Figure 3.3b. The fuzzy set "FULL" indicates if the node has stored a sufficient amount of energy to survive a period of energy scarcity. Once the node is completely "FULL", then the controller should be careful to avoid waste of energy. The fuzzy set "EMPTY" indicates how close the node is from emptying its energy stock. The "FAIL" fuzzy set serves as a safety to avoid power failures. If the "FAIL" set is activated, then the node is in energy distress state, and the priority of the controller is to avoid a power failure.

The parameter κ controls the shapes of the membership functions μ_{full} and μ_{empty}. The higher κ is, the faster μ_{full} tends to 1 and μ_{empty} tends to 0 when the residual energy increases. Therefore, choosing high values of κ makes Fuzzyman more tolerant about the fullness of the energy storage device. We denote E_{res} the amount of energy that is needed to be reserved in order for the node to ensure the minimum quality of service when no harvested energy is available. E_r^{full} indicates that the node has reserved sufficient energy E_{res}. E_r^{empty} indicates that all the reserved energy E_{res} was used up. Thus, $E_{res} = E_r^{full} - E_r^{empty}$. Having $E_r^{empty} > E_r^{fail}$ avoids power failure when all the reserved energy has been used. When the amount of residual energy falls below E_r^{empty}, the node enters the *energy distress state*. Finally, having $E_r^{full} < E_r^{max}$ avoids wasting energy by overflow of the storage device.

The output of the fuzzification unit is the tuple $(\mu_{weak}(e_h), \mu_{strong}(e_h), \mu_{fail}(e_r), \mu_{empty}(e_r), \mu_{full}(e_t))$, which forms the fuzzy inputs of the inference engine.

3.2.2 Inference Engine

The task of the inference engine is to create the control actions in fuzzy terms from the inputs provided by the fuzzification module. The inference engine strategy is described by a set of 6 fuzzy IF-THEN rules R_i with $i \in \{1 \dots 6\}$ shown by the Table 3.1. For each slot k, the output of the rule i is denoted $e_b^i[k]$. The output of the rules R_2 and R_3 are given by (3.11), and the rule R_6 output is the energy budget used at the previous slot.

e_h \ e_r	FAIL	EMPTY	FULL
STRONG	E_b^{eds} (R_1)	(3.11) (R_2)	(3.11) (R_3)
WEAK	E_b^{eds} (R_4)	E_b^{min} (R_5)	$e_b[k-1]$ (R_6)

Table 3.1 – Rule base used by the inference engine.

$$e_b^i[k] = E_b^{min} + \mu_{full}\left(e_r[k]\right) \left(e_h[k-1] - \frac{E_b^{min}}{\eta} - P_L T_s \right) \eta. \tag{3.11}$$

In (3.11), it is assumed that the energy harvesting rates for two consecutive time slots are similar. This assumption is reasonable for sufficiently small time slot duration. Energy prediction schemes can be used for better estimation of the energy harvesting rate in near future [26].

All rules share the following multi-input single-output form:

$$\begin{aligned} &\text{IF } e_r[k] \text{ is } X_r^i \ \wedge \ e_h[k-1] \text{ is } X_h^i \\ &\text{THEN } e_b[k] = e_b^i[k], \end{aligned}$$

where X_r^i can be either FAIL, EMPTY or FULL and X_h^i can be either STRONG or WEAK. It is important to notice that up to four rules can be activated at one run of Fuzzyman. The power strategy implemented by Table 3.1 corresponds to five different scenarios:

1. R_1 and R_4: If the residual energy is FAIL, then the node is in energy distress. In that case, the energy budget is set to the predefined value E_b^{eds}.

2. R_5: If the amount of harvested energy is WEAK and the energy storage device is EMPTY, then the energy budget is set to the amount of energy required to ensure minimum quality of service, *i.e.* E_b^{min}.

3. R_6: If the amount of harvested energy is WEAK and the energy storage device is FULL, then the energy budget is unchanged.

4. R_2: If the amount of harvested energy is STRONG and the energy storage device is not yet fully charged, *i.e.* $\mu_{full}(e_r[k]) < 1$, then part of the harvested energy is used to power the node, while the rest is stored. The fraction of the harvested energy used to power the node will be at least E_b^{min}, and depends on μ_{full} as shown by (3.11). Therefore, κ controls the energy allocation policy of Fuzzyman.

5. R_3: If the amount of harvested energy is STRONG and the energy storage device is fully charged, *i.e.* $\mu_{full}(e_r[k]) = 1$, then only the amount of energy required to compensate for the leakage is stored, while the rest is used to power the node, thus minimizing the risk of energy waste.

The fuzzy AND operator is implemented by the min function, as defined in the previous section, and the *activation value* $\alpha_{R^i}[k] \geqslant 0$ for each rule R_i corresponds to its firing strength, and is defined following the Takagi-Sugeno approach:

$$\alpha_{R^i}[k] = \min\left(\mu_{X_r^i}\left(e_r[k]\right), \mu_{X_h^i}\left(e_h[k-1]\right)\right). \tag{3.12}$$

The rule R_i is *activated* if its activation value is strictly positive. If the rule is not activated, then its output value $e_b^i[k]$ is simply set to 0. At every run of Fuzzyman, at least one rule is activated, and thus:

$$\sum_{i=1}^{6} \alpha_{R^i}[k] > 0. \tag{3.13}$$

The activation value of each rule is interpreted as the membership value of the energy budget to the output of the rule. The importance of κ can be seen here. Indeed, the κ parameter controls the membership functions of the FULL and EMPTY fuzzy sets, and therefore impacts the activation values of the rules. The highest κ is, the more tolerant is Fuzzyman about the fullness of the energy storage device, and therefore the less prudent it is. In Section 3.3, the choice of the adequate value of κ in the context of indoor ambient light harvesting is considered.

3.2.3 Defuzzification of the Energy Budget

The last unit of Fuzzyman is the defuzzification unit, which computes a physical value of the energy budget from the outputs of the inference engine. Following the Takagi-Sugeno approach, the "center-of-gravity" scheme is used, which is the most common formula [56] to perform defuzzification. Thus, the physical value of the energy budget is computed by:

$$e_b[k] = \frac{\sum_{i=1}^{6} \alpha_{R^i}[k] e_b^i[k]}{\sum_{i=1}^{6} \alpha_{R^i}[k]}, \tag{3.14}$$

which is always defined according to (3.13).

Finally, the algorithm of Fuzzyman is shown by Algorithm 1. The complexity of the proposed algorithm is $O(1)$, and incurs very few computations and memory overhead. Therefore, it is well-adapted to wireless sensor nodes.

Algorithm 1 Fuzzyman algorithm

Input: $e_r[k]$, $e_h[k-1]$
1: $i \leftarrow 1$
2: **while** $i \leqslant 6$ **do**
3: $\quad \alpha_{R^i}[k] \leftarrow \texttt{min}\{\mu_{X_r^i}(e_r[k]), \mu_{X_h^i}(e_h[k-1])\}$
4: $\quad$ **if** $\alpha_{R^i}[k] > 0$ **then**
5: $\quad\quad$ Set $e_b^i[k]$ according to Table 3.1
6: $\quad$ **else**
7: $\quad\quad e_b^i[k] \leftarrow 0$
8: $\quad i \leftarrow i + 1$
9: $e_b[k] \leftarrow \frac{\sum_{i=1}^{6} \alpha_{R^i}[k] e_b^i[k]}{\sum_{i=1}^{6} \alpha_{R^i}[k]}$
10: **return** $e_b[k]$

3.3 Tuning Fuzzyman

The κ parameter is the control parameter of Fuzzyman. Choosing κ inappropriately may lead to power failures or energy waste. The adequate value of κ depends on both the energy source and the energy storage device capacity E_r^{max}. We focus on the PowWow platform [59], which embeds a 0.9 F supercapacitor. Moreover, EH-nodes powered by indoor ambient light are considered in this work. Ambient light is the most common and mature among the different forms of energy harvesting. Indoor ambient light is usually a diurnal energy source, and the typical illumination level varies from 1 W/m^2 [60] to 10 W/m^2 [61]. Simulations are used to find the adequate value of κ when indoor ambient light is harvested.

3.3.1 Simulation Setup

Simulations were done using GreenCastalia [62], an open-source energy harvesting simulation framework for the Castalia/OMNeT++ simulator [63]. The simulated network consists of one sink that uses batteries as energy supply, and four EH-nodes powered by solar cells. The solar panel area is set to 30 cm^2, and the panel efficiency to 15%, which is a realistic value regarding current photovoltaic technologies [64]. The simulated platform embeds a TI CC1000 radio chip, which consumes 22.2 mW in receive state, 80.1 mW in transmit state and 0.0006 mW in sleep state. Because we want to evaluate the performance of the EM, only the energy waste due to energy storage device saturation *i.e.* harvested energy that cannot be stored because the energy storage device is full, is considered. Therefore, the power conversion efficiency η is set to 1 and the leakage power P_L is set to 0 W. Moreover, T_s is set to 300 s, and each simulation lasts 31 days (simulated time).

The energy consumption of EH-nodes is controlled by duty-cycling. As communication is usually the most consuming task, the idea of duty-cycling is to allow the node to switch its radio between the sleep state and the active state according to a schedule. At each wake up, the sensor node performs a measurement and sends the so-obtained value to the sink. Environmental power sources provide energy that varies with time and space, leading to decoupled and individual duty-cycle among EH-nodes. This makes synchronous MAC protocols unsuitable to EH-WSNs as they require synchronized duty-cycle [65]. In this work, the well-known Carrier Sense Multiple Access with Collision Avoidance (CSMA/CA) protocol is used.

3.3.2 Energy Traces

GreenCastalia needs energy traces to simulate the harvested energy. The Algorithm 2 is used to generate light power traces, with a time granularity of one second. The purpose of the trace generator is to allow the evaluation of the EMs in regard to energy source characteristics that influence significantly their behaviors, and which can be set by the user using input parameters in the proposed model. These characteristics are the average harvested power during daytime, the difference of harvested power from one day to another and the night-to-day duration ratio. The

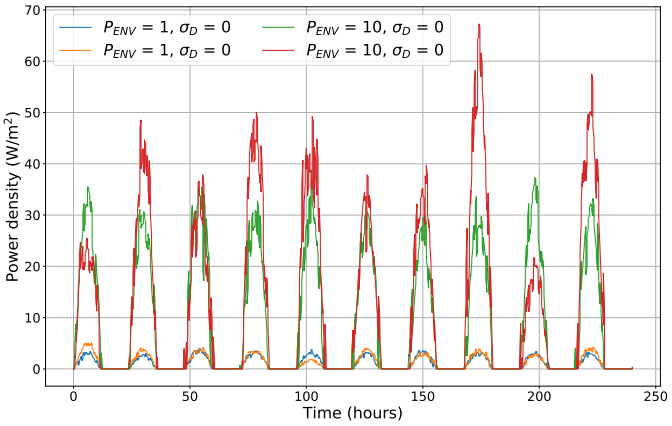

Figure 3.4 – Examples of generated power traces using Algorithm 2 with different values of P_{ENV} and σ_D.

input parameters allow the user to set up these characteristics. More precisely, P_{ENV} controls the average daytime power density and $\varphi \in [0, 1]$ is the night-to-day duration ratio. The difference of harvested power from one day to another is simulated using a coefficient (m in the Algorithm 2) that follows a normal distribution with a mean equal to one and a variance of σ_D^2. Moreover, L is the trace length in seconds, and small disturbances of the harvested energy are considered as noise (n in the Algorithm 2) and are simulated using a normal distribution with a zero mean and a variance of σ_N^2. Also, in real power traces, these variations do not occur as fast as every second. Therefore, we use the parameter N_W to set the duration between two variations of the noise variable.

Algorithm 2 Trace generation

Input: L, P_{ENV}, φ, σ_D, σ_N, N_W

Trace ← Empty Trace
$t \leftarrow 0$
loop
  $d \leftarrow t \ \% \ H$
  if $d = 0$ **then**
    $m \leftarrow \text{RandomGauss}(1, \sigma_D)$
  if $d < (1 - \varphi)H$ **then**
    if $t \ \% \ N_W = 0$ **then**
      $n \leftarrow \text{RandomGauss}(0, \sigma_N)$
    $y \leftarrow mP_{ENV}\left(\sin\left(\frac{\pi d}{T(1-\varphi)}\right) + n\right)$
    if $y < 0$ **then**
      $y \leftarrow 0$
  else
    $y \leftarrow 0$
  Trace[t] ← y
  $t \leftarrow t + 1$
  if $t = L$ **then**
    break

In the case of ambient light harvesting, typical power densities range from 1 W/m^2 [60] to 10 W/m^2 [61]. Therefore, using the trace generation algorithm, two pairs of energy traces were generated, one with P_{ENV} set to 1 W/m^2 and one with P_{ENV} set to 10 W/m^2. Each pair is made of two energy traces, one with important fluctuations generated with σ_D set to 0.4, and one with low fluctuations generated with σ_D set to 0.1. Figure 3.4 shows part of the traces using the Algorithm 2.

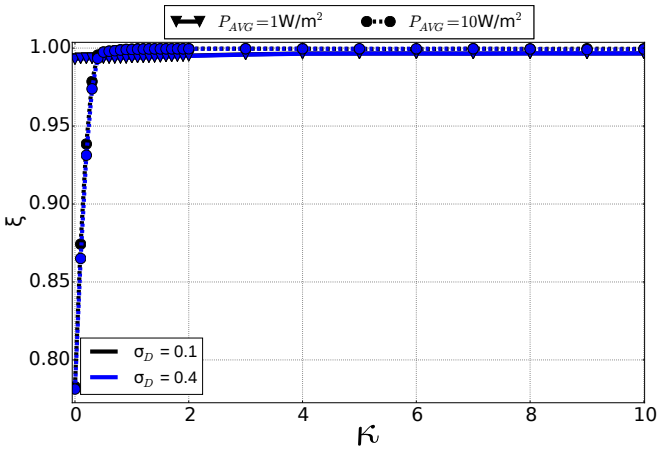

(a) Energy efficiency ξ as a function of κ.

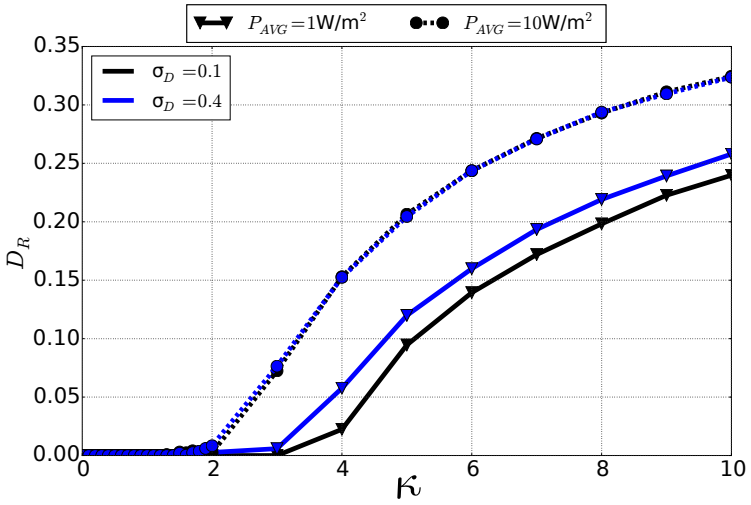

(b) Downtime ratio D_R as a function of κ.

Figure 3.5 – Simulation results for tuning Fuzzyman.

3.3.3 Simulations Results

Two metrics are considered for the choice of κ: the dead ratio D_R and the *energy efficiency* ξ, that were both introduced in Chapter 1. The downtime ratio is defined as the ratio of time spent in power failure state over the total application duration, while the energy efficiency is defined as follows:

$$\xi = 1.0 - \frac{\sum_k e_w[k]}{\sum_k e_h[k] + e_r[0]}. \tag{3.15}$$

Figure 3.5a and Figure 3.5b show respectively ξ and D_R for values of κ ranging from 0 to 10. We can see that for values of κ higher than 0.4, the energy efficiency is higher than 0.99 for the four scenarios, while for smaller values of κ the energy efficiency is significantly lower when $P_{ENV} = 10\,\mathrm{W/m^2}$. These results reveal that using low values of κ prevent Fuzzyman from taking advantage of all the harvested energy. Nonetheless, using too high values of κ causes Fuzzyman to incur power failures. Indeed, Figure 3.5b shows that for values of κ greater than 1.1 the downtime ratio stops being null and rapidly increases. According to these results, $\kappa = 1.1$ is the value that maximizes ξ while achieving a null downtime ratio for the four traces introduced in Section 3.3.2. Therefore, this value of κ is chosen for the evaluation of Fuzzyman presented in Section 3.4. Figure 3.3 shows the membership functions when $\kappa = 1.1$.

3.4 Evaluating Fuzzyman

We compared Fuzzyman to P-FREEN [55], a recent model-free EM that outperforms the reference scheme proposed by *Kansal et al.* [18]. The simulation setup is the same as in Section 3.3.1. Simulations were done with energy traces generated by the model introduced in Section 3.3.2. Two metrics in addition to D_R and ξ are considered: the wasted energy E_W, *i.e.* the harvested energy that could not be stored because the energy storage device was full, and the average energy budget $\overline{E_b}$. Simulations were run for values of P_{ENV} ranging from $1\,\mathrm{W/m^2}$ to $10\,\mathrm{W/m^2}$, and values of σ_D ranging from 0.1 to 0.4. Both Fuzzyman and P-FREEN achieve downtime ratio lower than 0.2 % in all the simulation scenarios. Therefore, we focus on the energy efficiency, the wasted energy and the average energy budget in the rest of this section.

Figure 3.6a exposes the impact of P_{ENV} and σ_D on ξ. If ξ is similar for both EMs when $P_{ENV} = 1\,\mathrm{W/m^2}$, Fuzzyman outperforms P-FREEN for higher values of P_{ENV}. σ_D has no impact on the performance of the EMs, whereas high values of P_{ENV} lead to lower values of ξ for P-FREEN, but do not influence the performance of Fuzzyman. As we will see below, these results are explained by the larger waste of energy incurred by P-FREEN.

Figure 3.6b shows the wasted energy E_W when P_{ENV} and σ_D vary. As we can see, Fuzzyman incurs significantly less energy waste than P-FREEN. As previously, σ_D does not impact the performance of the EMs. When P_{ENV} increases, the amount of wasted energy increases when P-FREEN is used, but stays low when Fuzzyman is used. This result explains the values of ξ exposed in Figure 3.6a.

In order to evaluate the impact of the more efficient harvested energy management achieved by Fuzzyman, the average packet generation rate $\overline{\chi_g}$ is considered. Figure 3.6c shows the impact of P_{ENV} and σ_D on $\overline{\chi_g}$. If the average energy budget is similar for both EMs for low values of P_{ENV}, Fuzzyman outperforms P-FREEN for high values of P_{ENV}. Moreover, the advantage of Fuzzyman over P-FREEN increases when P_{ENV} increases. Indeed, Fuzzyman achieves up to 25 % higher $\overline{\chi_g}$ than P-FREEN (when $P_{ENV} = 10\,\mathrm{mW}$ and $\sigma_D = 0.4$).

3.5 Conclusion

Fuzzy control theory applies fuzzy reasoning concepts from fuzzy logic to control, in the aim to extend conventional control techniques for a class of ill-modeled systems. As EH-nodes are usually hard-to-model systems because of the unstable and hard to predict behavior of the harvested energy, fuzzy control constitutes an appropriate framework for these systems. Fuzzyman was accordingly proposed in this chapter. Fuzzyman is a Takagi-Sugeno type of fuzzy controller, that is able to provide high harvested energy efficiency, while avoiding power failures. Fuzzyman was compared to P-FREEN, a recent EM using extensive trace-driven simulations, and the results showed that the proposed approach outperforms P-FREEN by allowing a higher energy efficiency, leading to better quality of service.

Fuzzyman does not relies on any forecasts of the harvested energy to operate, similarly to P-FREEN. However, it still needs measures of the harvested energy. In Chapter 8, an EM inspired by Fuzzyman was designed and implemented on the PowWow platform, but that uses the residual energy variation instead of the harvested energy as this latter value is hard to measure precisely in practice. Moreover, this consideration motivated the design of RLMan, presented in the next section, an EM for EH-nodes which is based on RL theory.

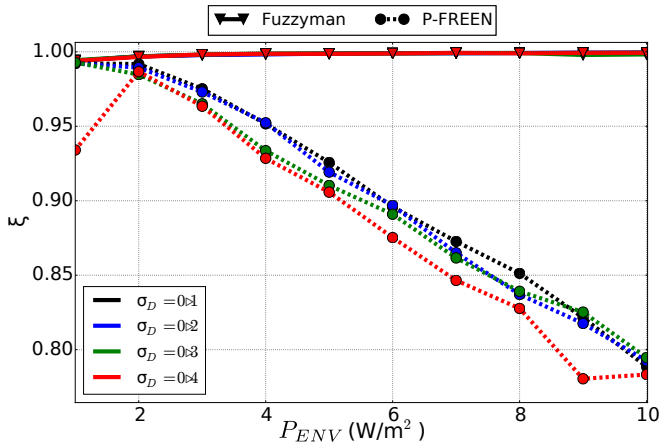

(a) Energy efficiency ξ as a function of P_{ENV} for different values of σ_D.

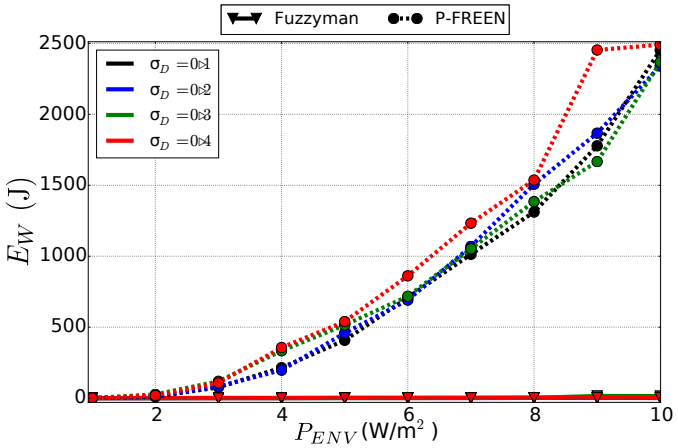

(b) Wasted energy E_W as a function of P_{ENV} for different values of σ_D.

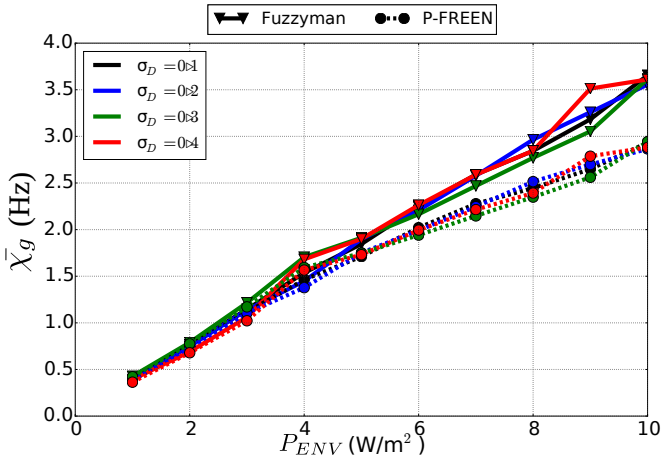

(c) Average packet generation rate $\overline{\chi_g}$ as a function of P_{ENV} for different values of σ_D.

Figure 3.6 – Simulation results for tunning Fuzzyman.

Chapter 4

RLMan: an Energy Manager Based on Reinforcement Learning

Most of the EMs introduced in Chapter 2 and Chapter 3 require an accurate control of the spent energy, as well as detailed tracking of the previously harvested and previously consumed energies to operate properly. However, in practice, such mechanisms are difficult to implement and incur significant overhead [66]. Considering these practical issues, we propose in this chapter RLMan [67], a novel EM scheme based on Reinforcement Learning (RL) theory, that requires only the state of charge of the energy storage device to operate. RLMan objective is to maximize the quality of service, defined as the packet generation rate, *i.e.* the frequency at which packets are generated (e.g. by performing measurements) and sent, while avoiding power failure. RLMan aims to set the packet generation rate by both exploiting the current knowledge of the environment and exploring it. The problem of maximizing the quality of service in EH-WSNs is formulated as a Markovian Decision Process (MDP), and a novel EM scheme based on RL theory is introduced. RLMan uses function approximation to minimize the memory footprint and computational overhead. RLMan as well as three state of the art EMs (P-FREEN, Fuzzyman and LQ-Tracker) that aim to maximize the quality of service were evaluated using extensive simulations with real measurements of both indoor light and outdoor wind.

The rest of this chapter is organized as follows: Section 4.1 presents the required background on RL theory. RLMan is introduced in Section 4.2. In Section 4.3, RLMan is evaluated. First, preliminary results are presented to show the behavior of RLMan, focusing on the learning phase (first few days). Next, the results of the comparison of RLMan with three other EMs are exposed. Finally, Section 4.4 concludes this chapter.

4.1 Background on Reinforcement Learning

RL is a framework for optimizing the behavior of an agent, or controller, that interacts with its environment. More precisely, RL algorithms can be used to solve optimization problems that can be formulated as MDPs. First, MDPs in continuous state and action spaces are introduced. Then, Temporal-Difference (TD) learning, an important method for online policy evaluation, is presented, focusing on the case where linear function approximators are used.

4.1.1 MDPs in Continuous State-Action Spaces

A MDP is a tuple $\langle \mathcal{S}, \mathcal{A}, \mathcal{T}, \mathcal{R} \rangle$ where $\mathcal{S}$ is the state space, $\mathcal{A}$ is the action space, $\mathcal{T} : \mathcal{S} \times \mathcal{A} \times \mathcal{S} \rightarrow [0, 1]$ is the state transition probability density function and $\mathcal{R} : \mathcal{S} \times \mathcal{A} \rightarrow \mathbb{R}$ is the reward function. In discrete time MDPs, which are considered in this work, at each time step k, the agent is in a state $S[k] \in \mathcal{S}$ and takes an action $A[k] \in \mathcal{A}$ according to a policy π. In response to this action, the environment provides a scalar feedback, called *reward* and denoted by $R[k+1]$, and the agent is, at the next time slot $k+1$, in the state $S[k+1]$. This process is illustrated in Figure 4.1. The aim of the RL algorithm is to find a policy which maximizes the accumulated reward called *return*.

In this work, MDPs are assumed to be stationary, *i.e.* the elements of the tuple $\langle \mathcal{S}, \mathcal{A}, \mathcal{T}, \mathcal{R} \rangle$ do not change over time.

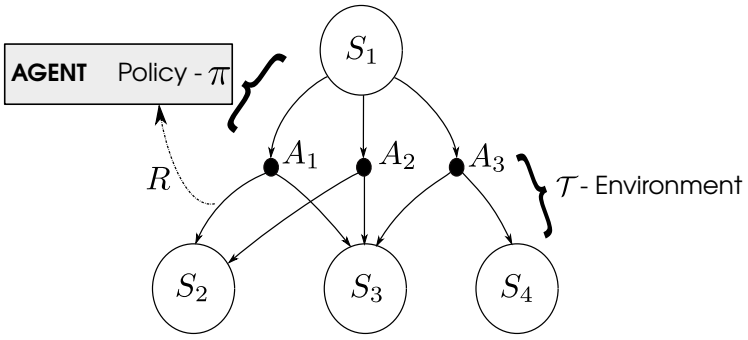

Figure 4.1 – Markovian decision process illustration.

Continuous state and action spaces are considered in this work, however in Figure 4.1, an illustration of a discrete state and action spaces MDP is shown for clarity. The stochastic process to be controlled is described by the transition probability density function $\mathcal{T}$, which models the dynamics of the environment. The probability of reaching a state $S[k+1]$ in the region $\mathcal{S}[k+1] \subseteq \mathcal{S}$ after taking the action $A[k]$ from the state $S[k]$ is therefore:

$$\Pr\left(S[k+1] \in \mathcal{S}[k+1] \mid S[k], A[k]\right) = \int_{\mathcal{S}[k+1]} \mathcal{T}\left(S[k], A[k], S\right) dS. \tag{4.1}$$

When taking an action $A[k]$ in a state $S[k]$, the agent receives a scalar reward $R[k+1]$ assumed to be bounded. The reward function is defined as the expected reward given a state and action pair:

$$\mathcal{R}(S, A) = \mathbb{E}\left[R[k+1] \mid S[k] = S,\ A[k] = A\right]. \tag{4.2}$$

The aim of the agent is to find a policy which maximizes the total discounted accumulated reward defined by:

$$J(\pi) = \mathbb{E}\left[\sum_{k=1}^{\infty} \gamma^{k-1} R[k] \;\middle|\; \rho_0,\ \pi\right], \tag{4.3}$$

where $\gamma \in [0, 1)$ is the discount factor, and ρ_0 the initial state distribution. From this last equation, it can be seen that choosing values of γ close to 0 leads to "myopic" evaluation as immediate rewards are preferred, while choosing a value of γ close to 1 leads to "far-sighted" evaluation.

Policies in RL can be either deterministic or stochastic. A deterministic policy π maps each state to an action: $\pi : \mathcal{S} \rightarrow \mathcal{A}$ in a unique way. When using a stochastic policy, actions are chosen randomly according to a distribution of actions given states:

$$\pi\left(A \mid S\right) = \Pr\left(A[k] = A \mid S[k] = S\right). \tag{4.4}$$

Using stochastic policies allows exploration of the environment, which is fundamental. Indeed, RL is similar to trail-and-error learning, and the goal of the agent is to discover a good policy from its experience with the environment, while minimizing the amount of reward "lost" while learning. This leads to a dilemma between exploration (learning more about the environment) and exploitation (maximizing the reward by exploiting known information). The initial state distribution is denoted by $\rho_0 : \mathcal{S} \rightarrow [0, 1]$, and the discounted accumulated reward can be defined by:

$$J(\pi) = \int_{\mathcal{S}} \rho_\pi(S) \int_{\mathcal{A}} \pi(A|S) \mathcal{R}(S, A) dA dS, \tag{4.5}$$

where:

$$\rho_\pi(S) = \int_{\mathcal{S}} \rho_0(S') \sum_{k=1}^{\infty} \gamma^{k-1} \Pr\left[S[k] = S \mid S_0 = S',\ \pi\right] dS' \tag{4.6}$$

is the discounted state distribution under the policy π.

During the learning, the agent evaluates a given policy π by estimating the J function (4.5). This estimate is called the value function of π and comes in two flavors. The *state value function*, denoted by V^π, is a function that gives for each state $S \in \mathcal{S}$ the expected return when the policy π is used:

$$V^\pi(S) = \mathbb{E}\left[\sum_{i=1}^{\infty} \gamma^{i-1} R[k+i] \;\middle|\; S[k] = S, \pi\right]. \tag{4.7}$$

This function aims to predict the future discounted reward if the policy π is used to walk through the MDP from a given state $S \in \mathcal{S}$, and thus evaluates the "goodness" of states. Similarly, the *state-action value function*, denoted by Q^π, evaluates the "goodness" of state-action couples when π is used:

$$Q^\pi(S, A) = \mathbb{E}\left[\sum_{i=1}^{\infty} \gamma^{i-1} R[k+i] \;\middle|\; S[k] = S, A[k] = A, \pi\right]. \tag{4.8}$$

These two value functions relate to each other as follows:

$$V^\pi(S) = \int_{\mathcal{A}} \pi(A \mid S) Q^\pi(S, A) dA. \tag{4.9}$$

Moreover, (4.7) and (4.8) can be written in a recursive form:

$$V^\pi(S) = \mathbb{E}\left[R[k+1] + \gamma V^\pi(S[k+1]) \mid S[k] = S, \pi\right], \tag{4.10}$$

and

$$Q^\pi(S, A) = \mathbb{E}\left[R[k+1] + \gamma Q^\pi(S[k+1], A[k+1]) \mid S[k] = S, A[k] = A, \pi\right], \tag{4.11}$$

which form the *Bellman Expectation Equations*. The intuition behind the Bellman Expectation Equations is that the value functions can be decomposed into immediate reward plus discounted value of the successor state.

The *optimal state value function* gives for each state $S \in \mathcal{S}$ the best possible return over all policies, and is formally defined by:

$$V^*(S) = \max_\pi V^\pi(S). \tag{4.12}$$

Similarly, the *optimal state-action value function* is the maximum state-action value function over all the policies:

$$Q^*(S, A) = \max_\pi Q^\pi(S, A). \tag{4.13}$$

The optimal value functions specify the best achievable performance in an MDP.

A partial ordering is defined over policies as follows:

$$\pi \geqslant \pi' \text{ if } \forall S \in \mathcal{S},\ V^\pi(S) \geqslant V^{\pi'}(S).$$

An important result in RL theory is that there exists an *optimal policy* π^* that is better than or equal to all the other policies, *i.e.* $\pi^* \geqslant \pi,\ \forall \pi$. Moreover, all optimal policies achieve the optimal state value function, *i.e.* $V^{\pi^*} = V^*$, and the optimal state-action value function, *i.e.* $Q^{\pi^*} = Q^*$. One can see that if Q^* is known, a deterministic optimal policy can be found by maximizing over Q^*: $\pi^*(S) = \text{argmax}_A Q^*(S, A)$. The optimal value functions are recursively related by the *Bellman Optimality Equations*, which intuitively express that a value from a state under an optimal policy must equal the expected return of the best action from the state. Formally:

$$V^*(S) = \max_{A \in \mathcal{A}} Q^*(S, A). \tag{4.14}$$

For the optimal state value function, we have:

$$V^*(S) = \max_{A \in \mathcal{A}} \mathbb{E}\left[R[k+1] + \gamma V^*(S[k+1]) \mid S[k] = S, A[k] = A, \pi\right] \tag{4.15}$$

$$= \max_{A \in \mathcal{A}} \int_{\mathcal{S}} \mathcal{T}(S, A, S') \left(R[k+1] + \gamma V^*(S')\right) dS', \tag{4.16}$$

and for the optimal state-action value function:

$$Q^*(S,A) = \mathbb{E}\left[\mathcal{R}(S,A) + \gamma \max_{A' \in \mathcal{A}} Q^*(S[k+1], A') \mid S[k] = S, A[k] = A, \pi\right] \tag{4.17}$$

$$= \int_{\mathcal{S}} \mathcal{T}(S,A,S') \left(R[k+1] + \gamma \max_{A' \in \mathcal{A}} Q^*(S', A')\right) dS'. \tag{4.18}$$

An agent uses its experience to evaluate a given policy by estimating its value function. The goal of the controller is to optimize the value function by finding an optimal policy. We next discuss a well-known approach for on-line policy evaluation, TD learning. Moreover, as continuous spaces are considered in this work, we focus on the case where function approximators are used.

4.1.2 Temporal-Difference Learning with Linear Function Approximation

When considering continuous state and action spaces MDPs, it is impossible to store the exact value for each state or state-action pair, and therefore function approximation is used to cover the full range of states and actions. There exist many function approximators [68], such as linear combination of features, neural networks, decision tree, Fourier or wavelet bases... However, linear function approximators are considered in this work, as they are simple to compute, which is important in the context of WSNs, and a number of convergence guarantees exists.

It is assumed that a feature-extraction function $\phi : \mathcal{S} \rightarrow \Phi$ is given, and maps the states into a feature vector in the feature space Φ. A feature vector is a representation of the state space which facilitates the processing. The feature vector corresponding to the state $S \in \mathcal{S}$ is denoted by $\phi(S)$. We denote by f_θ the function approximator of parameter vector θ, which approximates the function f. f can be the state value function V, the state-action value function Q or the policy π. f_θ is defined by:

$$f_\theta(S) = \theta^\intercal \phi(S). \tag{4.19}$$

where $\theta^\intercal$ is the transpose of θ. The function f_θ is linear in the parameters, and therefore is referred to as a linear function approximator. However, it may not be linear in state variable.

Let us now focus on how to approximate V^π by a function approximator V_θ. To do so, let us consider the Mean Square Error (MSE) objective function:

$$\text{MSE}(\theta) = \mathbb{E}\left[\left(V^\pi(S[k]) - V_\theta(S[k])\right)^2\right]. \tag{4.20}$$

A very popular method to adjust the parameter θ is following the gadient-descent method, by which the parameter is adjusted along the steepest direction of the MSE:

$$\begin{aligned} -\frac{1}{2}\text{MSE}\Big(\bigtriangledown_\theta(\theta)\Big) &= -\frac{1}{2} \bigtriangledown_\theta \left(\mathbb{E}\left[\left(V^\pi(S[k]) - V_\theta(S[k])\right)^2\right]\right) \\ &= \mathbb{E}\left[\left(V^\pi(S[k]) - V_\theta(S[k])\right) \bigtriangledown_\theta V_\theta(S[k])\right]. \end{aligned} \tag{4.21}$$

Because the value of V^π is unknown, and we do not have access to the MDP transition probabilities, it is not possible to compute this value in practice. The idea of TD learning in continuous spaces is to get around the unavailability of V^π by *bootstraping*, which intuition is to update a guess towards a guess, by approximating the target value:

$$V^\pi(S) \approx \mathbb{E}\left[R[k+1] + \gamma V_\theta(S[k+1]) \mid S[k] = S, \pi\right]. \tag{4.22}$$

As the agent does not have access to MDP transition probabilities, stochastic approximation is used: at every time step, direct sampling of equation (4.21) is performed, and the parameters are updated along the direction of:

$$\left(V^\pi(S[k]) - V_\theta(S[k])\right) \bigtriangledown_\theta V_\theta(S[k]).$$

The TD algorithm for continuous spaces, is obtained by putting these all together: at every time step k, the parameter $\theta[k]$ is updated:

$$\theta[k+1] = \theta[k] + \alpha[k]\delta[k] \bigtriangledown_\theta V_{\theta[k]}(S[k]), \tag{4.23}$$

where $\delta[k]$ is the TD-error defined by:

$$\delta[k] = R[k+1] + \gamma V_{\theta[k]}(S[k+1]) - V_{\theta[k]}(S[k]). \tag{4.24}$$

These methods have been extensively studied, e.g. [69]. An important result is the stability problem of this algorithm. Indeed, in the case of discrete state and action spaces, no function approximator is used, and the estimation of the value function is stored in a look-up table. In this case, TD is guaranteed to converge [70] under both on-policy training, *i.e.* when the agent follows the policy it tries to evaluate, and under off-policy training, *i.e.* when the agent follows a different policy that the one(s) it tries to evaluate. Off-policy learning enables a greater variety of exploration strategies by freeing the behavior policy from the evaluated policy. It also allows learning from training data generated by unrelated controllers, or learning multiple target policy.

It has been shown that the TD algorithm with function approximation, presented above, does not converge in general [71, 72]. However, it converges under standard assumptions when linear function approximator is used with on-policy training [71], in which case, if $V_\theta(S[k]) = \theta^\intercal \phi(S[k])$, equation (4.23) can be written:

$$\theta[k+1] = \theta[k] + \alpha[k]\delta[k]\phi(S[k]). \tag{4.25}$$

The TD method presented previously only uses one-step back-up to update the value function. Eligibility traces allow to look further ahead, and to assign credit to states (or state-action pairs) visited several steps earlier. The eligibility trace vector at time k is denoted by $\nu[k]$ and its update equation is:

$$\nu[k] = \lambda\gamma\nu[k-1] + \bigtriangledown_\theta V_{\theta[k]}(S[k]), \tag{4.26}$$

where $\lambda \in [0, 1]$ is the trace decay rate. The use of eligibility traces makes the recently used features more eligible for receiving credit. The update of the state value function approximator becomes:

$$\theta[k+1] = \theta[k] + \alpha[k]\delta[k]\nu[k], \tag{4.27}$$

which forms the TD(λ) algorithm. It has been shown that if linear approximator is used and on-policy training, TD(λ) algorithm converges [71]. More recently, *Maei et al.* proposed the GTD2 and TDC algorithms [73] which provide convergence guarantees when non-linear function approximators are used. These algorithms perform gradient descent on the projected Bellman error, and theoretical results guarantee convergence to a local optimum under standard assumptions.

In the next section, the energy management problem for EH-WSN is formulated using the RL framework presented in this section. Then, RLMan, an energy manager based on RL, is introduced.

4.2 Derivation of RLMan

It is assumed that time is divided into equal length time slots of duration T_s, and that the EM is executed at the beginning of every time slot. The amount of residual energy, *i.e.* the amount of energy stored in the energy storage device, is denoted by e_r and the energy storage device is assumed to have a finite capacity denoted by E_r^{max}. The hardware failure threshold, *i.e.* the minimum amount of residual energy required for the node to operate, is denoted by E_r^{fail}. It is assumed that the job of the node is to periodically send a packet at a packet generation rate denoted by $\chi_g \in [X^{min}, X^{max}]$, and that the goal of the EM is to dynamically adjust the performance of the node by setting χ_g. The goal of the EM is to maximize the packet generation rate χ_g while keeping the node sustainable, *i.e.* avoiding power failure.

In RL, it is assumed that all goals can be described by the maximization of expected cumulative reward. Formally, the problem is formulated as an MDP $\langle \mathcal{S}, \mathcal{A}, \mathcal{T}, \mathcal{R} \rangle$, detailed hereunder.

The set of states $\mathcal{S}$

The state of a node at time slot k is defined by the current residual energy e_r. Therefore, $\mathcal{S} = [E_r^{min}, E_r^{max}]$.

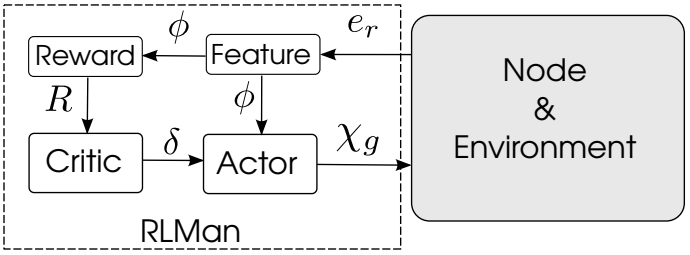

Figure 4.2 – Global architecture of RLMan.

The set of actions $\mathcal{A}$

An action corresponds to setting the packet generation rate χ_g at which packets are sent. Therefore, $\mathcal{A} = [X^{min}, X^{max}]$.

The transition function $\mathcal{T}$

The transition function gives the probability of a transition to $e_r[k+1]$ when action χ_g is performed in state $e_r[k]$.

The reward function $\mathcal{R}$

The reward is computed as a function of both χ_g and e_r:

$$R = \phi\chi_g, \tag{4.28}$$

where ϕ is the feature, which corresponds to the normalized residual energy:

$$\phi = \frac{e_r - E_r^{fail}}{E_r^{max} - E_r^{fail}}. \tag{4.29}$$

Therefore, maximizing the reward involves maximizing both the packet generation rate and the state of charge of the energy storage device. However, because the residual energy depends on the consumed energy and the harvested energy, and as these variables are stochastic, the reward function is defined by:

$$\mathcal{R}(e_r, \chi_g) = \mathbb{E}\left[R[k+1] \mid S[k] = e_r,\ A[k] = \chi_g\right]. \tag{4.30}$$

Energy management can be seen as a multiple reward functions system, in which both the normalized residual energy ϕ and the packet generation rate χ_g need to be maximized. These two rewards are combined by multiplication to form a single reward and to reduce to a single reward system. Exploring other approaches to combined the two rewards [74, 75] is considered as further work.

The EM scheme proposed in this work is an actor-critic algorithm, a class of RL techniques well-known for being capable to search for optimal policies using low variance gradient estimates [76]. This class of algorithms requires storing both a representation of the value function and the policy in memory, as opposite to other techniques such as critic-only or actor-only methods, which require only storing the value function or the policy respectively. Critic-only schemes require at each step deriving the policy from the value function, e.g. using a greedy method. However, this involves solving an optimization problem at each step, which may be computationally intensive, especially in the case of continuous action space and when the algorithm needs to be implemented on limited resource hardware, such as WSN nodes. On the other hand, actor-only methods work with a parameterized family of policies over which optimization procedure can be directly used, and a range of continuous action can be generated. However, these methods suffer from high variance, and therefore slow learning [76]. Actor-critic methods combine actor-only and critic-only methods by storing both a parameterized representation of the policy and a value function.

Figure 4.2 shows the relation between the actor and the critic. The actor updates a parameterized policy π_ψ, where ψ is the policy parameter, by gradient ascent on the objective function

J defined in (4.3). A fundamental result for computing the gradient of J is given by the *policy gradient theorem* [77]:

$$\begin{aligned}\nabla_\psi J(\pi_\psi) &= \int_{\mathcal{S}} \rho_{\pi_\psi}(e_r) \int_{\mathcal{A}} Q^{\pi_\psi}(e_r, \chi_g) \nabla_\psi \pi_\psi(\chi_g \mid e_r) d\chi_g de_r \\ &= \mathbb{E}\left[Q^{\pi_\psi}(e_r, \chi_g) \nabla_\psi \log \pi_\psi(\chi_g \mid e_r) \,\middle|\, \rho_{\pi_\psi},\ \pi_\psi \right].\end{aligned} \tag{4.31}$$

This result reduces the computation of the performance objective gradient to an expectation, and allows deriving algorithms by forming sample-based estimates of this expectation. In this work, a Gaussian policy is used to generate χ_g:

$$\pi_\psi(\chi_g \mid e_R) = \frac{1}{\sigma\sqrt{2\pi}} \exp\left(-\frac{(\chi_g - \mu)^2}{2\sigma^2} \right), \tag{4.32}$$

where σ is fixed and controls the amount of exploration, and μ is linear with the feature:

$$\mu = \psi\phi. \tag{4.33}$$

Defining μ as a linear function of the feature enables minimal memory footprint as only one floating value, ψ, needs to be stored. Moreover, the computational overhead is also minimal as $\nabla_\psi \mu = \phi$, leading to:

$$\nabla_\psi \log \pi_\psi(\chi_g \mid e_r) = \frac{(\chi_g - \mu)}{\sigma^2}\phi. \tag{4.34}$$

It is important to notice that other ways of computing μ from the feature can be used, e.g. artificial neural networks, in which case ψ is a vector of parameters, e.g. the weight of the neural network. However, these approaches incur higher memory usage and computational overhead, and might thus not be suited for WSN nodes.

Using the policy gradient theorem as formulated in (4.31) may lead to high variance and slow convergence [76]. A way to reduce the variance is to rewrite the policy gradient theorem using the *advantage function* $A^{\pi_\psi}(e_r, \chi_g) = Q^{\pi_\psi} - V^{\pi_\psi}$. Indeed, it can be shown that [77]:

$$\nabla_\psi J(\pi_\psi) = \mathbb{E}\left[A^{\pi_\psi}(e_r, \chi_g) \nabla_\psi \log \pi_\psi(\chi_g \mid e_r) \,\middle|\, \rho_{\pi_\psi},\ \pi_\psi \right]. \tag{4.35}$$

This can reduce the variance, without changing the expectation. Moreover, the TD-error, defined by:

$$\delta = R[k+1] + \gamma V^{\pi_\psi}(e_r[k+1]) - V^{\pi_\psi}(e_r[k]), \tag{4.36}$$

is an unbiased estimate of the advantage function, and therefore can be used to compute the policy gradient [76]:

$$\nabla_\psi J(\pi_\psi) = \mathbb{E}\left[\delta \nabla_\psi \log \pi_\psi(\chi_g \mid e_r) \,\middle|\, \rho_{\pi_\psi},\ \pi_\psi \right]. \tag{4.37}$$

The TD error can be intuitively interpreted as a critic of the previously taken action. Indeed, a positive TD error suggests that this action should be selected more often, while a negative TD error suggests the opposite. The critic computes the TD error (4.36), and, to do so, requires the knowledge of the value function V^{π_ψ}. As the state space is continuous, storing the value function for each state is not possible, and therefore function approximation is used to estimate the value function. Similarly to what was done for μ (4.33), linear function approximation was chosen to estimate the value function, as it requires very few computational overhead and memory:

$$V_\theta(e_r) = \theta\phi, \tag{4.38}$$

where ϕ is the feature (4.29), and θ is the approximator parameter. The critic, which estimates the value function by updating the parameter θ, is implemented using the well-known TD(λ) algorithm [70] introduced in the previous section:

$$\nu[k] = \gamma\lambda\nu[k-1] + \phi[k] \tag{4.39}$$

$$\theta[k] = \theta[k-1] + \alpha\delta[k]\nu[k] \tag{4.40}$$

Algorithm 3 Reinforcement learning based energy manager.

Input: $e_r[k]$, $R[k]$

1: $\phi[k] = \frac{e_r[k]-E_r^{fail}}{E_r^{max}-E_r^{fail}}$ ▷ Feature (4.29)

2: $\delta[k] = R[k] + \gamma\theta[k-1]\phi[k] - \theta[k-1]\phi[k-1]$ ▷ TD Error (4.36), (4.38)

3: ▷ Critic: update the value function estimate (4.39), (4.40):

4: $\nu[k] = \gamma\lambda\nu[k-1] + \phi[k]$

5: $\theta[k] = \theta[k-1] + \alpha\delta[k]\nu[k]$

6: ▷ Actor: updating the policy (4.33), (4.34), (4.37):

7: $\psi[k] = \psi[k-1] + \beta\delta[k]\frac{(f[k-1]-\psi[k-1]\phi[k-1])}{\sigma^2}\phi[k-1]$

8: Clamp μ_t to $[X^{min}, X^{max}]$

9: ▷ Generating a new action:

10: $\chi_g[k] \sim \mathcal{N}(\psi[k]\phi[k], \sigma)$

11: Clamp $\chi_g[k]$ to $[X^{min}, X^{max}]$

12: **return** $\chi_g[k]$

where $\alpha \in [0, 1]$ is a step-size parameter.

Algorithm 3 shows the proposed EM scheme. It can be seen that the algorithm has low memory footprint and incurs low computational overhead, and therefore is suitable for execution on WSN nodes. At each run, the algorithm is fed with the current residual energy $e_r[k]$ and the reward $R[k]$ computed using (4.28). First, the feature and the TD-error are computed (lines 1 and 2), and then the critic is updated using the TD(λ) algorithm (lines 4 and 5). Next, the actor is updated using the policy gradient theorem at line 7, where $\beta \in [0, 1]$ is a step-size parameter. The expectancy of the Gaussian policy is clamped to the range of allowed values at line 8. Finally, a frequency is generated using the Gaussian policy at line 10, which will be used in the current time slot. As the Gaussian distribution is unbounded, it is required to clamp the generated value to the allowed range (line 11).

4.3 Evaluation of RLMan

RLMan was evaluated and compared to three state of the art EMs using exhaustive simulations. The energy storage device was a supercapacitor with a maximum voltage of 5.2 V and a failure voltage of 2.8V. The task of the node consists of acquiring data by sensing, performing computation and then sending the data to a sink. However, in practice, the amount of energy consumed by one execution of this task varies, e.g. due to multiple retransmissions. Therefore, the amount of energy required to run one execution was simulated by a random variable which follows a beta distribution, with the mode of the distribution set to the energy consumed if only one transmission attempt is required, denoted by E_c^{typ}, and the maximum set to the energy consumed if five transmission attempts are necessary, denoted by E_c^{max}. Table 4.1 shows the values of E_c^{typ} and E_c^{max}, as well as the parameter values used when implementing the EMs. The rest of this section is organized as follows. First, preliminary results detail the behavior of the learning phase of the proposed algorithm, focusing on the first few days. Next, the comparison results of the proposed EM with three state of the art schemes are exposed.

4.3.1 Energy traces used for simulation

Indoor ambient light and wind were considered to evaluate the EMs as (i) they present very different behavior, as it can be seen in Figure 4.3, (ii) they correspond to many real applications and (iii) long energy traces from measurement campaigns are available, as opposite to other energy sources such as thermal energy and vibration/motion.

Regarding wind energy, an energy trace lasting 180 days from the National Renewable Energy Laboratory (NREL) available online [79] was used. However, the provided data are wind speed, in

All	E_c^{typ}	8.672 mJ
	E_c^{max}	36.0 mJ
	X^{min}	$\frac{1}{300}$ Hz
	X^{max}	5 Hz
	T_s	60 s
RLMan	α	0.1
	β	0.01
	σ	0.1
	γ	0.9
	λ	0.9
P-FREEN [55]	B_{OFL}	$0.95E_r^{max}$
	η	1.0
Fuzzyman	K	1.0
	η	1.0
	E_b^{eds}	$F^{min}T_sE_c^{typ}$
	E_b^{min}	$F^{min}T_sE_c^{typ}$
	E_h^{strong}	$F^{max}T_sE_c^{typ}$
	E_h^{weak}	$F^{min}T_sE_c^{typ}$
LQ-Tracker [19]	μ	0.001
	B*	$0.70E_r^{max}$
	α	0.5
	β	1.0

Table 4.1 – Parameter values used for simulations. For details about the parameters of P-FREEN, Fuzzyman and LQ-Tracker, the reader can refer to the respective literature.

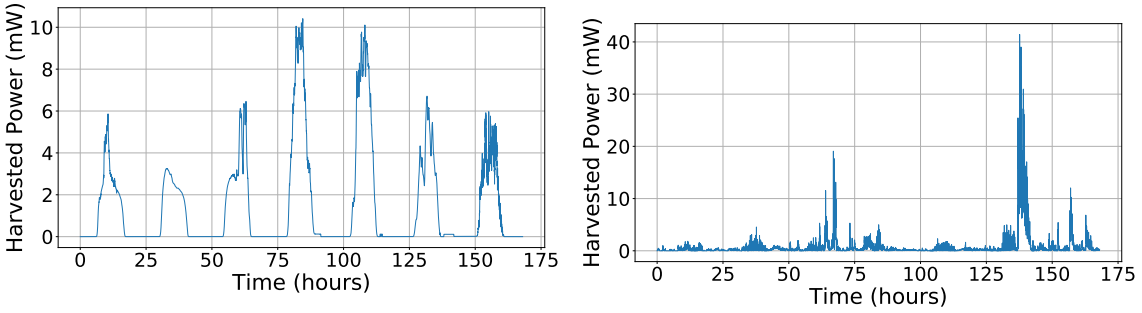

(a) Typical indoor ambient light power trace (from EnHANTs [78]).

(b) Typical wind power trace (from NREL [79]).

Figure 4.3 – Example of indoor ambient light power trace and wind power trace.

m/s, from which the corresponding extracted power by a turbine must be computed. Given the wind speed v, the power available from the wind kinetic energy is:

$$P_{wind} = \frac{1}{2}\rho A v^3, \tag{4.41}$$

where ρ is the air density (typically 1.25 kg/m^3) and A is the swept area of the turbine. The power actually harvested from the wind P_h is a fraction of P_{wind}:

$$P_h = C_P P_{wind}, \tag{4.42}$$

where C_P is the performance coefficient of the turbine. Albert Betz demonstrated in 1919 that no turbine can convert more than $\frac{19}{27}$ ($\approx 59.3\%$) of the kinetic energy of the wind into mechanical energy turning the rotor [80]. This is known as the Betz Limit, which provides a theoretical maximum power efficiency of any design of wind turbine:

$$C_P \leqslant \frac{19}{27}. \tag{4.43}$$

Wind turbine cannot operate at this maximum limit, and real-world turbine has limit below the Betz Limit. Small turbine used in EH-WSNs, with typical blades of 5 cm diameter, achieve efficiency less than 10% [80]. In this thesis, for simulations, blades of 5 cm diameter and efficiency of 10% were considered, which matches typical values [80]. However, these values lead to unreasonably

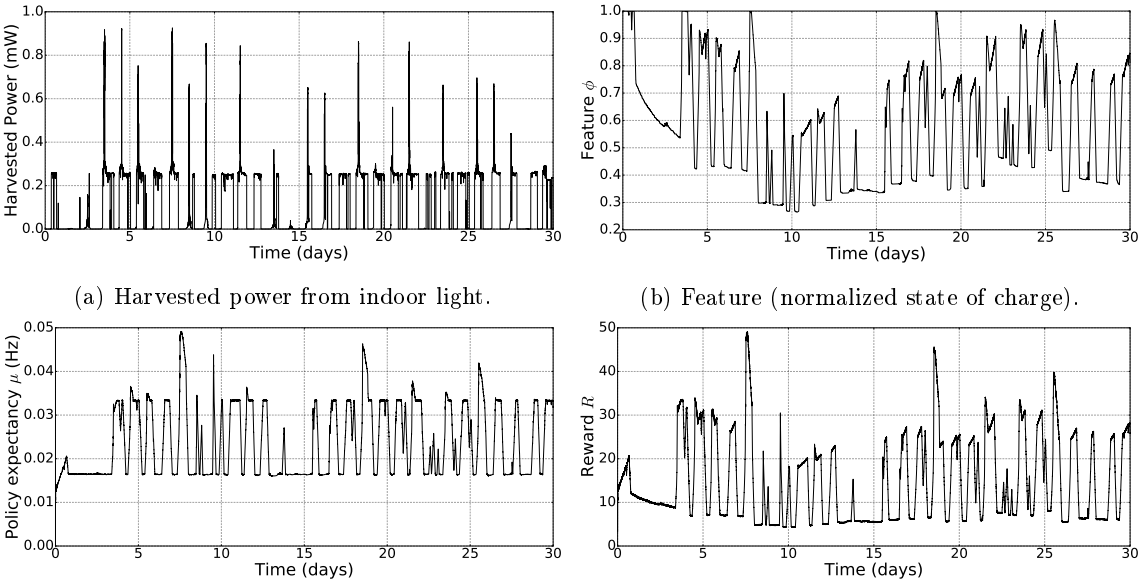

(a) Harvested power from indoor light.

(b) Feature (normalized state of charge).

(c) Gaussian policy expectation.

(d) Reward.

Figure 4.4 – Behavior of the EM scheme the first 30 days.

large amount of harvested energy, that will not be achieved in practice. Therefore, in order to keep the dynamic of wind sources while having consistent harvested energy values, a scaling factor of 10^{-2} was applied to these measurements. The trace shown in Figure 4.3b was generated using these settings.

Regarding indoor ambient light, the traces were obtained from the EnHANTs measurement campaign [47], during which continuous long-time measurements (up to a year) were performed in different locations of an office building. The provided data are irradiance measurements (in $\mathrm{W/m^2}$), and the harvested power is given by:

$$P_h = \eta I A, \tag{4.44}$$

where η is the photovoltaic cell efficiency, I is the irradiance and A is the cell area. To perform simulations, the cell area was set to 30 $\mathrm{cm^2}$, and the efficiency to 15%, which is realistic regarding current photovoltaic technologies [64]. The trace shown in Figure 4.3a was generated using these values.

4.3.2 Behavior of RLMan

Figure 4.4 shows the behavior of the proposed EM during the first 30 days of simulation using the indoor light energy trace. The capacitance of the energy storage device was set to 0.5 F. Figure 4.4a shows the harvested power, and Figure 4.4b shows the feature (ϕ), corresponding to the normalized residual energy. Figure 4.4c exposes the expectancy of the Gaussian distribution used to generate the packet generation rate (χ_g), and Figure 4.4d shows the reward (R), computed using (4.28). It can be seen that the first day the energy storage device was saturated (Figure 4.4b), as the average packet generation rate was progressively increasing (Figure 4.4c), leading to higher rewards (Figure 4.4d). As during the second and third days the amount of harvested energy was low, the residual energy dropped, causing a decrease of the rewards while the policy expectancy was stable. Starting the fourth day, energy was harvested again, enabling the node to increase its activity, as it can be seen on Figure 4.4c. Finally, it can be noticed that if a lot of energy was wasted by saturation of the energy storage device the first 5 days, this is no longer true once this period of learning is over.

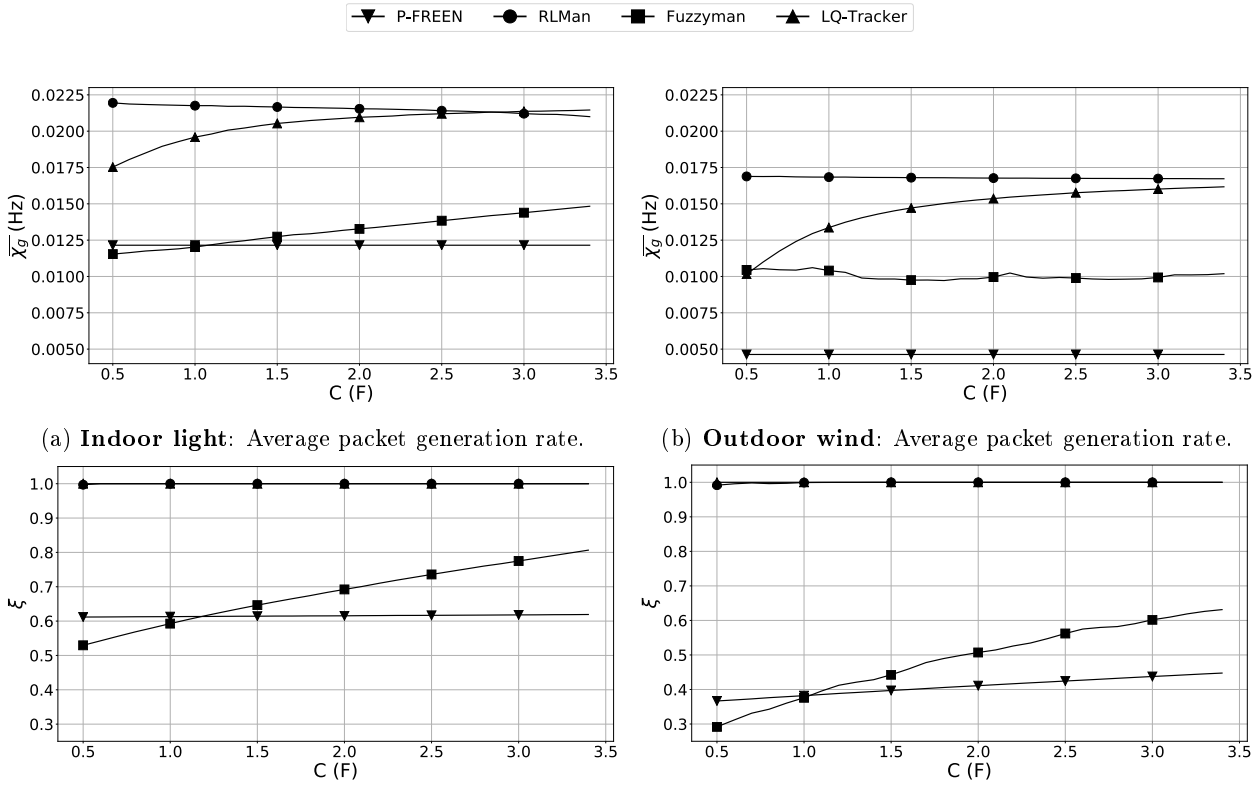

(a) **Indoor light**: Average packet generation rate.

(b) **Outdoor wind**: Average packet generation rate.

(c) **Indoor light**: Energy efficiency.

(d) **Outdoor wind**: Energy efficiency.

Figure 4.5 – Average packet generation rate and energy efficiency for different capacitance values, in the case of indoor light and outdoor wind.

4.3.3 Comparison to State of the Art Schemes

RLMan was compared to P-FREEN, Fuzzyman, and LQ-Tracker, three state of the art EM schemes that aim to maximize the packet generation rate. P-FREEN and Fuzzyman require the tracking of the harvested energy in addition to the residual energy, and were therefore executed with perfect knowledge of this value. RLMan and LQ-Tracker were only fed with the value of the residual energy. Both the indoor light and the wind energy traces were considered. The EMs were evaluated for different values of capacitances, ranging from 0.5 F to 3.5 F, as it strongly impacts the behavior of the EMs, but also both the cost and form factor of WSN nodes. In addition to the average packet generation rate, the energy efficiency denoted by ξ and introduced in Chapter 1 is also evaluated. ξ is defined as follows:

$$\xi = 1.0 - \frac{\sum_k e_w[k]}{\sum_k e_h[k] + e_r[0]}. \tag{4.45}$$

Each data point is the average of the results of ten simulations, each performed using different seeds for the random number generators.

All the EMs successfully avoid power failure when powered by indoor light or outdoor wind. Figure 4.5 exposes the comparison results. As it can be seen on Fig 4.5c and Figure 4.5d, both RLMan and LQ-Tracker achieve more than 99.9 % efficiency, for indoor light and outdoor wind, for all capacitance values, and despite the fact that they require only the residual energy as an input. In addition, when the node is powered by outdoor wind, RLMan always outperforms the other EMs in terms of average packet generation rate for all capacitance values, as shown in Figure 4.5b. When the node is powered by indoor light, RLMan also outperforms all the other EMs, except LQ-Tracker when the values of the capacitance are higher than 2.8 F. The advantage of RLMan over the other EMs is more significant for small values of the capacitance. Especially, the average packet generation rate is more than 20 % higher compared to LQ-Tracker in the case of indoor light, and almost 70 % higher in the case of outdoor wind, when the capacitance value is set to

0.5 F. This is encouraging as using small capacitance leads to lower cost and lower form factor.

Regarding Fuzzyman, results similar to the ones obtained in the previous chapter were expected, at least for a capacitance value of 0.9 F, as it was the one used previously. However, these results show that Fuzzyman does not behave on real traces as well as on the generated traces used in the previous chapter. Indeed, in this evaluation, the Fuzzyman parameters were set to the same values as in the previous chapter because (i) it allows fair comparison regarding to the previously presented results and (ii) the energy sources are in the same range as the generated traces. A better tuning may lead to higher efficiencies. These results highlight one of the drawback of Fuzzyman: it requires fine tuning to achieve high efficiency, as opposite to RLMan which can adapt to different sources with almost no tuning.

4.4 Conclusion

In this chapter, the problem of maximizing the quality of service in energy harvesting node is formulated using RL theory, and a novel EM scheme, named RLMan, is presented. RLMan requires only the state of charge of the energy storage device as an input, and uses function approximation to minimize the memory footprint and the computational overhead, which makes it practical to implement and suitable for WSN nodes. Exhaustive simulations showed the benefits enabled by RLMan in terms of packet generation rate and energy efficiency compared to three state of the art energy managers, in the case of both indoor light energy harvesting and outdoor wind energy harvesting. The advantage of RLMan is more significant when small energy storage devices are used.

As further work, it is intended to investigate other rewarding systems. Indeed, instead of reducing a multi-reward problem into a single-reward problem at is was done in this work, using multi-objective reinforcement learning approaches [74, 75] may lead to better results.

Also, increasing the number of inputs may also lead to better results as more information will be given to the controller. For example, in addition to the residual energy e_r, the residual energy variation $\Delta e_r[k] = e_r[k] - e_r[k-1]$ could also be considered as an input of the controller. This will however increase the complexity of the function approximators, and exploring approaches such as tile coding [81] seems promising. To reduce the memory footprint of such approximators, hash table could be used.

The next part of this dissertation is dedicated to Wake-up Receivers (WuRx) in WSNs. As communication is typically one of the most energy consuming task in WSNs, achieving energy efficient communications is important, and WuRx form a promising lead to tackle this challenge. Indeed, WuRx enable low power listening of the channel, as well as asynchronous communications, which is especially important in EH-WSNs as dynamic adaptation of the packet generation rate can lead to inefficient communications if the MAC layer require time synchronization.

Part II

MAC Protocols Leveraging Wake-up Receivers

Chapter 5

A Generic Framework for Modeling MAC Protocols

Great efforts are made to design network protocols that fulfill the requirements of WSNs, especially regarding the MAC layer [12]. The aim of the MAC layer is to provide mechanisms to allow several wireless nodes to share the wireless channel medium and access the network. The MAC layer fundamental tasks are to avoid collisions and to provide fair medium allocation among the nodes. Moreover, as the MAC layer controls the transceiver, it plays an important role in the energy efficiency of communication, and in the trade-off between power consumption and latency [82]. Because WSNs have many different applications with different requirements, and as the choice of an appropriate protocol strongly depends on the application requirements, the amount of proposed MAC protocols is large and multiple MAC protocols categories were defined over the last decade [12]. As a consequence, it is difficult to choose and tune the most appropriate MAC protocol given a specific application context or to compare new MAC schemes to state of the art, especially because of the lack of generic analytical models. Indeed, analytical models are required to investigate the performance of different schemes, to characterize their fundamental limitations and to optimize their parameters.

In this chapter, a generic framework for modeling MAC protocols is presented [83, 84]. The proposed framework is based on AMCs [85] and focuses on energy consumption, latency and reliability. Markov Chain (MC)s have already proved to be useful for modeling communications protocols, especially to study specific MAC protocols [86] and cross-layer designs [87]. The purpose of this generic framework is to permit the modeling of a wide range of MAC layer schemes to explore their parameters space and to compare them. To illustrate how to apply the proposed framework to model a specific MAC protocol, the state of the art PW-MAC [20] protocol, which is an improvement of RI-MAC [88], is modeled using the proposed framework, and the different modeling steps are explained. PW-MAC focuses on low energy consumption for both the receiver and the sender. Moreover, experimental measurements using real hardware were performed to set the model parameters using realistic and accurate energy consumption and latencies values and to validate the framework.

The rest of this chapter is organized as follows. Section 5.1 exposes previous works that aim to model MAC protocols for WSNs. In Section 5.2, the generic framework is presented. Finally, Section 5.3 exposes the modeling of PW-MAC using the framework and the experimental validation of the model.

5.1 Previous Works Related to Modeling MAC Protocols

The most widespread communication scheme for WSNs is the standard IEEE 802.15.4, which defines both a physical layer and a MAC protocol. Consequently, many dedicated models were proposed for characterizing and evaluating this scheme [89–93]. In [89], the authors evaluated the energy efficiency of the IEEE 802.15.4 MAC layer in dense networks, and concluded that this standard can be used to support communication in dense data-gathering networks. *Ramachandran et al.* [90] evaluated the throughput and energy consumption of the contention access period of

the IEEE 802.15.4 MAC layer by modeling it as a non-persistent Carrier Sense Multiple Access (CSMA) with backoff, and showed that shutting down the radio between transmissions improves the energy efficiency of the MAC layer in some applications. In [91], the IEEE 802.15.4 MAC protocol was modeled using MCs, assuming perfect channel conditions, to capture the performance of the scheme in terms of throughput and energy consumption, and in the case of saturated and unsaturated networks. Similarly, *Park et al.* [92] modeled the reliability, delay and energy consumption of the IEEE 802.15.4 MAC layer using MCs, and analyzed the impact of the MAC parameters on the performance metrics analyzed. More recently, *Vilajosana et al.* [93] proposed an energy consumption model for the time-slotted channel hopping scheme, which is at the heart of the IEEE 802.15.4e-2012 amendment of the IEEE 802.15.4-2011 standard. Experimental validation on real devices was done, and the model was applied to different network scenarios, to understand the potential effects of several network optimizations.

These previous works focus on modeling the IEEE 802.15.4 standard, and therefore do not aim to provide generic analytical frameworks. To the best of our knowledge, only a few generic models were proposed in the literature. *Vuran et al.* [94] proposed a theoretical framework to exploit spatial correlation of observed events between sensor nodes on the MAC layer to reduce unnecessary data transmissions. In [95], the authors analyzed the duty-cycle, energy efficiency and latency of a handful of MAC protocols in the context of low data rate WSNs regarding various network parameters such as the network density and the transceiver. If the proposed traffic and radio models are generic, the latency and energy models are specific to each MAC, making the proposed approach hard to extend to new protocols. *Asudeh et al.* [96] proposed a selection framework to choose the appropriate protocol that satisfies the requirements for a given context defined by a set of input parameters. Three categories of protocols (preamble sampling, common active period and scheduled) are defined and it is assumed that protocols in the same category have similar performance characteristics. The authors defined a combined performance function that relates different metrics (delay, energy consumption...) into a single scalar measure by scaling appropriately each metric. The aim of this performance function is to quantify the performance of each protocol to choose the most appropriate one regarding particular context and application requirements. However, the purpose of our work is not to provide a selection algorithm, but an analytical framework to evaluate different MAC schemes.

The generic framework proposed in this work can be used to model a wide range of MAC protocols and focuses on energy consumption, latency and reliability. It is based on AMCs, and using experimental measurements, we have proved that the model provides accurate estimations in the context of low throughput applications, typical for WSNs [97].

5.2 Modeling MAC Protocols using Absorbing Markov Chains

The proposed analytical framework for modeling the energy consumption, the latency and the reliability of MAC protocols is introduced in this section. For a given protocol, a MC describing the functioning of the protocol is established. The typical modeling of a MAC protocol by a MC is illustrated in Figure 5.1a. The "standby state" (STDBY) is defined as the state of the MAC when it is neither receiving nor transmitting a packet. The reception of a packet is usually preceded by a step such as the periodic check for incoming packets in preamble sampling protocols, or the asynchronous reception of a WuC when using WuRx. This step is called a *receive wake-up* and can lead to the reception of a packet. It corresponds to the R-WUP state in Figure 5.1a. We call *transmission process* the procedure defined by the protocol to transmit a packet, and *reception process* the procedure defined by the protocol to receive a packet. Each of these processes consists of one or more basic steps, e.g. the transmission of a beacon, the transmission of a data frame, the reception of an ACK. Some steps can possibly succeed or fail, e.g. the reception of an ACK may fail because of interference. When transmitting a packet, more than one attempt are typically allowed, and the number of allowed attempts is denoted by $N_A \in \mathbb{N}^*$. The failing of an attempt leads either to the starting of a new attempt, or to the failing of the transmission process if it was the last authorized attempt. The success of an attempt leads to the success of the transmission process.

In the proposed approach, the transmission and reception processes are individually modeled by

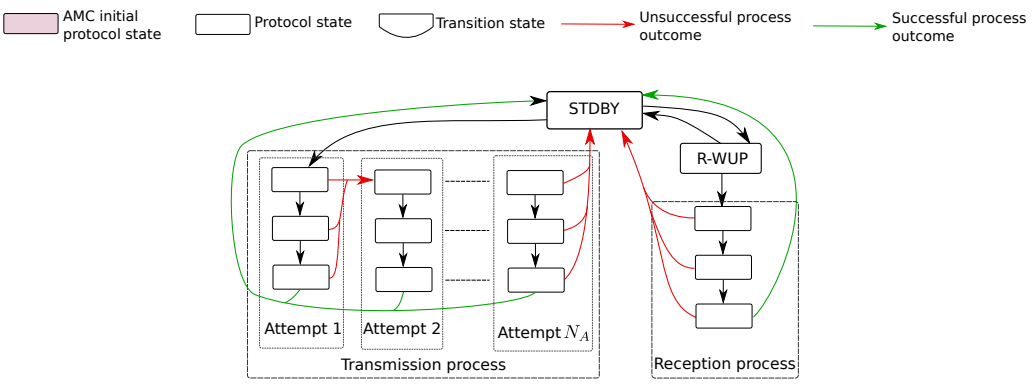

(a) Markov chain of the entire protocol.

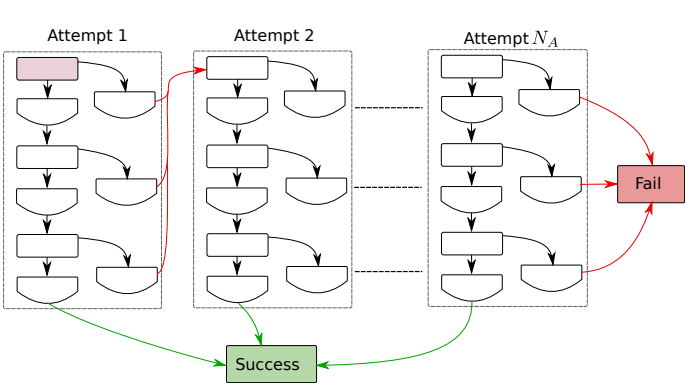

(b) AMC of the transmission process.

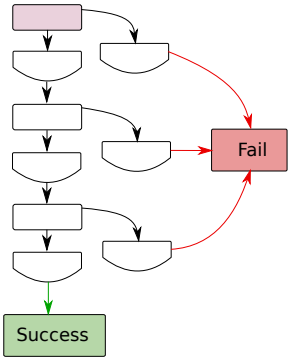

(c) AMC of the reception process.

Figure 5.1 – Markov chain models. States names of the transmission and reception processes are not indicated for clarity reason, as they are specific to each protocol.

two AMCs. These AMCs are constructed by extracting for each process the corresponding sub-MC of the MC modeling the entire protocol, and by defining two absorbing states, *i.e.* states which are impossible to leave, denoted "Success" and "Fail" and representing the two possible outcomes of the process. The AMC is termed to be "absorbed" by an absorbing state when it steps into an absorbing state. A success of the process leads to the absorption of the chain by the "Success" state and a failure of the process leads to the absorption of the chain by the "Fail" state. The modelings of the transmission and reception processes by AMCs are illustrated in Figure 5.1b and Figure 5.1c respectively. Three typologies of states are defined to build an AMC: *protocol states*, *transition states* and *final states*. Protocol states are defined by the protocol itself, and represent the steps that constitute the processes. However, to correctly evaluate the energy consumption and latency incurred by the protocol, transition states, which do not affect the behavior of the protocol, are needed to model the energy and latency cost of state transitions. The final states are the "Success" and "Fail" states that represent the possible outcomes of a packet transmission or reception process. All the states except the final ones are transient, *i.e.* can be left. In the rest of this chapter, mathematical objects (AMC, matrix, vector or scalar) associated to the packet transmission process are denoted with a "t" subscript, while mathematical objects associated to the packet reception process are denoted with a "r" subscript. When referring indifferently to both processes, the "$\bullet$" subscript is used.

Let $C_{\bullet}$ be an AMC modeling a packet transmission or reception process, and $\mathbf{P}_{\bullet}$ be its associ-

ated transition matrix defined by:

$$\mathbf{P_\bullet} = \begin{array}{c} \\ s_1 \\ \vdots \\ s_{M_\bullet} \\ \mathfrak{s} \\ \mathfrak{f} \end{array} \begin{array}{c} \begin{array}{cccccc} s_1 & \cdots & s_{M_\bullet} & \mathfrak{s} & \mathfrak{f} \end{array} \\ \begin{pmatrix} p_{1,1} & \cdots & p_{1,M_\bullet} & p_{1,\mathfrak{s}} & p_{1,\mathfrak{f}} \\ \vdots & \vdots & \vdots & \vdots & \vdots \\ p_{M_\bullet,1} & \cdots & p_{M_\bullet,M_\bullet} & p_{M_\bullet,\mathfrak{s}} & p_{M_\bullet,\mathfrak{f}} \\ 0 & \cdots & 0 & 1 & 0 \\ 0 & \cdots & 0 & 0 & 1 \end{pmatrix} \end{array}, \tag{5.1}$$

where $M_\bullet$ is the number of transient states $s_i, i \in \{1, \ldots, M_\bullet\}$, $\mathfrak{s}$ is the final "Success" state, $\mathfrak{f}$ is the final "Fail" state, $p_{i,j} \in [0,1]$ is the transition probability from the transient state s_i to the transient state s_j, $p_{i,\mathfrak{s}}$ is the transition probability from the transient state s_i to the final state $\mathfrak{s}$ and $p_{i,\mathfrak{f}}$ is the transition probability from the transient state s_i to the final state $\mathfrak{f}$. As $\mathfrak{s}$ and $\mathfrak{f}$ are absorbing states, the transition probabilities $p_{\mathfrak{s},\mathfrak{s}}$ and $p_{\mathfrak{f},\mathfrak{f}}$ take the value 1.

Applying classical AMC results, $\mathbf{P_\bullet}$ can be written without loss of generality as follows [85]:

$$\mathbf{P_\bullet} = \begin{pmatrix} \mathbf{Q_\bullet} & \mathbf{R_\bullet} \\ \mathbf{0_{2\times M_\bullet}} & \mathbf{I_2} \end{pmatrix}, \tag{5.2}$$

where $\mathbf{Q_\bullet}$ is a $M_\bullet-$by$-M_\bullet$ matrix, $\mathbf{R_\bullet}$ is a $M_\bullet-$by-2 matrix, $\mathbf{I_2}$ is the identity matrix of size 2 and $\mathbf{0_{2\times M_\bullet}}$ is the $2-$by$-M_\bullet$ null matrix. The *fundamental matrix* of $C_\bullet$ is [85]:

$$\mathbf{N_\bullet} = (\mathbf{I_{M_\bullet}} - \mathbf{Q_\bullet})^{-1}. \tag{5.3}$$

The $ij-$entry of $\mathbf{N_\bullet}$, denoted by $n_{i,j}$, is the expected number of times the chain was in the transient state s_j if it started in the transient state s_i before being absorbed. It is assumed without loss of generality that the initial state of $C_\bullet$ is s_{i_0} with $i_0 \in \{1, \ldots, M_\bullet\}$, *i.e.* s_{i_0} is the initial state of the transmission or reception process. Thus, only the i_0^{th} row of the $\mathbf{N_\bullet}$ matrix is considered, and the vector of size $M_\bullet$ corresponding to this row is denoted by $\mathbf{n_\bullet}$.

5.2.1 Probability of a Successful Packet Transmission or Reception

To evaluate the reliability of a protocol, the probability that a packet transmission or reception succeeds, *i.e.* that $C_\bullet$ is absorbed by the final state $\mathfrak{s}$, is considered. The *absorption probability matrix* denoted by $\mathbf{B_\bullet}$ is a $M_\bullet-$by-2 matrix in which the $ij-$entry, denoted by $b_{i,j}$, is the probability that the matrix will be absorbed by the j^{th} absorbing state, which is either $\mathfrak{s}$ or $\mathfrak{f}$, if it starts in the i^{th} transient state s_i, and can be computed as follows [85]:

$$\mathbf{B_\bullet} = \mathbf{N_\bullet}\mathbf{R_\bullet}. \tag{5.4}$$

As the initial state is s_{i_0}, only the i_0^{th} row is considered and the vector of size 2 corresponding to this row is denoted by $\mathbf{b_\bullet}$. We denote by $b_{\bullet,\mathfrak{s}}$ the entry of this vector corresponding to the probability that the chain $C_\bullet$ is absorbed by the final state $\mathfrak{s}$, *i.e.* that the process successfully terminates. $b_{\bullet,\mathfrak{s}}$ is given by:

$$b_{\bullet,\mathfrak{s}} = \sum_{j=1}^{M_\bullet} n_{i_0,j} p_{j,\mathfrak{s}}. \tag{5.5}$$

5.2.2 Energy Cost of a Packet Transmission/Reception Process

Let $\mathbf{c_\bullet}$ be the *energy cost vector*, *i.e.* the vector of size $M_\bullet$ in which the i^{th} entry is the energy cost incurred by the MAC protocol when traversing the transient state s_i. Hence, the average energy cost of a packet transmission or reception modeled by $C_\bullet$ is the scalar product of $\mathbf{n_\bullet}$ and $\mathbf{c_\bullet}$:

$$\bar{c_\bullet} = \mathbf{n_\bullet} \cdot \mathbf{c_\bullet}. \tag{5.6}$$

In (5.6), $\mathbf{n_\bullet}$ is related to the protocol, while $\mathbf{c_\bullet}$ is related to application and hardware specifics, *i.e.* transmission or reception time of frames and transceiver power consumption.

5.2.3 Average Number of Transmission Attempts

Let $\mathbf{a}$ be the vector of size M_t in which the i^{th} entry takes the value 1 if s_i corresponds to the initial state of an attempt in the AMC modeling the transmission process, 0 otherwise. Then, the expected number of transmission attempts denoted by $\bar{a}$, without considering the outcome of the transmission process, is given by:

$$\bar{a} = \mathbf{n_t} \cdot \mathbf{a}. \tag{5.7}$$

5.2.4 Latency of a Packet Transmission Process

We define the *latency costs vector* denoted by $\mathbf{l_.}$ as the vector of size $M_\mathbf{.}$ in which the i^{th} entry is the latency incurred by the MAC protocol when traversing the transient state s_i. The same reasoning as in (5.6) can not be applied for computing the packet transmission latency, as the scalar product of $\mathbf{n_t}$ and $\mathbf{l_t}$ gives the average duration of a packet transmission process without regard to its outcome. However, when the latency is evaluated, we are interested in the packet transmission duration when the transmission process succeeds. Therefore, the *conditional fundamental matrix* denoted by $\mathbf{N_{|a,t}}$ is introduced as the matrix in which the $ij-$entry, denoted by $n_{|a,i,j}$, is the expected number of times the chain was in the transient state s_j if it started in the transient state s_i and knowing that the chain was absorbed by the state $a \in \{\mathfrak{s}, \mathfrak{f}\}$. Moreover, it can be proved that:

$$n_{|a,i,j} = \frac{b_{j,a}}{b_{i,a}} n_{i,j}. \tag{5.8}$$

Proof. Let $X_{i,j}^{(m)}$ be the random variable that takes the value 1 if the chain is at the transient state s_j at the step m if it started at the transient state s_i, and 0 otherwise. Then:

$$\Pr\left(X_{i,j}^{(m)} = 1\right) = q_{i,j}^{(m)}, \tag{5.9}$$

where $q_{i,j}^{(m)}$ is the $ij-$entry of the matrix $\mathbf{Q_t}$ raised to the power m denoted by $\mathbf{Q_t^m}$. Let A_i be the random variable corresponding to the state, which will absorb the chain if it started at the transient state s_i. According to Bayes' theorem:

$$\Pr\left(X_{i,j}^{(m)} = 1 | A_i = a\right) = \frac{\Pr\left(A_i = a | X_{i,j}^{(m)} = 1\right) \Pr\left(X_{i,j}^{(m)} = 1\right)}{\Pr\left(A_i = a\right)}. \tag{5.10}$$

Because of the Markov property:

$$\Pr\left(A_i = a | X_{i,j}^{(m)} = 1\right) = \Pr\left(A_j = a\right), \tag{5.11}$$

hence, we have:

$$\Pr\left(X_{i,j}^{(m)} = 1 | A_i = a\right) = \frac{\Pr\left(A_j = a\right)}{\Pr\left(A_i = a\right)} \Pr\left(X_{i,j}^{(m)} = 1\right) = \frac{b_{j,a}}{b_{i,a}} q_{i,j}^{(m)}, \tag{5.12}$$

using the notation of the absorption probabilities matrix $\mathbf{B_.}$. The expected number of times the chain was in the transient state s_j in the first m steps given that it started in the transient state s_i and that it was absorbed by the state a is:

$$\mathbb{E}\left(X_{i,j}^{(0)} + \cdots + X_{i,j}^{(m)} | A_i = a\right) = \frac{b_{j,a}}{b_{i,a}} \left(q_{i,j}^{(0)} + \cdots + q_{i,j}^{(m)}\right), \tag{5.13}$$

because of the linearity of the expectancy. Hence, when m goes to infinity:

$$n_{|a,i,j} = \lim_{m \to +\infty} \mathbb{E}\left(X_{i,j}^{(0)} + \cdots + X_{i,j}^{(m)} | A_i = a\right) = \lim_{m \to +\infty} \frac{b_{j,a}}{b_{i,a}} \left(q_{i,j}^{(0)} + \cdots + q_{i,j}^{(m)}\right) = \frac{b_{j,a}}{b_{i,a}} n_{i,j}. \tag{5.14}$$

where the last equality holds because [85]:

$$\mathbf{N} = \sum_{k=0}^{\infty} \mathbf{Q_.}^k, \tag{5.15}$$

where $\mathbf{Q_.}^0 = \mathbf{I_{M_.}}$. □

The conditional fundamental matrix $\mathbf{N}_{|\mathbf{s},\mathbf{t}}$ is such that the $ij-$entry is the expected number of times the chain was in the transient state s_j if it started in the transient state s_i knowing that the packet transmission succeeds. As the initial state is assumed to be s_{i_0}, only the vector corresponding to the i_0^{th} row and denoted by $\mathbf{n}_{|\mathbf{s},\mathbf{t}}$ is considered. Hence, the expected latency incurred by the transmission of a packet is:

$$\bar{l_t} = \mathbf{n}_{|\mathbf{s},\mathbf{t}} \cdot \mathbf{l_t}, \tag{5.16}$$

where $\mathbf{l_t}$ is the latency cost vector of the transmission process.

5.2.5 Average Power Consumption

Knowing the expected energy costs of a packet transmission and a packet reception, respectively denoted by $\bar{c_t}$ and $\bar{c_r}$ and computed using (5.6), the average power consumption, denoted by $\overline{P_C}$, incurred by communications can be computed as follows:

$$\overline{P_C} = \bar{a}\chi_r\bar{c_r} + (\chi_g + b_{t,\mathfrak{s}}\chi_r)\,\bar{c_t} + \chi_u e_u + \Big(1 - \bar{a}\chi_r\,(\mathbf{n_r}\cdot\mathbf{l_r}) - (\chi_g + b_{t,\mathfrak{s}}\chi_r)\,(\mathbf{n_t}\cdot\mathbf{l_t}) - \chi_u l_u\Big)P_{SBY}, \tag{5.17}$$

assuming that a node forwards all packets that are successfully received. In (5.17), χ_r and χ_g are respectively the average packet reception and local packet generation rate. $b_{t,\mathfrak{s}}$ is the probability that a packet transmission succeeds and is given by (5.5). χ_u is the wake-up receive rate, and e_u and l_u are respectively the energy cost and the duration of a single receive wake-up operation. The scalar products $\mathbf{n_r}\cdot\mathbf{l_r}$ and $\mathbf{n_t}\cdot\mathbf{l_t}$ correspond to the duration of a packet reception and packet transmission process respectively, without regard to the outcome of the processes. Finally, P_{SBY} corresponds to the power consumption of the node when the MAC is in the STDBY state.

In (5.17), the first term corresponds to the power consumption due to packets reception, and the second term to the power consumption incurred by packets transmission. The third term accounts for the power consumption due to the receive wake-up operation (periodic listening to the channel or beacon transmission, WuCs reception...), and the final term accounts for the power consumption of the node in sleep state.

5.2.6 Constructing the AMCs Transition Matrices

The construction of the AMCs requires the calculation of the transition probabilities, which depend both on the protocol functioning and on the frame failure probabilities. In order to compute the frame failure probabilities, analytical models which focus on the wireless channel and interferences [98] can be used. Combining the framework proposed in this work with such models allows the evaluation of the MAC protocols regarding the scalability and channel quality. In the rest of this work, the frame failure probability is denoted by p_f, which can take different values for different frames. Hence, when constructing an AMC modeling a packet transmission or reception process, the states corresponding to a frame transmission or reception lead to a failure with a probability p_f, and to a success with a probability $1 - p_f$.

5.3 Case Study: Modeling PW-MAC using the Proposed Framework

In this section, PW-MAC [20], a receiver-initiated protocol that focuses on low energy consumption for both the sender and the receiver, is modeled using the proposed framework. As a receiver-initiated protocol, PW-MAC is similar to RICER presented in Chapter 1, but aims to reduce the energy cost of rendez-vous. PW-MAC was proposed by the same authors that introduced RI-MAC [88], to reduce the power consumption of the latter. Through this case study, the different stages required to apply the proposed framework to a particular MAC are illustrated. First, the AMCs modeling the transmission and reception processes are established. Then, the energy and latency cost vectors are set. Two different approaches are presented to set the energy and latency cost vectors. The first one solely relies on analytical estimations, while the second combines analytical estimations with measurements obtained by microbenchmarks to obtain accurate values

of the energy and latency overhead incurred by the software and hardware. By comparing the accuracy of the model achieved by each approach, the benefits enabled by the second approach are shown.

5.3.1 Building the AMCs

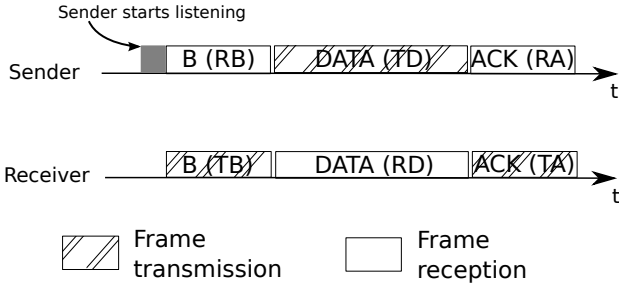

(a) Packet transmission using PW-MAC. For each frame transmission or reception, the corresponding state name is indicated in brackets: RB: Receive Beacon; TB: Transmit Beacon; RD: Receive Data; TD: Transmit Data; RA: Receive ACK; TA: Transmit ACK.

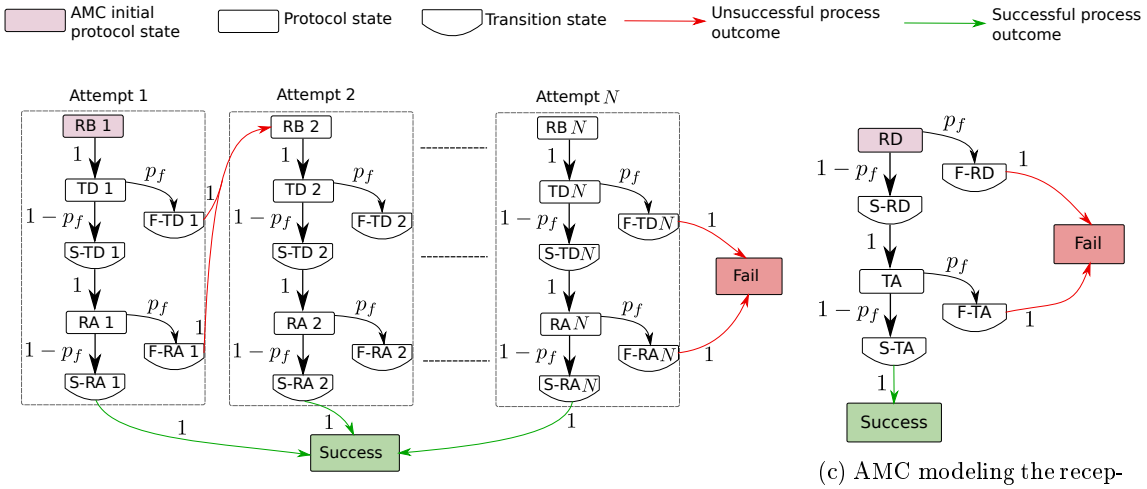

(b) AMC modeling the transmission process of PW-MAC.

(c) AMC modeling the reception process of PW-MAC.

Figure 5.2 – Packet transmission using PW-MAC and AMCs modeling the transmission and reception processes of this protocol.

The first step for modeling a particular MAC protocol using the proposed framework is to build the two AMCs describing the packet transmission and the packet reception processes. PW-MAC is based on the duty-cycling approach, in which the node keeps its transceiver in sleep state most of the time, and regularly switches it on to check for incoming packet. The proportion of time during which the node is active is called the duty-cycle. Because PW-MAC is a receiver-initiated protocol, each node regularly sends a beacon indicating that it is ready to receive. After each beacon sending, it listens to the channel for incoming data packet. If no packet is detected on the channel, the node goes back to sleep. The time interval between two beacon sendings is computed using a pseudo-random generator, avoiding nearby nodes to wake up at the same time repeatedly. A node learns the wake-up schedule of its forwarders, and when it needs to send a packet, it wakes up just before the receiving node sends a scheduled beacon. After receiving the beacon from the forwarder, it sends the data frame, and then listens to the ACK frame. A packet transmission using PW-MAC is shown in Figure 5.2a, in which the protocol state names associated to each frame sending or receiving are indicated in brackets.

Packet Transmission Process AMC

The transmission process of PW-MAC is modeled by the AMC shown in Figure 5.2b. Each protocol state corresponds to the transmission or reception of a frame. When a node needs to transmit a packet, it first listens to the channel until it receives a beacon. Therefore, the protocol states corresponding to this operation, named RB i where $i \in \{1, \ldots, N\}$ is the attempt number, only has one outcome as opposite to the other protocol states TD i and RA i, which possibly finish by a success or a failure. Transition states were added to take into account the energy and latency costs incurred by each possible outcome (success or failure) of the TD i and RA i protocol states. For example, if the TD i state fails, *i.e.* the transmission of the data frame fails at the i^{th} attempt, then the node will continue to listen for an ACK, which will incur energy consumption and latency. These energy and latency costs are accounted by the F-TD i transition state. As there are $M_t = 7$ transient states, the associated transition matrix is the $(7N + 2)-$by$-(7N + 2)$ matrix is defined by:

$$\mathbf{P_t} = \begin{array}{c} \\ \\ \\ \\ \\ \end{array} \begin{array}{c} \begin{array}{cccc} \multicolumn{4}{c}{\mathbf{Q_t}} & \mathbf{R_t} \end{array} \\ \left(\begin{array}{cccc|c} \mathbf{A} & \mathbf{B} & \mathbf{0_{7\times 7}} & \cdots & \mathbf{C} \\ \mathbf{0_{7\times 7}} & \ddots & \ddots & & \vdots \\ \vdots & \ddots & \mathbf{A} & \mathbf{B} & \mathbf{C} \\ \mathbf{0_{7\times 7}} & \cdots & \mathbf{0_{7\times 7}} & \mathbf{A} & \mathbf{D} \\ \hline \mathbf{0_{2\times 7}} & \cdots & \cdots & \mathbf{0_{2\times 7}} & \mathbf{I_2} \end{array} \right) \end{array},$$

where $\mathbf{A}$ is the $7-$by-7 matrix corresponding the to the intra-attempt transitions:

$$\mathbf{A} = \begin{array}{c} \\ \text{RB } i \\ \text{TD } i \\ \text{RA } i \\ \text{S-TD } i \\ \text{F-TD } i \\ \text{S-RA } i \\ \text{F-RA } i \end{array} \begin{array}{c} \begin{array}{ccccccc} \text{RB } i & \text{TD } i & \text{RA } i & \text{S-TD } i & \text{F-TD } i & \text{S-RA } i & \text{F-RA } i \end{array} \\ \begin{pmatrix} 0 & 1 & 0 & 0 & 0 & 0 & 0 \\ 0 & 0 & 0 & 1-p_f & p_f & 0 & 0 \\ 0 & 0 & 0 & 0 & 0 & 1-p_f & p_f \\ 0 & 0 & 1 & 0 & 0 & 0 & 0 \\ 0 & 0 & 0 & 0 & 0 & 0 & 0 \\ 0 & 0 & 0 & 0 & 0 & 0 & 0 \\ 0 & 0 & 0 & 0 & 0 & 0 & 0 \end{pmatrix} \end{array},$$

where $i \in \{1, \ldots, N\}$. Similarly, $\mathbf{B}$ is the $7-$by-7 matrix corresponding to the transitions between an attempt and the next attempt:

$$\mathbf{B} = \begin{array}{c} \\ \text{RB } i \\ \text{TD } i \\ \text{RA } i \\ \text{S-TD } i \\ \text{F-TD } i \\ \text{S-RA } i \\ \text{F-RA } i \end{array} \begin{array}{c} \begin{array}{cccc} \text{RB } i+1 & \text{TD } i+1 & \cdots & \text{F-RA } i+1 \end{array} \\ \begin{pmatrix} 0 & 0 & \cdots & 0 \\ 0 & 0 & \cdots & 0 \\ 0 & 0 & \cdots & 0 \\ 0 & 0 & \cdots & 0 \\ 1 & 0 & \cdots & 0 \\ 0 & 0 & \cdots & 0 \\ 1 & 0 & \cdots & 0 \end{pmatrix} \end{array},$$

where $i \in \{1, \ldots, N-1\}$. $\mathbf{C}$ is the matrix corresponding to the transitions between the non-last attempts and the final states:

$$\mathbf{C} = \begin{array}{c} \\ \text{RB } i \\ \text{TD } i \\ \text{RA } i \\ \text{S-TD } i \\ \text{F-TD } i \\ \text{S-RA } i \\ \text{F-RA } i \end{array} \begin{array}{c} \begin{array}{cc} s & f \end{array} \\ \begin{pmatrix} 0 & 0 \\ 0 & 0 \\ 0 & 0 \\ 0 & 0 \\ 0 & 0 \\ 1 & 0 \\ 0 & 0 \end{pmatrix} \end{array},$$

where $i \in \{1, \ldots, N-1\}$. Finally, $\mathbf{D}$ is the matrix corresponding to the transitions between the last attempt and the final states:

$$\mathbf{D} = \begin{array}{c} \\ \text{RB } N \\ \text{TD } N \\ \text{RA } N \\ \text{S-TD } N \\ \text{F-TD } N \\ \text{S-RA } N \\ \text{F-RA } N \end{array} \begin{array}{c} \begin{array}{cc} s & f \end{array} \\ \begin{pmatrix} 0 & 0 \\ 0 & 0 \\ 0 & 0 \\ 0 & 0 \\ 0 & 1 \\ 1 & 0 \\ 0 & 1 \end{pmatrix} \end{array}.$$

Packet Reception Process AMC

PW-MAC requires each node to wake up regularly to send a beacon indicating that it is ready to receive a packet. The node then listens to the medium for incoming packet, and if no preamble is detected, it returns to sleep after a short time. Otherwise, it continues to listen for the incoming packet. This operation is modeled by the R-WUP state of the MC modeling the protocol, and is therefore not considered by the AMC modeling the packet reception process. The initial state of the AMC modeling the packet reception process is the state corresponding to a data frame reception, as shown in Figure 5.2c. In this AMC, the state RD corresponds to a data frame reception, and the state TA to an acknowledgment transmission. Transition states were added to take into account the energy and latency costs incurred by each state possible outcome (success or failure). The corresponding transition matrix is the following 8−by−8 matrix:

$$\mathbf{P_r} = \begin{pmatrix} \mathbf{Q_r} & \mathbf{R_r} \\ \mathbf{0_{2\times 6}} & \mathbf{I_2} \end{pmatrix},$$

where $\mathbf{Q_r}$ is the 6−by−6 matrix that corresponds to transitions between non-final states:

$$\mathbf{Q_r} = \begin{array}{c} \\ \text{RD} \\ \text{TA} \\ \text{S-RD} \\ \text{F-RD} \\ \text{S-TA} \\ \text{F-TA} \end{array} \begin{array}{c} \begin{array}{cccccc} \text{RD} & \text{TA} & \text{S-RD} & \text{F-RD} & \text{S-TA} & \text{F-TA} \end{array} \\ \begin{pmatrix} 0 & 0 & 1-p_f & p_f & 0 & 0 \\ 0 & 0 & 0 & 0 & 1-p_f & p_f \\ 0 & 1 & 0 & 0 & 0 & 0 \\ 0 & 0 & 0 & 0 & 0 & 0 \\ 0 & 0 & 0 & 0 & 0 & 0 \\ 0 & 0 & 0 & 0 & 0 & 0 \end{pmatrix} \end{array},$$

and $\mathbf{R_r}$ is the 6−by−2 matrix that corresponds to transitions between the non-final states and the two final states:

$$\mathbf{R_r} = \begin{array}{c} \\ \text{RD} \\ \text{TA} \\ \text{S-RD} \\ \text{F-RD} \\ \text{S-TA} \\ \text{F-TA} \end{array} \begin{array}{c} \begin{array}{cc} s & f \end{array} \\ \begin{pmatrix} 0 & 0 \\ 0 & 0 \\ 0 & 0 \\ 0 & 1 \\ 1 & 0 \\ 0 & 1 \end{pmatrix} \end{array}.$$

5.3.2 Setting the Energy and Latency Cost Vectors

The proposed framework requires the energy cost and latency cost vectors, respectively denoted by $\mathbf{c.}$ and $\mathbf{l.}$, to be set carefully. When a node has to transmit a packet using PW-MAC, it first listens continuously until it receives a beacon. This operation corresponds to the RB i states of the AMC modeling the packet transmission process. It is assumed that the probability of a frame failure is p_f, therefore the number of failures before a beacon is successfully received, denoted by

X, is a discrete random variable that follows a geometric distribution of parameter $1 - p_f$. The expected number of beacon reception failures before the first beacon reception success is thus:

$$\mathbb{E}[X] = \frac{p_f}{1 - p_f}. \tag{5.18}$$

The average rate of beacon sending by a node is χ_u, and the expected listening time before a successful beacon reception starts, denoted by $\mathbb{E}[L]$, is therefore:

$$\mathbb{E}[L] = \frac{p_f}{\chi_u (1 - p_f)}, \tag{5.19}$$

which was accounted in the latency cost of the RB i state of the transmission process.

Focusing on the energy and latency costs incurred by the transmission and reception of frames (beacon, data and ACK), the size of a frame in bits is denoted by S, and the transmission bit rate in bps is denoted by R. When a protocol is implemented on a real platform, energy and latency overhead due to hardware and software overhead can incur as a consequence of radio setup, turn around... Therefore, the latency incurred by a frame transmission/reception is:

$$l = \frac{S}{R} + l_{ovh}. \tag{5.20}$$

where l_{ovh} is the hardware/software overhead. Moreover, the energy cost incurred by a frame transmission/reception is:

$$e = \frac{S}{R} P_C + e_{ovh}, \tag{5.21}$$

where P_C is the power consumed by the node, and takes different values depending on whether the node is transmitting or receiving, and e_{ovh} is the hardware/software energy overhead. The energy cost and latency cost incurred by the transmission/reception of each frame (beacon, data and ACK) were calculated using the appropriate values of S, R and P_C.

Microbenchmarks were performed to measure accurately the energy and latency costs (including the overhead) of a packet transmission, a packet reception, and a scheduled wake-up. The measurement results are shown in Figure 5.3a for the packet transmission process. These measurements were done using a Keysight N6705B DC power analyzer, with the PowWow platform [99]. The measurements were done using the Texas Instrument CC1120 transceiver, which consumes 34 mA when transmitting at +10 dBm, and 22 mA when receiving, according to the datasheet. On Figure 5.3a, the different steps of the packet transmission process can be seen, and the corresponding states are indicated. This figure shows that hardware and software overhead is introduced at the beginning and at the end of the processes, as well as between frames sendings and reception. These additional energy and latency costs were taken into account when setting the energy and latency cost vectors, and similar measurements were done for the reception process and the regular wake-ups.

To illustrate the importance of considering the hardware and software overhead when setting the cost vectors, measurements were done for different average values of χ_u, and compared to the analytical estimation obtained using the proposed framework. For both the latency and the power consumption, two analytical estimations were realized: one using cost vectors that do not take into account the hardware and software overhead, *i.e.* e_{ovh} and l_{ovh} were set to zero, qualified as "naive", and one that considers this overhead using the microbenchmark measurements qualified as "hybrid", as it uses both analytical estimation and experimental measurements from the microbenchmarks, as in [100, 101]. Figure 5.3b shows the two estimations as well as the obtained measurements. As it can be seen, the proposed framework is accurate regarding the latency both using the "naive" and the "hybrid" approaches. However, regarding the power consumption, the "hybrid" approach performs significantly better than the "naive" one. This is because most of the power consumption of PW-MAC is due to the scheduled wake-ups. Therefore having accurate measurement of the energy cost of this operation is essential to achieve accurate estimation of the power consumption. These results show the benefits of the "hybrid" approach compared to the "naive" one to achieve accurate estimation using the proposed framework.

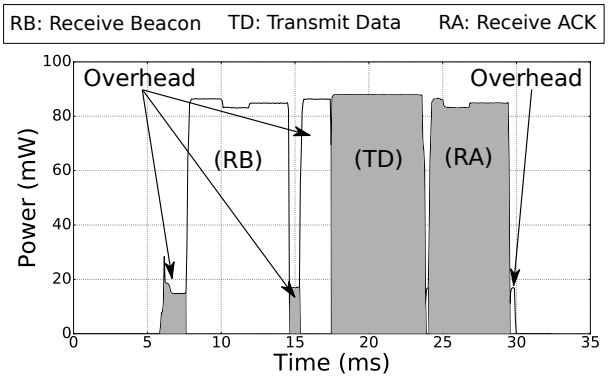

(a) Power consumption trace of a packet transmission using PW-MAC.

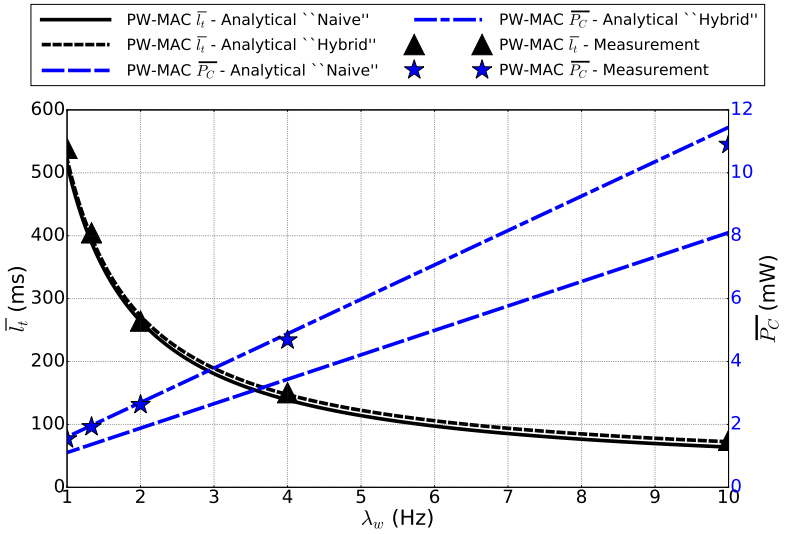

(b) Comparison of the “naive” setting of the cost vectors and “hybrid” setting.

Figure 5.3 – Microbenchmarks and comparison of the "naive" and "hybrid" approaches.

5.4 Conclusion

In this chapter, a new generic framework for modeling MAC protocols was presented. This framework is based on AMCs, and focuses on energy consumption, latency and reliability. The steps required to model a specific MAC protocol using the proposed framework were illustrated using the PW-MAC protocol, which aims to improve energy efficiency for both the receiver and the sender. Moreover, experimental measurements were performed to accurately set the energy and latency parameters required by the model, and to validate the framework.

While using the proposed framework to evaluate novel schemes, several lessons were learned about the potential and the limitations of the framework. Firstly, the energy and latency strongly depend on the hardware and the implementation, and therefore measurements are required if high accuracy is desired. In this work, microbenchmarks were used to get accurate values of both the latency and energy consumption incurred by each state. This can be seen as a limitation of the proposed framework as it requires measurements on real hardware. However, if one is interested only by the trends of the protocols, highly accurate estimation of the energy and latency is not necessary.

Another potential issue is the construction of the transition matrices, which requires the calculation of the transition probabilities. These probabilities depend on both the protocol algorithm and the frame failure probability. Computing realistic value of the frame failure probability for a given precise context may be difficult, as it depends on the channel state. However, as suggested

previously, the framework proposed in this work can be combined with other models focusing on the wireless channel. Also, letting the frame failure probability be a variable allows the exploration of the behaviors of MAC schemes under different channel conditions.

In the next chapter, the proposed generic framework combined with the "hybrid" approach are used to evaluate MAC protocols leveraging WuRx, compared to traditional approach, *i.e.* not using WuRx.

Chapter 6

Benefits of Wake-up Receivers

Traditional WSN MAC protocols switch on and off the transceiver according to a schedule, to reduce the energy consumption of communications. When two nodes need to communicate, preamble sampling is used to perform a *rendez-vous* between the two nodes, prior to the data packet exchange. In these approaches, each node is most of the time in sleep state, and regularly wakes up to check the channel for incoming packets. As energy is typically the limiting factor of long-term WSN applications, substantial efforts were devoted in the last decades to design energy efficient MAC protocols [12]. However, as nodes frequently wake-up while no incoming packets are pending, idle listening is usually an unavoidable and significant source of energy waste. Moreover, reducing the duty-cycle is not always a feasible solution, as it incurs higher expected latencies. Indeed, when setting the wake-up rate, *i.e.* the rate at which nodes wake up to check for incoming packets, a compromise is made between power consumption and latency. Therefore, decreasing the duty-cycle to reduce the energy cost of communications is not always a possible solution, as it can lead to unacceptable latencies.

In the recent years, Ultra Low Power (ULP) WuRx have emerged as a possible solution to achieve both energy efficient communications and low latencies. Indeed, these devices allow continuous channel monitoring while consuming orders of magnitude less power than traditional transceivers [13], therefore enabling "pure-asynchronous" communications. ULP WuRx wake up the node MCU or other sleeping subsystems using interrupts when a WuC is detected, thus removing the need for *rendez-vous* schemes [102]. In the rest of this thesis, we called ULP WuRx simply WuRx, to make the notation less cluttered.

The framework proposed in the previous chapter is used to evaluate the benefits enabled by WuRx, by modeling two simple MAC protocols that leverage these devices: TI-WuR and RI-WuR, both from [102]. These schemes are compared to PW-MAC, X-MAC [103], a popular transmitter-initiated protocol, and to the IEEE 802.15.4 standard in its beaconless mode, which is based on the well-known Carrier Sense Multiple Access with Collision Avoidance (CSMACA) scheme. Moreover, experimental measurements were realized to validate the presented results.

The rest of this chapter is organized as follows. Section 6.1 exposes the a state of the art of WuRx, focusing on both the hardware and the MAC protocols. Next, in Section 6.2, the latency-power consumption trade-off and the reliability of various MAC protocols, including two that leverage WuRx, are evaluated.

6.1 State of the Art of Wake-up Receivers

This section exposes the state of the art of WuRx. The first part focuses on the hardware of WuRx, while the second part concentrates on MAC protocols leveraging these devices.

6.1.1 Wake-up Radio Hardware

WuRx developed in the literature can be classified into two kinds: passive and active. Passive WuRx are entirely powered by the energy from incoming signals, and therefore incur almost no energy

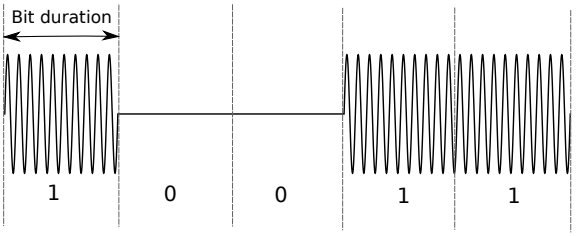

(a) OOK modulation.

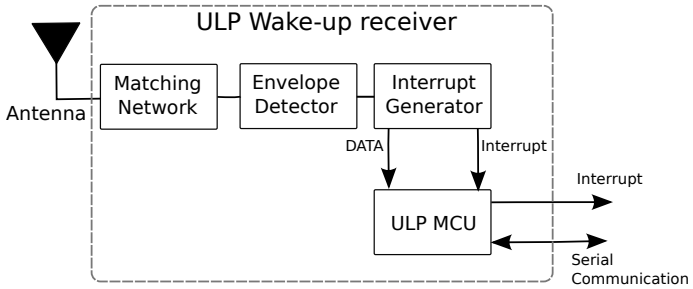

(b) WuRx block architecture.

Figure 6.1 – OOK modulation and WuRx architecture [2].

consumption overhead. However, this kind of devices suffers from a significant lower sensitivity than active WuRx, which require to be power supplied.

To the best of our knowledge, the first wireless sensor node that integrated a passive WuRx is the Wireless Identification and Sensing Platform (WISP) from *Sample et al.* [104]. WISP is a fully programmable platform which integrates a 16 bit MCU as part of a passive Radio Frequency IDentification (RFID) tag, as well as different kinds of sensors. WISP can operate only from the energy harvested from the input wireless signal, and achieves a range of 4.5 m. In [105], the WISP has been combined with the Tmote Sky mote as a passive WuRx, and the WISP-to-reader communication was disabled to permit a range of 5 m. Moreover, ID-based wake-up are supported by this device, as the WISP MCU is used to trigger the Tmote Sky MCU. *Chen et al.* proposed to combine the WISP with a RF energy harvesting circuit to enhance its wake-up ability in [106], forming the EH-WISP-Mote. This latter device benefits from a 20% higher wake-up range, while maintaining ID-based wake-up capabilities. Moreover, a trigger generator circuit has been developed which consumes less energy than the WISP, to wake up the MCU embedded in the WISP. The RF energy harvesting circuit and the trigger generator were combined to form the REACH-Mote, which achieves a wake-up range of 11 m. However, it suffers from a high wake-up latency, 235 ms at 1.5 m.

Regarding active WuRx, the first circuit proposed was PicoRadio, by *Rabaey et al.* [107] in 2002. PicoRadio is a very low power transceiver, designed to be always active, and which can be used either as a main radio or as a WuRx. This device achieves a sensitivity of -75 dBm, and consumes 1.6 mW in transmit mode and 380 μW in receive mode at 1 V. In [108], *Kolinko et al.* proposed a design that works in the 916 MHz band, consumes 20 μW and achieves a sensitivity of -69 dBm, enabling a range of 200 m when transmitting at $+30$ dBm. However, both these works do not permit selective wake-up without waking up the main MCU. In [109], the authors proposed to combine a front-end analog circuit with an ULP MCU, the PIC12F683, to form a WuRx able to filter the wake-up signals and to perform address matching. The WuRx MCU is responsible for waking up the main MCU. The proposed device operates in the 868 MHz band, and receives signals with On-Off Keying (OOK) modulation, the simplest form of amplitude shift keying modulation in which data is represented by the presence or absence of a carrier, as illustrated in Figure 6.1a. The proposed device consumes 171 μW, including the 48 μW consumed by the MCU, and achieves a maximum range of 3 m. *Gamm et al.* proposed in [110] a device which integrates 16 bit address coding for selective wake-up, using a low frequency wake-up signal that is modulated on a high frequency carrier in the main radio of the transmitting node. The WuRx provides a passive demodulation circuit which regains the low frequency signal and feds it to a low power low

frequency wake-up integrated circuit. This devices operates in the 868 MHz band, and consumes 2.78 μA. It achieves a -52 dBm sensitivity, which resulted in a wake-up range of 40 m at an output power of +10dBm. An improved version was proposed in [111], which consumes 3.5μA but achieves a wake-up range of 90 m in an open field when the wake-up signal is transmitted at +20 dBm.

In [112], *Sanchez et al.* proposed a WuRx which consumes 8.7 μW and can operate at 433 MHz, 868 MHz or 2.4 GHz. This device receives signal in OOK, and achieves a range of 15 m. An energy efficient addressing scheme was proposed in [113] by *Oller et al.*, called Time-Knocking (TicK). TicK uses the time intervals between WuCs to encode addresses, while putting the MCU in sleep state during these time intervals. This approach enables early detection of address mismatch, and the authors showed that this scheme outperforms MCU-based mechanism and correlation based mechanism in term of energy consumption. However, addressing duration is longer, varying between 48 ms and 68 ms. In [5], this TicK was integrated to a WuRx, which achieves a current consumption of 1 μW and a wake-up range of 10 m. A WuRx intended for WBAN was proposed in [3], which consumes a current of 270 nW at 1.5 V, and achieves a sensitivity of -51 dBm in the 433.92 MHz band. WuCs are sent using OOK modulation, and a preamble detection scheme is used to reduce false wake-ups due to interference sources. Moreover, the receiver integrates a Serial Peripheral Interface (SPI) to communicate with the MCU. In [6], a WuRx solution which uses a custom Complementary Metal Oxide Semiconductor (CMOS) rectifier and a comparator was proposed, and achieves a sensitivity of -41 dBm and a power consumption of 98 nW. *Takahagi et al.* proposed in [114] a WuRx that uses a rectifier, a high-band baseband amplifier and a wake-up signal recognition circuit that achieves a sensitivity of -47.2 dBm, but with a power consumption of 6 μW. A CMOS chip including external RF filter, antenna matching, reference generation and SPI interface to form a WuRx was proposed in [115]. This device achieves a sensitivity of -71 dBm at 868 MHz, a power consumption of 2.4 μW (1 V) and a latency of 7 ms.

Wake-up Receiver Used in this Work More recently, *Magno et al.* proposed in [2] a WuRx that was used in this thesis for experimentations, and which receives WuCs in OOK. The block architecture of the WuRx is shown in Figure 6.1b, and it can be seen that the WuRx is made up of four main blocks: the matching network, the envelope detector, the interrupt generator and the ULP MCU that provides computational resources to the WuRx and serial interface with the main node. The matching network guarantees maximum power transfer between the antenna and the rest of the circuit, and is optimized to work in the 868 MHz band. The second stage is a passive demodulation circuit, which consists of a passive envelope detector that discards the frequency and phase content and only detects amplitude. Once the signal is rectified, the third block performs interrupt generation by first reconstructing the bits of the WuC using a nano-power comparator, and a passive adaptive threshold circuit. The interrupt generator block also provides a preamble detector to avoid unwanted awakening due to noise. Finally, the PIC12LF1552 from Microchip provides computational capabilities. This on board processor is awaken by the interrupt generator when a WuC is detected, and can be programmed to partially incorporate the MAC layer, and in particular address matching, allowing nodes to wake up only a specific node and not all neighbors. The used version of the WuRx is optimized to work at a bit rate of 1 kbps, and the sensitivity in these conditions was measured to be -55 dBm. The power consumption of the whole WuRx was measured to be 1.83 μW in always-on listening mode and 284 μW when receiving and processing data with the MCU of the WuRx active.

The WuRx from [2] was chosen as it is a state of the art device that achieves competitive performances. Moreover, it embeds a programmable MCU that can implement some parts of MAC protocols, such as address matching. Finally, it is a device that we can easily acquire from the authors for experimentations.

6.1.2 Wake-up Radio MAC Protocols

We focus now on MAC schemes leveraging WuRx [116]. *Oller et al.* proposed in [102] two protocols, TI-WuR and RI-WuR, which are respectively transmitter and receiver initiated schemes. A packet reception using TI-WuR and the WuRx from [2] is illustrated in Figure 6.2. As a transmitter initiated protocol, the sender initiates the communication by sending a WuC containing the address of the target node. The analog front-end of the WuRx of its neighbors detects the activity on the

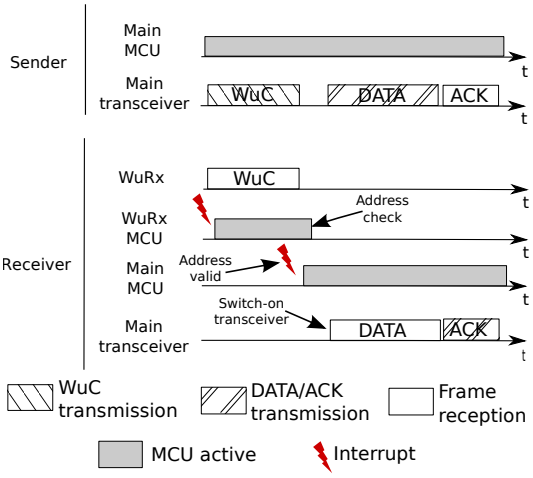

Figure 6.2 – Illustration of a packet transmission using TI-WuR.

channel, and trigger an interrupt to wake-up the MCU embedded in the WuRx. The WuRx MCU then reads the incoming data, and performs address matching. If the address embedded in the WuC matches the node address, the WuRx MCU triggers an interrupt to wake up the main MCU. The main MCU then switches on the main transceiver to receive the data frame from the sender. The data frame is sent using standard modulation schemes and bit rates. Finally, an ACK frame is sent by the receiver to acknowledge the reception of the data frame. Using RI-WuR, each node periodically broadcasts a WuC containing its address to inform its neighbors that it is ready to receive, and then listens for a data packet with its main radio. When a node receives a WuC, two scenarios are possible. If the node has no packet to send to the node that broadcasts the WuC, its WuRx simply ignores the WuC. Otherwise, the node is awaken, and the data transmission starts using the main transceiver in the same way that with TI-WuR.

Focusing on target tracking in dense wireless sensor networks, *Song et al.* proposed Low Energy Self Organizing Protocol (LESOP) in [117]. Using this scheme, the transport and network layer are excluded, and the MAC layer communicates directly with the application layer, making LESOP a cross layer protocol. Each node embeds a WuRx in addition to its main transceiver that is able to detect busy tones. When a node detects a target, it broadcasts a busy tone to wake up all its neighbors, and is labeled as the "leader". All the informations gathered by the nodes are sent to the leader which merges them. As the target moves, a new leader is elected and receives the target information from the former leader. In the context of critical infrastructure monitoring, *Ullah et al.* proposed a MAC protocol leveraging WuRx in [118]. In this approach, nodes are organized in a star topology, and communicate using a slotted Aloha approach. Nodes are equipped with WuRx, and the coordinator sends WuCs carrying synchronization information according to a schedule. After receiving a WuC, a node starts transferring its data after having chosen randomly a slot in the current frame. The authors extended their work to multi-hop networks in [119], where nodes are organized in clusters around a cluster head, which is the only node in the cluster to embed a WuRx. Focusing on WBAN, *Le et al.* proposed AWD-MAC [120], a receiver initiated scheme that uses WuRx to reduce collisions and power consumption. Nodes are assumed to be organized in a star topology, and cannot start a communication until the coordinator wakes them up. The coordinator performs nodes discovery at the network setup phase, and gathers all nodes addresses and data rate. Then, the coordinator is able to wake up each node when it is available, as it is aware of its data rate. Another MAC protocol for WBAN was proposed in [121] by *Ameen et al.*. The authors motivate the use of WuRx by a reduction of the power consumption, as well as by a reduction of the latency, which can be critical in emergency situations. For periodic non-urgent traffic, TDMA is used, and communications are initiated by the coordinator, which wakes up nodes according to a schedule which is established regarding the data rate requirement of each node. When a node has an urgent packet to send, it initiates the communication by sending a WuC to the coordinator, which responds by an ACK, followed by a beacon for resource allocation. The

node that initiated the communication then sends its urgent packet. Focusing on bats tracking and monitoring, *Dressler et al.* proposed in [122] a low power MAC protocol. Low power is an important constraint in bats tracking, as these animals cannot carry sensor heavier than 2 g, which forbids the use of big batteries. The authors focus on bat to ground communication, and the WuRx activates the mobile node only when it is in the communication range of the ground nodes. The bat-mounted system then starts transmitting information to the ground nodes.

Ravichandran et al. proposed in [123] to reduce the acquisition time of Ultra Wide Band (UWB) multi-hop sensor networks using passive WuRx. Indeed, UWB in WSNs enables very high data rates, but at the cost of high acquisition time which leads to energy waste. The authors proposed to use a passive WuRx in conjunction to the UWB radio to achieve fast channel control signaling. In [124], *Jurdak et al.* combined RFID to the IEEE 802.15.4 MAC standard beaconless mode, in a multi-hop context. In the proposed scheme, the IEEE 802.15.4 transceiver acts as a RFID reader, to avoid the extra cost of integrating such a device in each node. By using the RFID as passive WuRx, the overheads of periodic wake-ups required by the standard IEEE 802.15.4 were removed, increasing the energy efficiency of this protocol. Radio Triggered sensor MAC (RTM) [125] is another multi-hop MAC protocol leveraging passive WuRx. In this approach, the WuRx and the main radio operate on the same channel. When a node needs to transmit a packet, it first senses the channel, and, if the channel is found free, transmits a WuC which carries no information but serves only to energize the receiver WuRx. When a WuRx is energized by a WuC, it generates an interrupt to wake up the MCU, which switches on the main radio. The sender then transmits a frame containing the address of the target node, which responds to indicate that it is ready to receive. Finally, the data exchange takes place. *Ullah et al.* proposed Very Low Power MAC (VLPM) in [126] for WBAN, in which each node, including the coordinator, is assumed to be equipped with a passive WuRx. Moreover, it is assumed that WuCs embed the address of the target node, which can be processed by the nodes MCU to allow non-targeted nodes to go back in sleep state immediately after having performed address matching. The coordinator sends WuCs messages to a specific node containing synchronization information, as well as channel resources allocated to it. Combining passive WuRx and energy harvesting was proposed with WuR-TICER in [127]. WuR-TICER is a transmitter initiated protocol, and therefore when a node needs to send a packet, it first broadcasts a WuC embedding its address. Upon receiving the WuC, the receiver switches on its main radio to receive the data frame.

PicoRadio [128] is considered as the first MAC protocol for WSNs leveraging active WuRx. It is a multichannel approach, in which the frequency band is partitioned into multiple channels, and each node is assigned to a locally unique frequency. Spread spectrum Code Division Multiple Access (CDMA) is used for channel access, and a heuristic distributed solution is proposed to solve the NP-complete problem of channel assignment. Each node listens to a common control channel for a random period of time, and periodically broadcasts a channel assignment packet containing their own channel as well as their one-hop neighbors channels. Nodes keep a local channel assignment table which records channel usage by their one-hop and two-hop neighbors, and make sure its own channel is different from all its one-hop and two-hop neighbors. When a node gets a packet to be sent, it first sends a WuC addressed to the receiver on its channel. Then, it sends the data after a wake-up period on the receiver channel. Another multichannel protocol leveraging WuRx is CMAC [129]. Using CMAC, the WuRx of each node is tuned to the node specific channel, and is assumed to have transmission capabilities. When a node needs to send a packet, it first listens to the targeted node WuRx channel for a short time, and if the channel is found free, it sends a WuC containing the its channel number. If the targeted node can receive the data, it answers by another WuC on the sender WuRx channel, and then switches its main radio to the sender channel to receive the data. Otherwise, it answers by a WuC informing the sender that it cannot receive the data. In [130], *Nosovic et al.* proposed WuRx for WSNs in which nodes have a low power RFID in addition to their regular transceiver, and which are organized in a star topology where nodes communicate with each other through a base station. When data packets arrive at the base station destined for an embedded node, the base station first broadcast a WuC to prevent all the nodes from accessing the channel. Then, a unicast WuC addressed to the target node is sent to wake up it, followed by the data packet. When a node detects a unicast WuC, received by its RFID and attended to it, it turns on its main radio to receive the data packet at high speed.

Ansari et al. [131] proposed RTWAC, a simple MAC protocol that leverages WuRx with ad-

dressing capabilities. In this scheme, each node is equipped with a WuRx, and when a node needs to transmit a packet, it first performs a CCA, and, if the channel is found clear, sends a WuC which contains the target node address and some command. When a WuC is detected, an interrupt is generated by the WuRx using the energy from the received signal to wake up the MCU, which processes the data embedded in the WuC. More precisely, it performs address matching and eventually executes the command. ZeroMAC [132] is based on the 802.11 DFC standard [133], but unlike DFC, a node using ZeroMAC broadcasts a WuC before transmitting a packet, which significantly reduces the power consumption and latency of communications. When a node needs to send a packet, it first broadcasts a WuC, which wakes up all its neighbors as WuRx are assumed to not have address matching capabilities. The sender then transmits a packet containing the address if the target node. All the sender neighbors receive this packet, and all expect the target node go back to sleep mode after having performed address matching. Next, the target node sends a WuC to wake up all its neighbors, followed by a packet indicating the address of the sender. Finally, the data transfer takes place. A scheme based on clustering has been proposed in [134], in which nodes are organized around repeaters. Clusters creations are initiated by the repeaters. First, a repeater broadcasts a WuC to wake up all the neighboring nodes, followed by a binding request. Each node that receives the request responds by a confirmation containing its address, after a backoff time. All sensor nodes report their information to the repeater to which they are bind.

To evaluate the benefits of WuRx, TI-WuR and RI-WuR were chosen as they represent the two big categories of protocols, receiver-initiated and transmitter-initiated, and most of the MAC protocols for WuRx rely on these schemes. Moreover, they do not focus on specific applications, and are compatible with the WuRx device used in this work.

6.2 Comparison of MAC Protocols

6.2.1 Evaluation Setup

TI-WuR and RI-WuR are compared to the PW-MAC, X-MAC and CSMA/CA protocols using the framework introduced in the previous chapter and experimentations. PW-MAC is an improvement of RI-MAC, proposed by the same authors, which focuses on low energy consumption. The details of PW-MAC modeling using the proposed framework are given in the previous chapter. X-MAC is a well-known transmitter-initiated protocol in which the receiver periodically wakes up to listen to the channel for a short time. When a node needs to send a packet, it first sends short preambles containing the target address. Once the receiver detects a short preamble frame with its address, it sends an early ACK, and the transmitter then sends the data frame. The CSMA/CA scheme was also evaluated. CSMA/CA is used by the IEEE 802.15.4 MAC standard in beaconless mode, and requires the node to be continuously listening to the channel. Therefore, when a node needs to send a data frame, it sends the data frame directly to the addressee node, possibly after a random backoff. The reception of the data frame is acknowledged by an ACK frame. If this approach incurs high power consumption, it provides benchmark values for latency. Similarly to PW-MAC, TI-WuR, RI-WuR, CSMA/CA and X-MAC were modeled using the proposed framework and following the procedure illustrated in the previous chapter.

These five protocols were implemented on a testbed of PowWow platforms (Figure 8.6). Each PowWow node was equipped with a Texas Instrument CC1120 transceiver, which is able to handle OOK modulation and therefore can send WuC. When TI-WuR or RI-WuR were evaluated, each node was also equipped with an instance of the WuRx presented in Section 6.1.1. The transmission power of the WuCs was +10 dBm, allowing a range up to 25 m using +3 dBi antennas for both transmitters and receivers, while the transmission power of the non-WuC frames was −6 dBm as it was found experimentally to be the minimal power required to achieve the same range. Moreover, the size of the data payload frame was 14 B. Each measurement was done on a node that was receiving packets at the rate $\chi_r = 0.10$ Hz (not considering the outcome of the reception process), locally generating packets at the rate $\chi_g = 0.10$ Hz, and transmitting both the generated and the received packets.

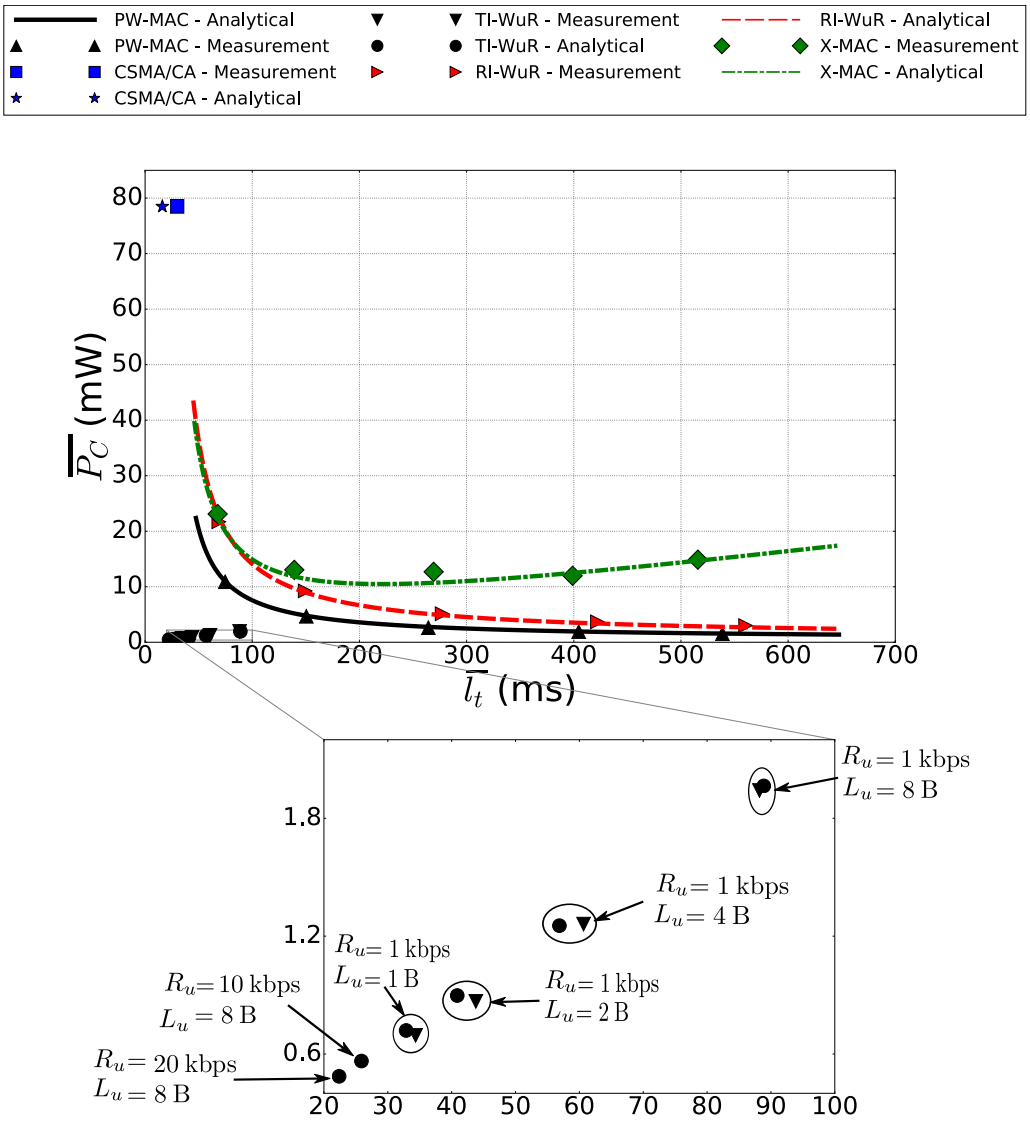

Figure 6.3 – Power consumption and latency of the five evaluated protocols.

6.2.2 Beyond the Latency-Power Consumption Trade-off

Figure 6.3 exposes the latency and the power consumption incurred by the evaluated protocols. Both analytical and experimental results are shown. For the analytical evaluation, p_f was set to 0 as this value leads to the closest fit with the experimental measurements. Concerning RI-WuR, PW-MAC and X-MAC, latency and power consumption were computed with the proposed framework for values of the average wake-up rate χ_u in the range $[1, 20]$Hz. Moreover, experimental measurements of these two quantities are shown for values of χ_u of 1, 1.3, 2, 4 and 10 Hz. In the case of TI-WuR, results for different values of the bit rate at which WuCs are sent, denoted by R_u, and different values of WuCs size, denoted by L_u, are exposed. Regarding CSMA/CA, only one couple of points (analytical and experimental) is shown as the protocol has no tuning parameters. It can be seen that the model fits well the numerical results for the five evaluated protocols.

These results show that a trade-off between the latency and the power consumption must be made when using RI-WuR and PW-MAC, and this trade-off is set by the wake-up rate χ_u. Indeed, high values of χ_u incur low power consumption at the cost of high latency, while low values of χ_u lead to low latency at the cost of high power consumption. Therefore, minimizing both latency and power consumption using this approach is not straightforward. Regarding X-MAC, an optimal value of χ_u permits the minimization of the power consumption. However, this optimal value depends on both χ_r and χ_g, which makes this optimization process difficult. When using X-MAC, choosing low values of χ_u allows low latencies at the cost of high power consumption, similarly to PW-MAC and RI-WuR. However, as X-MAC sends short preambles before each packet transmission, using high values of χ_u incurs high power consumption as the overhead incurred by the preamble sending becomes significant. PW-MAC and RI-WuR do not suffer from this drawback. Indeed, with PW-MAC the transmitter is synchronized with the receiver, and RI-WuR uses WuRx to avoid the need of preamble sending. CSMA/CA minimizes the latency as nodes are always listening: no synchronization nor WuC sending is required. However, this comes at the cost of high power consumption.

TI-WuR allows significantly lower latency and power consumption compared to the other considered protocols as it can be seen on Figure 6.3. As WuCs are sent at higher transmission power and lower bit rate than the other frames, decreasing the WuCs transmission time leads to lower latency and power consumption. Therefore, for $R_u = 1$ kbps, smaller WuC sizes lead to better performance, as shown in Figure 6.3 for WuCs sizes ranging from 1 B to 8 B. However, reducing the WuCs size is not always a solution as it implies reducing the amount of information that WuCs embed. Therefore, a more promising solution is to increase the bit rate of WuRx. As the WuRx device used for experimentation is optimized for a bit rate of 1 kbps, the evaluation of TI-WuR for values of R_u higher than 1 kbps was only done analytically, and Figure 6.3 shows the latency and power consumption incurred by TI-WuR when $L_u = 8$ B and R_u equals 10 kbps and 20 kbps. TI-WuR achieves a latency of 25.9 ms when $R_u = 10$ kbps, and 22.0 ms when $R_u = 20$ kbps, while CSMA/CA achieves a latency of 16.2 ms, but at the cost of a power consumption 130 times higher.

These results show the benefits of the pure-asynchronous approach enabled by WuRx when TI-WuRx is used. Trade-offs between the power consumption and the latency are no longer required in the context of low data rate WSNs, as packet exchanges are done without requiring regular wake-ups as with preamble sampling protocols, or continuous listening of the main transceiver as with CSMA/CA. Performance of current schemes can be improved by increasing the bit rate of WuRx, however this comes at the cost of a trade-off with the range and the power consumption of the WuRx device [2].

6.2.3 Reliability Evaluation

This section focuses on the impact of the frame failure probability p_f on the performance of three MAC protocols, TI-WuR, PW-MAC and CSMA/CA. TI-WuR and PW-MAC were chosen as they present the best performance as shown in Section 6.2.2, while CSMA/CA was chosen as it gives benchmark values for the latency. High values of p_f can be caused by interferences or collisions, e.g. due to dense networks or poor channel quality. As it is difficult to control the frame failure probability experimentally, the impact of this parameter was only analytically evaluated. Figure 6.4a shows the impact of p_f on $\overline{P_c}$ when $\chi_u = 4$ Hz, $R_u = 1$ kbps and $L_u = 1$ B. It can

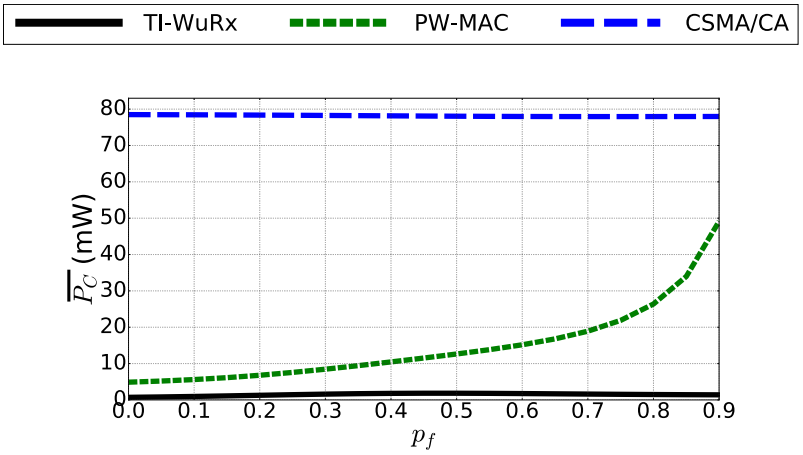

(a) $\overline{P_C}$ as a function of p_f.

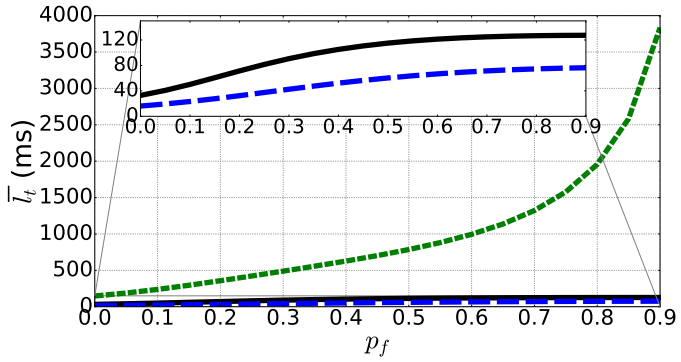

(b) $\overline{l_t}$ as a function of p_f.

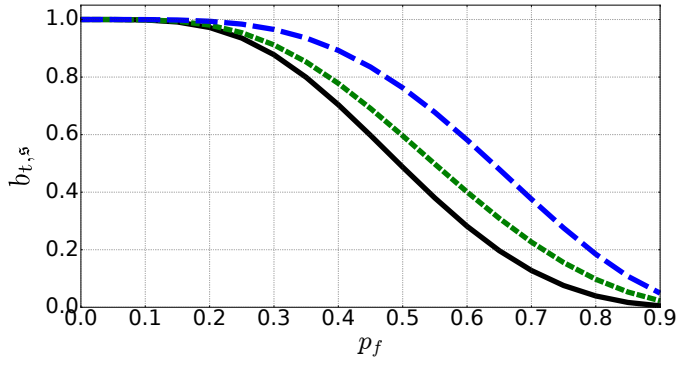

(c) $b_{t,s}$ as a function of p_f.

Figure 6.4 – Average power consumption, average transmission latency and probability of transmission success regarding the frame failure probability.

be seen that while p_f has a low impact on the average power consumption incurred by TI-WuR and CSMA/CA, it has a strong impact on the average power consumption incurred by PW-MAC. Indeed, when a node sends a packet using PW-MAC to a forwarder node, the sending node first wakes up just before the forwarder sends its scheduled beacon. If no beacon is received, then the sending node assumes that the synchronization with the forwarder node was lost, keeping its transceiver active until a beacon from the forwarder node is received to resynchronize. Therefore, a high frame failure probability causes frequent resynchronization activities and therefore significantly increases the power consumption. This unwanted effect also leads to high transmission latency when p_f becomes high as shown in Figure 6.4b, as the sending node waits for a valid beacon from the forwarder node. On the other hand, when an attempt to transmit a packet fails with TI-WuR or CSMA/CA, the sending node makes a new attempt until the transmission succeeds or exceeds a predefined number of re-transmissions (set to 4 in this work), each re-transmission being preceded by a random backoff. The functioning of PW-MAC leads to higher probability of successfully delivering the packet compared to TI-WuR as shown in Figure 6.4c. However, the difference becomes significant only when the probability of frame failure is higher than 20 %. CSMA/CA is the more reliable protocol, as only two frames must successfully be transmitted for the communication to be successful (the data frame and the ACK), while three frames must be successfully transmitted for TI-WuR and PW-MAC.

6.3 Conclusion

The proposed framework was used in this chapter to evaluate pure-asynchronous approaches enabled by emerging WuRx. In addition to evaluate these emerging schemes, this work illustrates how the framework introduced in the previous chapter can be used to explore new MAC paradigms. Five MAC schemes were modeled using the proposed framework, two leveraging emerging WuRx (TI-WuR and RI-WuR), and three traditional protocols (PW-MAC, X-MAC and CSMA/CA used by IEEE 802.15.4 beaconless). In addition to analytical evaluation of the pure-asynchronous approach, experimental measurements were conducted to support our conclusions. Results show the benefits enabled by emerging pure-asynchronous schemes, especially when a transmitter-initiated approach is used, in terms of both power consumption and latency as no more trade-off between these two critical quantities is required.

However, a drawback of many state of the art WuRx is the sensitivity, which is typically significantly lower than with traditional transceivers, and allows only a few tens of meters of range. If this range is sufficient for many applications, such as WBAN, this can be a critical limiting factor.

The rest of this part presents diverse approaches for leveraging WuRx. A new opportunistic MAC protocol leveraging WuRx is proposed in Chapter 7. In chapter 8, a modified version of Fuzzyman, introduced in Chapter 3 combined with a new MAC protocol leveraging WuRx are implemented on a star network. Finally, in Appendix B, WuRx were combined with emerging long-range communication schemes in a new network architecture.

Chapter 7

An opportunistic MAC protocol Leveraging Wake-up Receivers

In WSNs, traditional routing schemes predefine fixed paths before transmissions. Then, at each hop, a fixed neighbor is used to forward a packet. These schemes do not suit well to dynamic environment with lossy, unreliable and varying link qualities as they incur excessive retransmissions and thus waste network resources [135]. Opportunistic forwarding [136, 137] has emerged as a promising approach to tackle the problem of varying link qualities. The basic idea of this technique is to take advantage of the broadcast nature of the wireless medium to choose the next forwarding node at every hop instead of taking one predefined path to the destination. Therefore, this approach allows intermediate nodes to collaborate on packet forwarding in a localized manner. However, cross-layer MAC protocols must be carefully designed to achieve efficient collaboration.

Research in opportunistic forwarding is a hot topic and many solutions were proposed [138–147] In traditional approaches, neighborhood knowledge is achieved by periodic packets exchange called `Hello` packets, which leads to out of date information and is usually very costly in terms of energy. Another approach is formed by timer-based contention [144–147], which is a promising technique to allow opportunistic next relay selection while minimizing information exchange between nodes and their neighbors. With timer-based contention mechanism, information is encoded in time difference, avoiding `Hello` packets exchanges between a node and its neighbors. When a node wants to send a packet, it sends an RTS frame. Then, a *contention window* begins, during which a subset of the sender neighbors, called *potential receivers*, answers by sending a CTS frame using a backoff, called *contention backoff*, computed from a *state metric* (e.g. the remaining energy). The better a potential receiver behaves according to the state metric, the smaller its contention backoff should be. The receiver which answers first is chosen by the sender to receive its packet, and therefore the best next hop relay with respect to the chosen state metric is selected.

The main drawback of this technique is that it can be exceedingly energy costly as it requires the sender to keep its transceiver in the receive state for an arbitrary long period during the next hop relay election process, incurring high idle listening. Many applications such as environmental monitoring, home automation and assisted living require long-term sustainability, especially when the nodes are deployed in harsh environments. A severe bottleneck for many long-term applications is the limited lifetime of WSNs due to the finite amount of embedded energy in each node. As wireless communications are usually the most power consuming tasks over all other nodes activities such as sensing and computing [148], we proposed to use WuRx to reduce the energy consumption incurred by communications in the context of timer-based contention.

In this chapter, we present OPportunistic Wake-Up MAC (OPWUM) [149], a novel MAC protocol for WSNs in which each node embeds a WuRx. OPWUM uses timer-based contention to allow nodes to opportunistically select a receiver among their potential receivers at each packet sending. Potential receivers are chosen using a routing algorithm not addressed in this work [150]. By doing all the next hop relay election phase using WuCs only, OPWUM enables timer-based contention to become an energetically interesting solution. This chapter presents the design of OPWUM and presents comparison of OPWUM and 1-hopMAC [147], a state of the art protocol also based on timer-based contention, using exhaustive network simulations.

The remainder of this chapter is organized as follows: Section 7.1 presents the related work. The design of OPWUM is detailed in Section 7.2. In Section 7.3, OPWUM is compared to 1-hopMAC using exhaustive simulations. An application case is shown in Section 7.4 in order to demonstrate the effectiveness of OPWUM. Finally, Section 7.5 concludes this chapter.

7.1 Related Work

Opportunistic forwarding solutions can be classified according to the selection metric of relay [151]: geographical information [138], delivery rate [139], hop count [140] or not restricted to a specific kind of metric [141]. Some protocols code the packets when they are emitted [142]. However, most of these proposals do not consider the MAC layer, and assume the existence of a MAC protocol on which they rely. In this work, we focus on the MAC layer and assume the existence of a routing protocol that realizes a preselection of the forwarders among the neighboring nodes. The result of this preselection constitutes the set of potential receivers.

Zhang et al. proposed Reservation-based OPportunistic forwarding MAC (ROP-MAC) [143], in which each node keeps two synchronization tables, one mapping destination nodes to their reserved time (the transmitting table) and one mapping source nodes to their reserved time (the receiving table). When a node needs to transmit a packet, it first checks if the destination ID of the packet is present in the destination table. If it is, the node transmits the packet at the reserved time. Otherwise, a synchronization process is launched to synchronize the node with its potential receivers. During this process, a reservation is made for the following transmissions from the source node. Multiple transmissions from the same source node can profit from one synchronization. Moreover, the reservation tables of each node are used to avoid collisions of simultaneous transmissions from different source nodes.

Timer-based contention has been mainly addressed at the network layer [144–146]. *Watteyne et al.* proposed to use this approach in the MAC layer with 1-hopMAC [147], which is a semi-asynchronous transmitter initiated protocol. Using this scheme, nodes periodically wake up to listen the channel to check for forwarding requests. When a node needs to send a packet, it first sends a preamble long enough for neighboring nodes to receive it. The preamble must therefore lasts at least as long as the wake-up period. The preamble is made of micro-frames, each containing the instant at which the contention window begins. The node that initiated the communication, *i.e.* the sender, must keep its transceiver in the receive state from the beginning of the contention window until the first CTS frame is received. At the end of the contention window, all potential receivers, which have sent a CTS frame during the contention window, put their transceiver in the receive state to receive a small header from the sender containing the address of the selected next hop relay, *i.e.* the node that first sent a CTS. Then, all the receivers but the selected one turn their radio off, and the data exchange takes place between the selected node and the sender.

As OPWUM is also using timer-based contention, 1-hopMAC is the closest work to ours. However, 1-hopMAC suffers from high energy consumption caused by idle listening. With OPWUM, we propose to exploit emerging WuRx technologies to make timer-based contention energetically interesting.

7.2 Design of OPWUM

Timer-based contention enables the node to select a next hop relay according to a given metric without having any knowledge about its neighbors. When a node u wants to transmit a packet, it first broadcasts an RTS beacon. Then, each node v that received the RTS and is a potential receiver of u sets a backoff of duration $B(v) \in [0, D_c]$ where D_c is the contention window duration. $B(v)$ is function of a state metric $M(v)$: $B(v) = f(M(v))$. The better v behaves according to $M(v)$, the shorter $B(v)$ is. For example, if $M(v)$ is the remaining energy of v, the larger $M(v)$ is, the smaller $B(v)$ should be. When the backoff expires, a CTS is sent by v. u selects as the next hop relay the node which answered the first, and thus which has the best status according to the state metric. Thus, the next hop forwarder is opportunistically selected, and without requiring from the sender to have any knowledge about its neighbors. The choice of the metric is not discussed in this work, as it is application dependent.

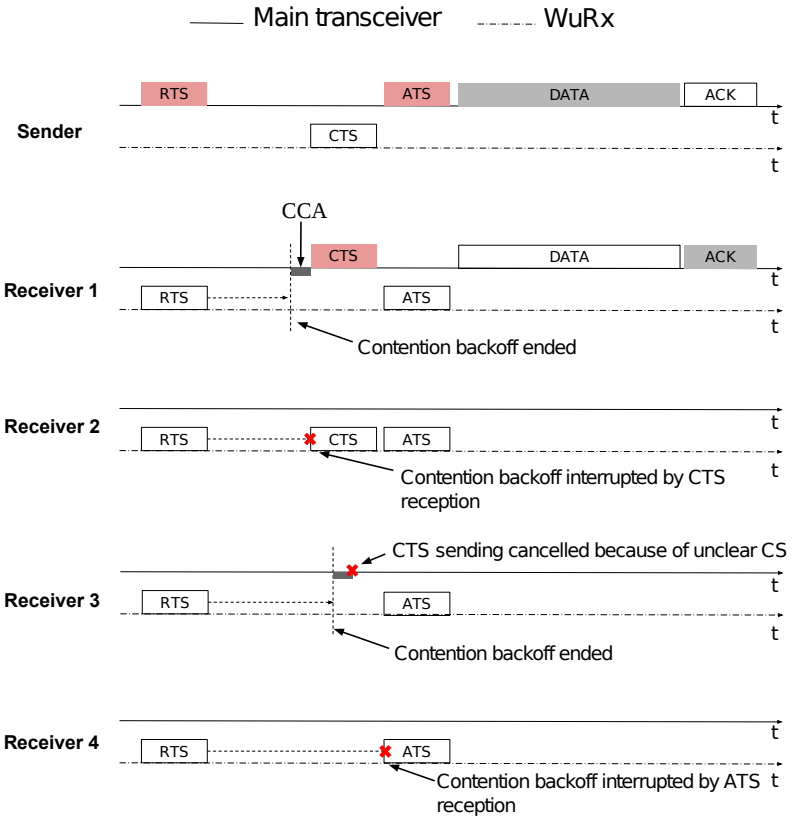

Figure 7.1 – Packet forwarding using OPWUM. Red color is used to represent WuCs transmission, gray color is used to represent data and ACK frames transmission, and white color is used to represented reception. The main transceiver channel is represented by a solid time line and the WuRx channel is represented by a dashed time line. CCA are represented by dark gray rectangles located under the time line.

Using OPWUM, it is assumed that each node is equipped with both a WuRx and a main transceiver that offers CCA capabilities. Figure 7.1 shows an example of packet forwarding using OPWUM. In this case, the sender has four potential receivers. After receiving an RTS WuC from the sender, each receiver sets a backoff computed from a state metric. In this example, the receiver 1 computes the shortest backoff, and thus is the first node to answer by sending a CTS WuC. Therefore, it is chosen by the sender to become the next hop relay. The receiver 2 also received the CTS sent by the receiver 1, causing the interruption of its backoff. Yet, the receivers 3 and 4 did not receive the CTS, for example because the receiver 1 is out of range of their WuRx, and must be informed that they have lost the contention. The receiver 3 backoff expires while the receiver 1 is sending a CTS WuC. Before each CTS sending, a CCA operation is performed to avoid CTS collisions. The receiver 3 CCA detects the activity on the channel, and thus cancels the CTS sending. Because the main transceivers usually have a much higher sensitivity than WuRx, it is possible that the CCA operation detects the CTS sending even if the CTS was not detected by the WuRx. When the sender receives the CTS from the first receiver, it sends an About To Send (ATS) WuC to inform the remaining nodes still competing that a next hop relay was already chosen. In this example, the receiver 4 receives the ATS and thus cancels its backoff. Finally, the data exchange takes place between the sender and the first receiver using the main transceiver.

WuC structure When using state of the art WuRx with data processing capabilities, only a few bytes of data can be embedded in the WuC. Moreover, because of the low sensitivity and bit rates of current WuRx, sending long WuC is energetically costly. Indeed, WuCs must be sent at high power to cope with the low sensitivity of WuRx, and at relatively low data rates (few kbps), incurring longer transmission time. Therefore, reducing the size of WuCs is an important

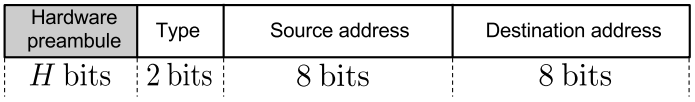

Figure 7.2 – Structure of WuC with OPWUM.

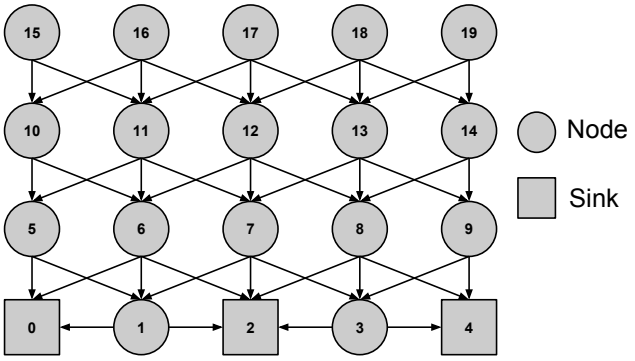

Figure 7.3 – Network used to compare OPWUM and 1-hopMAC. Arrows show the potential receivers of each node.

consideration when designing MAC protocols exploiting WuRx. The structure shared by the three WuCs types defined in OPWUM (RTS, CTS and ATS) is shown in Figure 7.2. The length of a WuC is $18 + H$ bits, where H is the length of the hardware preamble required by the WuRx (2 to 8 bits usually). The first field after the hardware preamble is the WuC type (RTS, CTS or ATS), which is indicated by a 2 bits field. Finally, the WuRx addresses of the sender and receiver are indicated, each using a 8 bits field. Allowing only 8 bits addresses may seem limiting regarding scalability, but WuRx addresses do not have to be similar to network addresses used by higher network layers. Indeed, as they are only used for one hop communications, they can be reused by nodes which do not share neighbors, while network addresses must be unique across the network.

Collisions and retransmission Collisions may lead to retransmissions, and therefore reducing collisions is an important issue when designing energy efficient sensor networks. Current semi-asynchronous MAC protocols use *rendez-vous* schemes to synchronize the source and destination nodes, increasing the risk of collisions when two nodes want to transmit to a same destination at the same time. OPWUM uses WuRx to achieve pure-asynchronous communication. Moreover, a node captures all the RTS, CTS and ATS WuCs sent by its neighbors allowing it to be informed when a transmission in which it is not involved is about to happen. In that case, the node enters a *silent state* for a predefined period during which it will not respond to RTS WuCs and postpones the sending of all packets to the end of the silent period. When the silent period expires, if there are packets to send, the node will wait for a random backoff before starting a transmission process to avoid collisions between multiple nodes leaving the silent state at the same time. Finally, to reduce the risk of collision between WuCs, a CCA is done before sending RTS or CTS WuCs.

Nevertheless, collisions can still occur when multiple nodes wake up at the same time and perform a CCA simultaneously. Wireless channel interference may also lead to the need of packet retransmission. When retransmission is needed, backoff strategy such as binary exponential backoff is used to efficiently resolve collisions.

7.3 Performance Evaluation

In this section, OPWUM and 1-hopMAC [147] are compared using exhaustive network simulations. 1-hopMAC is a state of the art MAC protocol using timer-based contention and described in Section 7.1. A converge-cast tree network shown in Figure 7.3, which is a common scenario in

Power consumed in the sleep state	0.6 μW
Power consumed in the receive state	22.2 mW
Power consumed when transmitting WuCs	80.1 mW
Power consumed when transmitting regular data frames	26.7 mW
Power consumed by the WuRx	196 nW

Table 7.1 – Values used for simulations.

WSN literature, is used.

7.3.1 Node Modeling and Simulation Settings

OPWUM and 1-hopMAC were implemented in GreenCastalia [62], an open-source simulation framework for the Castalia/OMNeT++ simulator [63] that focuses on energy modeling. A GreenCastalia module to model the WuRx from [2] was also implemented. All results were obtained by averaging the outcomes of a number of simulations large enough to obtain 95 % confidence interval and 5 % accuracy. Each run lasted 3600 s (simulated time). The WuRx considered presents data passing capabilities, a minimal power consumption of 1.83 μW and a sensitivity of -55 dBm. The hardware preamble length of WuCs was set to 1 byte, leading to a total WuC size of 26 bits. The main radio chip was a Texas Instrument CC1000, and the transmission powers were set to 10 dBm for WuCs and -5 dBm for non-WuC frames. WuCs were transmitted at a bit rate of 5 kbps and non-WuC frames were transmitted at 19.2 kbps. The size of the data frames was set to 30 bytes and the size of ACK frames to 8 bytes using the IEEE 802.15.4 physical layer. In these conditions, the power consumption of the radio chip and the transmission durations of the different frames are shown by Table 7.1.

7.3.2 Evaluated Scenario

The network shown in Figure 7.3 was considered. It is a static multi-hop network, with multiple sinks, which is widely used in monitoring applications. Given that it is a multi-hop network, intermediate nodes are in charge of forwarding packets from their immediate predecessors, and their immediate children do so for them. Moreover, every node, except the sinks, generates packets periodically. The packet generation period is denoted by T_g and is equal for all the nodes. Three sinks were used to avoid saturation of these when the packet generation period was set to low values. Because opportunistic routing is considered in this work, each node has multiple potential forwarders, shown by the arrows on Figure 7.3. By using timer-based contention, OPWUM and 1-hopMAC choose the next hop relay among these potential forwarders at each packet transmission attempt. For the latter, different wake-up periods, denoted by T_w, ranging from 100 ms to 400 ms are considered. Moreover, as we do not make any assumption about the state metric from which the contention backoff is computed, we assume that the contention backoff has no other constraint that being in the interval $[0, D_c]$. Therefore, it is chosen uniformly within this interval. OPWUM and 1-hopMAC are evaluated with respect to the following metrics:

- The total energy consumed by the network.
- The PDR.

7.3.3 Simulations Results: Energy Consumption

Figure 7.4 depicts the energy consumed by OPWUM and 1-hopMAC as a function of the packet generation period T_g, when the contention window D_c is set to 50 ms. We observe that the energy consumption of 1-hopMAC depends on the value of T_w. Indeed, in typical WSN scenarios, with relatively low traffic, high values of T_w tend to reduce the energy consumption of 1-hopMAC. OPWUM allows significant improvement on energy consumption, spending up to 5 times less

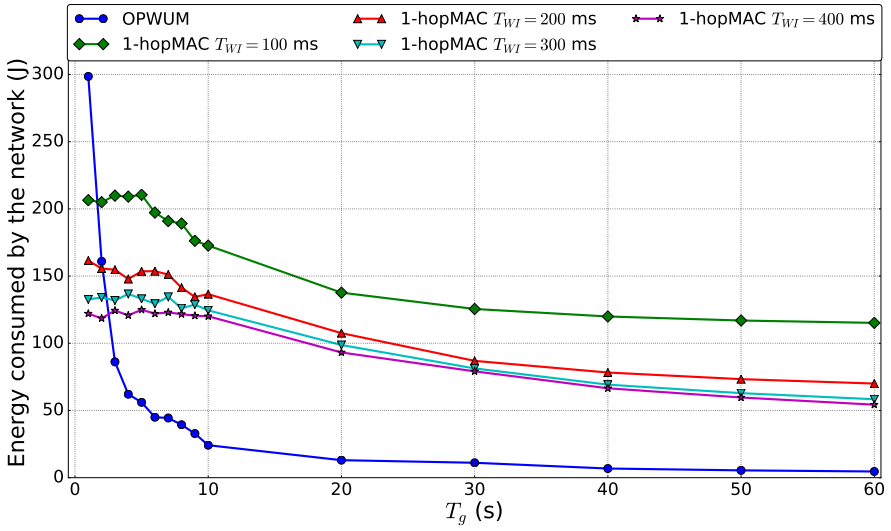

Figure 7.4 – Energy spent by the network as a function of packet generation period T_g. The contention window D_c is set to 50 ms.

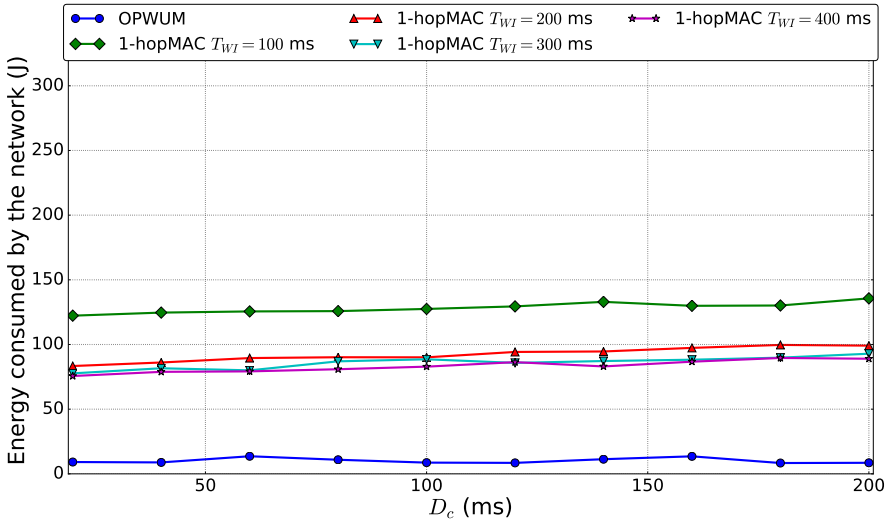

Figure 7.5 – Energy spent by the network as a function of the contention window duration D_c. T_g is set to 30 s.

energy than 1-hopMAC. The only exception is for high traffic, *i.e.* when T_g is less than 5 s. But, as we will see later, the PDR of 1-hopMAC collapses to almost 0 % when the traffic is high. In order to minimize the power consumption of 1-hopMAC, the optimal value of the T_{WI} needs to be computed for each node, and depends on both T_g and the packet arrival rate. As the packet arrival rate is usually not stationary, especially in the context of opportunistic routing, minimizing the power consumption of 1-hopMAC is not easy in practice, and the wake-up period is fixed once for all at the deployment of the network.

Figure 7.5 shows the energy spent by the network as a function of the contention window duration, when the packet generation period is set to 30 s. We can see that the contention window duration does not affect the power consumption of OPWUM, because all the next hop relay selection phase is done using WuCs only. Regarding 1-hopMAC, the consumed energy slowly increases with the contention window duration. Indeed, during the next hop relay selection phase, the sender must keep its transceiver in the receive state until it receives a CTS from a potential next hop relay. As higher contention window duration increases the average waiting time, it leads to higher

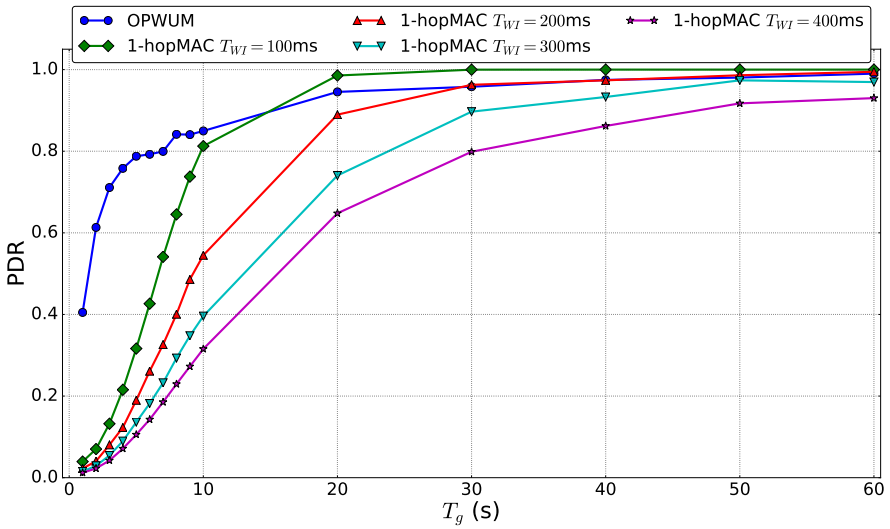

Figure 7.6 – Packet delivery ratio as a function of packet generation period T_g. The contention window D_c is set to 50 ms.

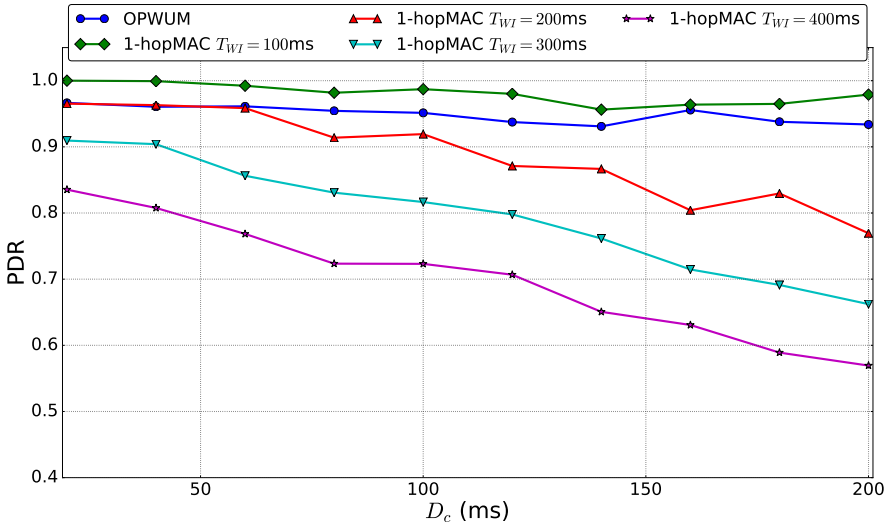

Figure 7.7 – Packet delivery ration as a function of contention period duration D_c. The packet generation period T_g is set to 30 s.

energy consumption.

7.3.4 Simulation Results: Packet Delivery Ratio

The PDRs of OPWUM and 1-hopMAC are shown in Figure 7.6 as a function of T_g, when D_c is set to 50 ms. For relatively high traffic, *i.e.* when T_g is less than 10 s, OPWUM outperforms 1-hopMAC. Moreover, the PDR never falls bellow 40 % with OPWUM, while it can reach almost 0 % with 1-hopMAC. For small traffic rates, *i.e.* when T_g is higher than 10 s, OPWUM performs similarly to 1-hopMAC with T_w set to 100 ms. But as shown in Figure 7.4, this configuration of 1-hopMAC is highly energy expensive. The other configurations of 1-hopMAC perform significantly worse, even when low traffic is considered. Figure 7.7 shows the PDR as a function of D_c, when T_g is set to 30 s. We can see that the PDR decreases when D_c increases for both protocols, but the decay rate is more significant for 1-hopMAC with high T_{WI} values. Indeed, longer contention windows increases the chances that neighboring nodes initiate a communication during the contention period, leading

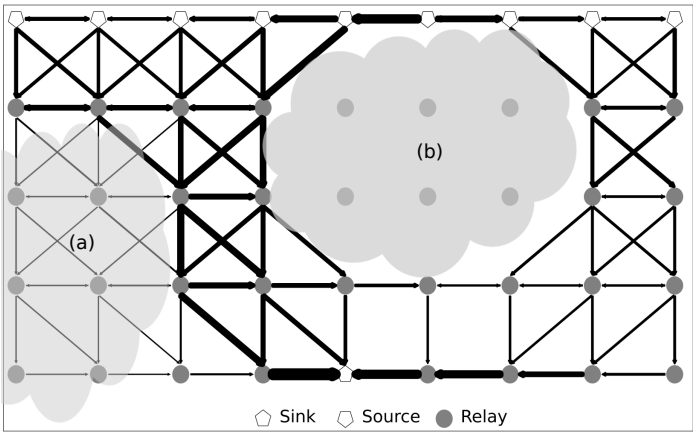

Figure 7.8 – Study case showing the effectiveness of OPWUM.

to collisions that can cause both communications to fail. Because of the silent state feature of OPWUM, presented in Section 7.2, this scenario is less likely to happen.

7.4 Application Case: Energy Harvesting Wireless Sensor Networks

To illustrate the effectiveness of OPWUM, the context of energy harvesting WSNs is considered, the grid network presented in Figure 7.8 was implemented in GreenCastalia. In this study case, the nodes of the upper row generate packets at an average frequency of one packet every 10 s (the source nodes), while one node gathers the generated packets (the sink node). All the other nodes only serve as relays. Every node, except the sink, is equipped with an energy harvesting device, e.g. a solar panel. The nodes located under the clouds (a) and (b) harvest less energy than the other nodes, and the cloud (a) is "thinner" than the cloud (b), meaning that energy harvesting rate of nodes located under the cloud (a) is higher than these of nodes under the cloud (b). The state metric $M(\cdot)$ used to compute contention backoffs is the energy harvesting rate, and thus the contention backoff is inversely proportional to the energy harvesting rate, *i.e.* high energy harvesting rate incurs small contention backoff. The simulation lasted 10000 s (simulated time). The set of potential receivers of each node is set using static routing tables, while OPWUM is used to opportunistically choose a forwarder among this set every time a packet needs to be sent. Potential receivers are neighboring nodes on the grid, located either on the same row or on the lower row.

Figure 7.8 shows the used links. In this figure, thicker arrows show the most used links. As we can see, only a few routing paths contain nodes from the area (a), while no routing paths contain nodes from the area (b). OPWUM enables the nodes to choose the potential receivers which harvest the most energy. As a result, the routing paths bypass the cloudy areas to reach the sink, thus allowing nodes to survive periods of energy scarcity.

7.5 Conclusion

In this chapter, WuRx and timer-based contention approach were combined to achieve energy efficient opportunistic forwarding. Indeed, the timer-based contention approach enables opportunistic relay selection without the requirement of extensive information exchange between a node and its neighbors. However, this is at the cost of high energy consumption in traditional implementation of this scheme. If reducing the contention window duration leads to lower energy consumption, this is at the cost of a significant drop of the PDR. The proposed cross-layer protocol, OPWUM, leverages WuRx to make timer-based contention energetically interesting. Indeed, OPWUM enables significantly lower power consumption that state of the art traditional approaches. Moreover, OPWUM leads to more reliable communications (higher PDR) when the traffic is dense.

In the context of energy harvesting, opportunistic forwarding is especially interesting to choose the most promising paths in the network, *i.e.* the ones that enable high quality of service while avoiding power outage of nodes. Further work includes studying OPWUM more deeply in this context and implementing this protocol on real hardware to perform more extensive evaluation.

Chapter 8

Combining Wake-up Receivers and Energy Harvesting in Star Networks

The first part of this thesis focuses on energy harvesting in WSNs, and two EMs were proposed to tackle the challenge of achieving energy neutrality in EH-WSNs. The aim of this chapter is to combine energy harvesting and WuRx in the context of data gathering star networks, in which a central sink to which all the other nodes are connected collects the data.

Our first goal was to implement Fuzzyman as it is presented in chapter 3. However, it was quickly found that the amount of harvested energy, required by Fuzzyman as an input, cannot be accurately estimated on the considered hardware. This led to the design of a novel EM inspired by Fuzzyman, called Rule-based EM (REM), which unlike most state of the art EMs, requires only the residual energy as an input.

As we focus on data gathering star networks, a novel MAC protocol, called Star NetWork MAC (SNW-MAC) leveraging WuRx is proposed [152]. SNW-MAC enables asynchronous communications, minimizes the cost of packet transmissions, and allows error corrections. SNW-MAC significantly reduces the energy cost variability of packet transmissions allowing accurate control of the consumed energy by the EM. The scalability of SNW-MAC is analytically studied in this chapter.

In addition to the new EM, SNW-MAC as well as PW-MAC and X-MAC were implemented on a testbed using the WuRx from [2] for evaluation. Experimentations were done in the context of indoor light, and the Energy Utilization Coefficient (EUC), is defined and used as an evaluation metric.

The remainder of this chapter is organized as follows. Section 8.1 presents REM, and introduces the EUC metric. Section 8.2 details the design of SNW-MAC, and presents an analytical study of its scalability. Section 8.3 exposes the experimental setup used to evaluate our approach, and Section 8.4 presents the experimental results. Finally, Section 8.5 concludes this chapter.

8.1 Design of REM

The design of REM is presented in this section. The task of the EM is to dynamically adjust the performance of the node, evaluated in this work by the packet generation rate, according to the current residual energy. REM can be used in collaboration with various MAC protocols. Later, we show the benefits of combining REM with the SNW-MAC protocol leveraging WuRx introduced in Section 8.2.

We assume that the time is divided into time slots of equal duration T_s, and that the EM is executed at the beginning of each slot to set the packet generation rate of the node for the current slot k. At each execution, REM measures the current residual energy denoted by e_r, and computes the wake-up interval for the next slot denoted by T_{WI}, *i.e.* the time between the sending of two packets. Two submodules compose REM as shown in Figure 8.1. The Energy Budget Computation (EBC) module evaluates the energy that the node should consume in the next time slot k to remain sustainable. This amount of energy is the energy budget and is denoted by $e_b[k]$. The inputs to the EBC are the current residual energy and the variation of residual energy, respectively denoted

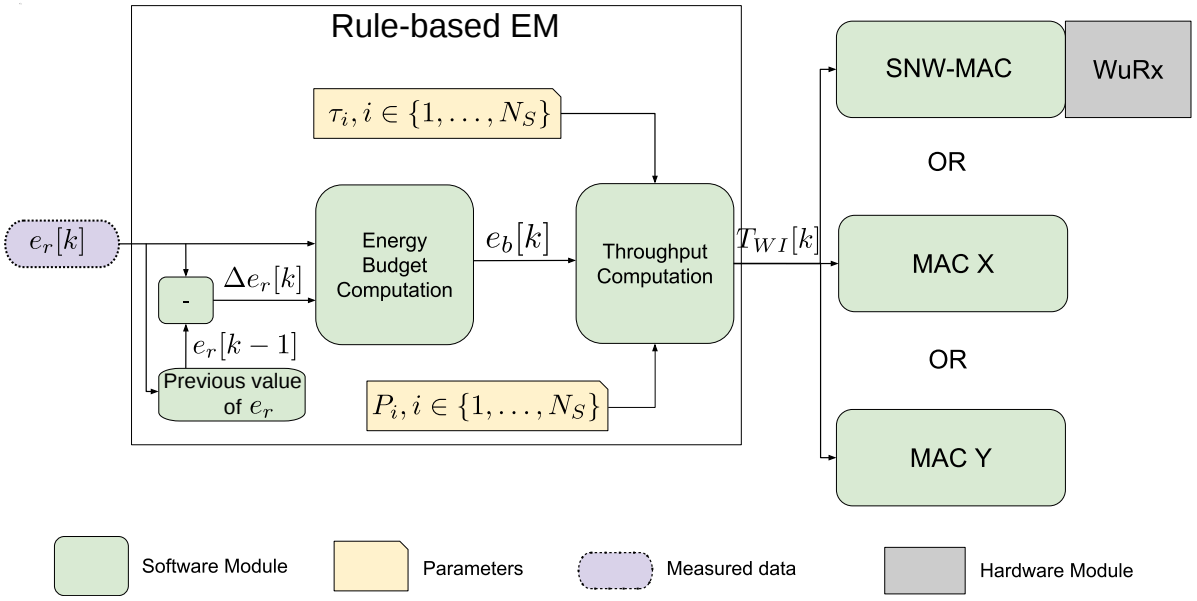

Figure 8.1 – Software architecture with detailed view of REM structure. The design of the propSNW-MACprotocol is detailed Section 8.2.

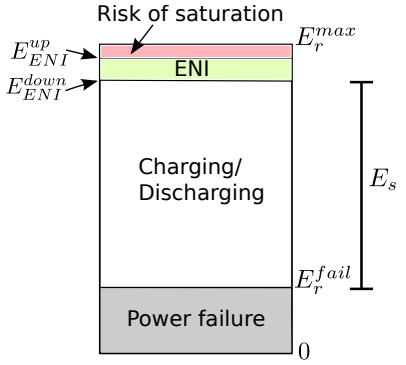

Figure 8.2 – Energy storage device levels.

by $e_r[k]$ and $\Delta e_r[k]$ defined by:

$$\Delta e_r[k] = e_r[k] - e_r[k-1]. \tag{8.1}$$

The second module is the Throughput Computation (TC) module, which calculates the wake-up interval $T_{WI}[k]$ according to the energy budget $e_b[k]$. When the topology is a star network, the only task of a node is to perform a measurement and to send the so generated data to the sink. In multi-hop networks, each node must also relay packets sent by other nodes.

8.1.1 EBC Design

Most of the EMs presented in the literature assume the availability of the harvested and consumed energy values [18,44]. However, precise tracking of these values is difficult and their implementation incurs high overhead [66], which motivates the design of an EM that only requires the residual energy. The aim of the EBC is to keep the device in the ENO-MAX state, *i.e.* the amount of consumed energy equals the amount of harvested energy over long period of time [19], by dynamically adapting the energy budget. Four residual energy levels of the energy storage device are defined and shown in Figure 8.2. E_r^{max} is the energy storage capacity, and E_r^{fail} is the hardware failure threshold, which identifies the minimal energy level ensuring the correct supply of the device. E_r^{fail} and E_r^{max} are hardware dependent. An Energy Neutral Interval (ENI) is defined by two

Δe_r \ e_r	$[E_r^{fail}, E_{ENI}^{down}]$	$[E_{ENI}^{down}, E_{ENI}^{up}]$	$[E_{ENI}^{up}, E_r^{max}]$
< 0	$\mu_D(e_r)\,\Delta e_r$	$-\Delta e_b$	0
$= 0$	$-\Delta e_b$	0	Δe_b
> 0	$\mu_C(e_r)\,\Delta e_r$	Δe_b	Δe_b

Table 8.1 – Energy storage levels and rule base used to compute δe_b.

energy thresholds E_{ENI}^{up} and E_{ENI}^{down} such that $E_r^{fail} < E_{ENI}^{down} < E_{ENI}^{up} < E_r^{max}$ as illustrated in Figure 8.2. If the stored energy falls below E_r^{fail}, a power outage occurs. On the other hand, if the energy storage device is full, *i.e.* the amount of stored energy is E_r^{max}, then the excess of harvested energy is wasted, as it cannot be stored. This situation is called a *saturation* of the energy storage device. To avoid saturation, E_{ENI}^{up} should be chosen such that $E_{ENI}^{up} < E_r^{max}$, which allows the EBC to avoid waste of energy by overflow of the storage device. Moreover, the *energy stock* $E_s = E_{ENI}^{down} - E_R^{fail}$ is defined as the amount of energy required to ensure the operating of the device during periods without intake energy from the harvester, and depends on the application and the energy source characteristics. Therefore, E_s is the amount of energy that should be stored in the energy storage device to avoid power outage in case of energy scarcity periods. The aim of the EBC is to keep the state of charge of the energy storage device in the ENI $[E_{ENI}^{down}, E_{ENI}^{up}]$ when environmental energy is available, thus avoiding waste of energy by saturation of the storage device, while storing enough energy to survive periods during which no energy is harvested.

Ensuring the minimum quality of service required by the application necessitates a minimum energy budget per slot denoted by E_b^{min}. At each execution of the EBC, the energy budget of the next slot k is computed as follows:

$$e_b[k] = \max\Big(E_b^{min}, e_b[k-1] + \delta e_b[k]\Big), \tag{8.2}$$

where $\delta e_b[k]$ is the *energy budget correction*, which is calculated according to the current values of e_r and Δe_r. Table 8.1 summarizes the EBC strategy. In this table, Δe_b is a positive parameter of the EM and corresponds to the energy budget correction when the amount of stored energy is either in the ENI interval or in the risk of saturation interval. As most applications do not perform well under strong variations of the allocated energy budget, choosing Δe_b requires a compromise between the reactiveness of the EBC and the variability of the allocated energy budget. Four scenarios can be considered from Table 8.1 and are detailed thereafter.

Risk of saturation A risk of saturation occurs when $e_r > E_{ENI}^{up}$. To avoid waste of energy by overflow of the energy storage device, the EBC increases the energy budget until the residual energy decreases to bring it to a value belonging to the ENI.

Energy neutral interval If the amount of residual energy belongs to the energy neutral interval, the EBC goal is to keep the node in the ENO-MAX state. The ENO-MAX state is achieved when the residual energy is kept constant with regard to time, and the EBC thus corrects the energy budget regarding the sign of Δe_r to keep the node in the ENO-MAX state.

Charging State The node is considered to be in charging state when $e_r < E_{ENI}^{down}$ and Δe_r is positive. The node is thus re-filling its energy stock. In these conditions, the goal of the EBC is to keep the residual energy increasing for the amount of stored energy to be greater or equal than E_s, *i.e.* for the residual energy to reach the ENI in a reasonable time, while allocating a high enough energy budget to ensure a good quality of service. A trade-off must be made between the charging time and the quality of service. Indeed, at one extreme, a conservative policy is to allocate the minimal energy budget while the energy storage device is not fully charged, leading to a quick refill of the storage device at the cost of a low quality of service during the charging phase. On the other hand, allocating almost all the harvested energy will lead to a slow charging rate, but to a

good quality of service, regarding the currently available environmental energy, during the charging phase. As the choice of an appropriate strategy is dependent on the application, a tunable strategy is proposed. The energy budget correction δe_b is set to a value proportional to the residual energy variation Δe_r and the proportionality factor is a function of e_r denoted by $\mu_C(e_r)$:

$$\mu_C(e_r) = \kappa'_C \left(1 - \left(1 - \frac{e_r - E_r^{fail}}{E_{ENI}^{down} - E_r^{fail}}\right)^{\kappa_C}\right), \tag{8.3}$$

where κ'_C and κ_C are positive parameters allowing the tuning of the charging strategy. μ_C increases with e_r as the more energy is stored, the less conservative we need to be. While κ'_C sets the maximum value of the proportionality factor, κ_C sets the growth rate of μ_C. If $\kappa_C = 1$, δe_b increases linearly with e_r. For values of κ_C lower than one, the growth rate increases when the residual energy increases, while for values of κ_C higher than one, the growth rate decreases when e_r increases.

Discharging State The node is considered to be in discharging state when $e_r < E_{ENI}^{down}$ and Δe_r is negative. The node is thus using its energy stock. In this scenario, a trade-off must be made between the allocated energy budget and the lifetime of the node, *i.e.* the time it can last before running into a power outage. A conservative policy is to set the energy budget to the minimum required, hence maximizing the lifetime at the cost of a low quality of service. On the other hand, setting the energy budget to an arbitrary high value leads to high quality of service at the cost of short lifetime. Similarly to what has been done for the charging state, a customizable energy management, that can be tuned according to the need of an application, is proposed. The energy budget correction δe_b is set at a value proportional to the residual energy variation Δe_r and the proportionality factor is a function of e_r denoted by $\mu_D(e_r)$:

$$\mu_D(e_r) = \kappa'_D \left(1 - \frac{e_r - E_{ENI}^{down}}{E_{ENI}^{down} - E_r^{fail}}\right)^{\kappa_D}, \tag{8.4}$$

where κ'_D and κ_D are positive parameters allowing the tuning of the discharging strategy. μ_D decreases with e_r as the less energy is stored, the more conservative we must be, and the impact of κ_D and κ'_D on the discharging strategy are similar to the ones of κ_C and κ'_C on the charging strategy.

8.1.2 TC Design

The TC aims to compute the packet generation rate of the node over a time slot to consume the amount of energy specified by the EBC. As wireless communications are usually the most consuming task over all the other tasks such as sensing and computing [10], the packet generation rate of the node given an energy budget strongly depends on the MAC protocol.

To transmit a single packet, a given MAC protocol typically requires many steps, such as receiving/sending a beacon frame, sending a data frame, receiving an ACK... The number of states in which the node can be when communicating using a given protocol is denoted by N_S. Each state is defined by the state of the MCU (typically sleeping or active) and the state of the radio chip (typically sleeping, idle, receiving, transmitting). The time spent in the state $i \in \{1, \ldots, N_S\}$ during a single packet transmission is denoted by τ_i, and the corresponding power consumption of the node is denoted by P_i. The energy cost of the whole process to send a single packet is therefore:

$$c_t = \sum_{i=1}^{N_S} \tau_i P_i, \tag{8.5}$$

and the energy consumed by the node over one time slot k is:

$$e_c[k] = \frac{T}{T_{WI}[k]} c_t + \left(T - \frac{T}{T_{WI}[k]} \tau_t\right) P_S, \tag{8.6}$$

where P_S is the power consumption of the node when both the MCU and the radio chip are sleeping, and τ_t is the total time required to send a packet and is equal to $\tau_t = \sum_{i=1}^{N_S} \tau_i$. Therefore, in order

for the consumed energy $e_c[k]$ to be equal to the energy budget $e_b[k]$, the wake-up interval is set to the following value:

$$T_{WI}[k] = \frac{c_t - \tau_t P_S}{\frac{e_b[k]}{T} - P_S}. \tag{8.7}$$

This equation is obtained by replacing $e_c[k]$ by $e_b[k]$ in (8.6). The associated packet generation rate, in packets per minute, is thus $\frac{60}{T_{WI}[k]}$.

If we assume low data-rate application, typical in EH-WSNs, usual MAC protocols are based on pseudo-asynchronous approaches, which make the estimation of the τ_i values challenging. Indeed, *rendez-vous* schemes incur high variability of the time spent in the idle state and receive state for different packet transmissions. As a consequence of an inaccurate estimation of these values, the energy consumed by the node can be significantly different from the energy budget calculated by the EBC, which can lead to power failures or energy wastes. Therefore, in Section 8.2, a new protocol reducing the energy consumption variability of packet transmission is proposed.

8.1.3 Energy Utilization Coefficient

To evaluate the energy efficiency of different MAC protocols, the EUC, denoted by ζ, is defined as the ratio of the packet generation rate to the energy budget:

$$\zeta(e_b) = \frac{\text{Packet rate in packets per minute}}{e_b} = \frac{60}{e_b T_{WI}}. \tag{8.8}$$

It is expressed in packets per minute and per Joule. For notational simplicity, the slot number indication "$[k]$" is omitted in the rest of this section, and all the following equations refer to a single time slot. The EUC quantifies the achieved packet generation rate of a MAC protocol regarding the available energy budget, and is similar to other energy efficiency metrics e.g. [153, 154].

By combining (8.7) and (8.8) we obtain:

$$\zeta(e_b) = \frac{1}{HT} - \frac{P_S}{H}\frac{1}{e_b}, \tag{8.9}$$

where H (in Joule) is defined by:

$$H = c_t - \tau_t P_S. \tag{8.10}$$

H is a constant particular to a given hardware and MAC protocol. Indeed, the τ_i values depend on the MAC protocol while the P_i and P_S values depend on the hardware. Two remarks can be done regarding (8.9). First, the EUC is not constant for a given hardware and MAC but increases with the energy budget e_b. Secondly, the EUC is bounded, as:

$$\zeta_\infty = \lim_{e_b \to \infty} \zeta(e_b) = \frac{1}{HT}. \tag{8.11}$$

From (8.11) it can be observed that the maximum EUC ζ_∞ is higher for small values of H. Therefore, the smaller H is, the better it is. For the rest of this work, the P_i values are assumed to be fixed and the power consumption in sleep state P_S is supposed to be much smaller than the power consumption of the other states P_i. This assumption holds true for all the WSN platforms. Hence, minimizing H is done by minimizing the τ_i values. In order for H to be minimal, only the data frame should be sent at each packet transmission. However, most of the MAC protocols introduce an overhead to synchronize the nodes (e.g. *rendez-vous* process in pseudo-asynchronous MAC protocols) or for error control (e.g. ACK frames). As we will see in the next section, using WuRx allows the minimization of H, and hence the maximization of the EUC.

8.2 Leveraging Wake-up Receivers in Star Networks

SNW-MAC leverages WuRx to enable asynchronous communication, minimizing the energy required to transmit a packet and making collisions impossible between packets sent by nodes belonging to a same SNW-MAC-based network. It is assumed that a physical layer providing an error detection mechanism is used. For example, the widespread IEEE 802.15.4 physical layer provides a Cyclic Redundancy Check (CRC) error detecting code.

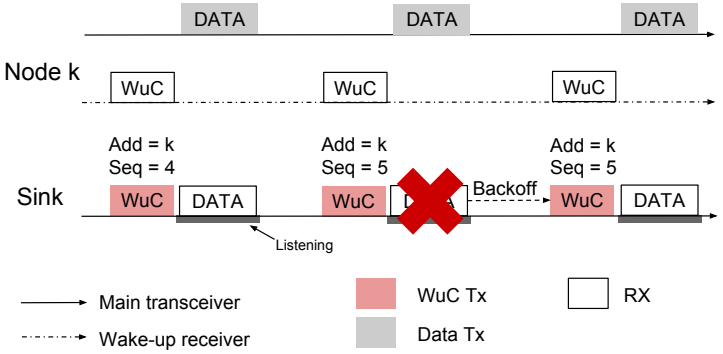

(a) Packet transmission using SNW-MAC

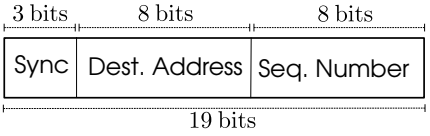

(b) WuC structure.

Figure 8.3 – SNW-MAC packet transmission illustration and WuC format.

8.2.1 Design of SNW-MAC

SNW-MAC is an asynchronous scheme that uses the receiver-initiated approach to minimize the energy consumption of WSN nodes. As the power consumption of WuRx has to be orders of magnitude less than the main radio, these devices are usually characterized by low sensitivity and low data rate [2, 155], as seen in Chapter 6. For this reason, sending WuCs to a WuRx can be energy-wise costly as it is done at low bit rate and high transmission power to achieve the same range as the main radio.

Packet transmission using SNW-MAC is illustrated in Figure 8.3a. The sink initializes a communication by sending a WuC containing the address of a specific sensor node, and then listens to the channel to receive the data packet. The targeted sensor node is awaken by its WuRx, and starts sending the data packet. Each sensor node piggybacks its wake-up interval in data packets. The sink keeps an updated table that associates for each node its wake-up interval, and polls each node at the right time. Compared to traditional receiver-initiated protocols, this approach reduces the energy consumption of the sink and the nodes as no *rendez-vous* process is required. The sink energy consumption is further reduced as useless periodic WuCs sendings are avoided. Because the wake-up interval is typically a 16 bit integer, minimal overhead is incurred by the piggybacking of this information. Moreover, the sink can use it to monitor the sensor node activity.

Error control and retransmission By coordinating data packet transmission at the sink, SNW-MAC cancels the risk of collisions compared to traditional pseudo-asynchronous schemes as each node is specifically polled. However, wireless channel interferences may lead to corrupted frames, and energy-efficient error control and packet retransmission is therefore an important issue. As the sink is entirely in charge of coordinating the packet transmission, it is responsible for detecting transmission errors and scheduling another attempt. Each WuC embeds an 8 bit sequence number of the expected data packet in addition to the 8 bit address of the wireless sensor node to be polled and 3 synchronization bits (imposed by the hardware) as shown in Figure 8.3b. Therefore, a WuC is 19 bit long. The sink keeps an updated table that associates for each node the next packet sequence number to poll. When a sensor node WuRx acquires a WuC, it reads both the address and the sequence number. The WuRx is assumed to embed data processing capabilities, as explained in Section 6.1, and it wakes up the node MCU only if the address is valid, and then sends to it the sequence number. All the packets, which have sequence number lower than the one received are considered as either successfully received or dropped because of a too high number of transmission attempts, and are erased from the transmission buffer. The packet which has the sequence number asked by the sink is then sent. Using this mechanism, when the sink detects

a transmission failure, e.g. the received data packet is corrupted, it sets a random backoff and, when the backoff expires, it initiates a new communication using the same sequence number, as illustrated in Figure 8.3a. Compared to traditional error-control schemes that require ACK frames, the energy overhead is significantly reduced for sensor nodes as they do not need to listen to ACK frames after each data packet transmission. On the sink side, as no ACK frame is sent, energy is also saved. Nonetheless, this energy saving is counterbalanced by longer WuCs sent by the sink due to the sequence number.

Using SNW-MAC, only the data frame is sent by the nodes, thus minimizing the per-packet energy consumption and the H value introduced in Section 8.1.2. Moreover, the per-packet energy consumption variability is also minimized if the data frame length does not change. Indeed, the only possible cause of energy consumption variability is due to retransmissions. Having a low energy consumption variability is important to allow the EM to accurately control the energy consumption of the node.

8.2.2 Analytical Study of the Scalability

In this section, the scalabilities of SNW-MAC and traditional pseudo-asynchronous MAC protocols are evaluated in the context of star networks. The number of nodes that compose the network is denoted by N_N (not including the sink), and the packet generation rate is modeled by a Poisson distribution of parameter λ packets per minute. Next, expressions of the packet arrival rate at the sink are derived for SNW-MAC and pseudo-asynchronous MAC protocols when it is assumed that the only cause of packet loss is collisions, and that all collisions are destructive, *i.e.* lead to corrupted packets.

SNW-MAC Packets collisions are impossible SNW-MACas the sink specifically polls each node. Nonetheless, as receiving a packet requires a non-null duration, the receiving rate is still bounded. The total time required to receive a packet is denoted by τ_r and is defined by:

$$\tau_r = \tau_d + \tau_o, \tag{8.12}$$

where τ_d is the time required to receive the data payload and τ_o is the overhead incurred by the hardware and the protocol at each packet reception (WuC sending, radio setup, turn-around time, software overhead). The maximum receiving rate in packets per minute is thus:

$$\Gamma = \left\lfloor \frac{60}{\tau_r} \right\rfloor, \tag{8.13}$$

where $\lfloor \cdot \rfloor$ is the floor function. We assume that the packet generation rates of the nodes are independent from each other and are modeled by Poisson distributions of mean λ packets per minute, and we denote by A the aggregate rate. As Poisson distributions are stable by sum, A follows a Poisson distribution of mean λN_N packets per minute. However, because the maximum receiving rate of the sink is Γ, the receiving rate of the sink, denoted by R, is modeled by the following distribution:

$$\Pr(R=k) = \begin{cases} \Pr(A=k) = \frac{(\lambda N_N)^k}{k!} e^{-\lambda N_N} & \text{if } 0 \leqslant k < \Gamma \\ \sum_{i=\Gamma}^{\infty} \Pr(A=i) = \sum_{i=\Gamma}^{\infty} \frac{(\lambda N_N)^i}{i!} e^{-\lambda N_N} & \text{if } k = \Gamma \\ 0 & \text{if } k > \Gamma \end{cases} \tag{8.14}$$

Indeed, the sink saturates when the receiving packet generation rate reaches Γ, and therefore higher receiving packet generation rates are impossible as the sink cannot poll the nodes quickly enough. The average packet generation rate is thus:

$$\chi_{r,SNW-MAC} = \mathbb{E}[R] = \sum_{k=0}^{\infty} k \Pr(R=k) = \sum_{k=1}^{\Gamma-1} k \frac{(\lambda N_N)^k}{k!} e^{-\lambda N_N} + \Gamma \sum_{k=\Gamma}^{\infty} \frac{(\lambda N_N)^k}{k!} e^{-\lambda N_N}. \tag{8.15}$$

As:

$$\sum_{k=\Gamma}^{\infty} \frac{(\lambda N_N)^k}{k!} = e^{\lambda N_N} - \sum_{k=0}^{\Gamma-1} \frac{(\lambda N_N)^k}{k!}, \tag{8.16}$$

we finally have:

$$\chi_{r,SNW-MAC} = e^{-\lambda N_N} \sum_{k=0}^{\Gamma-1} k \frac{(\lambda N_N)}{k!} + \left(1 - e^{-\lambda N_N} \sum_{k=0}^{\Gamma-1} \frac{(\lambda N_N)^k}{k!}\right) \Gamma. \tag{8.17}$$

Pseudo-asynchronous MAC Using traditional pseudo-asynchronous MAC, the sink periodically wakes up to receive data packets, and the sink wake-up interval is denoted by T_u. The time is thus divided into equal length time slots of duration T_u. When a node generates a packet, it typically tries to send it at the sink next wake-up. The number of packets, denoted by X, generated by a given node over a time slot can be modeled by a Poisson distribution of parameter $\frac{\lambda T_u}{60}$. Therefore, the probability that a node generates packets in a time slot is:

$$p_g = \Pr(X \geqslant 1) = 1 - \Pr(X = 0) = 1 - e^{-\frac{\lambda T_u}{60}}. \tag{8.18}$$

Let Y be the number of nodes that have generated packets over a time slot. Y can be modeled by a binomial distribution of parameter p_g. As the Y nodes will try to send a packet at the next sink wake-up, and if we assume that all the collisions are destructive, the number of packets received by the sink during a time slot is a function of Y denoted by $R'(Y)$ and defined by:

$$R'(Y) = \begin{cases} 0 & \text{if } Y = 0 \\ \mathbb{E}[X|X \geqslant 1] & \text{if } Y = 1 \\ 0 & \text{if } Y > 1 \end{cases} \tag{8.19}$$

the last case being the collision scenario. Also:

$$\mathbb{E}[X|X \geqslant 1] = \sum_{k=1}^{\infty} k \Pr(X = k|X \geqslant 1), \tag{8.20}$$

and for $k \geqslant 1$:

$$\Pr(X = k|X \geqslant 1) = \frac{\Pr(X = k, X \geqslant 1)}{\Pr(X \geqslant 1)} = \frac{\Pr(X = k)}{p_g}, \tag{8.21}$$

leading to:

$$\mathbb{E}[X|X \geqslant 1] = \frac{\mathbb{E}(X)}{p_g} = \frac{\lambda T_u}{60 p_g}. \tag{8.22}$$

Therefore, the average number of packets received during a time slot is:

$$\mathbb{E}\left[R'(Y)\right] = \sum_{i=1}^{n} R'(Y = i) \Pr(Y = i) = \mathbb{E}[X|X \geqslant 1] \Pr(Y = 1) = \frac{N_N \lambda T_u}{60} e^{-(N-1)\frac{\lambda T_u}{60}}, \tag{8.23}$$

and the average receiving rate $\chi_{r,PAM}$ in packets per minute is thus:

$$\chi_{r,PAM} = \frac{60\mathbb{E}[R'(Y)]}{T_u} = N_N \lambda e^{-(N-1)\frac{\lambda T_u}{60}}. \tag{8.24}$$

Figure 8.4 shows $\chi_{r,SNW-MAC}$ and $\chi_{r,PAM}$ for values of N_N ranging from 0 to 100 and values of λ ranging from values of 0 to 300 packets per minute. Both τ_r and T_u where set to 40 ms for fairness, leading to $\Gamma = 1500$ packets per minute for SNW-MAC. As we can see, $\chi_{r,SNW-MAC}$ increases until reaching Γ. The sink then saturates and the receiving packet generation rate stops increasing. On the other hand, $\chi_{r,PAM}$ first increases with λ and N_N, but decreases after reaching a maximum because of collisions, limiting its scalability. Moreover, the maximum reached by $\chi_{r,PAM}$ is more than twice smaller than the maximum reached by $\chi_{r,SNW-MAC}$. These numerical results show the better scalability of SNW-MAC. Finally, it is important to notice that T_u was set to the same value as τ_r when plotting Figure 8.4 for fairness. However, in real scenario, the sink wake-up interval is usually set to a much higher value than the packet reception duration to achieve low duty cycles and save energy, reducing moreover the scalability of pseudo-asynchronous MAC protocols.

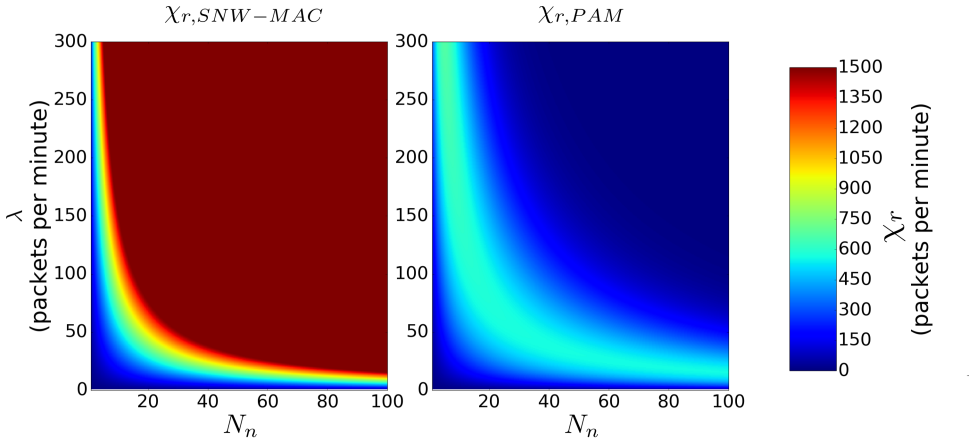

Figure 8.4 – $\chi_{r,SNW-MAC}$ and $\chi_{r,PAM}$ as a function of n and λ when $T_u = \tau_r = 40\,\text{ms}$.

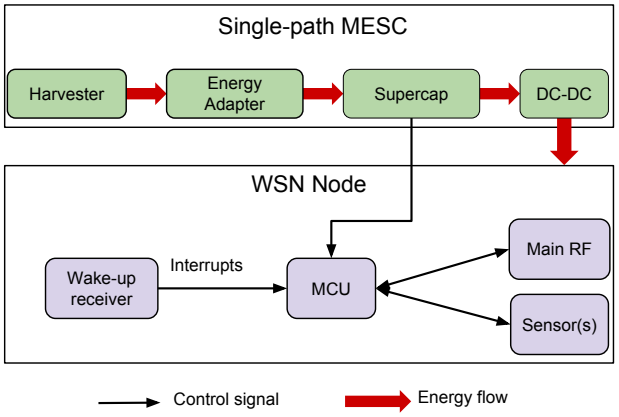

Figure 8.5 – Hardware architecture of a WSN node using the MESC architecture and a WuRx.

8.3 Experimental Setup

8.3.1 Node Architecture

Multiple EH-WSN platforms have been proposed by academia and industry over the last decade [156, 157]. In this work, we consider a single-path architecture version of the Multiple Energy Source Converter (MESC) architecture proposed in [158]. In single-path architecture, there is only one energy storage device and all the harvested energy is used to charge the storage device which directly powers the node through a DC-DC converter. Figure 8.5 shows the block architecture of MESC that can be used with a variety of energy harvesters (photo-voltaic cells, thermoelectric generators and wind turbines) using the appropriate energy adapter to normalize the output energy. Supercapacitors were chosen as storage devices as they are more durable and offer a higher power density than batteries [159]. In this work, the PowWow platform [99], based on the MESC architecture and equipped with a Texas Instrument CC1120 radio chip, is used as testbed. The energy storage device is a 0.9 F supercapacitor with a maximum voltage of 5.0 V, and the minimum voltage required to power the node is 2.8 V. PowWow embeds a voltage measurement chip, the INA3221 from Texas Instrument, which allows measurement of the supercapacitor voltage, denoted by V_c, with a precision of 0.1 mV. The residual energy e_r can thus easily be computed as follows:

$$e_r = \frac{1}{2} C {V_c}^2, \tag{8.25}$$

where C is the supercapacitor capacitance. When SNW-MAC is evaluated, the WuRx is added to the node, and the so-obtained mote is shown in Figure 8.6. REM, introduced in Section 8.1, was

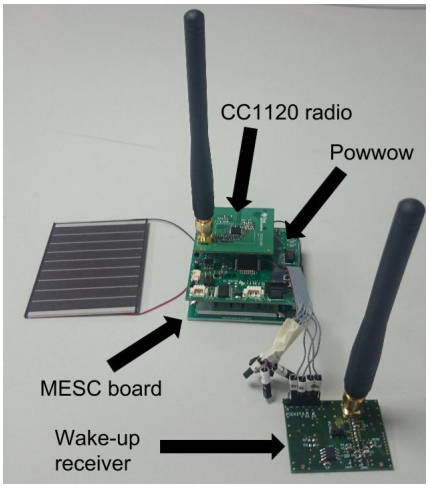

Figure 8.6 – PowWow node equipped with an ULP WuRx.

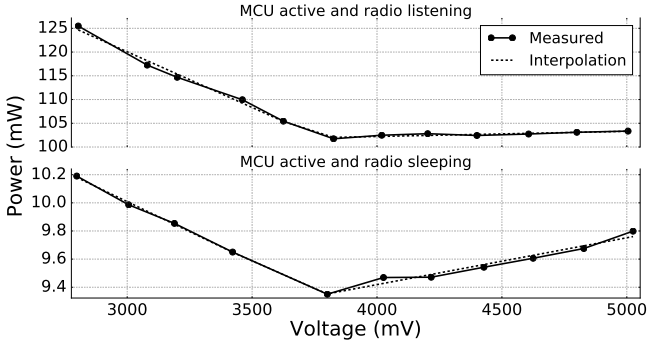

Figure 8.7 – Power consumption of the node when (i) the MCU is active and the radio is listening and when (ii) the MCU is active and the radio is sleeping for different input voltages of the DC-DC converter.

implemented on PowWow, as well as SNW-MAC introduced in Section 8.2 and two other state of the art MAC protocols presented in Section 6.2. The parameters used for experimentations are shown by Table 8.2.

As the supercapacitor supplies the node via a DC-DC converter as shown in Figure 8.5 and the efficiency of the DC-DC converter varies with the input voltage, the power consumed by the node depends on the charge of the supercapacitor. Therefore, the power consumption of each of the N_S states (introduced in section 8.1.2) was measured for different input voltages of the DC-DC converter ranging from 2.8 V to 5.0 V, and piecewise linear interpolation was used to get the P_i values as functions of the supercapacitor voltage. The considered states were: MCU active and transceiver sleeping, MCU active and transceiver idle, MCU active and transceiver listening, MCU active and transceiver transmitting data frame and MCU active and transceiver transmitting WuC frames. Figure 8.7 shows the so obtained measures and the corresponding interpolated functions for two states of the node. As we can see, piecewise linear interpolation permits an accurate modeling of the node power consumption. This model is used by the nodes, and more precisely by the TC unit, to achieve accurate control of the energy consumed.

One of the requirements of a WuRx is the very low power consumption as it is always active, even when all the other components are in sleep state. The power consumption of the WuRx was measured to be 1.83 μW when the radio front-end is active and the PIC is in sleep state and 284 μW when the PIC is active at 3.3 V and is parsing the received data at 2 MHz. Therefore, the WuRx power consumption becomes significant when the PIC is active. At each wake-up, the PIC is active for 19 ms to perform address matching. Hence, the energy consumed by the WuRx at each wake-up of the PIC is 5.40 μJ. If we consider a typical node, not using a WuRx, but using the duty-cycling approach with a duty-cycle set to a typical value of 0.05% and consuming 100 mW when the transceiver is active, then the total energy consumed by this node over a period of 24 h is

Parameters		Values
MAC	Sink wake-up interval (X-MAC and PW-MAC)	250 ms
	Maximum number of retransmissions	2
Physical layer	WuB bit rate	1 kbps
	Data/ACK/beacon bit rate	20 kbps
	WuB transmission power	12.5 dBm
	Data/ACK/beacon transmission power	−6 dBm
EBC	κ'_C	0.01
	κ_C	2.0
	κ'_D	0.5
	κ_D	2.0
	Δe_b	5 mJ
	E_r^{fail}	3.528 J
	E_{ENI}^{down}	12.40 J
	E_{ENI}^{up}	12.45 J
	E_r^{max}	12.50 J

Table 8.2 – Parameters used for the experimentations.

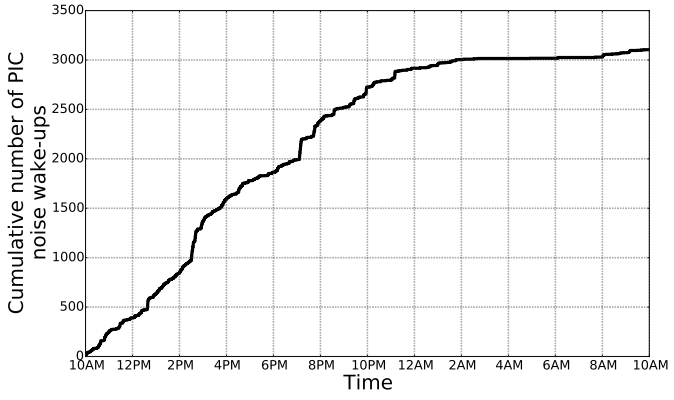

Figure 8.8 – False wake-ups of the PIC over a 24 h period in an indoor environment.

4.32 J. This amount of energy corresponds to more than 8×10^5 wake-ups of the PIC. The number of "false" PIC wake-ups, *i.e.* wake-ups not caused by WuCs but by the wireless channel noise, was measured over a period of 24 h in an indoor environment. Figure 8.8 shows the total cumulative number of false wake-ups according to time. It is not surprising to observe that most of the false wake-ups happen during daytime. In total, 3110 false wake-ups were accounted over a 24 h period, which is two orders of magnitude below the previously considered scenario assuming a typical 0.05% duty-cycle. Moreover, no false wake-ups of the main MCU happened. These results show the importance of the ULP MCU embedded in the WuRx. Indeed, performing address matching by a ULP MCU avoids numerous false wake-ups of the node MCU, which power consumption is significantly higher.

8.4 Experimental Results

This section starts by exposing the results of the microbenchmarks realized to provide detailed insights on the energy cost of the transmission and reception of a packet using the evaluated protocols, and to compute the H and ζ_∞ values related to the EUC metric introduced in Section 8.1. Next, the benefits of SNW-MAC are shown by comparing it to the two state of the art MAC protocols. Finally, our scheme is evaluated under variable energy harvesting conditions to show the benefits of the EM in collaboration with the MAC protocols, and the higher performance of the proposed approach.

8.4.1 Energy Microbenchmarks

To evaluate the energy efficiency of a MAC protocol, it is important to measure the energy consumption of the transmission and the reception of a single packet. Therefore, the energy traces of both operations were measured for the three evaluated protocols, by capturing the voltage drop across a 10.2 Ω resistor in series with a 3.5 V power supply using an Agilent Technologies MSO-X-3024A oscilloscope. In addition to allow detailed analysis of the energy consumption, these microbenchmarks were used to set the τ_i values introduced in Section 8.1.2, and to compute the H and ζ_∞ values related to the EUC metric.

The results of the measurements are exposed in Figure 8.9, in which P_c is the power consumption of the node. Figure 8.9a shows that sending a data packet using the proposed SNW-MAC protocol achieves the lowest power consumption compared with the other protocols, as it requires only the sending of the data frame (B). Moreover, the energy cost of sending a packet is constant if the data payload length is fixed. Regarding the sink on Figure 8.9b, the two stages of a packet reception, sending the WuB (A) then receiving the data frame (B), can be seen on this figure. As sending the WuC is done at lower bit rate and higher transmission power than for non-WuC frames, polling a node is energetically expensive for the sink. This result motivates the piggybacking of the wake-up interval of each node in data packets, allowing the sink to poll them only at the right time (see Section 8.2).

Figure 8.9c and Figure 8.9d show respectively the energy cost of a packet transmission and reception using PW-MAC. Sending a packet with this protocol requires the receiving of a beacon (A) and an ACK (C) frame, making the energy cost of sending a packet higher than with SNW-MAC. Moreover, the sender wakes up a short time before the sink transmits a beacon to prevent prediction errors. This time interval varies at each transmission, leading to a non-constant energy cost per packet transmission. The prediction error becomes significant due to the clock drift, and when it exceeds a fixed threshold an update of the prediction state is triggered leading to even higher energy consumption. Regarding the sink, receiving a data packet does not require the sending of a WuC, and is thus less energetically expensive than with SNW-MAC. Nonetheless, SNW-MAC does not require the transmission of an ACK frame, which partially counterbalances the energy overhead incurred by the WuB transmission when compared to PW-MAC.

Figure 8.9e shows the energy cost of sending a packet for a node using X-MAC. In this case, the packet was successfully received by the sink at the sixth attempt. For each attempt, the two stages, sending the data packet (B) and listening for an ACK (C), can be seen. As shown in Figure 8.9f, the sink woke up during the fifth attempt (B), and thus did not receive the complete data packet.

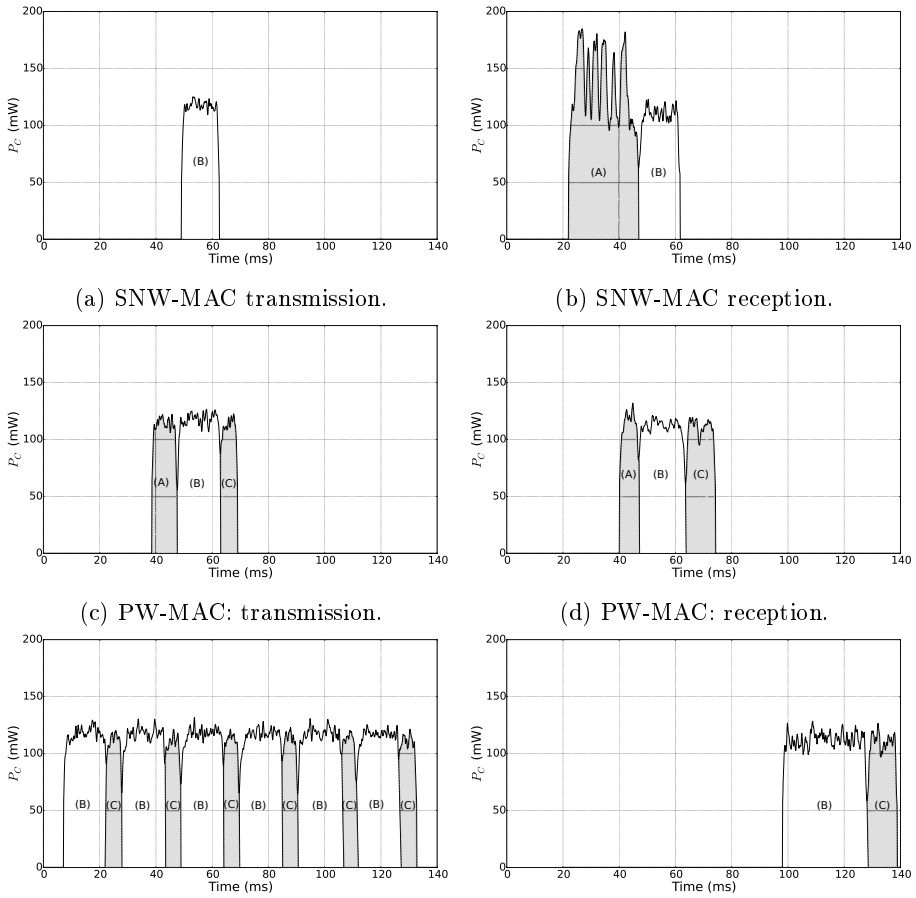

(a) SNW-MAC transmission.

(b) SNW-MAC reception.

(c) PW-MAC: transmission.

(d) PW-MAC: reception.

(e) X-MAC: transmission.

(f) X-MAC: reception.

Figure 8.9 – Microbenchmarks of the MAC protocols. (A), (B) and (C) respectively correspond to the transmission/reception of a beacon/WuC, data frame and ACK.

Protocol	H (Joule)	ζ_∞ (packets per minute and per Joule)
X-MAC	0.0125	0.666
PW-MAC	0.00313	2.660
SNW-MAC	0.00135	6.156

Table 8.3 – Best values of H and ζ_∞ for the different MAC protocols.

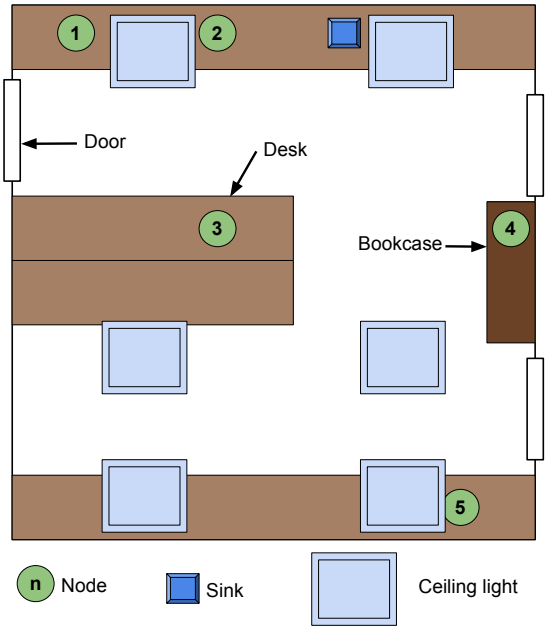

Figure 8.10 – Setup of the star network.

It stayed awake to receive it at the next attempt (B) and sent an ACK (C). The cost of sending one packet with X-MAC greatly varies for different transmissions because of the randomness of the sink wake-up time relatively to the node transmission starting time. In average, a node has to wait half of the wake-up interval of the sink before a data packet is successfully received. This makes the sending of a packet with this protocol energetically more expensive than with SNW-MAC or PW-MAC. On the sink side, the energy cost of a packet reception is also highly variable, and requires in average the listening of one and a half data packets in addition to the transmission of an ACK frame.

Using these microbenchmarks, the τ_i values introduced in Section 8.1.2 were measured and H and ζ_∞ were calculated for the different MAC protocols using the lowest measured values of the P_i, leading to the best achievable values of H and ζ_∞. Table 8.3 presents the obtained results. It can be observed that using SNW-MAC allows a significantly better use of the energy budget. Indeed, SNW-MAC permits values of H (resp. ζ_∞) more than twice smaller (resp. bigger) than with PW-MAC, and more than nine times smaller (resp. bigger) than with X-MAC.

Energy overhead of the EM The EM is periodically executed by each node, and therefore incurs an energy overhead. Using micro-benchmarks, it was measured that each execution of the EM consumes 207.41 μJ at most. For the rest of this work, the duration between two executions of the EM T_s is set to 120 s and the power consumption overhead incurred by the EM is thus equivalent to a constant power draw of 1.73 μW, which is similar to the power consumption of state of the art electronic components for WSN nodes in sleep state.

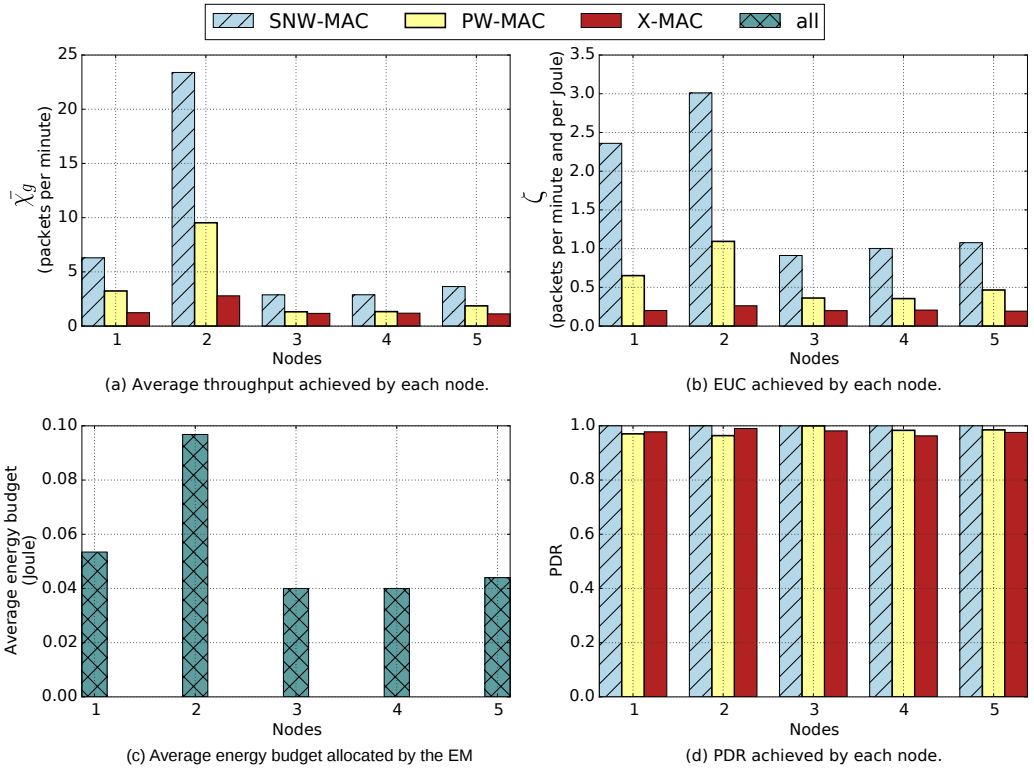

Figure 8.11 – Results of the experimentations on a star network.

8.4.2 Evaluation on a Star Network

The proposed EM and the evaluated MAC protocols were implemented on a testbed made of 6 PowWow nodes including one sink, in a star topology. The nodes were exclusively powered by indoor fluorescent light, allowing reproducibility of the experiments. Moreover, the nodes were deployed under different lighting conditions, as shown in Figure 8.10. Nodes 1, 2 and 5 were located on desks, directly under the ceiling lights while node 3 was deployed in a more shadowed area and node 4 was located on a bookcase, close to the ceiling, thus receiving less light than the others. Each experiment lasted for 3 hours, and the PowWow nodes have been equipped with a WuRx only when the SNW-MAC protocol was evaluated. Figure 8.11 shows the obtained results, where Figure 8.11a presents the packet generation rate, in packets per minute, achieved with the different MAC protocols. SNW-MAC significantly outperforms the two other protocols, allowing up to twice higher packet generation rate than PW-MAC for the node 2 due to the lower energy cost of packet transmissions. The performance of SNW-MAC is confirmed by the Figure 8.11b, which shows that the EUC is much higher for SNW-MAC, revealing a better use of the energy budget. It is not surprising to notice that the results obtained for each node are strongly linked to the average energy budget allocated by the EBC shown in Figure 8.11c. As the amount of harvested energy varies for different nodes, the average allocated energy budget also differs. Finally, Figure 8.11d shows the PDR achieved by the three protocols. SNW-MAC is the only protocol to achieve a 100 % PDR on all the nodes.

8.4.3 Evaluation Under Variable Light Conditions

The benefits in terms of achievable packet generation rate of the proposed approach have been evaluated under variable light conditions. The residual energy of a node was tracked when the node was exposed to fluorescent lighting, typical from an indoor environment, then without any available environmental energy (the lights were off) for 2 hours, and finally exposed to indoor light again. The whole experiment lasted for 5 hours, starting with the storage fully charged, and the

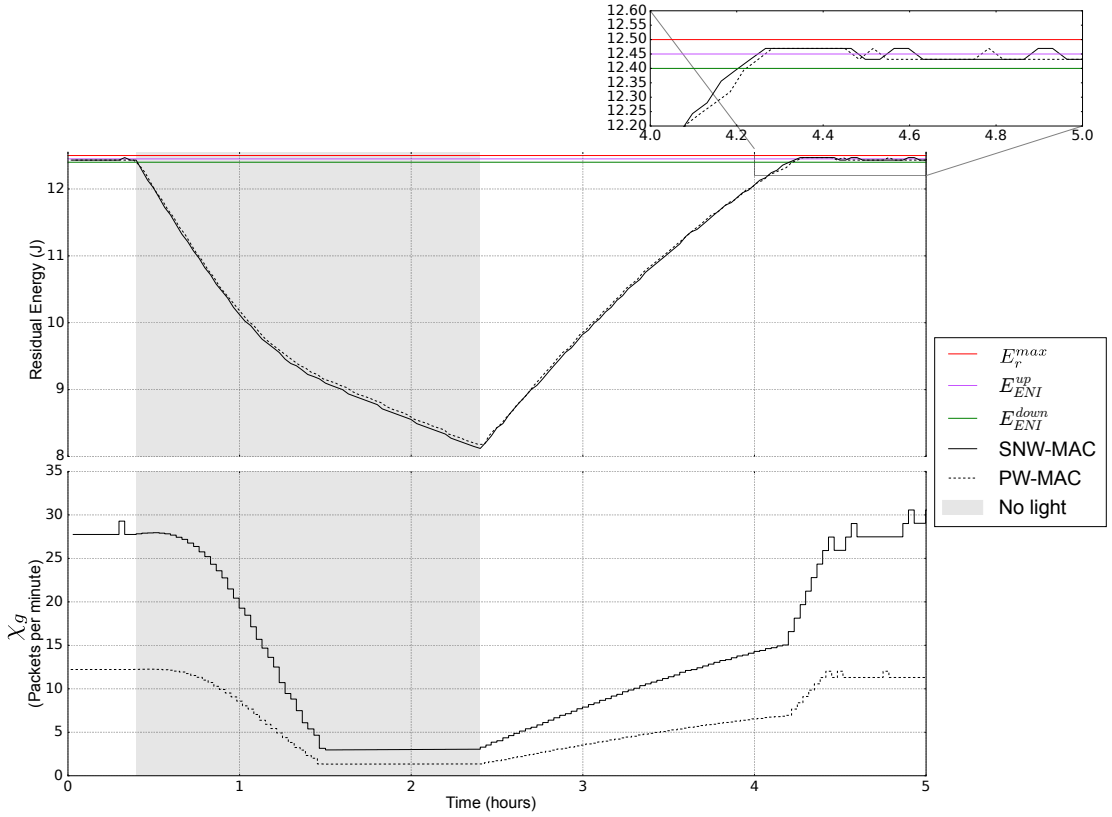

Figure 8.12 – Behavior of the EM and achievable packet generation rate with variable lighting conditions.

results are shown in Figure 8.12. This figure shows the residual energy and the throughput. In this evaluation, only PW-MAC has been compared to SNW-MAC, as it allows higher packet generation rate than X-MAC as we have previously seen.

Figure 8.12 shows that the EM successfully adapts the packet generation rate of the node to keep it sustainable. Indeed, when few or no energy is harvested, a decrease of the residual energy leads the EM to reduce the energy budget, incurring a reduction of the packet generation rate, both with SNW-MAC and PW-MAC, demonstrating how the EM and the MAC protocol work together to keep the node sustainable. It can be observed that during periods of harvested energy availability, and when the residual energy is in the ENI, the EM successfully keeps the node in the ENO-MAX state, avoiding waste of energy by saturation of the storage device.

From this evaluation, we observe that the packet generation rate using SNW-MAC is in all conditions higher than with PW-MAC, showing the better energy efficiency of SNW-MAC. Especially, the packet generation rate of the proposed approach is up to 2.5 times higher than PW-MAC in periods during which harvesting energy is possible.

These results demonstrate the ability of the EM to achieve energy neutrality with different MAC protocols and the benefits of its combination with the highly efficSNW-MACprotocol, which exploits a WuRx to enable asynchronous communication.

8.5 Conclusion

In this chapter, an EM was combined with an asynchronous MAC protocol leveraging WuRx in the context of WSN organized in a star topology and with energy harvesting capabilities. The proposed scheme has been implemented on real hardware, and experimental results have shown that the proposed approach enables up to 2.5 times higher packet generation rate compared to PW-MAC and even more compared to X-MAC.

These experimental results show the benefits of combining EH and WuRx in the context of

star networks, which form an important application case in practice (smart buildings, body area networks, etc.). Moreover, if the monitoring area may be limited due to the low sensitivity of current WuRx compared to traditional transceivers for WSNs, new network topologies, formed of multiple clusters each organized in a star network and leveraging WuRx, and connected together using emerging long-range radio technologies for the IoT such as LoRa^{TM}, can be considered (see Appendix B).

Chapter 9

Conclusions and Perspectives

9.1 Conclusions

Energy is the main bottleneck of long-term wireless sensor networks applications, as typical wireless sensor nodes are battery-powered and batteries can only store a finite amount of energy. A promising solution is to enable each node to harvest energy directly from its environment. As the energy sources are dynamic and uncontrolled, it is required to perform online adaptation of the nodes performance in order to maximize the application quality of service, while avoiding power failures.

In this thesis, two new energy management approaches were proposed. The first one, called Fuzzyman, is based on fuzzy control theory. Fuzzyman is a model-free scheme, *i.e.* it does not require predictions of the future harvested energy. With Fuzzyman, an intuitive strategy is formally expressed as a set of fuzzy IF-THEN rules. Fuzzyman requires as an input both the residual energy and the amount of harvested energy since the previous execution of the energy manager. Fuzzyman was compared to P-FREEN, a state of the art energy manager, using extensive simulations, and it was found that Fuzzyman achieves higher energy efficiency and no power failure. The main drawbacks of Fuzzyman are that it requires the amount of energy harvested which can be unpractical to measure, and the lack of objective way to set the parameters, such as the rule base and fuzzy membership functions.

The second energy manager that was proposed is called RLMan, and relies on reinforcement learning theory. In RLMan, linear function approximators are used to reduce the computational and memory overheads, even if continuous state and action spaces are considered. Moreover, RLMan requires only the residual energy as an input, as opposite to Fuzzyman, which makes it more practical to implement as this value may be difficult and energy costly to measure in practice. Using simulations, RLMan was compared to three other state of the art energy managers, including Fuzzyman, in the case of both energy harvesting from indoor light and outdoor wind. Results show that RLMan outperforms other state of the art approaches with regard both to energy efficiency and average packet generation rate, while incurring no power failure.

Achieving efficient energy management is not sufficient to attain sustainable energy harvesting wireless sensor networks. As communication is typically one of the most, if not the most, consuming task in a wireless sensor node, enabling energy efficient communication is also critical. Medium Access Control (MAC) protocols are especially important as they are responsible for point-to-point communications and control the transceiver. A popular way to reduce the power consumption of communications is duty-cycling, which allow significant power savings, but still incur non-negligible energy waste. Recent advances have made possible the realization of ultra-low power wake-up receivers, able to listen to the wireless channel while having a power consumption similar to the other wireless node components in sleep state. These devices are capable of waking-up the microcontroller when a wake-up command is detected. Some wake-up receivers are able to decode and process information embedded in the wake-up commands. The cost of ultra low power consumption is significantly lower sensitivity and bitrate than traditional wireless sensor network transceivers, and as a consequence the wake-up commands must be transmitted at higher power and lower bitrates than the other frames, making their transmission energetically expensive.

In this thesis, we proposed a generic analytical framework based on absorbing Markov chain to model MAC protocols. This model enables the studying and comparison of the power consumption, latency and reliability of different MAC protocols. To show practically how the proposed framework can be used to model MAC protocols, PW-MAC, a receiver-initiated pseudo-asynchronous scheme, was modeled and the details were exposed. To achieve high accuracy, experimental measurements were performed to feed to analytical model, and to support our results.

The proposed framework was used to compare traditional pseudo-asynchronous schemes to a simple MAC leveraging wake-up receivers in order to show the potential benefits that such approaches can enable. Using traditional pseudo-asynchronous schemes, a trade-off exists between latency and power consumption, and this tradeoff is controlled by the wake-up interval. Analytical results, supported by experimental measurements, show that using wake-up receivers allows going beyond this tradeoff, as both low power and low latency communications can be achieved.

An opportunistic MAC protocol was also proposed in this thesis, called OPportunistic Wake-Up Mac (OPWUM). OPWUM relies on the timer-based contention mechanism in order to enable "on-the-fly" packet forwarding according to some application metric. If such a mechanism was already present in the literature, OPWUM leverages wake-up receiver to make them energetically interesting. Using network simulation, it was shown that OPWUM outperforms other opportunistic MAC schemes.

Finally, energy harvesting and wake-up receivers were put together in the context of data gathering star networks. In star networks, each wireless sensor node can send directly its data packets to the sink, without the need of relays. An energy manager inspired by Fuzzyman and which require as an input only the residual energy was implemented on a testbed of PowWow nodes equipped with a state of the art wake-up receivers. Moreover, a MAC protocol for data gathering star networks and leveraging wake-up receivers was designed and implemented. Results show how wake-up receivers combined with the proposed scheme enable energy efficiency communications and sustainable energy harvesting networks.

To conclude, the results of this thesis encourage us to believe that achieving energy neutral operation while efficiently using the harvested energy is a feasible goal. High energy efficiency requires careful design of adaptation algorithms as well as communication protocols. Moreover, wake-up receivers, enabled by the progress of microelectronics, have the potential to significantly reduce the energy consumption and the latency of communication tasks in some applications that do not require high range such as smart buildings or body are networks.

9.2 Perspectives

Many doors were opened by this thesis, and this section presents the issues that in our opinion are worthwhile subjects for future works.

9.2.1 Fuzzyman: self adaption

A drawback of Fuzzyman is the lack of objective method for establishing the controller parameters, e.g. the rule-base and the membership functions. A solution may be to use adaptive control, in which an adaptation mechanism is used to dynamically tune the controller parameters. In this approach, the adaptation mechanism algorithm observes both the inputs and the outputs of the control system, and adapts the parameter of the controller in the aim to achieve the required performance.

9.2.2 RLMan: considering other rewarding systems

In RLMan, the reward is the product between the normalized residual energy (feature) and the packet generation rate. However, other rewarding systems can be considered. In particular, multi-objective reinforcement learning seems to be an interesting lead to follow, where for example the normalized residual energy and the packet generation rate are two distinct rewards to maximize. Moreover, adopting a multi-objective approaches can enable the adding of other quality of service metrics, each one associated with a distinct reward, making the algorithm more flexible.

9.2.3 RLMan: Multiple inputs

RLMan requires only one input, which is the residual energy. An interesting extension can be to give additional inputs to RLMan, such as the variation of the residual energy between the current and previous time slots. The intuition is that having additional information available may lead to better results. However, additional inputs means more complex function approximators, such as tile coding. In tile coding, the input space is divided into multiple tiles, each tile taking only one value. Moreover, to make generalization easier and speed-up learning, multiple overlapping tile layers can be considered. In order to reduce the memory requirement, which is critical in wireless sensor networks, a hash table, possibly mapping multiple tiles to the same value, can be considered. Investigating this approach as well as the impact on a hash table on the memory overhead and approximator performance in the context of energy management in energy harvesting wireless sensor networks seems to be an interesting lead.

9.2.4 Multi-source energy harvesting

In this thesis, when evaluating the energy managers by simulations or experimentations, the nodes were powered by one energy source at the time. However, it is possible to equip each node with multiple energy harvesters [157,160], and therefore to power the nodes with multiple energy sources simultaneously. If the energy managers presented in this thesis are model-free and do not make assumptions on a particular kind of energy source, they were not evaluated in this context, which could be an interesting lead to explore.

9.2.5 MAC analytical framework

The proposed MAC analytical framework only considers the MAC layer, but not the topology of the network which could also affect the performance of the MAC protocol. An improvement of the proposed framework would be to extend it to incorporate such network-level considerations. Indeed, MAC protocols typically incorporate collision avoidance mechanism (e.g. RTS-CTS handshake), and considering network level knowledge will enable more realistic modeling of such mechanisms.

Incorporating analytical model of the wireless channel in the model is also an open problem, to set the transition probabilities in a more realistic manner. A software is currently under development for making the modeling of MAC protocols using the proposed framework easy, as well as the incorporation of additional analytical models, e.g. for the physical layer.

9.2.6 Energy management in multi-hop networks

Multi-hop network, in which each node is both a sensor that generates packets and a relay for the network, where not tackled in this thesis. In such network, when setting the packet generation rate of a sensor node, the energy conditions of its relays should also be considered, as well as the network-level fairness. Therefore, energy efficiency as defined in this thesis is not anymore a relevant metric. Designing distributed energy managers for such network is a field worth being investigated. Appendix A shows an approach that we propose to tackle this challenge, using convex optimization and the alternate direction of multipliers method. Other approaches, such as multi-agent reinforcement learning, can be considered.

9.2.7 Combining wake-up receiver and long-range technologies

In recent years, a handful technologies enabling long-range communication of several kilometers with power consumption similar to usual wireless sensor node transceivers, have emerged. LoRa^{TM}and SIGFOX^{TM}are example of such technologies. The cost of long-range is low bitrate, of typically a few kbps. Using LoRa^{TM}, communication from the nodes to the gateway, is done with low latency, as the gateway is always listening to the channel, while communication from the gateway to the nodes requires a trade-off between the latency and the power consumption of the nodes. Wake-up receivers and LoRa^{TM}present orthogonal features and combining them into novel network architectures could be interesting. The Appendix B explores this track in more details, focusing on MAC protocols.

9.2.8 Energy Traces

An issue when evaluating energy management algorithms using simulations is the lack of energy traces. If many meteorological data sets, such as solar irradiance and wind speed, are available from meteorological laboratories such as the National Renewable Energy Laboratory (NREL), they typically do not correspond to many realistic environments in which sensor nodes of the Internet of Things are expected to be deployed. For example, the sunlight or wind received by a sensor node located in a city is strongly impacted by the surrounding buildings, whereas the irradiance data sets available from meteorological laboratories are typically recored in clear spaces.

Moreover, other energy sources are considered for powering sensor nodes such as human heat, motion, indoor light... If a few data sets are available for indoor light from the EnHANTs project [161], to the best of our knowledge, there is in general a real lack of energy traces for exhaustive simulations.

Appendices

Appendix A

Distributed Computation of Fair Packet Rates in Energy Harvesting Wireless Sensor

In multi-hop networks, in addition to perform measurements and send the so-obtained data to a sink, each node is also a relay that forwards packets from other nodes. Therefore, the energy consumed by each node is shared between packet generation, *i.e.* performing sensing to produce new data and sending the so-obtained data, and relaying, *i.e.* forwarding packets from other nodes. An important consideration in multi-hop networks is the fairness of the packet generation rates of the nodes given the amount of energy harvested by each node. To illustrate the idea of packet generation rate fairness, we consider the toy example shown in Figure A.1. In this example, each node i has a given amount of available resources R_i, and the cost of generating a packet and relaying a packet are both equal to 1 for convenience. Both A and B are feasible allocations, as none of them require more resources than the ones available for each node. However, it can be seen that the allocation B is more fair than the allocation A, given the amount of resources available for each node. Indeed, with the allocation B, the nodes 1 and 2 have the same packet generation rates, whereas with the allocation A the node 1 is clearly favored. In both cases, the node 3 is limited as it has much less available resources.

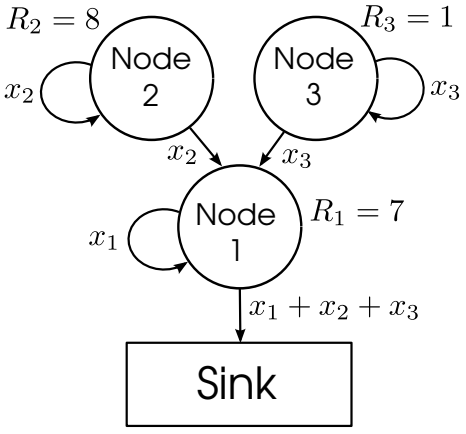

(a) Toy example of a multi-hop sensor network.

Allocations	A	B
x_1	5	3
x_2	1	3
x_3	1	1
$x_1 + x_2 + x_3$	7	7
log utility	1.6	2.2

(b) Two different packet generation rate allocations.

Figure A.1 – Illustration of packet generation rate fairness in multi-hop sensor networks. The cost of generating a packet and the cost of relaying a packet are both 1 for all the nodes.

In order to maximize packet generation rates while achieving a fair allocation, the proportional fairness metric is used and maximized. Proportional fairness [162, 163] is widely used in wireless networks to balance fairness and packet rate sum. Formally, an allocation $\mathbf{x}$ is said to be

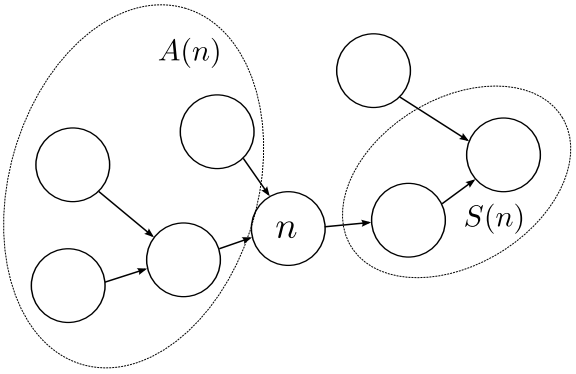

Figure A.2 – Tree topology network. $A(n)$ is the set of all nodes for which the node n serves as a relay, and $S(n)$ is the set of all nodes that relay the packets sent by n.

proportionally fair if for any other feasible allocation $\mathbf{x}'$ we have:

$$\sum_i \frac{x'[i] - x[i]}{x[i]} \leqslant 0, \tag{A.1}$$

which states that any change in the solution must have a negative average change. Proportional fairness can be achieved by maximizing logarithmic utility function defined by $\sum_i \log x[i]$, over the set of feasible allocations. Indeed, it is proved that if the set of feasible allocations is convex, then the allocation that maximizes the logarithmic utility is proportionally fair [162]. Fig A.1 gives for each allocation its associated logarithmic utility, and, unsurprisingly, allocation A achieves a less good utility than allocation B. Actually, allocation B maximizes the logarithmic utility over the convex set of feasible allocations, and is therefore optimal in the sense of proportional fairness.

The main contribution of this appendix is the design of a distributed algorithm for setting the packet generation rates of sensor nodes forming a multi-hop EH-WSN [164]. Routing is not considered, and it is assumed to be either imposed by the network topology, or established by a routing algorithm [150]. The nodes are supposed to be organized in a routing tree, where each node has a one-hop successor to which it forwards packets, as illustrated in Figure A.2. No assumption is made on the energy source type. The problem of energy management was formulated as a convex optimization problem, with logarithmic utility function. The problem was then reformulated such that, using the ADMM [165], it can be decomposed into smaller subproblems that can be solved in parallel. More precisely, a variation of the ADMM is used in this work, called fast ADMM [166], which enables higher convergence rates.

The rest of this appendix is organized as follows. First, the energy management problem formulation and the derivation of the proposed distributed algorithm are presented in Section A.1. Next, the proposed approach was validated by simulations of a network of 15 nodes powered by real measurements of indoor light in Section A.2.

A.1 Distributed and Fair Optimization

This section starts by formulating the packet generation rate assignment problem as a convex optimization problem. Then, the derivation of a distributed algorithm is presented, which is based on the fast ADMM.

A.1.1 Problem Formulation

As in the previous chapters, time is divided into equal length time slots of duration T_s, and the EM is executed at the beginning of every time slot. An energy predictor (e.g. [8]) provides predictions of the harvested energy over a window of K time slots, and the number of nodes forming the network is denoted by N_N. For convenience, the sets $\mathcal{K} = \{1, \ldots, K\}$ and $\mathcal{N} = \{1, \ldots, N_N\}$ are defined. The current time slot is denoted by t, and the predicted harvested energy for the time slot $t + k$ is denoted by $\widehat{e_h}[n, k],\ n \in \mathcal{N},\ k \in \mathcal{K}$. Each node embeds an energy buffer of finite

capacity denoted by $B[n]$. The energy failure threshold, *i.e.* the minimum energy level required by the node n to operate, is denoted by $b[n]$. At each execution of the EM, each node n measures the residual energy denoted by $e_r[n,0]$. The energy cost for the node n of a packet generation is denoted by $C_L[n]$, while the energy cost of relaying a packet is denoted by $C_R[n]$. For each node n, the sets $A(n)$ and $S(n)$ are respectively defined as the set of all nodes for which n is a relay, and the set of all nodes that serve as a relay for n, as illustrated in Figure A.2. Formally:

$$A(n) \coloneqq \{m \in \mathcal{N} \mid \exists m \rightsquigarrow n\} \tag{A.2}$$
$$S(n) \coloneqq \{m \in \mathcal{N} \mid \exists n \rightsquigarrow m\}, \tag{A.3}$$

where $m \rightsquigarrow n$ designates a path from m to n in the routing tree. The energy variation during the time slot $t+k$ for the node n is defined by:

$$\Delta e(n,k,\boldsymbol{\chi_g}) \coloneqq \widehat{e_h}[n,k] - C_L[n]\chi_g[n,k] - C_R[n] \sum_{m \in A(n)} \chi_g[m,k], \tag{A.4}$$

where $\boldsymbol{\chi_g}$ is the packet generation rate vector and $\chi_g[n,k]$ corresponds to the packet generation rate of the node n at the time slot $t+k$. The residual energy of the node n and at the time slot $t+k$ is denoted by $e_r[n,k]$ and is defined by:

$$e_r(n,k,\boldsymbol{\chi_g}) \coloneqq \begin{cases} e_r[n,0], & n \in \mathcal{N},\ k = 0 \\ \texttt{min}\left\{B[n], e_r(n,k-1,\boldsymbol{\chi_g}) + \Delta e(n,k,\boldsymbol{\chi_g})\right\}, & n \in \mathcal{N}, k \in \mathcal{K} \end{cases} \tag{A.5}$$

The energy management problem is formulated as follows:

$$\begin{aligned} \underset{\boldsymbol{\chi_g}}{\text{minimize}}\ & f_0(\boldsymbol{\chi_g}) \coloneqq -\sum_{n=1}^{N_N} \sum_{k=1}^{K} \log \chi_g[n,k] \\ \text{subject to: } & e_r(n,k,\boldsymbol{\chi_g}) \geqslant b[n],\ n \in \mathcal{N},\ k \in \mathcal{K} \end{aligned} \tag{P_0}$$

where the constraint requires no power failure.

While (P_0) is quite intuitive to formulate, it is not easy to work with because of the `min` operator present in the constraint. Therefore, in order to make (P_0) more tractable, the energy waste vector $\boldsymbol{e_w}$ is introduced and the energy management problem is re-formulated as a convex optimization problem defined as follows:

$$\begin{aligned} \underset{\boldsymbol{\chi_g}, \mathbf{e_w}}{\text{minimize}}\ & f_0(\boldsymbol{\chi_g}) \\ \text{subject to: } & e_w[n,k] \geqslant 0,\ n \in \mathcal{N},\ k \in \mathcal{K} && (C_W) \\ & f(n,k,\boldsymbol{\chi_g},\boldsymbol{e_w}) \leqslant B[n],\ n \in \mathcal{N},\ k \in \mathcal{K} && (C_S) \\ & f(n,k,\boldsymbol{\chi_g},\boldsymbol{e_w}) \geqslant b[n],\ n \in \mathcal{N},\ k \in \mathcal{K} && (C_F) \end{aligned} \tag{P_1}$$

where f is defined by:

$$f(n,k,\boldsymbol{\chi_g},\boldsymbol{e_w}) \coloneqq \begin{cases} e_r[n,0], & n \in \mathcal{N},\ k = 0 \\ e_r[n,0] + \sum_{i=1}^{k} \Delta e(n,i,\boldsymbol{\chi_g}) - \sum_{i=1}^{k} e_w[n,i], & n \in \mathcal{N},\ k \in \mathcal{K} \end{cases} \tag{A.6}$$

In (P_1), the first constraint requires positive wasted energy, the second constraint represents the energy buffer capacity and the last constraint requires no power failure. (P_1) is convex, and the logarithmic utility function f_0 leads to proportional fairness [162] with regard to nodes and time, *i.e.* if $\boldsymbol{\chi_g}$ is an optimal solution of (P_1), then for any feasible solution $\boldsymbol{\chi'_g}$ of (P_1) we have:

$$\sum_{n=1}^{N_N} \sum_{k=1}^{K} \frac{\chi'_g[n,k] - \chi_g[n,k]}{\chi_g[n,k]} \leqslant 0. \tag{A.7}$$

In the rest of this section, it is shown than (P_1) is equivalent to (P_0), in the sense that they have the same optimal solution. Moreover, this optimal solution is unique.

The set of feasible points of (P_0) is denoted by $\mathcal{F}_0$:

$$\mathcal{F}_0 \coloneqq \left\{ \boldsymbol{\chi_g} \;\middle|\; \boldsymbol{\chi_g} \in \mathrm{dom} f_0,\ e_r(n,k,\boldsymbol{\chi_g}) \geqslant b[n],\ n \in \mathcal{N},\ k \in \mathcal{K} \right\}.$$

where $\mathrm{dom} f$ is the domain of function f, and the set of feasible points of (P_1) is denoted by $\mathcal{F}$:

$$\begin{aligned} \mathcal{F} \coloneqq \{ \boldsymbol{\chi_g} \oplus \boldsymbol{e_w} \;\big|\; & \boldsymbol{\chi_g} \in \mathrm{dom} f_0,\ e_w[n,k] \geqslant 0,\ f(n,k,\boldsymbol{\chi_g},\boldsymbol{e_w}) \leqslant B[n], \\ & f(n,k,\boldsymbol{\chi_g},\boldsymbol{e_w}) \geqslant b[n],\ n \in \mathcal{N},\ k \in \mathcal{K} \}. \end{aligned} \tag{A.8}$$

where $\oplus$ is the concatenation operator, *i.e.* if $\mathbf{a} = (a[1], \ldots, a[n])^\intercal$ and $\mathbf{b} = (b[1], \ldots, b[m])^\intercal$, then $\mathbf{a} \oplus \mathbf{b} = (a[1], \ldots, a[n], b[1], \ldots, b[m])^\intercal$. Moreover, the projection of $\mathcal{F}$ onto the $\boldsymbol{\chi_g}$ components: $\mathcal{F}_{\chi_g} \coloneqq \left\{ \boldsymbol{\chi_g} \;\middle|\; \boldsymbol{\chi_g} \oplus \boldsymbol{e_w} \in \mathcal{F} \right\}$ is convex, as the projection of a convex set onto some of its coordinates is convex [167].

Definition 1. *A point (not necessarily feasible)* $\boldsymbol{\chi_g} \oplus \boldsymbol{e_w}$ *is said to be* realistic *if the energy waste vector is such that:*

$$e_w[n,k] = \max\left\{0, f(n,k-1,\boldsymbol{\chi_g}) + \Delta e(n,k,\boldsymbol{\chi_g}) - B[n]]\right\},\ n \in \mathcal{N},\ k \in \mathcal{K}, \tag{A.9}$$

Intuitively, a realistic point is such that the wasted energy is exactly the energy that could not be stored because the energy buffer is saturated. We can see that, if $\boldsymbol{\chi_g} \oplus \boldsymbol{e_w}$ is realistic, then:

$$e_w[n,k] > 0 \rightarrow f(n,k,\boldsymbol{\chi_g},\boldsymbol{e_w}) = B[n]. \tag{A.10}$$

For every packet generation vector $\boldsymbol{\chi_g}$, a corresponding realistic point $\boldsymbol{\chi_g} \oplus \boldsymbol{e_w^r}$ can be constructed using the definition of a realistic solution. The vector denoted by $\boldsymbol{e_w^r}$ and constructed such that $\boldsymbol{\chi_g} \oplus \boldsymbol{e_w^r}$ is a realistic point is called the realistic energy waste vector associated to $\boldsymbol{\chi_g}$ and $\boldsymbol{\chi_g} \oplus \boldsymbol{e_w^r}$ is called the realistic point associated to $\boldsymbol{\chi_g}$. Moreover, this realistic point is unique for each packet generation vector by construction. It can be seen that if $\boldsymbol{\chi_g} \oplus \boldsymbol{e_w^r}$ is a realistic solution, then the constraints (C_W) and (C_S) of (P_1) are checked by construction.

The set of feasible realistic solutions of (P_1) is denoted by $\mathcal{F}^r$, which is a subset of $\mathcal{F}$. The projection of $\mathcal{F}^r$ onto the $\boldsymbol{\chi_g}$ components is denoted by $\mathcal{F}^r_{\chi_g}$ and is defined as: $\mathcal{F}^r_{\chi_g} \coloneqq \left\{ \boldsymbol{\chi_g} \;\middle|\; \boldsymbol{\chi_g} \oplus \boldsymbol{e_w^r} \in \mathcal{F}^r \right\}$.

Proposition 1. *For any* $\boldsymbol{\chi_g} \in \mathcal{F}_{\chi_g}$*, its associated realistic energy waste vector* $\boldsymbol{e_w^r}$ *is such that, for any other energy waste vector such that* $\boldsymbol{\chi_g} \oplus \boldsymbol{e_w} \in \mathcal{F}$*:*

$$\sum_{i=1}^{k} e_w^r[n,i] \leqslant \sum_{i=1}^{k} e_w[n,i],\ n \in \mathcal{N},\ k \in \mathcal{K}. \tag{A.11}$$

Proof. Indeed, let us assume that for some $n \in \mathcal{N}$ and $k \in \mathcal{K}$, we have:

$$\sum_{i=1}^{k} e_w^r[n,i] > \sum_{i=1}^{k} e_w[n,i]. \tag{A.12}$$

As $\boldsymbol{\chi_g} \oplus \boldsymbol{e_w}$ is feasible and from (A.6):

$$f(n,k,\boldsymbol{\chi_g},\boldsymbol{e_w^r}) < f(n,k,\boldsymbol{\chi_g},\boldsymbol{e_w}) \leqslant B[n],$$

and therefore from (A.10): $e_w^r[n,k] = 0$. We define:

$$k' \coloneqq \mathtt{argmax}_i \left\{ i \leqslant k : e_w^r[n,i] > 0 \right\}, \tag{A.13}$$

and, if such k' exists, it is necessarily such that $k' < k$. Two cases can now be distinguished:

- If k' does not exist, *i.e.* $e_w^r[n,i] = 0$ for all $i \in \{1, \ldots, k\}$, then $\sum_{i=1}^{k} e_w^r[n,i] = 0$ which contradicts (A.12) as $\boldsymbol{\chi_g} \oplus \boldsymbol{e_w}$ is feasible.

- If k' exists, then:

$$\sum_{i=1}^{k'} e_w[n,i] \leqslant \sum_{i=1}^{k} e_w[n,i] < \sum_{i=1}^{k} e_w^r[n,i] = \sum_{i=1}^{k'} e_w^r[n,i],$$

and hence:

$$f(n,k',\boldsymbol{\chi_g},\boldsymbol{e_w}) > f(n,k',\boldsymbol{\chi_g},\boldsymbol{e_w^r}) = B[n],$$

where the equality stands from (A.10). This contradicts the feasibility of $\boldsymbol{\chi_g} \oplus \boldsymbol{e_w}$.

In conclusion, (A.12) being true for some $n \in \mathcal{N}$ and $k \in \mathcal{K}$ always leads to a contradiction, and therefore (A.11) stands for all $n \in \mathcal{N}$ and $k \in \mathcal{K}$. □

Proposition 2. *The sequence $(e_r(n,k,\boldsymbol{\chi_g}))_{n,k}$ defined in (A.5) and associated to a packet generation rate vector $\boldsymbol{\chi_g}$ and the sequence $(f(n,k,\boldsymbol{\chi_g},\boldsymbol{e_w^r}))_{n,k}$ defined in (A.6) and associated to the realistic point $\boldsymbol{\chi_g} \oplus \boldsymbol{e_w^r}$ are equal,* i.e.*:*

$$e_r(n,k,\boldsymbol{\chi_g}) = f(n,k,\boldsymbol{\chi_g},\boldsymbol{e_w^r}),\ n \in \mathcal{N},\ k \in \mathcal{K}. \tag{A.14}$$

Proof. Indeed, if it is assumed that for some n and $k-1$, with $n \in \mathcal{N}$ and $k \in \{2,\dots,K\}$ the equality (A.14) holds, then:

$$\begin{aligned} f(n,k,\boldsymbol{\chi_g},\boldsymbol{e_w^r}) &= f(n,k-1,\boldsymbol{\chi_g},\boldsymbol{e_w^r}) + \Delta e(n,k,\boldsymbol{\chi_g}) - e_w^r[n,k] \\ &= e_r(n,k-1,\boldsymbol{\chi_g}) + \Delta e(n,k,\boldsymbol{\chi_g}) - e_w^r[n,k]. \end{aligned}$$

Two cases can be distinguished:

- If $e_r(n,k-1,\boldsymbol{\chi_g}) + \Delta e(n,k,\boldsymbol{\chi_g}) \leqslant B[n]$, then $e_w^r[n,k] = 0$, as $\boldsymbol{\chi_g} \oplus \boldsymbol{e_w^r}$ is realistic. Therefore:

$$f(n,k,\boldsymbol{\chi_g},\boldsymbol{e_w^r}) = e_r(n,k-1,\boldsymbol{\chi_g}) + \Delta e(n,k,\boldsymbol{\chi_g}).$$

In this case, from (A.5):

$$e_r(n,k,\boldsymbol{\chi_g}) = e_r(n,k-1,\boldsymbol{\chi_g}) + \Delta e(n,k,\boldsymbol{\chi_g}),$$

leading to: $e_r(n,k,\boldsymbol{\chi_g}) = f(n,k,\boldsymbol{\chi_g},\boldsymbol{e_w^r})$.

- If $e_r(n,k-1,\boldsymbol{\chi_g}) + \Delta e(n,k,\boldsymbol{\chi_g}) > B[n]$, and from the definition of a realistic solution (A.9):

$$e_w^r[n,k] = e_r(n,k-1,\boldsymbol{\chi_g}) + \Delta e(n,k,\boldsymbol{\chi_g}) - B[n], \tag{A.15}$$

and:

$$f(n,k,\boldsymbol{\chi_g},\boldsymbol{e_w^r}) = B[n]. \tag{A.16}$$

Moreover, from (A.5):

$$e_r(n,k,\boldsymbol{\chi_g}) = B[n], \tag{A.17}$$

and therefore: $e_r(n,k,\boldsymbol{\chi_g}) = f(n,k,\boldsymbol{\chi_g},\boldsymbol{e_w^r})$.

As $e_r(n,0,\boldsymbol{\chi_g}) = f(n,0,\boldsymbol{\chi_g},\boldsymbol{e_w^r}) = e_r[n,0]$ by definition, it can be concluded by induction that for all $n \in \mathcal{N}$ and $k \in \mathcal{K}$, $e_r(n,k,\boldsymbol{\chi_g}) = f(n,k,\boldsymbol{\chi_g},\boldsymbol{e_w^r})$. □

We now give the last proposition of this section, which allows us to conclude that solving (P_1) is equivalent to solving (P_0).

Proposition 3. $\mathcal{F}_0 = \mathcal{F}_{\chi_g}^r = \mathcal{F}_{\chi_g}$.

Proof. For any $\boldsymbol{\chi_g} \in \mathcal{F}_{\chi_g}^r$, the realistic solution $\boldsymbol{\chi_g} \oplus \boldsymbol{e_w^r}$ associated to $\boldsymbol{\chi_g}$ is feasible by definition of $\mathcal{F}_{\chi_g}^r$, *i.e.* $\boldsymbol{\chi_g} \oplus \boldsymbol{e_w^r} \in \mathcal{F}^r \subset \mathcal{F}$, and therefore $\boldsymbol{\chi_g} \in \mathcal{F}_{\chi_g}$. Hence: $\mathcal{F}_{\chi_g}^r \subset \mathcal{F}_{\chi_g}$.

Let $\boldsymbol{\chi_g}$ be an element of $\mathcal{F}_{\chi_g}$, and $\boldsymbol{e_w^r}$ be its associated realistic energy waste vector. Because $\boldsymbol{\chi_g} \in \mathcal{F}_{\chi_g}$, there exists $\boldsymbol{e_w}$ such that $\boldsymbol{\chi_g} \oplus \boldsymbol{e_w}$ is feasible. Therefore, for all $n \in \mathcal{N}$ and $k \in \mathcal{K}$:

$$f(n,k,\boldsymbol{\chi_g},\boldsymbol{e_w}) \geqslant b[n],$$

and from Proposition 1, for all $n \in \mathcal{N}$ and $k \in \mathcal{K}$:

$$f(n,k,\boldsymbol{\chi_g},\boldsymbol{e_w^r}) \geqslant f(n,k,\boldsymbol{\chi_g},\boldsymbol{e_w}) \geqslant b[n], \tag{A.18}$$

which means that $\boldsymbol{\chi_g} \oplus \boldsymbol{e_w^r}$ checks the constraint (C_F). Moreover, as this point also checks the constraints (C_W) and (C_S) by construction, then $\boldsymbol{\chi_g} \oplus \boldsymbol{e_w^r}$ is feasible, and $\boldsymbol{\chi_g} \in \mathcal{F}^r_{\chi_g}$. It can be concluded that $\mathcal{F}_{\chi_g} \subset \mathcal{F}^r_{\chi_g}$. As we already seen that $\mathcal{F}^r_{\chi_g} \subset \mathcal{F}_{\chi_g}$, we finally have $\mathcal{F}^r_{\chi_g} = \mathcal{F}_{\chi_g}$.

Let $\boldsymbol{\chi_g}$ be an element of $\mathcal{F}_0$, and $\boldsymbol{e_w^r}$ its associated realistic vector. Then, because $\boldsymbol{\chi_g}$ is feasible for (P_0) and from Proposition 2, then $\boldsymbol{\chi_g} \oplus \boldsymbol{e_w^r}$ verifies the condition (C_F). Moreover, as it also checks the conditions (C_W) and (C_S) by construction, we have $\boldsymbol{\chi_g} \oplus \boldsymbol{e_w^r} \in \mathcal{F}^r$, and thus $\mathcal{F}_0 \subset \mathcal{F}^r_{\chi_g}$. If we now choose $\boldsymbol{\chi_g} \in \mathcal{F}^r_{\chi_g}$, then from Proposition 2, and because $\boldsymbol{\chi_g} \oplus \boldsymbol{e_w^r}$ checks the constraint (C_F), then $\boldsymbol{\chi_g}$ is feasible for (P_0), *i.e.* $\boldsymbol{\chi_g} \in \mathcal{F}_0$. Hence, $\mathcal{F}^r_{\chi_g} \subset \mathcal{F}_0$. Therefore we have $\mathcal{F}^r_{\chi_g} = \mathcal{F}_0$. Finally, $\mathcal{F}_0 = \mathcal{F}^r_{\chi_g} = \mathcal{F}_{\chi_g}$.

□

The sets $\mathcal{F}_0$, $\mathcal{F}^r_{\chi_g}$, and $\mathcal{F}_{\chi_g}$ are hence the same convex set. Because the utility function f_0 only depends on $\boldsymbol{\chi_g}$, for any optimal solution of (P_1) denoted by $\boldsymbol{\chi_g^*} \oplus \boldsymbol{e_w^*}$, $\boldsymbol{\chi_g^*}$ is also an optimal solution of (P_0). Moreover, as the utility function f_0 is strictly convex, it admits a unique minimum on $\mathcal{F}_0$ $(= \mathcal{F}_{\chi_g} = \mathcal{F}^r_{\chi_g})$ [167], and all the optimal solutions $\boldsymbol{\chi_g^*} \oplus \boldsymbol{e_w^*}$ therefore share the same packet generation rate vector $\boldsymbol{\chi_g^*}$ (which is an optimal solution of (P_0)). It is therefore enough to solve (P_1) in order to solve (P_0). The rest of this section is dedicated to the derivation of a distributed algorithm in that purpose.

A.1.2 Decomposition of (P_1)

To decompose (P_1), each node n keeps a local copy of the packet generation rate of its predecessors, denoted by $\mathbf{c_n}$, and (P_1) is reformulated as follows:

$$\begin{aligned} \underset{\boldsymbol{\chi_g},\mathbf{e_w},\{\mathbf{c_n}\}}{\text{minimize}}\ & f_0(\boldsymbol{\chi_g}) \\ \text{subject to: } & e_w[n,k] \geqslant 0,\ n \in \mathcal{N},\ k \in \mathcal{K} \\ & g(n,k,\boldsymbol{\chi_g},\mathbf{e_w},\mathbf{c_n}) \leqslant B[n],\ n \in \mathcal{N},\ k \in \mathcal{K} \\ & g(n,k,\boldsymbol{\chi_g},\mathbf{e_w},\mathbf{c_n}) \geqslant b[n],\ n \in \mathcal{N},\ k \in \mathcal{K} \\ & c_n[m,k] = \chi_g[m,k],\ n \in \mathcal{N},\ k \in \mathcal{K},\ m \in A(n) \end{aligned} \tag{P_2}$$

where $\{\mathbf{c_n}\}$ denotes the set of vectors $\{\mathbf{c_1},\ldots,\mathbf{c_N}\}$, and $c_n[m,k]$ is the local copy of the packet generation rate of the node m at the time slot $t+k$ stored by the node n for any $m \in A(n)$, and g is similar to f:

$$g(n,k,\boldsymbol{\chi_g},\mathbf{e_w},\mathbf{c_n}) \coloneqq e_r[n,0] + \sum_{i=1}^{k} \Delta e(n,i,\boldsymbol{\chi_g}) - \sum_{i=1}^{k} e_w[n,i]. \tag{A.19}$$

Let $\mathcal{C}$ be the convex set of feasible solutions of (P_2), defined by:

$$\mathcal{C} \coloneqq \Big\{ (\boldsymbol{\chi_g},\mathbf{e_w},\{\mathbf{c_n}\}) \mid n \in \mathcal{N},\ k \in \mathcal{K},\ e_w[n,k] \geqslant 0, \\ g(n,k,\boldsymbol{\chi_g},\mathbf{e_w},\mathbf{c_n}) \leqslant B[n],\ g(n,k,\boldsymbol{\chi_g},\mathbf{e_w},\mathbf{c_n}) \geqslant b[n] \Big\}. \tag{A.20}$$

The indicator function of $\mathcal{C}$ denoted by $\mathcal{I}_{\mathcal{C}}$ is defined by:

$$\mathcal{I}_{\mathcal{C}}(\boldsymbol{\chi_g},\mathbf{e_w},\{\mathbf{c_n}\}) \coloneqq \begin{cases} 0, & \text{if } (\boldsymbol{\chi_g},\mathbf{e_w},\{\mathbf{c_n}\}) \in \mathcal{C} \\ \infty, & \text{otherwise} \end{cases} \tag{A.21}$$

Using $\mathcal{I}_{\mathcal{C}}$, (P_2) can be reformulated as:

$$\begin{aligned} \underset{\boldsymbol{\chi_g},\mathbf{e_w},\mathbf{r},\{\mathbf{c_n}\}}{\text{minimize}}\ & f_0(\boldsymbol{\chi_g}) + \mathcal{I}_{\mathcal{C}}(\boldsymbol{\chi_g},\mathbf{e_w},\{\mathbf{c_n}\}) \\ \text{subject to: } & \chi_g[m,k] = c_n[m,k],\ n \in \mathcal{N},\ k \in \mathcal{K},\ m \in A(n) \end{aligned} \tag{P_3}$$

Algorithm 4 Original ADMM applied to (P_4).

1: **for** $i = 1, \dots$ **do**
2: $\quad \boldsymbol{\chi}_{\boldsymbol{g}}^{\mathbf{i+1}}[\boldsymbol{n}] \leftarrow \arg\min_{\boldsymbol{\chi}_{\boldsymbol{g}}} L_\rho(\boldsymbol{\chi}_{\boldsymbol{g}}, \mathbf{r^i}, \mathbf{e_w^i}, \{\mathbf{c_n^i}\}, \{\mathbf{u_n^i}\}, \mathbf{v^i})$
3: $\quad \mathbf{r^{i+1}}, \mathbf{w^{i+1}}, \{\mathbf{c_n^{i+1}}\} \leftarrow \arg\min_{\mathbf{r},\mathbf{w},\{\mathbf{c_n}\}} L_\rho(\boldsymbol{\chi}_{\boldsymbol{g}}^{\mathbf{i+1}}, \mathbf{r}, \mathbf{e_w}, \{\mathbf{c_n}\}, \{\mathbf{u_n^i}\}, \mathbf{v^i})$
4: $\quad \mathbf{u_n^{i+1}}[\mathbf{m}] \leftarrow \mathbf{u_n^i}[\mathbf{m}] + \boldsymbol{\chi}_{\boldsymbol{g}}^{\boldsymbol{i+1}}[\boldsymbol{m}] - \mathbf{c_n^{i+1}}[\mathbf{m}],\ m \in A(n),\ n \in \mathcal{N}$
5: $\quad \mathbf{v^{i+1}} \leftarrow \mathbf{v^i} + \boldsymbol{\chi}_{\boldsymbol{g}}^{\mathbf{i+1}} - \mathbf{r^{i+1}}$

In order to make (P_3) suitable for the ADMM, the variable $\boldsymbol{\chi}_{\boldsymbol{g}}$ is replicated by a variable $\mathbf{r}$, and (P_3) is equivalent to:

$$\begin{aligned} \underset{\boldsymbol{\chi}_{\boldsymbol{g}},\mathbf{e_w},\mathbf{r},\{\mathbf{c_n}\}}{\text{minimize}}\ & f_0(\boldsymbol{\chi}_{\boldsymbol{g}}) + \mathcal{I}_{\mathcal{C}}(\mathbf{r}, \mathbf{e_w}, \{\mathbf{c_n}\}) \\ \text{subject to: } & \chi_g[m,k] = c_n[m,k],\ n \in \mathcal{N},\ k \in \mathcal{K},\ m \in A(n) \\ & \chi_g[n,k] = r[n,k],\ n \in \mathcal{N},\ k \in \mathcal{K} \end{aligned} \tag{P_4}$$

The augmented Lagrangian of (P_4) in the scaled form is:

$$\begin{aligned} L_\rho(\boldsymbol{\chi}_{\boldsymbol{g}}, \mathbf{r}, \mathbf{e_w}, \{\mathbf{c_n}\}, \{\mathbf{u_n}\}, \mathbf{v}) \coloneqq f_0(\boldsymbol{\chi}_{\boldsymbol{g}}) + \mathcal{I}_{\mathcal{C}}(\mathbf{r}, \mathbf{e_w}, \{\mathbf{c_n}\}) + \frac{\rho}{2} \sum_{n=1}^{N_N} \Big(\|\boldsymbol{\chi}_{\boldsymbol{g}}[\boldsymbol{n}] - \mathbf{r}[\mathbf{n}] + \mathbf{v}[\mathbf{n}]\|_2^2 \\ + \sum_{m \in A(n)} \|\boldsymbol{\chi}_{\boldsymbol{g}}[\boldsymbol{m}] - \mathbf{c_n}[\mathbf{m}] + \mathbf{u_n}[\mathbf{m}]\|_2^2 \Big), \end{aligned} \tag{A.22}$$

where $\rho > 0$ is the penalty parameter, and $\mathbf{v},\ \mathbf{u_1}, \dots, \mathbf{u_N}$ are the scaled dual variables. For a vector $\mathbf{y}$, the notation $\mathbf{y}[\mathbf{n}]$ denotes the sub-vector $(y[n,1], \dots, y[n,K])^\intercal$.

A.1.3 Derivation of a Distributed Algorithm

The original ADMM applied to (P_4) consists of the iterations shown in Algorithm 4. In Algorithm 4, $\mathbf{y^i}$ denotes the value of the vector $\mathbf{y}$ at the i^{th} iteration. One common way to measure how far the iterates are from the optimal allocation is to define the primal and dual residuals, respectively:

$$\mathbf{p^i} \coloneqq \left(\bigoplus_{n=1}^{N_N} \bigoplus_{m \in A(n)} \left(\boldsymbol{\chi}_{\boldsymbol{g}}^{\boldsymbol{i}}[\boldsymbol{m}] - \mathbf{c_n^i}[\mathbf{m}] \right) \right) \oplus \left(\boldsymbol{\chi}_{\boldsymbol{g}}^{\boldsymbol{i}} - \mathbf{r^i} \right), \tag{A.23}$$

$$\mathbf{d^i} \coloneqq \rho \left(\bigoplus_{n=1}^{N_N} \left(\mathbf{c_n^i} - \mathbf{c_n^{i-1}} \right) \right) \oplus \left(\mathbf{e_w^i} - \mathbf{e_w^{i-1}} \right) \oplus \left(\mathbf{r^i} - \mathbf{r^{i-1}} \right), \tag{A.24}$$

where $\bigoplus_{n=1}^{N} \mathbf{y_i} = \mathbf{y_1} \oplus \mathbf{y_2} \cdots \oplus \mathbf{y_N}$. It is proved that the utility value of the ADMM iterates approaches the optimal value and that $\lim_{i \to \infty} \mathbf{p^i} = \lim_{i \to \infty} \mathbf{d^i} = \mathbf{0}$ [165]. In [166], two fast ADMM algorithms were proposed to enable quicker decay of these residuals compared to the original ADMM. The first algorithm is proved to achieve the following rates:

$$\|\mathbf{p^i}\|_2^2 \leqslant \mathcal{O}(\frac{1}{i^2}), \tag{A.25}$$

$$\|\mathbf{d^i}\|_2^2 \leqslant \mathcal{O}(\frac{1}{i^2}), \tag{A.26}$$

but requires both the objective functions to be strongly convex, which is not the case of (P_4). The second scheme introduced in [166] does not require strong convexity of the objective functions, but does not guarantee any global convergence rate. This algorithm applied to (P_4) is shown in Algorithm 5. The fast ADMM is similar to the original ADMM, but introduces an acceleration step (lines 8–13) which requires additional variables $\alpha, \bar{\mathbf{r}}, \bar{\mathbf{e}}_\mathbf{w}, \{\bar{\mathbf{c}}_\mathbf{n}\}, \{\bar{\mathbf{u}}_\mathbf{n}\}, \bar{\mathbf{v}}$. To enforce stability, a "restart" rule is used (lines 15–21) which relies on a combined residual defined by $C^i \coloneqq \sum_n C_n^i$

Algorithm 5 Fast ADMM for weakly convex problems applied to (P_4).

1: **for** $i = 1, \dots$ **do**
2: $\quad \boldsymbol{\chi}_{\boldsymbol{g}}^{\boldsymbol{i}} \leftarrow \arg\min_{\boldsymbol{\chi}_{\boldsymbol{g}}} L_\rho(\boldsymbol{\chi}_{\boldsymbol{g}}, \bar{\mathbf{r}}^{\mathbf{i}}, \bar{\mathbf{e}}_{\mathbf{w}}^{\mathbf{i}}, \{\bar{\mathbf{c}}_{\mathbf{n}}^{\mathbf{i}}\}, \{\bar{\mathbf{u}}_{\mathbf{n}}^{\mathbf{i}}\}, \bar{\mathbf{v}}^{\mathbf{i}})$
3: $\quad \mathbf{r}^{\mathbf{i}}, \mathbf{w}^{\mathbf{i}}, \{\mathbf{c}_{\mathbf{n}}^{\mathbf{i}}\} \leftarrow \arg\min_{\mathbf{r},\mathbf{w},\{\mathbf{c_n}\}} L_\rho(\boldsymbol{\chi}_{\boldsymbol{g}}^{\boldsymbol{i+1}}, \mathbf{r}, \mathbf{e}_{\mathbf{w}}, \{\mathbf{c}_{\mathbf{n}}\}, \{\bar{\mathbf{u}}_{\mathbf{n}}^{\mathbf{i}}\}, \bar{\mathbf{v}}^{\mathbf{i}})$
4: $\quad \mathbf{u}_{\mathbf{n}}^{\mathbf{i}}[\mathbf{m}] \leftarrow \bar{\mathbf{u}}_{\mathbf{n}}^{\mathbf{i}}[\mathbf{m}] + \boldsymbol{\chi}_{\boldsymbol{g}}^{\boldsymbol{i}}[\boldsymbol{m}] - \mathbf{c}_{\mathbf{n}}^{\mathbf{i}}[\mathbf{m}],\ m \in A(n),\ n \in \mathcal{N}$
5: $\quad \mathbf{v}^{\mathbf{i}} \leftarrow \bar{\mathbf{v}}^{\mathbf{i}} + \boldsymbol{\chi}_{\boldsymbol{g}}^{\boldsymbol{i}} - \mathbf{r}^{\mathbf{i}}$
6: $\quad$ Compute the combined residual C^i
7: $\quad$ **if** $C^i < \eta C^{i-1}$ **then**
8: $\quad\quad \alpha^{i+1} \leftarrow \frac{1+\sqrt{1+(\alpha^i)^2}}{2}$
9: $\quad\quad \bar{\mathbf{r}}^{\mathbf{i+1}} \leftarrow \mathbf{r}^{\mathbf{i}} + \frac{\alpha^i - 1}{\alpha^{i+1}}(\mathbf{r}^{\mathbf{i}} - \mathbf{r}^{\mathbf{i-1}})$
10: $\quad\quad \bar{\mathbf{e}}_{\mathbf{w}}^{\mathbf{i+1}} \leftarrow \mathbf{e}_{\mathbf{w}}^{\mathbf{i}} + \frac{\alpha^i - 1}{\alpha^{i+1}}(\mathbf{e}_{\mathbf{w}}^{\mathbf{i}} - \mathbf{e}_{\mathbf{w}}^{\mathbf{i-1}})$
11: $\quad\quad \bar{\mathbf{c}}_{\mathbf{n}}^{\mathbf{i+1}} \leftarrow \mathbf{c}_{\mathbf{n}}^{\mathbf{i}} + \frac{\alpha^i - 1}{\alpha^{i+1}}(\mathbf{c}_{\mathbf{n}}^{\mathbf{i}} - \mathbf{c}_{\mathbf{n}}^{\mathbf{i-1}}),\ n \in \mathcal{N}$
12: $\quad\quad \bar{\mathbf{u}}_{\mathbf{n}}^{\mathbf{i+1}} \leftarrow \mathbf{u}_{\mathbf{n}}^{\mathbf{i}} + \frac{\alpha^i - 1}{\alpha^{i+1}}(\mathbf{u}_{\mathbf{n}}^{\mathbf{i}} - \mathbf{u}_{\mathbf{n}}^{\mathbf{i-1}}),\ n \in \mathcal{N}$
13: $\quad\quad \bar{\mathbf{v}}^{\mathbf{i+1}} \leftarrow \mathbf{v}^{\mathbf{i}} + \frac{\alpha^i - 1}{\alpha^{i+1}}(\mathbf{v}^{\mathbf{i}} - \mathbf{v}^{\mathbf{i-1}})$
14: $\quad$ **else**
15: $\quad\quad C^i = \frac{C^{i-1}}{\rho}$
16: $\quad\quad \alpha^{i+1} \leftarrow 1$
17: $\quad\quad \bar{\mathbf{r}}^{\mathbf{i+1}} \leftarrow \mathbf{r}^{\mathbf{i-1}}$
18: $\quad\quad \bar{\mathbf{e}}_{\mathbf{w}}^{\mathbf{i+1}} \leftarrow \mathbf{e}_{\mathbf{w}}^{\mathbf{i-1}}$
19: $\quad\quad \bar{\mathbf{c}}_{\mathbf{n}}^{\mathbf{i+1}} \leftarrow \mathbf{c}_{\mathbf{n}}^{\mathbf{i-1}},\ n \in \mathcal{N}$
20: $\quad\quad \bar{\mathbf{u}}_{\mathbf{n}}^{\mathbf{i+1}} \leftarrow \mathbf{u}_{\mathbf{n}}^{\mathbf{i-1}},\ n \in \mathcal{N}$
21: $\quad\quad \bar{\mathbf{v}}^{\mathbf{i+1}} \leftarrow \mathbf{v}^{\mathbf{i-1}}$

that measures both the primal and dual residuals and where:

$$C_n^i := \frac{1}{\rho}\left(\|\mathbf{u}_{\mathbf{n}}^{\mathbf{i}} - \bar{\mathbf{u}}_{\mathbf{n}}^{\mathbf{i}}\|_2^2 + \|\mathbf{v}^{\mathbf{i}}[\mathbf{n}] - \bar{\mathbf{v}}^{\mathbf{i}}[\mathbf{n}]\|_2^2\right) + \rho\left(\|\mathbf{r}^{\mathbf{i}}[\mathbf{n}] - \bar{\mathbf{r}}^{\mathbf{i}}[\mathbf{n}]\|_2^2 + \|\mathbf{e}_{\mathbf{w}}^{\mathbf{i}}[\mathbf{n}] - \bar{\mathbf{e}}_{\mathbf{w}}^{\mathbf{i}}[\mathbf{n}]\|_2^2 + \|\mathbf{c}_{\mathbf{n}}^{\mathbf{i}} - \bar{\mathbf{c}}_{\mathbf{n}}^{\mathbf{i}}\|_2^2\right). \quad \text{(A.27)}$$

The "restart" rule throws up the most recent iteration and "restarts" the algorithm if the combined residual has not decreased by a factor of at least $\eta \in (0, 1)$. It is proved that $\lim_{i\to\infty} C^i = 0$ [166]. Indeed, each "restart" iteration, *i.e.* iteration that triggered a "restart", is followed by an original ADMM iteration ($\alpha^i = 1$), and it is proved that the original ADMM decreases the combined residual monotonically [168]. Also, for each "accelerated" iteration, *i.e.* iteration with $\alpha^i > 1$ and that did not triggered a "restart", the combined residual decreases by a factor of at least η. Therefore, if the number of "accelerated" iterations is infinite, it is clear that $\lim_{i\to\infty} C^i = 0$. In the case that the number of "restart" iterations is finite, then each pair of "restart" and original ADMM iteration is equivalent to a single original ADMM iteration, for which convergence of the combined residual is known.

Let us now look at how Algorithm 5 can be distributed. The first step (line 2) of an iteration is to solve:

$$\boldsymbol{\chi}_{\boldsymbol{g}}^{\boldsymbol{i}} = \arg\min_{\boldsymbol{\chi}_{\boldsymbol{g}}} L_\rho(\boldsymbol{\chi}_{\boldsymbol{g}}, \bar{\mathbf{r}}^{\mathbf{i}}, \bar{\mathbf{e}}_{\mathbf{w}}^{\mathbf{i}}, \{\bar{\mathbf{c}}_{\mathbf{n}}^{\mathbf{i}}\}, \{\bar{\mathbf{u}}_{\mathbf{n}}^{\mathbf{i}}\}, \bar{\mathbf{v}}^{\mathbf{i}}). \quad \text{(A.28)}$$

If it is assumed that the vector $(\bar{\mathbf{r}}, \bar{\mathbf{e}}_{\mathbf{w}}, \{\bar{\mathbf{c}}_{\mathbf{n}}\}) \in \mathcal{C}$, then (A.28) can be written as follows:

$$\boldsymbol{\chi}_{\boldsymbol{g}}^{\boldsymbol{i}} = \arg\min_{\boldsymbol{\chi}_{\boldsymbol{g}}} \left\{ f_0(\boldsymbol{\chi}_{\boldsymbol{g}}) + \frac{\rho}{2} \sum_{n=1}^{N_N} \left(\|\boldsymbol{\chi}_{\boldsymbol{g}}[\boldsymbol{n}] - \bar{\mathbf{r}}^{\mathbf{i}}[\mathbf{n}] + \bar{\mathbf{v}}^{\mathbf{i}}[\mathbf{n}]\|_2^2 + \sum_{m \in S(n)} \|\boldsymbol{\chi}_{\boldsymbol{g}}[\boldsymbol{n}] - \bar{\mathbf{c}}_{\mathbf{m}}^{\mathbf{i}}[\mathbf{n}] + \bar{\mathbf{u}}_{\mathbf{m}}^{\mathbf{i}}[\mathbf{n}]\|_2^2 \right) \right\}, \quad \text{(A.29)}$$

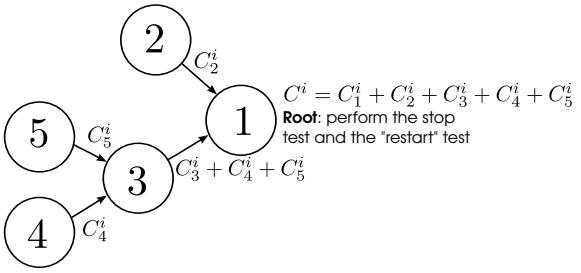

Figure A.3 – Illustration of the combined residual calculation: each node n gathers the combined residuals calculated by its one-hop predecessors, sums these values, add to the result its own local combined residual C_n^i, and then sends the so-obtained value to its successor.

by noticing that:

$$\sum_{n=1}^{N_N} \sum_{m \in A(n)} \|\boldsymbol{\chi_g}[\boldsymbol{m}] - \bar{\mathbf{c}}_\mathbf{n}[\mathbf{m}] + \bar{\mathbf{u}}_\mathbf{n}[\mathbf{m}]\|_2^2 = \sum_{n=1}^{N_N} \sum_{m \in S(n)} \|\boldsymbol{\chi_g}[\boldsymbol{n}] - \bar{\mathbf{c}}_\mathbf{m}[\mathbf{n}] + \bar{\mathbf{u}}_\mathbf{m}[\mathbf{n}]\|_2^2. \tag{A.30}$$

To solve this problem, each node computes:

$$\boldsymbol{\chi}_{\boldsymbol{g}}^{\boldsymbol{i}}[\boldsymbol{n}] = \underset{\boldsymbol{\chi_g[n]}}{\arg\min} \left\{ \sum_{k=1}^{K} \log \chi_g[n,k] + \frac{\rho}{2} \sum_{m \in S(n)} \|\boldsymbol{\chi_g}[\boldsymbol{n}] - \bar{\mathbf{c}}_\mathbf{m}^\mathbf{i}[\mathbf{n}] + \bar{\mathbf{u}}_\mathbf{m}^\mathbf{i}[\mathbf{n}]\|_2^2 \right.$$
$$\left. + \frac{\rho}{2} \|\boldsymbol{\chi_g}[\boldsymbol{n}] - \bar{\mathbf{r}}^\mathbf{i}[\mathbf{n}] + \bar{\mathbf{v}}^\mathbf{i}[\mathbf{n}]\|_2^2 \right\}. \tag{A.31}$$

The second step (line 3) of an iteration is to solve:

$$\begin{bmatrix} \mathbf{r}^\mathbf{i} \\ \mathbf{e}_\mathbf{w}^\mathbf{i} \\ \{\mathbf{c}_\mathbf{n}^\mathbf{i}\} \end{bmatrix} = \underset{\mathbf{r},\mathbf{e_w},\{\mathbf{c_n}\}}{\arg\min} L_\rho(\boldsymbol{\chi}_{\boldsymbol{g}}^{\boldsymbol{i}}, \mathbf{r}, \mathbf{e_w}, \{\mathbf{c_n}\}, \{\bar{\mathbf{u}}_\mathbf{n}^\mathbf{i}\}, \bar{\mathbf{v}}^\mathbf{i}), \tag{A.32}$$

which can be done if each node computes:

$$\begin{aligned} \underset{\mathbf{r[n]},\mathbf{e_w[n]},\mathbf{c_n}}{\text{minimize}} & \left\{ \|\boldsymbol{\chi}_{\boldsymbol{g}}^{\boldsymbol{i}}[\boldsymbol{n}] - \mathbf{r}[\mathbf{n}] + \bar{\mathbf{v}}^\mathbf{i}[\mathbf{n}]\|_2^2 + \sum_{m \in A(n)} \|\boldsymbol{\chi}_{\boldsymbol{g}}^{\boldsymbol{i}}[\boldsymbol{m}] - \mathbf{c_n}[\mathbf{m}] + \bar{\mathbf{u}}_\mathbf{n}^\mathbf{i}[\mathbf{m}]\|_2^2 \right\} \\ \text{subject to: } & e_w[n,k] \geqslant 0, \ k \in \mathcal{K} \\ & g(n,k,\mathbf{r[n]},\mathbf{e_w[n]},\mathbf{c_n}) \leqslant B[n], \ k \in \mathcal{K} \\ & g(n,k,\mathbf{r[n]},\mathbf{e_w[n]},\mathbf{c_n}) \geqslant b[n], \ k \in \mathcal{K} \end{aligned} \tag{A.33}$$

The constraints of (A.33) guarantee that the global solution of this problem $(\mathbf{r}^\mathbf{i}, \mathbf{w}^\mathbf{i}, \{\mathbf{c}_\mathbf{n}^\mathbf{i}\}) \in \mathcal{C}$, and therefore $\mathcal{I}_\mathcal{C}(\mathbf{r}^\mathbf{i}, \mathbf{e}_\mathbf{w}^\mathbf{i}, \{\mathbf{c}_\mathbf{n}^\mathbf{i}\}) = 0$. The third step of an iteration is to update the scaled dual variables $\{\mathbf{u_n}\}$ and $\mathbf{v}$ (lines 4–5).

The next step is the calculation of the combined residual (line 6). In order to reduce the amount of message passing, the combined residual is computed as illustrated in Figure A.3: each node n gathers the combined residuals calculated by its one-hop predecessors, sums these values, add to the result its own local combined residual C_n^i, and sends the so-obtained value:

$$C_n^i + \sum_{m \in A(n)} C_m^i \tag{A.34}$$

to its successor. By starting from the leaf nodes, the value thus calculated by the root node corresponds to the global combined residual. Therefore, the root node performs the "restart" test (line 7). If the "restart" test is passed, the root node broadcasts a "restart" instruction to all

Algorithm 6 Executed by the node n at the end of each slot.

Init: $\alpha^1 = 1,\ \bar{\mathbf{r}}^{\mathbf{1}} = \mathbf{r}^{\mathbf{0}},\ \bar{\mathbf{w}}^{\mathbf{1}} = \mathbf{w}^{\mathbf{0}},\ \bar{\mathbf{c}}^{\mathbf{1}}_{\mathbf{n}} = \mathbf{c}^{\mathbf{0}}_{\mathbf{n}},\ \bar{\mathbf{u}}^{\mathbf{1}}_{\mathbf{n}} = \mathbf{u}^{\mathbf{0}}_{\mathbf{n}},\ \bar{\mathbf{v}}^{\mathbf{1}} = \mathbf{v}^{\mathbf{0}}$
for $i = 1, \dots$ **do**
  if $A(n) \neq \varnothing$ **then**
    Send $\bar{\mathbf{c}}^{\mathbf{i}}_{\mathbf{n}}$ and $\bar{\mathbf{u}}^{\mathbf{i}}_{\mathbf{n}}$ to all predecessors
  if $S(n) \neq \varnothing$ **then**
    Wait for all $\bar{\mathbf{c}}^{\mathbf{i}}_{\mathbf{m}}$ and $\bar{\mathbf{u}}^{\mathbf{i}}_{\mathbf{m}}$, $m \in S(n)$
  Compute $\boldsymbol{\chi}^{\boldsymbol{i}}_{\boldsymbol{g}}[\boldsymbol{n}]$ by solving (A.31)
  if $S(n) \neq \varnothing$ **then**
    Send $\boldsymbol{\chi}^{\boldsymbol{i}}_{\boldsymbol{g}}[\boldsymbol{n}]$ computed at previous step to all successors
  if $A(n) \neq \varnothing$ **then**
    Wait for all $\boldsymbol{\chi}^{\boldsymbol{i}}_{\boldsymbol{g}}[\boldsymbol{m}]$, $m \in A(n)$
  Compute $\mathbf{r}^{\mathbf{i}}[\mathbf{n}]$, $\mathbf{w}^{\mathbf{i}}[\mathbf{n}]$ and $\mathbf{c}^{\mathbf{i}}_{\mathbf{n}}$ by solving (A.33)
  $\mathbf{u}^{\mathbf{i}}_{\mathbf{n}}[\mathbf{m}] \leftarrow \bar{\mathbf{u}}^{\mathbf{i}}_{\mathbf{n}}[\mathbf{m}] + \boldsymbol{\chi}^{\boldsymbol{i}}_{\boldsymbol{g}}[\boldsymbol{m}] - \mathbf{c}^{\mathbf{i}}_{\mathbf{n}}[\mathbf{m}],\ m \in A(n)$
  $\mathbf{v}^{\mathbf{i}}[\mathbf{n}] \leftarrow \bar{\mathbf{v}}^{\mathbf{i}}[\mathbf{n}] + \boldsymbol{\chi}^{\boldsymbol{i}}_{\boldsymbol{g}}[\boldsymbol{n}] - \mathbf{r}^{\mathbf{i}}[\mathbf{n}]$
  Compute C^i_n according to (A.27)
  Wait the residuals sent by the one-hop predecessors
  Compute $C^i_n + \sum_{m \in A(n)} C^i_m$ and send it to the successor
  $\alpha^{i+1} \leftarrow \frac{1+\sqrt{1+(\alpha^i)^2}}{2}$
  $\bar{\mathbf{r}}^{\mathbf{i+1}}[\mathbf{n}] \leftarrow \mathbf{r}^{\mathbf{i}}[\mathbf{n}] + \frac{\alpha^i - 1}{\alpha^{i+1}}(\mathbf{r}^{\mathbf{i}}[\mathbf{n}] - \mathbf{r}^{\mathbf{i-1}}[\mathbf{n}])$
  $\bar{\mathbf{w}}^{\mathbf{i+1}}[\mathbf{n}] \leftarrow \mathbf{w}^{\mathbf{i}}[\mathbf{n}] + \frac{\alpha^i - 1}{\alpha^{i+1}}(\mathbf{w}^{\mathbf{i}}[\mathbf{n}] - \mathbf{w}^{\mathbf{i-1}}[\mathbf{n}])$
  $\bar{\mathbf{c}}^{\mathbf{i+1}}[\mathbf{n}] \leftarrow \mathbf{c}^{\mathbf{i}}[\mathbf{n}] + \frac{\alpha^i - 1}{\alpha^{i+1}}(\mathbf{c}^{\mathbf{i}}[\mathbf{n}] - \mathbf{c}^{\mathbf{i-1}}[\mathbf{n}])$
  $\bar{\mathbf{u}}^{\mathbf{i+1}}[\mathbf{n}] \leftarrow \mathbf{u}^{\mathbf{i}}[\mathbf{n}] + \frac{\alpha^i - 1}{\alpha^{i+1}}(\mathbf{u}^{\mathbf{i}}[\mathbf{n}] - \mathbf{u}^{\mathbf{i-1}}[\mathbf{n}])$
  $\bar{\mathbf{v}}^{\mathbf{i+1}}[\mathbf{n}] \leftarrow \mathbf{v}^{\mathbf{i}}[\mathbf{n}] + \frac{\alpha^i - 1}{\alpha^{i+1}}(\mathbf{v}^{\mathbf{i}}[\mathbf{n}] - \mathbf{v}^{\mathbf{i-1}}[\mathbf{n}])$
  if Is root **then**
    $C^i = \sum_{n=1}^{N_N} C^i_n$
    if $C^i < \epsilon$ **then**
      Broadcast stop instruction
      break
    else if $C^i \geqslant \eta C^{i-1}$ **then**
      $C^i = \frac{C^{i-1}}{\rho}$
      Broadcast restart instruction for slot i
      RESTART(i)

Set the packet generation rate to $\chi_g[n, 0]$
▷ Executed if a restart instruction is received:
function RESTART(i)
  $\alpha^{i+1} \leftarrow 1$
  $\bar{\mathbf{r}}^{\mathbf{i+1}}[\mathbf{n}] \leftarrow \mathbf{r}^{\mathbf{i-1}}[\mathbf{n}]$
  $\bar{\mathbf{w}}^{\mathbf{i+1}}[\mathbf{n}] \leftarrow \mathbf{w}^{\mathbf{i-1}}[\mathbf{n}]$
  $\bar{\mathbf{c}}^{\mathbf{i+1}}_{\mathbf{n}} \leftarrow \mathbf{c}^{\mathbf{i-1}}_{\mathbf{n}}$
  $\bar{\mathbf{u}}^{\mathbf{i+1}}_{\mathbf{n}} \leftarrow \mathbf{u}^{\mathbf{i-1}}_{\mathbf{n}}$
  $\bar{\mathbf{v}}^{\mathbf{i+1}} \leftarrow \mathbf{v}^{\mathbf{i-1}}$
  Start iteration $i + 1$

its predecessors, *i.e.* all the other nodes in the tree. As the combined residual converges to 0, a reasonable stop criteria is $C^i < \epsilon$, where $\epsilon > 0$ is a parameter of the algorithm. The root node is responsible for performing the stop test, as it is aware of the global combined residual. If the stop test is passed, the root node broadcasts a "stop" instruction to all the other nodes in the tree, to inform them that the algorithm has converged.

The complete algorithm executed by each node n at the end of each time slot is shown in Algorithm 6. To solve (A.31) (line 6), each node n needs the values of $\mathbf{c_m}$ and $\mathbf{u_m}$ of all its successors m (lines 4–5), and therefore each node that is not a leaf of the routing tree sends its values of $\mathbf{c_n}$ and $\mathbf{u_n}$ to its predecessors (lines 2–3). This is done before solving the local problem, to avoid stopping the predecessors from starting solving (A.31). Solving (A.33) (line 11) requires each node n to have the newly computed packet generation rate values $\boldsymbol{\chi_g[m]}$ of its predecessors (lines 9–10), and therefore each node sends its value of $\boldsymbol{\chi_g[n]}$ (lines 7–8) before starting solving (A.33). The node n then performs the residual calculation step (lines 14–16), and the acceleration steps of fast ADMM (lines 17–22). The root, which is the only node aware of the global combined residual, performs the stop criteria (line 25–27) and, if the stop criteria is passed, it broadcasts the "stop" instruction. In that case, each node n sets its packet generation rate to the value of $\chi_g[n, 0]$ just calculated (line 33). The root also performed the "restart" test (line 28). If the "restart" test is passed, the root broadcasts the "restart" instruction. The function RESTART is used to perform the "restart" operation. It is called synchronously by the root (line 31), or at the reception of a "restart" instruction by the other nodes.

A.2 Performance Evaluation

A network made of 15 PowWow [99] nodes organized in a binary tree was simulated, the root node having as a one-hop successor the sink. To simulate the harvested energy, indoor light energy traces from [47] were used. These traces correspond to real measurements, and each node was powered with a different trace. All the nodes were equipped with a 0.9 F capacitance, with a maximum voltage of 5.2 V and a minimum voltage of 2.8 V, and therefore $B[n] = 12.168\,\text{J},\ n \in \mathcal{N}$ and $b[n] = 3.528\,\text{J},\ n \in \mathcal{N}$. Moreover, the energy costs C_R and C_L were set to 25 mJ and 15 mJ respectively, and these values were used for all the nodes. The EM was executed every $T_s = 2$ hours, and the prediction window was $K = 12$, corresponding to 24 hours. The simulated time was 10 days. ρ and η were set to the typical values of 1.0 and 0.999 respectively [166]. In order to accelerate the convergence of the algorithm, warm starting was used, *i.e.* the allocation calculated at the iteration i was used as the start point for the iteration $i + 1$.

Two performance metrics were considered: the average packet generation rate, and fairness which was measured using Jain's fairness index defined as follows:

$$J(\boldsymbol{\chi_g}, t) := \frac{\left(\sum_{n=1}^{N_N} \chi_g[n,t]\right)^2}{N \sum_{n=1}^{N_N} \chi_g[n,t]^2}. \tag{A.35}$$

The Jain's fairness index ranges from $\frac{1}{N}$ to 1, this latter value corresponding to all the nodes having the same packet generation rate. The proposed algorithm was evaluated for different values of ϵ in the range $[0.1, 3.0]$. Moreover, (P_1) was also solved by a regular solver and the so-obtained optimal solution serves as a reference for comparison. For all the simulation runs, no power failure was observed.

The proposed algorithm was evaluated using both perfect predictions, referred to as the "oracle case", and the predictor from [8], referred to as "predictor case". Results are presented in Figure A.4. Figure A.4a and Figure A.4b show the cumulative relative error between the utility value (f_0) obtained by the proposed algorithm and the optimal utility for each time slot, for the predictor case and the oracle case respectively. As expected, the higher is ϵ, the higher is the relative error and therefore the less accurate is the allocation computed by the proposed scheme compared to the optimal solution. Moreover, it can be seen that the relative error is significantly higher in the predictor case than in the oracle case.

The average packet generation rate as a function of ϵ is shown for in Figure A.4c for the predictor case and in Figure A.4d for the oracle case. It can be seen that the average packet generation rate

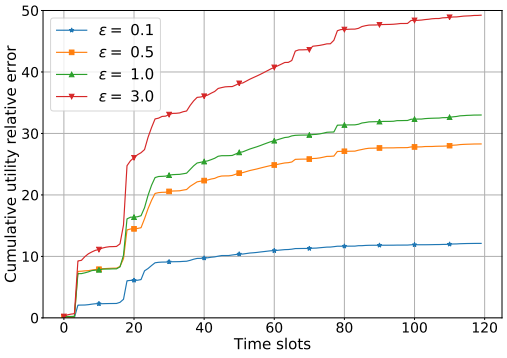

(a) Predictor case: utility value.

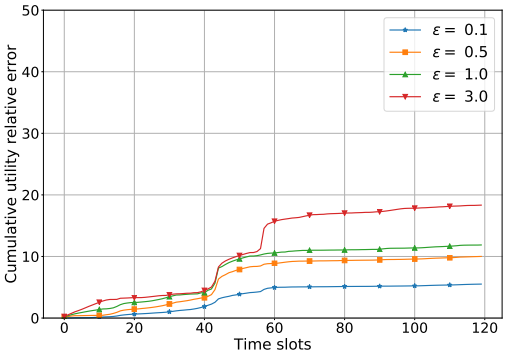

(b) Oracle case: utility value.

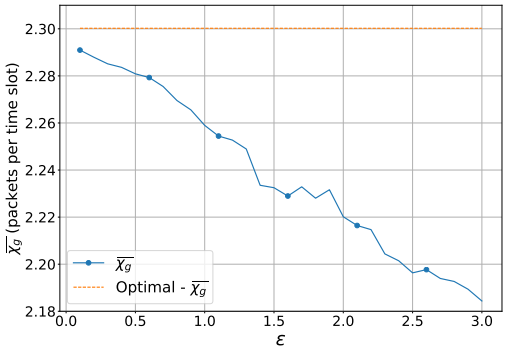

(c) Predictor case: packet generation rate.

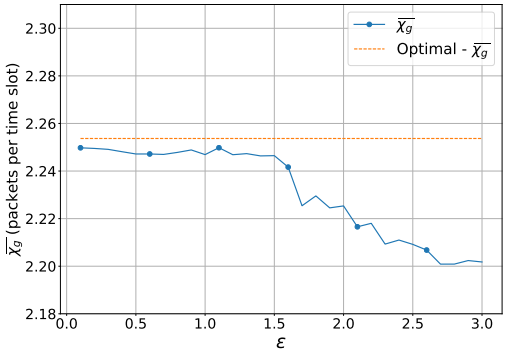

(d) Oracle case: packet generation rate.

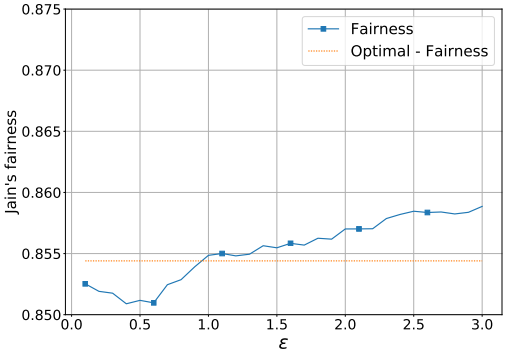

(e) Predictor case: Jain's fairness.

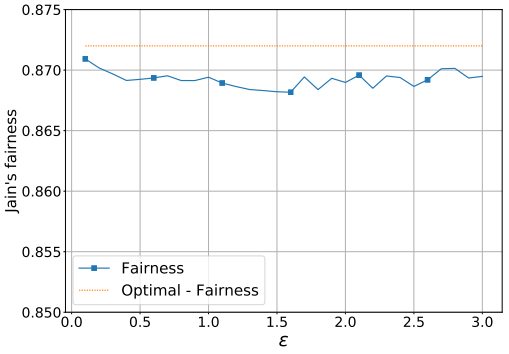

(f) Oracle case: Jain's fairness.

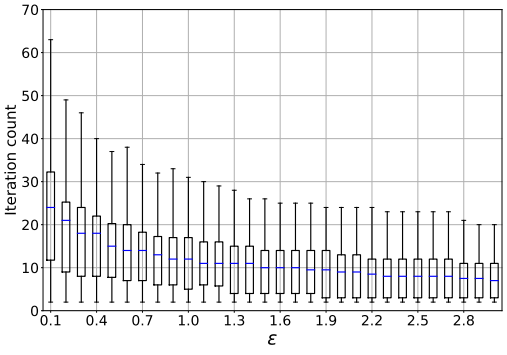

(g) Predictor case: iteration count.

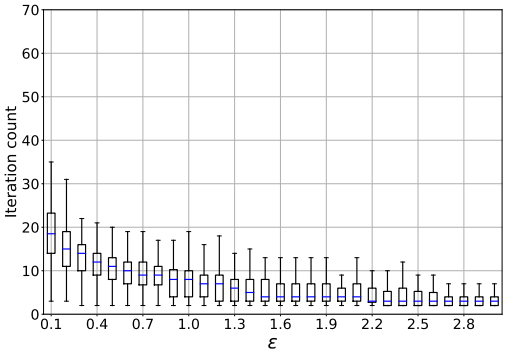

(h) Oracle case: iteration count.

Figure A.4 – Performance evaluation with the predictor from [8] and an oracle giving perfect predictions.

achieved in the oracle case and predictor case are very similar, as the difference between the optimal packet generation rate for the predictor case and the optimal packet generation rate for the oracle case is 2%. Moreover, in both cases, increasing ϵ leads to lower average packet generation rate. However, in the oracle case, the performance decay is less strong than in the predictor case.

Regarding Jain's fairness (Figure A.4e and Figure A.4f), in both the oracle and the predictor case, the optimal Jain's fairness is not 1. Indeed, nodes that harvest more energy will have a higher throughput as long as it is fair to the other nodes giving the amount of energy that they harvest. Therefore, a Jain's fairness of 1, corresponding to all the nodes having the same packet generation rate, is generally not optimal. The achieved Jain's fairness is however close to 1, which indicates that the nodes have similar packet generation rates. Similarly to the results obtained for the packet generation rate, the fairness obtained in the predictor case and in the oracle case are very similar. Moreover, increasing ϵ does not lead to significantly worse fairness in both cases, as it stays within a 0.5% range of the optimal Jain's fairness.

If increasing ϵ leads to less accurate solutions, it significantly decreases the overhead of the EM. Indeed, on constrained systems such as WSNs, the overhead incurred by the EM is not negligible. As shown in Figure A.4g and FigureA.4h, increasing ϵ significantly reduces the number of iterations required by the proposed algorithm. Moreover, it can be seen that the number of iterations required in the oracle case is significantly lower than the number of iterations required in the predictor case. This might be because using the oracle (perfect prediction), the predicted harvested energy does not change significantly from one iteration to the other, while using a predictor, the predicted harvested energy can change significantly from one iteration to the other, making the warm starting less efficient.

A.3 Conclusion

In this appendix, a distributed algorithm for fair packet generation rate assignment targeting multi-hop EH-WSNs was proposed. In EH-WSNs, each node both performs measurements to produce data to be sent to a sink, and relays data packets from other nodes. The packet rate assignment problem was formulated as a convex optimization problem, and using the fast ADMM, the original problem was decomposed into smaller subproblems that can be solved in parallel. Simulations using real indoor light energy traces showed that the results obtained using a state of the art predictor are similar to the ones obtained using perfect predictions. Moreover, simulations showed that the algorithm enables packet generation rates and fairness close to the optimal, even with a low number of iterations. Also, by setting the stop criteria parameter, a compromise can be set between the accuracy of the solution and the computational overhead incurred by the algorithm.

Appendix B

Long-Short range Communication with LoRa™ and Wake-up Receivers

The most widely-used communication scheme for WSNs is the IEEE 802.15.4 standard, which provides both physical layer and MAC layer specifications. This standard enables low-cost and low power transceivers, but suffers from a range of only a few tens of meters. In recent years, a handful of wireless technologies enabling Long Range (LR) communication of several kilometers with power consumption similar to usual WSN nodes transceivers [169] have emerged. An example of such a technology in use is LoRa™ [170], by the LoRa™ Alliance. LoRa™ operates in the 868/915 MHz ISM bands, allows a theoretical range up to a few tens of kilometers, and a bit rate in the range between 0.37 and 46.9kbps [171]. Using LoRa™, uplink communication, *i.e.* from the nodes to the gateway, is done with low latency, as the gateway is always listening to the channel. On the other hand, downlink communication, *i.e.* from the gateway to the nodes, requires a trade-off between the latency and the power consumption of the nodes [172]. However, some applications, such as industrial machine health monitoring, require both low latency and low power consumption [173], which motivates the network architecture proposed in this chapter.

As one can notice, WuRx and LoRa™ provide orthogonal features that are often required together in WSNs applications. Moreover, many application scenarios are comprised by many nodes clustered in short range areas, but with the need to communicate with remote hosts which can be several kilometers apart. In this chapter, we propose to combine the LoRa™ communication scheme with ULP WuRx in a network architecture [174, 175], which exploits radio diversity to achieve energy efficiency and low latency in both uplink and downlink communications. The nodes that form the network embed a communication module that is able to handle LoRa™ as well as the well-known Gaussian Frequency-Shift Keying (GFSK) and OOK modulation schemes, in combination with WuRx. The proposed network architecture achieves uplink communication by using only the LoRa™ scheme, while downlink communication is done using the LoRa™ stack to transmit the message to one of the sensors nodes designated as the Cluster Head (CH), which then forwards the message to the addressee nodes by first waking them up using their WuRx, and then transmitting the message using standard GFSK modulation. WuCs are sent using OOK modulation. The LoRa™ communication protocol has been analytically modeled as well as the proposed approach to evaluate the power consumption and latency. The designed architecture was experimentally evaluated in terms of power consumption and latency, and results show that the proposed scheme removes the required trade-off between power consumption and latency. The main contributions of this work are:

- A network architecture allowing low power and low latency LR communications,
- Experimental evaluation of the proposed architecture on a new platform that embeds both a LoRa™ transceiver and a WuRx,
- Analytical comparisons of the power consumption and latency of the proposed architecture to LoRa™ standard schemes.

The rest of this chapter is organized as follows: Section B.1 presents the related work. Section B.2 exposes the proposed network architecture, as well as the MAC layer. In Section B.3, an

analytical model is derived to compare the power consumption and latency of the proposed scheme to the standard LoRa™ approaches. Section B.4 presents the experimental setup and the power consumption and sensitivity measurement results of the LoRa™scheme. Section B.5 shows results of analytical comparisons between standard LoRa™schemes and the proposed architecture, and finally, Section B.6 concludes this chapter.

B.1 Related Work

B.1.1 Long-Range Communication Schemes

LR communication schemes can be grouped according to the spectrum use, *i.e.* Ultra Narrow Band (UNB) techniques, which aim to minimize the bandwidth to increase the sensitivity, or spread spectrum schemes, which take advantage of spectral diversity.

The physical layer developed and patented by the French company SigFox achieves UNB by broadcasting binary data using Binary Phase-Shift Keying (BPSK) modulation at very low bitrate (100 bps), on a much larger band, typically 192 kHz in the 868 MHz or 915 MHz band. Frequency hopping inside the band is supported to improve reliability, and medium access is done using a modified Aloha scheme, where nodes randomly access to the channel both in time and frequency domain.

Another narrow band physical layer is proposed by Weightless, an organization which aims to provide wireless standards for internet of things networks. Multiple standards, targeting different use cases, are proposed. The Weightless-N standard, based on Differential Binary Phase-Shift Keying (DBPSK) modulation, is unidirectional and allows a range of 5km. Similarly to SigFox, frequency hopping is used to counteract interference and fading. The Weightless-P standards is based on the Weightless-N standard, but enables bidirectional communication and acknowledgement. It uses Frequency Division Multiple Access (FDMA) and Time Division Multiple Access (TDMA) to scale to a large number of devices, but reduces the range to 2 km in urban environment. The last proposed standard, Weightless-W is not narrow band, but is a spread spectrum scheme. It operates in TV white space spectrum, and uses variable modulation modes coupled with spreading codes, to enable 5 km range and bidirectional communication.

The scheme proposed by Ingenu differs from the other long-range communication methods as it operates in the 2.4GHz ISM band. It is a spread spectrum technique, called Random Phase Multiple Access (RPMA), that enables a range of 10 km, using a typical channel bandwidth of 1 MHz. Both uplink and downlink transmission are allowed, and performed in a half-duplex way with a downlink period of 2 s, followed by an uplink period of 2 s. The spreading factor is dynamically adapted based on the received power.

Another spread spectrum technique for LR communication was patented by Cycléo, and is based on Chirp Spread Spectrum (CSS). Named LoRa™, this physical layer operates in the 868 MHz or 915 MHz ISM bands, and enables a range up to a few tens of kilometers. In the LoRa™network architecture [172], all WSN nodes communicate directly with the gateway, which serves as a bridge between the nodes and a network server. The gateway is always active listening to the channel, while three types of classes are defined for end-devices: A, B and C. Class A is the lowest power consuming class, as nodes only leave the sleep state to send their data. Each uplink transmission is followed by two short downlink receive windows. Class B devices open additional receive windows at scheduled time in addition to class A receive windows, and time synchronized beacons from the gateway are used to allow the gateway to know when devices are listening. Finally, class C devices are continuously listening, except when they are transmitting. Therefore, using the LoRa™network architecture, a trade-off must be made between latency and energy consumption for downlink communications.

B.1.2 Heterogeneous Communication Networks

As many devices embed more than one radio module, exploiting radio diversity was previously proposed to reduce energy consumption and latency for opportunistic networking [176]. The main idea is to use a low power radio combined with a high power radio. It is expected that using two radio modules instead of one account for higher energy expense, but exploiting the low power

radio to save power on the high power radio can ultimately reduce power consumption of the whole system. Some combinations of low power radio (typically Bluetooth or Zigbee) and high power radio (typically Wi-Fi or cellular) were previously proposed [177–179].

In many devices such as smartphones, the low power radio is a Bluetooth or Zigbee module, while the high power radio is a Wi-Fi or cellular module. *Pering et al.* [177] proposed to use a low level radio to discover, configure and activate a high level radio link when a connection is needed. The authors experimented on a platform that provides Bluetooth, Zigbee and Wi-Fi, and revealed that the lower power consumption is achieved by employing Zigbee and Wi-Fi. However, using Bluetooth and Zigbee as a low power radio is still too energy costly for WSN applications, which is the focus of this work. Moreover, neither Bluetooth, Zigbee nor Wi-Fi allow kilometer-range communication. Other proposals combining Wi-Fi and Zigbee for power saving purpose are present in literature [178,179]. Differently from these previous works, we are using a single transceiver that is dynamically configured to work in combination with LoRa^{TM}for the LR, and WuRx for the Short Range (SR).

To the best of our knowledge, the closest work to ours is [180]. The authors proposed the OpenMote+ platform, targeting industrial applications, which combines three communication modules: one for LR (kilometers-range) communication, one for hundreds of meters communication, and one for contact-based communication. Each module is implemented by a specific hardware chip. LR communication is implemented by the Sub-GHz EZRadioPRO radio transceiver, which provides a sensitivity of −133 dBm and a transmission power up to 20 dBm. In addition to this radio interface, a low-energy Atmel AT86RF233 is present. This transceiver operates in the 2.4 GHz band, and supports IEEE 802.15.4 standards. Finally, contact-based communication is implemented by the NXP NT3H1201 chip, which operates in the 13.56 MHz band and supports the Near Field Communication (NFC) standard. However, contrary to our proposal, no WuRx is used to eliminate idle listening and perform purely asynchronous communication for SR communications. In this work, we propose to combine the LoRa^{TM}communication scheme, able to achieve kilometer-range communication, with WuRx, which enable SR distant wake-up of the nodes with no significant power consumption increase, and low downlink latency. This work emphasizes on the network architecture and the MAC protocols.

B.2 Long-Short Range Network Architecture

B.2.1 Communication Module Architecture

This work addresses the use of heterogeneous radio systems to enhance energy and latency of LR communications. The block diagram of the proposed WSN node is illustrated in Figure B.1. Each node embeds a MCU, sensors, actuators, an energy storage device and a communication module. The communication stack allows both LR and SR communications.

LR communication relies on the LoRa^{TM}physical layer, which can recover data from weak signal, even under the noise level. SR communications relies on GFSK and OOK modulations.

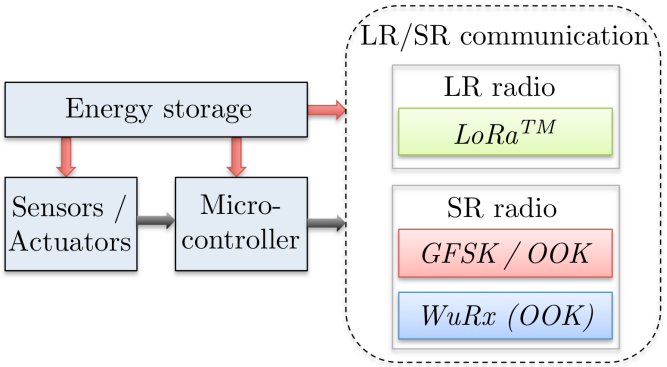

Figure B.1 – Long-Short range node architecture.

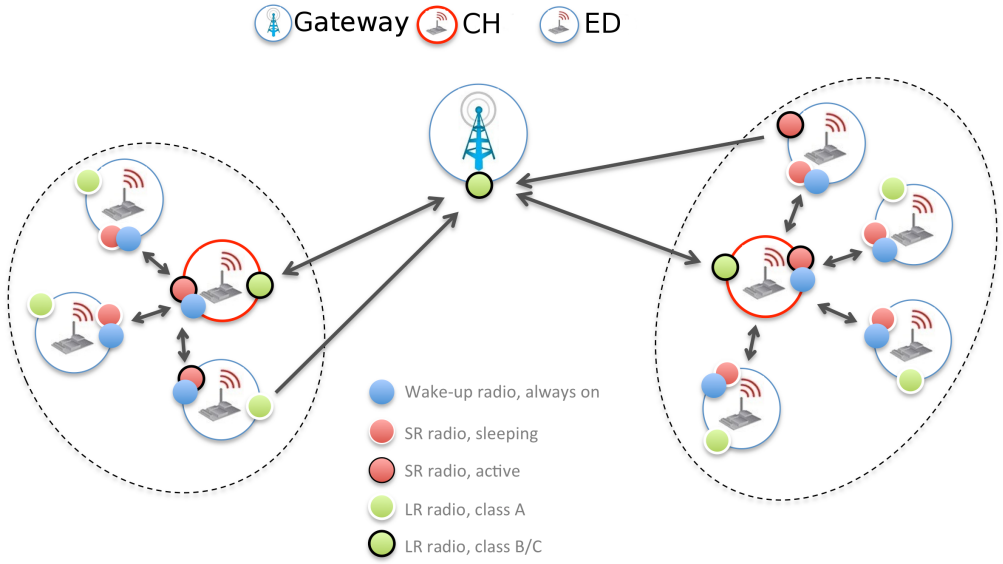

Figure B.2 – Cluster-based network architecture for Long-Short range communication.

GFSK modulation is compatible with IEEE 802.15.4 frame allowing bit rate up to 300 kbps, while OOK modulation is used to wake up the WuRx devices. Indeed, each WSN node is equipped with a WuRx, which receives data with OOK modulation. Typically, the WuRx is continuously listening to the wireless medium while the main transceivers (*i.e.* LoRa™ and GFSK) are in a power saving state. Moreover, the WuRx embeds address matching features, which allows a node to wake up only a specific subset of its neighbors.

B.2.2 Cluster-Based Network Architecture

In the proposed network architecture, WSN nodes are organized in clusters as shown in Figure B.2. A gateway, located at a large distance (few kilometers) from the clusters, collects the sensed data, and sends commands to the nodes, e.g. to activate actuators or to set sensing parameters. Each cluster is organized in a star topology network composed of long-short range nodes introduced previously. In a cluster, a CH is in charge of bidirectional LR communications with the gateway and of SR communications with the other nodes of the clusters, referred to as End Devices (EDs). The EDs are distributed in a range of a few tens of meters around the CH.

The gateway is assumed to have no energy constrains, and therefore operates in LoRa™ class C. The CHs operate in class B or C according to their energy constrains and the application requirements. EDs are energetically constrained, and therefore spend most of their time in the sleep state. EDs only wake up when an interrupt occurs. This interrupt can be triggered on a timer expiration, e.g. to perform periodic sensing or action, or on an event from the environment detected by an embedded sensor. These interrupts may lead to the sending of a data message intended for the gateway. To this aim, the EDs directly send the data to the gateway using LR communication, as shown in Figure B.2. For the EDs, LoRa™ class A is used to send the data.

Another kind of interrupts that can wake up the EDs is the reception of a WuC detected by the WuRx. Indeed, as each ED is equipped with a WuRx, the CH can wake up one or more EDs by sending WuCs. This interrupt occurs in the "data request" scenario when the gateway first sends a command attended to one or more EDs and the EDs transmit in a second step data to the gateway in response to the command. This scenario will be experimented in the following as it leads to interesting performance gains (both energy and latency) compared to LR-only communication schemes.

In this scenario, the gateway first transmits the command to the CHs using standard LoRa™ communication schemes, the CH being in class B or C. Then, the CHs forwards the command to the addressee EDs, by waking up the addressee EDs by sending a WuC to their WuRx. Finally, the EDs sends the requested data to the gateway using the standard LoRa™ approach. Hence, direct LR com-

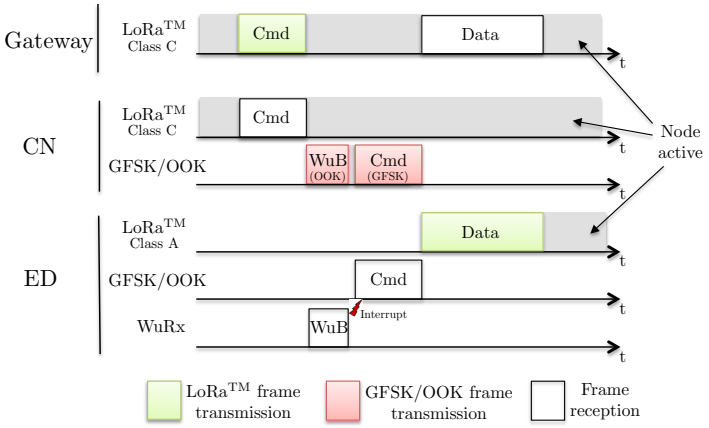

Figure B.3 – Long-Short range MAC protocol using WuRx.

munication is unidirectional between the EDs and the gateway (ED → gateway), and bidirectional between the gateway and the CH. The protocol dedicated to this scenario is detailed in the next section.

B.2.3 MAC Layer Design

The protocol that addresses the "data request" scenario is illustrated in Figure B.3. The gateway first sends the command (Cmd) to the CH of the addressee cluster. Once the command is received, the CH wakes up the ED by sending a 2 bytes long WuC, using OOK modulation. The WuC consists of a 1 byte preamble, and a 1 byte address, corresponding to the address of the addressee ED. To handle the broadcasting use case, one address is reserved for broadcasting. All the ED WuRx receive the WuC sent by the CH, but as the WuRx performs address matching, only the addressee ED is awaken. The addressee ED then switches-on its main transceiver to receive the data frame. As the data frame may be significantly larger than the WuC, GFSK modulation is used as well as the standard IEEE 802.15.4 packet frame structure which provides error detection using Cyclic Redundancy Check (CRC) code. Finally, the ED sends its requested data (Data) to the gateway using LoRa™class A. The transmission is followed by two short receive windows (not shown on the figure).

To ensure good SR transmission, an ACK frame can be sent by the addressee ED to the CH to indicate the successful reception of the data frame. If a transmission error occurs, e.g. due to interferences, a new transmission attempt is initiated after a random backoff.

While with the standard LoRa™scheme a trade-off must be made between latency and power consumption, the proposed architecture combined with the proposed MAC protocol allows bidirectional low latency and energy efficient communications in heterogeneous long-short range networks. This is achieved by organizing the EDs around a CH in a star network topology, and exploiting WuRx to allow pure-asynchronous communications between the CH and the EDs. Using this approach, the EDs do not have to periodically (class B) or continuously (class C) listen to the channel to receive data from the gateway, and no trade-off must be made between power consumption and latency as with the standard LoRa™scheme.

B.3 Power Consumption and Latency Analytical Models

Analytical models of the power consumption incurred by the downlink transmission of the EDs are derived in this section, as well as analytical models of the packet reception latency. First, the models of the LoRa™approaches are presented. Then, the models of the WuRx-based approach proposed in this work are exposed.

B.3.1 Models of LoRa™ Communication Schemes

The average rate at which commands are sent by the gateway to EDs is denoted λ_{CMD}. As previously explained, LoRa™ proposes three operating modes for the EDs, called class A, B and C. Using the class A operating mode, commands from the gateway can only be transmitted to an ED after an uplink transmission, and the average power consumption of an ED incurred by downlink communication, denoted P_C^{LA}, is therefore:

$$P_C^{LA} = e_{CMD}^L \lambda_{CMD}, \text{ with } \lambda_{CMD} \leqslant \lambda_{SND}, \tag{B.1}$$

where e_{CMD}^L is the energy cost to receive a command using LoRa™ and λ_{SND} is the packet transmission rate of EDs. At each command transmission, the gateway waits for the ED to perform an uplink transmission before sending a command. In average, the waiting time is $\frac{1}{2\lambda_{SND}}$ seconds, and the average latency of the command transmission, denoted L^{LA} is thus:

$$L^{LA} = \frac{1}{2\lambda_{SND}} + l_{CMD}^L, \tag{B.2}$$

where l_{CMD}^L is the time required for the command transmission using LoRa™.

Using the class B operating mode, each ED periodically opens receive windows, called ping slots, at a rate λ_{PING}. If no preamble is detected during a ping slot, the ED immediately returns to sleep. If a preamble is detected the radio transceiver stays on until the frame is demodulated. The gateway provides time reference to the EDs by periodically broadcasting beacon, at a rate λ_{BCN}. The average power consumption incurred by downlink communication of an ED using this operating scheme is thus:

$$P_C^{LB} = \lambda_{BCN} e_{BCN} + (\lambda_{PING} - \lambda_{CMD})\, e_{PING} + \lambda_{CMD} e_{CMD}^L, \tag{B.3}$$

where e_{BCN} is the cost of receiving a synchronization beacon and e_{PING} is the cost of opening a receiving window that leads to no preamble detection. The gateway has to wait in average $\frac{1}{2\lambda_{PING}}$ seconds for the ED to open a ping slot, and the average latency of command transmission is thus:

$$L^{LB} = \frac{1}{2\lambda_{PING}} + l_{CMD}^L. \tag{B.4}$$

The class C option is designed for EDs with sufficient available power. Using this operating mode, EDs are always listening to the channel, except when they are transmitting. Therefore, the average power consumption of an ED incurred by the downlink transmission is:

$$P_C^{LC} = (1 - \lambda_{SND} l_{SND})\, P_{C,RX}, \tag{B.5}$$

where $P_{C,RX}$ is the power consumption of the transceiver when receiving, and l_{SND} is the time required to send a periodic uplink packet. The latency of a downlink transmission using class C operating mode is only due to the packet transmission duration:

$$L^{LC} = l_{CMD}^L. \tag{B.6}$$

B.3.2 Models of LoRa™-WuRx Communication Scheme

The ED power consumption incurred by the proposed approach for receiving packets from the gateway is:

$$P_C^{WuRx} = \lambda_{CMD} e_{CMD}^W + (1 - \lambda_{CMD} l_{WuC})\, P_{WuRx}, \tag{B.7}$$

where e_{CMD}^W is the energy cost of receiving a packet using the SR MAC approach presented in the previous section, l_{WuC} is the transmission time of a WuC, and P_{WuRx} is the power consumption of the WuRx when only the analog font-end is active listening to the channel, while the ULP MCU is in the sleep state. Assuming that the CH uses the class C operating mode, the latency of a packet reception is:

$$L^W = l_{CMD}^L + l_{CMD}^W, \tag{B.8}$$

where the first term is the latency of the packet transmission from the gateway to the CH, while the second term is the time required for a packet transmission using SR MAC approach presented in the previous section.

B.4 Experimental Measurements

This section presents power consumption and sensitivity measurements. First, the experimental setup is exposed. Then, the measurements results are given.

B.4.1 Experimental Setup

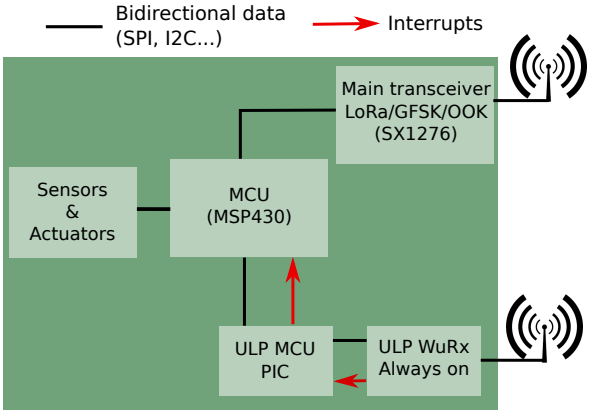

(a) Block diagram of the prototype.

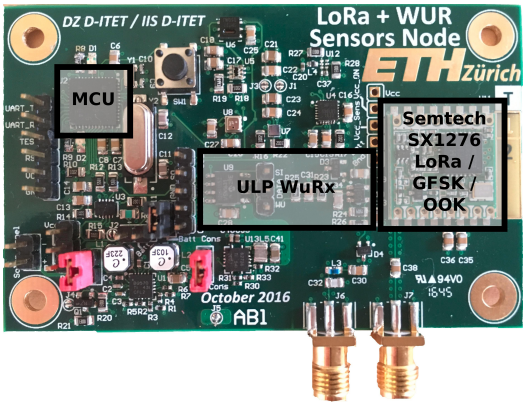

(b) Picture of the prototype.

Figure B.4 – Prototype used for experimentations, developed by the Swiss Federal Institute of Technology in Zurich.

A prototype developed by the Swiss Federal Institute of Technology in Zurich and shown in Figure B.4, was used for experimentations. It includes a Texas Instrument MSP430FR5969 MCU, the WuRx from [2], multiple sensors and a Semtech SX1276 transceiver, was used to evaluate the proposed architecture. The transceiver SX1276 from Semtech provides GFSK and OOK modulations, as well as the LoRa^{TM}physical layer. Moreover, it allows switching between the different modulation schemes, enabling coexistence between different modulation approaches. LoRa^{TM} relies on CSS modulation [181], where a chirp is a sinusoidal waveform whose frequency varies with time. SF is the spreading factor which takes value in the range between 6 and 12.

The spreading factor (SF), bandwidth (B), coding rate (CR) and transmission power (P_{Tx}) are critical parameters that control the trade-off between energy consumption and the immunity to interference in LoRa^{TM}communications. The CR parameter corresponds to the additional data overhead ratio incurred by the cyclic error coding to perform forward error detection and correction, and takes value in the range between $\frac{4}{8} \ldots \frac{4}{5}$. Using LoRa^{TM}, the bit rate denoted R_b can be calculated as follows [171]:

$$R_b = SF \frac{B}{2^{SF}}. \tag{B.9}$$

	SH	SD	SL
CR	$\frac{4}{5}$	$\frac{4}{5}$	$\frac{4}{8}$
B (kHz)	500	125	125
SF	6	7	12
R_b (kbps)	46.9	6.84	0.367

Table B.1 – Setups use for LoRa™ energy measurement.

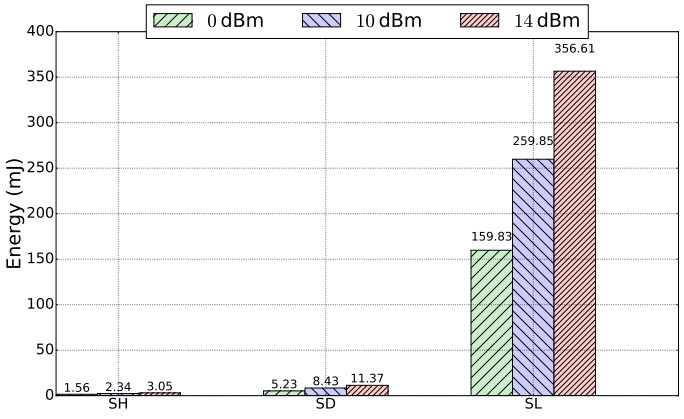

(a) Energy cost of sending a packet using LoRa™.

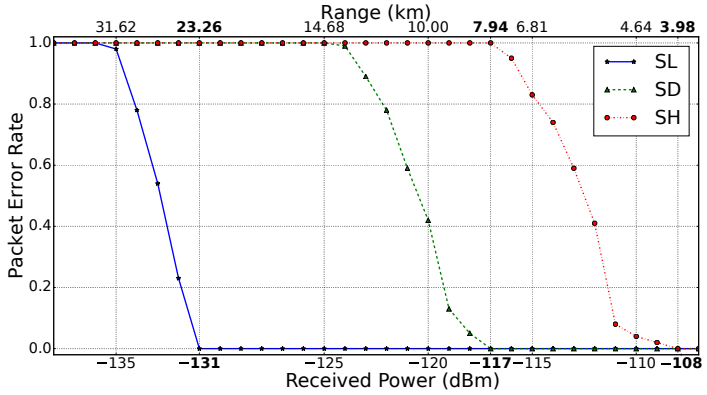

(b) LoRa™ sensitivity and theoretical range for different setups.

Figure B.5 – LoRa™ experimental evaluations.

Because the space defined by these four parameters is large, 3 setups corresponding respectively to the highest bit rate setup (SH), the LoRa™ default setup (SD) and the lowest bit rate setup (SL) were considered in this work. Table B.1 details the parameter values used for each setup.

In addition to the SX1276 transceiver, each WSN node is equipped with an instance of the WuRx designed in [2]. Finally, the platform embeds the ultra low-power TI MSP430FR5969 micro-controller that is connected with the sensors, the actuators and the communication module. The micro-controller executes data collection from sensors and sending data or commands with the SX1276 module (using LoRa™ or OOK modulation).

B.4.2 Measurements Results

Figure B.5a exposes the energy required for sending a 14 bytes payload using each setup and for different transmission powers P_{Tx}. As it can be seen, the energy required to send a packet using the SL setup is two orders of magnitude higher than the energy required to send a packet using the SH setup. This is due to the much lower bit rate incurred by the lower bandwidth and the higher spreading factor, as well as the data overhead caused by a higher code rate. However, if increasing the throughput reduces both the latency and the consumed energy, it also significantly decreases the communication range as shown in Figure B.5b. This figure shows the packet error rate achieved for different received powers, and the sensitivity is estimated for a packet error rate of 0 %. A theoretical range was computed using the log-normal shadowing propagation model with a path loss exponent of 3 and a power transmission of 0 dBm. These measurements were done using two nodes connected by a variable attenuator, and radio-frequency leakages were canceled by isolating one node in an anechoic chamber. The measured sensitivities show a 13 dBm difference between the SL and SD setups and a 7 dBm difference between the SD and SH setups. As it can be seen, the range is strongly impacted by the used setup, as using the SL setup theoretically improves the range by a factor of 5.8 compared to the SH setup. Therefore, the SR, B and CR parameters must be chosen very carefully to fulfill the application requirements in terms of range and energy consumption.

Figure B.6 shows the power consumption of the gateway, CH and ED when using the proposed scheme. In this example, the CH is operating in class C. These measurements were obtained using an Agilent N6705 DC analyzer. The different stages of the proposed MAC protocol, detailed in Section B.2.3, can be seen here, as well as the two receiving windows required by the class A LoRa$^{\text{TM}}$scheme. Moreover, the hardware and software overhead can also be seen, between two frame transmissions/receptions. These measurements were used to compute the energy costs needed by the analytical model.

B.5 Analytical Comparison

The communication scheme proposed in this work for transmitting commands from the gateway to the EDs was analytically compared to the standard LoRa$^{\text{TM}}$approaches by including experimental measurements in the models presented in Section B.3. The three setups introduced in the previous section (SL, SD and SH) were considered. Energy values were calculated using power consumption measurements and by taking into account the physical layer and MAC layer overheads of LoRa$^{\text{TM}}$, and the default value of λ_{BCN} was used [172].

Figure B.7 shows the power consumption and the latency of an ED node operating using the different evaluated schemes. The LoRa$^{\text{TM}}$class B was evaluated for values of λ_{PING} ranging from 0.1 to 33 Hz, and, when evaluating the proposed approach, the CH node was assumed to operate in class C. The size of the LoRa$^{\text{TM}}$frame was set to 14 bytes, λ_{CMD} to $\frac{1}{90}$ Hz, λ_{BCN} to $\frac{1}{128}$ Hz, and λ_{SND} to $\frac{1}{10}$ Hz. It can be seen that using LoRa$^{\text{TM}}$, a trade-off between power consumption and latency is required. Indeed, the class A allows very low power consumption, but at the cost of high latency as the gateway can send commands to an ED only after an uplink transmission. On the other hand, if the ED operates in class C, downlink communications are performed with low latency, as the node is always listening to the channel, but at the cost of high power consumption preventing long-term applications. The class B allows a trade-off between these two extremes, by taking advantage of the well-known duty-cycled approach. When operating in class B, the ED periodically wakes up to listen to the channel, and the trade-off between power consumption and latency is set using the λ_{PING} parameter. The WuRx-based approach proposed in this work, which combines SR and LR communications, achieves a latency close to the one of the classC mode, while incurring a low power consumption. The proposed approach requires the use of an extra hardware device, the WuRx, which power consumption is negligible as it is 1.83μW in always-on listening mode. Hence, no more trade-off is required for downlink communication, as it is the case with standard LoRa$^{\text{TM}}$approaches.

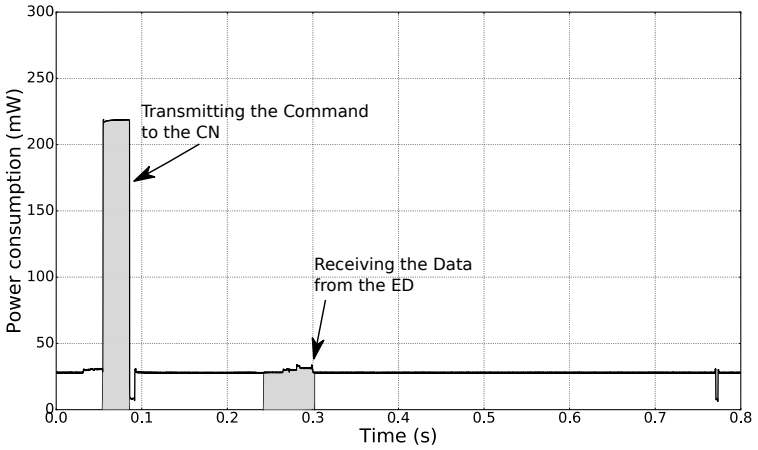

(a) Gateway (GW).

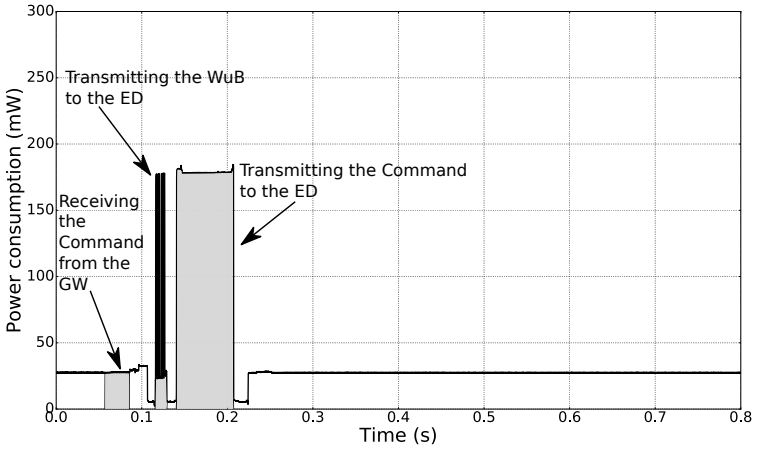

(b) CN.

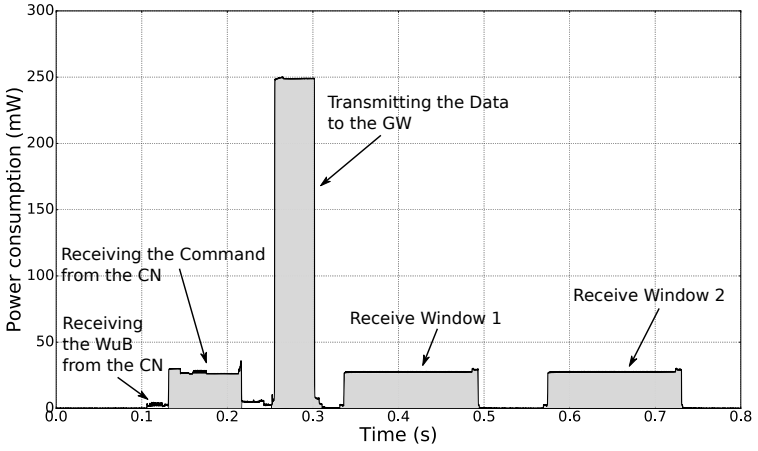

(c) ED.

Figure B.6 – Microbenchmarks showing the "data request" scenario. The SD setup is used.

B.6 Conclusion

This chapter presents a new network architecture exploiting radio diversity by combining LoRa™ and wake-up receivers. Using LoRa™, a trade-off between latency and power consumption for packet transmission from the gateway to the nodes must be made. Therefore, it does not suit applications that require low latency and low power consumption in short range. We proposed in this chapter

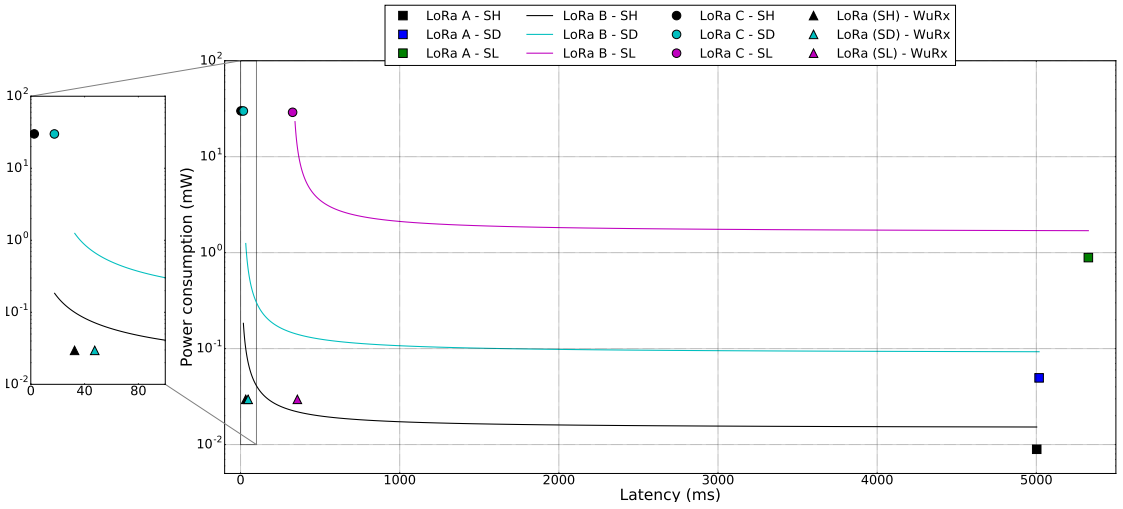

Figure B.7 – Power consumption vs Latency.

to combine LoRa™ with WuRx, which enables pure-asynchronous communication, and eliminates idle listening, but operates in the range of tens of meters. The proposed network architecture combines these two schemes for applications where sensor and actuator nodes are deployed in a small range area, but need to communicate with a distant gateway, to which they send data and from which they receive commands. To this aim, nodes must be organized in clusters with a central node in charge of bidirectional long range communications with the gateway and short range communications with sensor and actuator nodes.

The long-short range architecture is validated with an hybrid approach that combines analytical models with experimental measurements. A dedicated platform that embeds both LoRa™ and WuRx technologies has been prototyped for the experiments. Experimental and analytical comparison showed the benefits of the proposed scheme, as it removes the trade-off between power consumption and latency.

Personal Publications

International Journals

- *(To appear)* Fayçal Aït Aoudia, Matthieu Gautier, Olivier Berder, **Distributed Computation of Fair Packet Rates in Energy Harvesting Wireless Sensor Networks**, *IEEE Wireless Communications Letters*
- Fayçal Aït Aoudia, Matthieu Gautier, Michele Magno, Olivier Berder, Luca Benini, **A Generic Framework for Modeling MAC Protocols in Wireless Sensor Networks**, *IEEE/ACM Transactions on Networking*, vol. 25, no. 3, pp. 1489-1500, June 2017
- Fayçal Aït Aoudia, Matthieu Gautier, Olivier Berder, **OPWUM: Opportunistic MAC Protocol Leveraging Wake-Up Receivers in WSNs**, *Journal of Sensors*, Article ID 6263719, 2016
- (SUBMITTED) Fayçal Aït Aoudia, Matthieu Gautier, Michele Magno, Mickaël Le Gentil, Olivier Berder, Luca Benini, **Long-Short Range Communication Network Leveraging LoRa and Wake-up Receiver**, *Elsevier Microprocessors and Microsystems*
- (SUBMITTED) Fayçal Aït Aoudia, Michele Magno, Matthieu Gautier, Olivier Berder, Luca Benini, **Leveraging Energy Harvesting and Wake-up Receivers for Long-Term Wireless Sensor Networks**, *ACM Transactions on Sensor Networks*

International Conferences

- Fayçal Aït Aoudia, Matthieu Gautier, Olivier Berder, **Learning to Survive: Achieving Energy Neutrality in Wireless Sensor Networks Using Reinforcement Learning**, *IEEE International Conference on Communications (ICC)*, May 2017, Paris, France
- Michele Magno, Fayçal Aït Aoudia, Matthieu Gautier, Olivier Berder and Luca Benini, **WULoRa: An Energy Efficient IoT End-Node for Energy Harvesting and Heterogeneous Communication**, *IEEE/ACM Design, Automation & Test in Europe Conference & Exhibition (DATE)*, pp. 1528-1533, Lausanne, Switzerland, March 2017
- Fayçal Aït Aoudia, Michele Magno, Matthieu Gautier, Olivier Berder, Luca Benini, **Analytical and Experimental Evaluation of Wake-up Receivers based protocols**, *IEEE Global Communications Conference (Globecom)*, December 2016, Washington, United States
- Fayçal Aït Aoudia, Matthieu Gautier, Michele Magno, Olivier Berder, Luca Benini, **SNW-MAC: an Asynchronous Protocol Leveraging Wake-up Receivers for Data Gathering in Star Networks**, *EAI International Conference on Sensor Systems and Software (S-cube)*, December 2016, Nice, France
- Fayçal Aït Aoudia, Michele Magno, Matthieu Gautier, Olivier Berder and Luca Benini, **A Low Latency and Energy Efficient Communication Architecture for Heterogeneous Long-Short Range Communication**, *Euromicro Conference on Digital System Design (DSD)*, Limassol, 2016, pp. 200-206
- Fayçal Aït Aoudia, Matthieu Gautier, Olivier Berder, **Fuzzy Power Management for Energy Harvesting Wireless Sensor Nodes**, *IEEE International Conference on Communications (ICC)*, May 2016, Kuala Lumpur, Malaysia

- Fayçal Aït Aoudia, Matthieu Gautier and Olivier Berder, **GRAPMAN: Gradual Power Manager for Consistent Throughput of Energy Harvesting Wireless Sensor Nodes**, *IEEE 26th Annual International Symposium on Personal, Indoor, and Mobile Radio Communications (PIMRC)*, Hong Kong, 2015, pp. 954-959

National Conferences

- Fayçal Aït Aoudia, Matthieu Gautier, Olivier Berder, **Comment bénéficier de la wake-up radio pour les réseaux de capteurs à récupération d'énergie ?**, *Journées Scientifiques URSI France - Energie et radiosciences*, March 2016, Rennes, France. Actes des journées scientifiques URSI France

- Fayçal Aït Aoudia, Matthieu Gautier, Olivier Berder, **Adaptation dynamique de la qualité de service dans les réseaux de capteurs avec récupération d'énergie**, *Gretsi*, September 2015, Lyon, France

Posters and Demos

- Fayçal Aït Aoudia, Matthieu Gautier, Antoine Courtay, Olivier Berder, **Etude du compromis entre latence et consommation d'énergie des radio longues portées**, *Colloque du GDR SoC-SiP*, June 2017, Bordeaux, France

- Fayçal Aït Aoudia, Matthieu Gautier, Olivier Berder, **Protocoles de communication faibles latences et faibles consommations à base de wake-up radio**, *Colloque du GDR SoC-SiP*, June 2016, Nantes, France

- Fayçal Aït Aoudia, Michele Magno, Matthieu Gautier, Olivier Berder, and Luca Benini, **Wake-up receivers for energy efficient and low latency communication: poster abstract**, *15th International Conference on Information Processing in Sensor Networks (IPSN)*, April 2016, Vienna, Austria

- Fayçal Aït Aoudia, Matthieu Gautier, Mickaël Le Gentil, Olivier Berder, **Demo Abstract: How Fuzzy Logic can enhance Energy Management in autonomous Wireless Sensor Nodes ?**, *Conference on Design and Architectures for Signal and Image Processing (DASIP), Demo Night*, October 2016, Rennes, France

Bibliography

[1] E.-Y. Lin, J. Rabaey, and A. Wolisz, "Power-efficient rendez-vous schemes for dense wireless sensor networks," in *IEEE International Conference on Communications (ICC)*, June 2004.

[2] M. Magno, V. Jelicic, B. Srbinovski, V. Bilas, E. Popovici, and L. Benini, "Design, Implementation, and Performance Evaluation of a Flexible Low-Latency Nanowatt Wake-Up Radio Receiver," *IEEE Transactions on Industrial Informatics*, vol. 12, no. 2, pp. 633–644, April 2016.

[3] S. Marinkovic and E. Popovici, "Nano-Power Wireless Wake-Up Receiver With Serial Peripheral Interface," *IEEE Journal on Selected Areas in Communications*, vol. 29, no. 8, pp. 1641–1647, September 2011.

[4] J. Oller, I. Demirkol, J. Casademont, J. Paradells, G. Gamm, and L. Reindl, "Performance Evaluation and Comparative Analysis of SubCarrier Modulation Wake-up Radio Systems for Energy-Efficient Wireless Sensor Networks," *Sensors*, vol. 14, no. 1, p. 22–51, December 2013. [Online]. Available: http://dx.doi.org/10.3390/s140100022

[5] J. Oller, I. Demirkol, J. Casademont, and J. Paradells, "Design, Development, and Performance Evaluation of a Low-cost, Low-power Wake-up Radio System for Wireless Sensor Networks," *ACM Transaction on Sensor Networks*, vol. 10, no. 1, 2013.

[6] N. E. Roberts and D. D. Wentzloff, "A 98nW wake-up radio for wireless body area networks," in *IEEE Radio Frequency Integrated Circuits Symposium*, June 2012, pp. 373–376.

[7] H. Milosiu, F. Oehler, M. Eppel, D. Frühsorger, S. Lensing, G. Popken, and T. Thönes, "A 3-μW 868-MHz wake-up receiver with- 83 dBm sensitivity and scalable data rate," in *2013 Proceedings of the ESSCIRC (ESSCIRC)*, Sept 2013, pp. 387–390.

[8] A. Cammarano, C. Petrioli, and D. Spenza, "Online Energy Harvesting Prediction in Environmentally Powered Wireless Sensor Networks," *IEEE Sensors Journal*, vol. 16, no. 17, pp. 6793–6804, September 2016.

[9] R. J. M. Vullers, R. v. Schaijk, H. J. Visser, J. Penders, and C. V. Hoof, "Energy Harvesting for Autonomous Wireless Sensor Networks," *IEEE Solid-State Circuits Magazine*, vol. 2, no. 2, pp. 29–38, Spring 2010.

[10] T. Rault, A. Bouabdallah, and Y. Challal, "Energy Efficiency in Wireless Sensor Networks: A Top-Down Survey," *Computer Networks*, vol. 67, pp. 104–122, July 2014.

[11] Y. R. Thomas, M. Picot, A. Carer, O. Berder, O. Sentieys, and F. Barrière, "A single sediment-microbial fuel cell powering a wireless telecommunication system," *Journal of Power Sources*, vol. 241, pp. 703 – 708, 2013.

[12] P. Huang, L. Xiao, S. Soltani, M. W. Mutka, and N. Xi, "The Evolution of MAC Protocols in Wireless Sensor Networks: A Survey," *IEEE Communications Surveys Tutorials*, vol. 15, no. 1, pp. 101–120, January 2013.

[13] N. S. Mazloum and O. Edfors, "Performance Analysis and Energy Optimization of Wake-Up Receiver Schemes for Wireless Low-Power Applications," *IEEE Transactions on Wireless Communications*, vol. 13, no. 12, pp. 7050–7061, December 2014.

[14] Y. Ammar, S. Bdiri, and F. Derbel, "An Ultra-Low Power Wake Up Receiver with Flip Flops Based Address Decoder," in *International Multi-Conference on Systems, Signals and Devices (SSD)*, March 2015, pp. 1–5.

[15] L. Chen, J. Warner, P. L. Yung, D. Zhou, W. Heinzelman, I. Demirkol, U. Muncuk, K. Chowdhury, and S. Basagni, "REACH2-Mote: A Range-Extending Passive Wake-Up Wireless Sensor Node," *ACM Transaction On Sensor Networks*, vol. 11, no. 4, December 2015.

[16] D. Spenza, M. Magno, S. Basagni, L. Benini, M. Paoli, and C. Petrioli, "Beyond Duty Cycling: Wake-up Radio with Selective Awakenings for Long-Lived Wireless Sensing Systems," in *IEEE INFOCOM*, April 2015, pp. 522–530.

[17] F. Sutton, B. Buchli, J. Beutel, and L. Thiele, "Zippy: On-Demand Network Flooding," in *ACM Conference on Embedded Networked Sensor Systems (SenSys)*, November 2015, pp. 45–58.

[18] A. Kansal, J. Hsu, S. Zahedi, and M. B. Srivastava, "Power Management in Energy Harvesting Sensor Networks," *ACM Transactions on Embedded Computing Systems*, vol. 6, no. 4, 2007.

[19] C. M. Vigorito, D. Ganesan, and A. G. Barto, "Adaptive Control of Duty Cycling in Energy-Harvesting Wireless Sensor Networks," in *4th Annual IEEE Communications Society Conference on Sensor, Mesh and Ad Hoc Communications and Networks (SECON)*, June 2007.

[20] L. Tang, Y. Sun, O. Gurewitz, and D. B. Johnson, "PW-MAC: An Energy-Efficient Predictive-Wakeup MAC Protocol for Wireless Sensor Networks," in *IEEE INFOCOM*, April 2011, pp. 1305–1313.

[21] F. Ait Aoudia, M. Gautier, and O. Berder, "GRAPMAN: Gradual Power Manager for Consistent Throughput of Energy Harvesting Wireless Sensor Nodes," in *IEEE 26th Annual International Symposium on Personal, Indoor, and Mobile Radio Communications (PIMRC)*, August 2015.

[22] F. K. Shaikh and S. Zeadally, "Energy harvesting in wireless sensor networks: A comprehensive review," *Renewable and Sustainable Energy Reviews*, vol. 55, pp. 1041 – 1054, 2016.

[23] G. M. d. Araújo, A. R. Pinto, J. Kaiser, and L. B. Becker, *Genetic Machine Learning Approach for Link Quality Prediction in Mobile Wireless Sensor Networks.* Berlin, Heidelberg: Springer Berlin Heidelberg, 2014, pp. 1–18.

[24] G. M. de Araújo, J. Kaiser, and L. B. Becker, "An optimized Markov model to predict link quality in mobile wireless sensor networks," in *IEEE Symposium on Computers and Communications (ISCC)*, July 2012, pp. 000 307–000 312.

[25] T. Liu and A. E. Cerpa, "Data-driven Link Quality Prediction Using Link Features," *ACM Transactions Sensor Networks*, vol. 10, no. 2, pp. 37:1–37:35, 2014.

[26] J. R. Piorno, C. Bergonzini, D. Atienza, and T. S. Rosing, "Prediction and Management in Energy Harvested Wireless Sensor Nodes," in *1st International Conference on Wireless Communication, Vehicular Technology, Information Theory and Aerospace Electronic Systems Technology. (Wireless VITAE)*, May 2009.

[27] C. Bergonzini, D. Brunelli, and L. Benini, "Comparison of energy intake prediction algorithms for systems powered by photovoltaic harvesters," *Microelectronics Journal*, vol. 41, no. 11, pp. 766 – 777, 2010, {IEEE} International Workshop on Advances in Sensors and Interfaces.

[28] C. Moser, L. Thiele, D. Brunelli, and L. Benini, "Adaptive Power Management in Energy Harvesting Systems," in *Proceedings of the Conference on Design, Automation and Test in Europe (DATE)*, San Jose, CA, USA, 2007, pp. 773–778.

[29] C. Bergonzini, D. Brunelli, and L. Benini, "Algorithms for harvested energy prediction in batteryless wireless sensor networks," in *3rd International Workshop on Advances in sensors and Interfaces*, June 2009, pp. 144–149.

[30] J. Lu and K. Whitehouse, "SunCast: Fine-grained Prediction of Natural Sunlight Levels for Improved Daylight Harvesting," in *Proceedings of the 11th International Conference on Information Processing in Sensor Networks (IPSN)*. New York, NY, USA: ACM, 2012, pp. 245–256.

[31] A. Cammarano, C. Petrioli, and D. Spenza, "Pro-Energy: A novel energy prediction model for solar and wind energy-harvesting wireless sensor networks," in *IEEE 9th International Conference on Mobile Adhoc and Sensor Systems (MASS)*, October 2012, pp. 75–83.

[32] ——, "Improving Energy Predictions in EH-WSNs with Pro-Energy-VLT," in *Proceedings of the 11th ACM Conference on Embedded Networked Sensor Systems (SenSys)*, 2013, pp. 41:1–41:2.

[33] C. Renner, "Solar Harvest Prediction Supported by Cloud Cover Forecasts," in *Proceedings of the 1st International Workshop on Energy Neutral Sensing Systems (ENSSys)*, New York, NY, USA, 2013, pp. 1:1–1:6.

[34] S. Kosunalp, "A New Energy Prediction Algorithm for Energy-Harvesting Wireless Sensor Networks With Q-Learning," *IEEE Access*, vol. 4, pp. 5755–5763, 2016.

[35] D. Porcarelli, D. Spenza, D. Brunelli, A. Cammarano, C. Petrioli, and L. Benini, "Adaptive Rectifier Driven by Power Intake Predictors for Wind Energy Harvesting Sensor Networks," *IEEE Journal of Emerging and Selected Topics in Power Electronics*, vol. 3, no. 2, pp. 471–482, June 2015.

[36] A. Jushi, A. Pegatoquet, and T. N. Le, "Wind Energy Harvesting for Autonomous Wireless Sensor Networks," in *Euromicro Conference on Digital System Design (DSD)*, August 2016, pp. 301–308.

[37] I. T. Christou, *Quantitative methods in supply chain management: models and algorithms*. Springer Science & Business Media, 2011.

[38] D. Fan, L. L. Ruiz, J. Gong, and J. Lach, "Profiling, modeling, and predicting energy harvesting for self-powered body sensor platforms," in *IEEE 13th International Conference on Wearable and Implantable Body Sensor Networks (BSN)*, June 2016, pp. 402–407.

[39] C. Moser, J.-J. Chen, and L. Thiele, "An Energy Management Framework for Energy Harvesting Embedded Systems," *J. Emerg. Technol. Comput. Syst.*, vol. 6, no. 2, pp. 7:1–7:21, 2008.

[40] C. Moser, L. Thiele, D. Brunelli, and L. Benini, "Robust and Low Complexity Rate Control for Solar Powered Sensors," in *Proceedings of the Conference on Design, Automation and Test in Europe (DATE)*. ACM, 2008, pp. 230–235.

[41] ——, "Adaptive Power Management for Environmentally Powered Systems," *IEEE Transactions on Computers*, vol. 59, no. 4, pp. 478–491, April 2010.

[42] C. Moser, J. J. Chen, and L. Thiele, "Reward Maximization for Embedded Systems with Renewable Energies," in *14th IEEE International Conference on Embedded and Real-Time Computing Systems and Applications*, August 2008, pp. 247–256.

[43] C. Moser, J.-J. Chen, and L. Thiele, "Optimal Service Level Allocation in Environmentally Powered Embedded Systems," in *Proceedings of the ACM Symposium on Applied Computing (SAC)*, 2009, pp. 1650–1657.

[44] A. Castagnetti, A. Pegatoquet, C. Belleudy, and M. Auguin, "A Framework for Modeling and Simulating Energy Harvesting WSN Nodes with Efficient Power Management Policies," *EURASIP Journal on Embedded Systems*, no. 1, 2012.

[45] T. N. Le, A. Pegatoquet, O. Berder, and O. Sentieys, "A Power Manager with Balanced Quality of Service for Energy-harvesting Wireless Sensor Nodes," in *Proceedings of the 2Nd International Workshop on Energy Neutral Sensing Systems (ENSSys)*, 2014, pp. 19–24.

[46] ——, "Energy-Efficient Power Manager and MAC Protocol for Multi-Hop Wireless Sensor Networks Powered by Periodic Energy Harvesting Sources," *IEEE Sensors Journal*, vol. 15, no. 12, pp. 7208–7220, 2015.

[47] M. Gorlatova, A. Wallwater, and G. Zussman, "Networking Low-Power Energy Harvesting Devices: Measurements and Algorithms," in *IEEE INFOCOM*, April 2011.

[48] ——, "Networking Low-Power Energy Harvesting Devices: Measurements and Algorithms," *IEEE Transactions on Mobile Computing*, vol. 12, no. 9, pp. 1853–1865, September 2013.

[49] M. Gorlatova, J. Sarik, G. Grebla, M. Cong, I. Kymissis, and G. Zussman, "Movers and Shakers: Kinetic Energy Harvesting for the Internet of Things," *IEEE Journal on Selected Areas in Communications*, vol. 33, no. 8, pp. 1624–1639, August 2015.

[50] S. Yang, X. Yang, J. A. McCann, T. Zhang, G. Liu, and Z. Liu, "Distributed Networking in Autonomic Solar Powered Wireless Sensor Networks," *IEEE Journal on Selected Areas in Communications*, vol. 31, no. 12, pp. 750–761, December 2013.

[51] S. Moeller, A. Sridharan, B. Krishnamachari, and O. Gnawali, "Routing Without Routes: The Backpressure Collection Protocol," in *Proceedings of the 9th ACM/IEEE International Conference on Information Processing in Sensor Networks (IPSN)*. New York, NY, USA: ACM, 2010, pp. 279–290.

[52] K.-W. Fan, Z. Zheng, and P. Sinha, "Steady and fair rate allocation for rechargeable sensors in perpetual sensor networks," in *Proceedings of the 6th ACM Conference on Embedded Network Sensor Systems (SenSys)*. New York, NY, USA: ACM, 2008, pp. 239–252.

[53] R. C. Hsu, C. T. Liu, and H. L. Wang, "A Reinforcement Learning-Based ToD Provisioning Dynamic Power Management for Sustainable Operation of Energy Harvesting Wireless Sensor Node," *IEEE Transactions on Emerging Topics in Computing*, vol. 2, no. 2, pp. 181–191, June 2014.

[54] A. G. Watts, M. Prauzek, P. Musilek, E. Pelikan, and A. Sanchez-Azofeifa, "Fuzzy power management for environmental monitoring systems in tropical regions," in *2014 International Joint Conference on Neural Networks (IJCNN)*, July 2014, pp. 1719–1726.

[55] S. Peng and C. P. Low, "Prediction free energy neutral power management for energy harvesting wireless sensor nodes," *Ad Hoc Networks*, vol. 13, Part B, 2014.

[56] G. Chen and T. T. Pham, *Introduction to Fuzzy Sets, Fuzzy Logic, and Fuzzy Control Systems*. CRC Press, 2000.

[57] F. Ait Aoudia, M. Gautier, and O. Berder, "Fuzzy power management for energy harvesting Wireless Sensor Nodes," in *IEEE International Conference on Communications (ICC)*, May 2016.

[58] T. Takagi and M. Sugeno, "Fuzzy identification of systems and its applications to modeling and control," *IEEE Transactions on Systems, Man, and Cybernetics*, vol. SMC-15, no. 1, pp. 116–132, January 1985.

[59] "PowWow: Power Optimized Hardware and Software FrameWork for Wireless Motes," http://powwow.gforge.inria.fr/, 2014, [Online; accessed December-2015].

[60] J. Paradiso and T. Starner, "Energy scavenging for mobile and wireless electronics," *IEEE Pervasive Computing*, vol. 4, no. 1, pp. 18–27, Jan 2005.

[61] C. Ó. Mathúna, T. O'Donnell, R. V. Martinez-Catala, J. Rohan, and B. O'Flynn, "Energy scavenging for long-term deployable wireless sensor networks," *Talanta*, vol. 75, no. 3, pp. 613 – 623, 2008, Special Section: Remote Sensing.

[62] D. Benedetti, C. Petrioli, and D. Spenza, "GreenCastalia: An Energy-harvesting-enabled Framework for the Castalia Simulator," in *Proceedings of the 1st ACM International Workshop on Energy Neutral Sensing Systems (ENSSys)*, 2013.

[63] A. Boulis, "Castalia: Revealing Pitfalls in Designing Distributed Algorithms in WSN," in *Proceedings of the 5th International Conference on Embedded Networked Sensor Systems (SenSys)*, 2007.

[64] M. A. Green, K. Emery, Y. Hishikawa, W. Warta, and E. D. Dunlop, "Solar cell efficiency tables (version 45)," *Progress in Photovoltaics: Research and Applications*, vol. 23, no. 1, pp. 1–9, 2015.

[65] X. Fafoutis and N. Dragoni, "Analytical comparison of MAC schemes for Energy Harvesting - Wireless Sensor Networks," in *Ninth International Conference on Networked Sensing Systems (INSS)*, June 2012.

[66] R. Margolies, M. Gorlatova, J. Sarik, G. Stanje, J. Zhu, P. Miller, M. Szczodrak, B. Vigraham, L. Carloni, P. Kinget, I. Kymissis, and G. Zussman, "Energy-Harvesting Active Networked Tags (EnHANTs): Prototyping and Experimentation," *ACM Transactions on Sensor Networks*, vol. 11, no. 4, pp. 62:1–62:27, November 2015.

[67] F. Ait Aoudia, M. Gautier, and O. Berder, "Learning to Survive: Achieving Energy Neutrality in Wireless Sensor Networks Using Reinforcement Learning," in *IEEE International Conference on Communications (ICC)*, May 2017.

[68] H. Van Hasselt, "Reinforcement Learning in Continuous State and Action Spaces," in *Reinforcement Learning*. Springer, 2012, pp. 207–251.

[69] D. P. Bertsekas and J. Tsitsiklis, *Neuro-Dynamic Programming*. Athena Scientific, 1996.

[70] R. S. Sutton, "Learning to Predict by the Methods of Temporal Differences," *Machine Learning*, vol. 3, no. 1, pp. 9–44, 1988.

[71] J. N. Tsitsiklis and B. V. Roy, "An analysis of temporal-difference learning with function approximation," *IEEE Transactions on Automatic Control*, vol. 42, no. 5, pp. 674–690, May 1997.

[72] L. Baird, "Residual Algorithms: Reinforcement Learning with Function Approximation," in *In Proceedings of the Twelfth International Conference on Machine Learning*. Morgan Kaufmann, 1995, pp. 30–37.

[73] S. Bhatnagar, D. Precup, D. Silver, R. S. Sutton, H. R. Maei, and C. Szepesvári, "Convergent Temporal-Difference Learning with Arbitrary Smooth Function Approximation," in *Advances in Neural Information Processing Systems 22*, Y. Bengio, D. Schuurmans, J. D. Lafferty, C. K. I. Williams, and A. Culotta, Eds. Curran Associates, Inc., 2009, pp. 1204–1212.

[74] C. Liu, X. Xu, and D. Hu, "Multiobjective Reinforcement Learning: A Comprehensive Overview," *IEEE Transactions on Systems, Man, and Cybernetics: Systems*, vol. 45, no. 3, pp. 385–398, March 2015.

[75] C. R. Shelton, "Balancing Multiple Sources of Reward in Reinforcement Learning," in *Advances in Neural Information Processing Systems 13*, T. K. Leen, T. G. Dietterich, and V. Tresp, Eds. MIT Press, 2001, pp. 1082–1088. [Online]. Available: http://papers.nips.cc/paper/1831-balancing-multiple-sources-of-reward-in-reinforcement-learning.pdf

[76] I. Grondman, L. Busoniu, G. A. D. Lopes, and R. Babuska, "A Survey of Actor-Critic Reinforcement Learning: Standard and Natural Policy Gradients," *IEEE Transactions on Systems, Man, and Cybernetics, Part C (Applications and Reviews)*, vol. 42, no. 6, pp. 1291–1307, November 2012.

[77] R. S. Sutton, D. A. McAllester, S. P. Singh, and Y. Mansour, "Policy Gradient Methods for Reinforcement Learning with Function Approximation." in *Advances in Neural Information Processing Systems 12*, vol. 99, 2000, pp. 1057–1063.

[78] M. Gorlatova, M. Zapas, E. Xu, M. Bahlke, I. J. Kymissis, and G. Zussman, "CRAWDAD dataset columbia/enhants (v. 2011-04-07)," Downloaded from http://crawdad.org/columbia/enhants/20110407, Apr. 2011.

[79] "National Renewable Energy Laboratory (NREL)," http://www.nrel.gov/.

[80] J. A. R. Azevedo and F. E. S. Santos, "Energy harvesting from wind and water for autonomous wireless sensor nodes," *IET Circuits, Devices Systems*, vol. 6, no. 6, pp. 413–420, November 2012.

[81] R. S. Sutton, "Generalization in Reinforcement Learning: Successful Examples Using Sparse Coarse Coding," in *Advances in Neural Information Processing Systems 8*. MIT Press, 1996, pp. 1038–1044.

[82] R. Zhang, O. Berder, J.-M. Gorce, and O. Sentieys, "Energy–delay tradeoff in wireless multihop networks with unreliable links," *Ad Hoc Networks*, vol. 10, no. 7, pp. 1306 – 1321, 2012.

[83] F. Ait Aoudia, M. Magno, M. Gautier, O. Berder, and L. Benini, "Analytical and Experimental Evaluation of Wake-up Receivers based protocols," in *IEEE Global Communications Conference (Globecom 2016)*, Washington, United States, Dec. 2016. [Online]. Available: https://hal.inria.fr/hal-01412792

[84] F. Ait Aoudia, M. Gautier, M. Magno, O. Berder, and L. Benini, "A Generic Framework for Modeling MAC Protocols in Wireless Sensor Networks," *IEEE/ACM Transactions on Networking*, vol. 25, no. 3, pp. 1489–1500, June 2017.

[85] C. M. Grinstead and J. L. Snell, *Grinstead and Snell's Introduction to Probability*. Chance Project, 2006.

[86] Q. Zhao and L. Tong, "A Dynamic Queue Protocol For Multiaccess Wireless Networks With Multipacket Reception," *IEEE Transactions on Wireless Communications*, vol. 3, no. 6, pp. 2221–2231, November 2004.

[87] Y. Wang, M. Vuran, and S. Goddard, "Cross-Layer Analysis of the End-to-End Delay Distribution in Wireless Sensor Networks," *IEEE/ACM Transactions on Networking*, vol. 20, no. 1, pp. 305–318, February 2012.

[88] Y. Sun, O. Gurewitz, and D. B. Johnson, "RI-MAC: A Receiver-initiated Asynchronous Duty Cycle MAC Protocol for Dynamic Traffic Loads in Wireless Sensor Networks," in *ACM Conference on Embedded Network Sensor Systems (SenSys)*, November 2008, pp. 1–14.

[89] B. Bougard, F. Catthoor, D. C. Daly, A. Chandrakasan, and W. Dehaene, "Energy Efficiency of the IEEE 802.15.4 Standard in Dense Wireless Microsensor Networks: Modeling and Improvement Perspectives," in *Conference on Design, Automation and Test in Europe (DATE)*, March 2005, pp. 196–201 Vol. 1.

[90] I. Ramachandran, A. K. Das, and S. Roy, "Analysis of the Contention Access Period of IEEE 802.15.4 MAC," *ACM Transaction on Sensor Networks (ToSN)*, vol. 3, no. 1, March 2007.

[91] S. Pollin, M. Ergen, S. C. Ergen, B. Bougard, L. V. D. Perre, I. Moerman, A. Bahai, P. Varaiya, and F. Catthoor, "Performance Analysis of Slotted Carrier Sense IEEE 802.15.4 Medium Access Layer," *IEEE Transactions on Wireless Communications*, vol. 7, no. 9, pp. 3359–3371, September 2008.

[92] P. Park, P. D. Marco, P. Soldati, C. Fischione, and K. H. Johansson, "A Generalized Markov Chain Model for Effective Analysis of Slotted IEEE 802.15.4," in *IEEE International Conference on Mobile Adhoc and Sensor Systems*, October 2009, pp. 130–139.

[93] X. Vilajosana, Q. Wang, F. Chraim, T. Watteyne, T. Chang, and K. S. J. Pister, "A Realistic Energy Consumption Model for TSCH Networks," *IEEE Sensors Journal*, vol. 14, no. 2, pp. 482–489, February 2014.

[94] M. C. Vuran and I. F. Akyildiz, "Spatial correlation-based collaborative medium access control in wireless sensor networks," *IEEE/ACM Transactions on Networking*, vol. 14, no. 2, pp. 316–329, April 2006.

[95] K. Langendoen and A. Meier, "Analyzing MAC Protocols for Low Data-Rate Applications," in *ACM Transactions on Sensor Networks (ToSN)*, vol. 7, no. 1, 2010, pp. 1–34.

[96] A. Asudeh, G. V. Záruba, and S. K. Das, "A General Model For MAC Protocol Selection in Wireless Sensor Networks," *Ad Hoc Networks*, vol. 36, Part 1, pp. 189 – 202, January 2016.

[97] Y. Liu, Y. He, M. Li, J. Wang, K. Liu, and X. Li, "Does Wireless Sensor Network Scale? A Measurement Study on GreenOrbs," *IEEE Transactions on Parallel and Distributed Systems*, vol. 24, no. 10, pp. 1983–1993, October 2013.

[98] M. Haenggi, J. G. Andrews, F. Baccelli, O. Dousse, and M. Franceschetti, "Stochastic geometry and random graphs for the analysis and design of wireless networks," *IEEE Journal on Selected Areas in Communications*, vol. 27, no. 7, pp. 1029–1046, September 2009.

[99] O. Berder and O. Sentieys, "PowWow: Power Optimized Hardware/Software Framework for Wireless Motes," in *International Conference on Architecture of Computing Systems (ARCS)*, February 2010.

[100] M. Alam, O. Berder, D. Menard, and O. Sentieys, "TAD-MAC: Traffic-Aware Dynamic MAC Protocol for Wireless Body Area Sensor Networks," *IEEE Journal on Emerging and Selected Topics in Circuits and Systems*, vol. 2, no. 1, pp. 109 –119, 2012. [Online]. Available: https://hal.inria.fr/hal-00741556

[101] M. M. Alam, O. Berder, D. Menard, T. Anger, and O. Sentieys, "A Hybrid Model for Accurate Energy Analysis of WSN nodes," *EURASIP Journal on Embedded Systems*, 2011. [Online]. Available: https://hal.inria.fr/inria-00554188

[102] J. Oller, I. Demirkol, J. Casademont, J. Paradells, G. U. Gamm, and L. Reindl, "Has Time Come to Switch From Duty-Cycled MAC Protocols to Wake-Up Radio for Wireless Sensor Networks?" *IEEE/ACM Transactions on Networking*, vol. 24, no. 2, pp. 674–687, April 2016.

[103] M. Buettner, G. V. Yee, E. Anderson, and R. Han, "X-MAC: A Short Preamble MAC Protocol for Duty-cycled Wireless Sensor Networks," in *Proceedings of the 4th International Conference on Embedded Networked Sensor Systems (SenSys)*, October 2006.

[104] A. P. Sample, D. J. Yeager, P. S. Powledge, and J. R. Smith, "Design of a Passively-Powered, Programmable Sensing Platform for UHF RFID Systems," in *IEEE International Conference on RFID*, March 2007, pp. 149–156.

[105] H. Ba, I. Demirkol, and W. Heinzelman, "Feasibility and Benefits of Passive RFID Wake-Up Radios for Wireless Sensor Networks," in *IEEE Global Telecommunications Conference (GLOBECOM)*, December 2010, pp. 1–5.

[106] L. Chen, S. Cool, H. Ba, W. Heinzelman, I. Demirkol, U. Muncuk, K. Chowdhury, and S. Basagni, "Range extension of passive wake-up radio systems through energy harvesting," in *IEEE International Conference on Communications (ICC)*, June 2013, pp. 1549–1554.

[107] J. M. Rabaey, J. Ammer, T. Karalar, S. Li, B. Otis, M. Sheets, and T. Tuan, "PicoRadios for wireless sensor networks: the next challenge in ultra-low power design," in *IEEE International Solid-State Circuits Conference (ISSCC)*, vol. 1, February 2002, pp. 200–201 vol.1.

[108] P. Kolinko and L. E. Larson, "Passive RF Receiver Design for Wireless Sensor Networks," in *IEEE/MTT-S International Microwave Symposium*, June 2007, pp. 567–570.

[109] B. Van der Doorn, W. Kavelaars, and K. Langendoen, "A prototype low-cost wakeup radio for the 868 MHz band," *International Journal of Sensor Networks*, vol. 5, no. 1, pp. 22–32, 2009.

[110] G. U. Gamm, M. Sippel, M. Kostic, and L. M. Reindl, "Low power wake-up receiver for wireless sensor nodes," in *Sixth International Conference on Intelligent Sensors, Sensor Networks and Information Processing*, December 2010, pp. 121–126.

[111] G. U. Gamm and L. M. Reindl, "Range extension for wireless wake-up receivers," in *International Multi-Conference on Systems, Sygnals Devices*, March 2012, pp. 1–4.

[112] A. Sanchez, J. Aguilar, S. Blanc, and J. J. Serrano, "RFID-based wake-up system for wireless sensor networks," pp. 806 708–806 708–12, 2011. [Online]. Available: http://dx.doi.org/10.1117/12.887039

[113] J. Oller, I. Demirkol, J. Paradells, J. Casademont, and W. Heinzelman, "Time-Knocking: A novel addressing mechanism for wake-up receivers," in *IEEE 8th International Conference on Wireless and Mobile Computing, Networking and Communications (WiMob)*, October 2012, pp. 268–275.

[114] K. Takahagi, H. Matsushita, T. Iida, M. Ikebe, Y. Amemiya, and E. Sano, "Low-power wake-up receiver with subthreshold CMOS circuits for wireless sensor networks," *Analog Integrated Circuits and Signal Processing*, vol. 75, no. 2, pp. 199–205, 2013. [Online]. Available: http://dx.doi.org/10.1007/s10470-012-9929-1

[115] C. Hambeck, S. Mahlknecht, and T. Herndl, "A 2.4 μW Wake-up Receiver for wireless sensor nodes with -71 dBm sensitivity," in *IEEE International Symposium of Circuits and Systems (ISCAS)*, May 2011, pp. 534–537.

[116] F. Z. Djiroun and D. Djenouri, "MAC Protocols with Wake-up Radio for Wireless Sensor Networks: A Review," *IEEE Communications Surveys Tutorials*, vol. PP, no. 99, pp. 1–1, 2016.

[117] L. Song and D. Hatzinakos, "A Cross-layer Architecture of Wireless Sensor Networks for Target Tracking," *IEEE/ACM Transactions on Networking*, vol. 15, no. 1, pp. 145–158, 2007. [Online]. Available: http://dx.doi.org/10.1109/TNET.2006.890084

[118] N. Ullah, M. S. Chowdhury, M. A. Ameen, and K. S. Kwak, "Energy Efficient MAC Protocol for Low-Energy Critical Infrastructure Monitoring Networks Using Wakeup Radio," *International Journal of Distributed Sensor Networks*, vol. 8, no. 4, p. 504946, 2012. [Online]. Available: http://dx.doi.org/10.1155/2012/504946

[119] N. Ullah, M. S. Chowdhury, P. Khan, and K. S. Kwak, "Multi-hop medium access control protocol for low energy critical infrastructure monitoring networks using wake-up radio," *International Journal of Communication Systems*, vol. 27, no. 11, pp. 2536–2554, 2014.

[120] T. N. Le, A. Pegatoquet, and M. Magno, "Asynchronous on demand MAC protocol using wake-up radio in wireless body area network," in *6th International Workshop on Advances in Sensors and Interfaces (IWASI)*, June 2015, pp. 228–233.

[121] M. Al Ameen, N. Ullah, M. S. Chowdhury, S. R. Islam, and K. Kwak, "A power efficient MAC protocol for wireless body area networks," *EURASIP Journal on Wireless Communications and Networking*, vol. 2012, no. 1, p. 33, 2012. [Online]. Available: http://dx.doi.org/10.1186/1687-1499-2012-33

[122] F. Dressler, B. Bloessl, M. Hierold, C. Y. Hsieh, T. Nowak, R. Weigel, and A. Koelpin, "Protocol design for ultra-low power wake-up systems for tracking bats in the wild," in *IEEE International Conference on Communications (ICC)*, June 2015, pp. 6345–6350.

[123] K. Ravichandran, K. Sivalingam, and P. Agrawal, "Design and analysis of a dual radio node architecture and medium access control protocols for Ultra Wide Band based sensor networks," in *Fourth International Conference on Broadband Communications, Networks and Systems (BROADNETS)*, September 2007, pp. 889–897.

[124] R. Jurdak, A. G. Ruzzelli, and G. M. P. O'Hare, "Multi-Hop RFID Wake-Up Radio: Design, Evaluation and Energy Tradeoffs," in *Proceedings of 17th International Conference on Computer Communications and Networks*, August 2008, pp. 1–8.

[125] P. Sthapit and J. Y. Pyun, "Effects of Radio Triggered Sensor MAC Protocol over Wireless Sensor Network," in *IEEE 11th International Conference on Computer and Information Technology*, August 2011, pp. 546–551.

[126] N. Ullah, P. Khan, and K. S. Kwak, "A Very Low Power MAC (VLPM) protocol for wireless body area networks," *Sensors*, vol. 11, no. 4, pp. 3717–3737, 2011.

[127] T. N. Le, M. Magno, A. Pegatoquet, O. Berder, O. Sentieys, and E. Popovici, "Ultra Low Power Asynchronous MAC Protocol Using Wake-up Radio for Energy Neutral WSN," in *Proceedings of the 1st ACM International Workshop on Energy Neutral Sensing Systems (ENSSys)*, November 2013.

[128] C. Guo, L. C. Zhong, and J. M. Rabaey, "Low power distributed MAC for ad hoc sensor radio networks," in *IEEE Global Telecommunications Conference (GLOBECOM)*, vol. 5, 2001, pp. 2944–2948 vol.5.

[129] K. R. Chowdhury, N. Nandiraju, D. Cavalcanti, and D. P. Agrawal, "CMAC - A multi-channel energy efficient MAC for wireless sensor networks," in *IEEE Wireless Communications and Networking Conference (WCNC)*, vol. 2, April 2006, pp. 1172–1177.

[130] W. Nosovic and T. D. Todd, "Scheduled rendezvous and RFID wakeup in embedded wireless networks," in *IEEE International Conference on Communications (ICC)*, vol. 5, 2002, pp. 3325–3329 vol.5.

[131] J. Ansari, D. Pankin, and P. Mähönen, "Radio-triggered Wake-ups with Addressing Capabilities for Extremely Low Power Sensor Network Applications," *International Journal of Wireless Information Networks*, vol. 16, no. 3, p. 118, 2009. [Online]. Available: http://dx.doi.org/10.1007/s10776-009-0100-6

[132] S. H. Lee, Y. S. Bae, and L. Choi, "On-demand radio wave sensor for wireless sensor networks: Towards a zero idle listening and zero sleep delay MAC protocol," in *IEEE Global Communications Conference (GLOBECOM)*, December 2012, pp. 560–566.

[133] *802.11-2007, Part 11: Wireless LAN Medium Access Control (MAC) and Physical Layer (PHY) Specifications*, IEEE Std.

[134] E. Umbdenstock, S. Frank, M. Kleinsteuber, and H. Meyer, "Wake-Up-Receiver in energy efficient Wireless Sensor Networks for security applications," in *Proceedings of the 7th Edition of the Interdisciplinary Workshop on Global Security*, 2013.

[135] H. Liu, B. Zhang, H. Mouftah, X. Shen, and J. Ma, "Opportunistic routing for wireless ad hoc and sensor networks: Present and future directions," *IEEE Communications Magazine*, vol. 47, no. 12, pp. 103–109, Dec 2009.

[136] V. F. Mota, F. D. Cunha, D. F. Macedo, J. M. Nogueira, and A. A. Loureiro, "Protocols, mobility models and tools in opportunistic networks: A survey," *Computer Communications*, vol. 48, pp. 5 – 19, 2014.

[137] R. Zhang, J.-M. Gorce, O. Berder, and O. Sentieys, "Lower Bound of Energy-Latency Tradeoff of Opportunistic Routing in Multihop Networks," *EURASIP Journal on Wireless Communications and Networking*, vol. 2011, no. 1, p. 265083, Oct 2010.

[138] L. Cheng, J. Niu, J. Cao, S. Das, and Y. Gu, "QoS Aware Geographic Opportunistic Routing in Wireless Sensor Networks," *IEEE Transactions on Parallel and Distributed Systems*, vol. 25, no. 7, pp. 1864–1875, July 2014.

[139] Y. WenZhong, H. Chuanhe, W. Bo, Z. Zhenyu, and W. Tong, "A reliable multicast for MANETs based on opportunistic routing and network coding," in *IEEE International Conference on Wireless Communications, Networking and Information Security (WCNIS)*, June 2010, pp. 540–545.

[140] S. Jain and S. R. Das, "Exploiting path diversity in the link layer in wireless ad hoc networks," *Ad Hoc Networks*, vol. 6, no. 5, pp. 805–825, 2008.

[141] Y. Yuan, H. Yang, S. H. Wong, S. Lu, and W. Arbaugh, "ROMER: resilient opportunistic mesh routing for wireless mesh networks," in *IEEE workshop on wireless mesh networks (WiMesh)*, vol. 12, 2005.

[142] Y. Yan, B. Zhang, J. Zheng, and J. Ma, "Core: a coding-aware opportunistic routing mechanism for wireless mesh networks," *IEEE Wireless Communications*, vol. 17, no. 3, pp. 96–103, 2010.

[143] R. Zhang, O. Berder, and O. Sentieys, "Energy efficient reservation-based opportunistic MAC scheme in multi-hop networks," in *IEEE 24th International Symposium on Personal Indoor and Mobile Radio Communications (PIMRC)*, Sept 2013, pp. 1660–1665.

[144] H. Füßler, J. Widmer, M. Käsemann, M. Mauve, and H. Hartenstein, "Contention-based forwarding for mobile ad hoc networks," *Ad Hoc Networks*, vol. 1, no. 4, pp. 351–369, 2003.

[145] A. Bachir and D. Barthel, "Localized max-min remaining energy routing for WSN using delay control," in *IEEE International Conference on Communications (ICC)*, vol. 5, May 2005, pp. 3302–3306.

[146] F. Ye, G. Zhong, S. Lu, and L. Zhang, "Gradient broadcast: A robust data delivery protocol for large scale sensor networks," *Wireless Networks*, vol. 11, no. 3, pp. 285–298, 2005.

[147] T. Watteyne, A. Bachir, M. Dohler, D. Barthel, and I. Auge-Blum, "1-hopMAC: An Energy-Efficient MAC Protocol for Avoiding 1 -hop Neighborhood Knowledge," in *3rd Annual IEEE Communications Society on Sensor and Ad Hoc Communications and Networks (SECON)*, vol. 2, Sept 2006, pp. 639–644.

[148] R. A. de Freitas Mini and A. A. F. Loureiro, "Energy in Wireless Sensor Networks," in *Middleware for Network Eccentric and Mobile Applications*, 2009, pp. 3–24.

[149] F. Ait Aoudia, M. Gautier, and O. Berder, "OPWUM: Opportunistic MAC Protocol Leveraging Wake-Up Receivers in WSNs," *Journal of Sensors*, January 2016, Article ID 6263719.

[150] N. Pantazis, S. Nikolidakis, and D. Vergados, "Energy-Efficient Routing Protocols in Wireless Sensor Networks: A Survey," *IEEE Communications Surveys Tutorials*, vol. 15, no. 2, pp. 551–591, 2013.

[151] A. Triviño-Cabrera and S. Canadas-Hurtado, "Survey on opportunistic routing in multihop wireless networks," *International Journal of Communication Networks and Information Security (IJCNIS)*, vol. 3, no. 2, pp. 170–177, 2011.

[152] F. Ait Aoudia, M. Gautier, M. Magno, O. Berder, and L. Benini, "SNW-MAC: an Asynchronous Protocol Leveraging Wake-up Receivers for Data Gathering in Star Networks," in *EAI International Conference on Sensor Systems and Software (S-cube)*, Nice, France, 2016.

[153] S. Nawaz, S. A. Hassan, S. A. R. Zaidi, and M. Ghogho, "Throughput and energy efficiency of two-tier cellular networks: Massive mimo overlay for small cells," in *International Wireless Communications and Mobile Computing Conference (IWCMC)*, September 2016, pp. 874–879.

[154] C. Huang and Y. Tang, "On the Energy Efficiency and Effective Throughput Tradeoff of Fading Channels," *IEEE Transactions on Vehicular Technology*, vol. 65, no. 4, pp. 2758–2762, April 2016.

[155] V. Jelicic, M. Magno, D. Brunelli, V. Bilas, and L. Benini, "Analytic Comparison of Wake-up Receivers for WSNs and Benefits over the Wake-on Radio Scheme," in *Proceedings of the 7th ACM Workshop on Performance Monitoring and Measurement of Heterogeneous Wireless and Wired Networks (PM2HW2N)*, October 2012.

[156] S. Sudevalayam and P. Kulkarni, "Energy Harvesting Sensor Nodes: Survey and Implications," *IEEE Communications Surveys & Tutorials*, vol. 13, no. 3, pp. 443–461, March 2011.

[157] A. S. Weddell, M. Magno, G. V. Merrett, D. Brunelli, B. M. Al-Hashimi, and L. Benini, "A survey of multi-source energy harvesting systems," in *Proceedings of the Conference on Design, Automation and Test in Europe (DATE)*, San Jose, CA, USA, 2013, pp. 905–908.

[158] T. N. Le, A. Pegatoquet, O. Berder, O. Sentieys, and A. Carer, "Energy-Neutral Design Framework for Supercapacitor-Based Autonomous Wireless Sensor Networks," *ACM Journal on Emerging Technologies in Computing Systems (JETC)*, vol. 12, no. 2, pp. 19:1–19:21, September 2015.

[159] A. Kailas, D. Brunelli, and M. A. Weitnauer, "Comparison of Energy Update Models for Wireless Sensor Nodes with Supercapacitors," in *Proceedings of the 1st International Workshop on Energy Neutral Sensing Systems (ENSSys)*, 2013.

[160] P.-D. Gleonec, J. Ardouin, M. Gautier, and O. Berder, "Architecture exploration of multi-source energy harvester for IoT nodes," in *IEEE Online Conference on Green Communications (Online GreenComm 2016)*, n/a, United States, Nov. 2016, pp. 27 – 32. [Online]. Available: https://hal.inria.fr/hal-01400418

[161] "Irradiance Datasets," http://enhants.ee.columbia.edu/indoor-irradiance-meas/, 2014, [Online; accessed August-2015].

[162] W. H. Wang, M. Palaniswami, and S. H. Low, "Application-Oriented Flow Control: Fundamentals, Algorithms and Fairness," *IEEE/ACM Transactions on Networking*, vol. 14, no. 6, pp. 1282–1291, December 2006.

[163] P. D. Diamantoulakis and G. K. Karagiannidis, "Maximizing Proportional Fairness in Wireless Powered Communications," *IEEE Wireless Communications Letters*, vol. 6, no. 2, pp. 202–205, April 2017.

[164] F. Ait Aoudia, M. Gautier, and O. Berder, "(To Apprear) Distributed Computation of Fair Packet Rates in Energy Harvesting Wireless Sensor Networks," *IEEE Wireless Communications Letters*.

[165] S. Boyd, N. Parikh, E. Chu, B. Peleato, and J. Eckstein, "Distributed Optimization and Statistical Learning via the Alternating Direction Method of Multipliers," *Foundations and Trends in Machine Learning*, vol. 3, no. 1, pp. 1–122, January 2011.

[166] T. Goldstein, B. O'Donoghue, S. Setzer, and R. Baraniuk, "Fast Alternating Direction Optimization Methods," *SIAM Journal on Imaging Sciences*, vol. 7, no. 3, pp. 1588–1623, 2014.

[167] S. Boyd and L. Vandenberghe, *Convex optimization*. Cambridge university press, 2004.

[168] B. He and X. Yuan, "On non-ergodic convergence rate of Douglas–Rachford alternating direction method of multipliers," *Numerische Mathematik*, vol. 130, no. 3, pp. 567–577, 2015.

[169] B. Martinez, M. Monton, I. Vilajosana, and J. Prades, "The Power of Models: Modeling Power Consumption for IoT Devices," *IEEE Sensors Journal*, vol. 15, no. 10, pp. 5777–5789, October 2015.

[170] "LoRa Family | Wireless & RF ICs for ISM Band Applications | Semtech," http://www.semtech.com/wireless-rf/lora.html, 2016.

[171] C. Goursaud and J.-M. Gorce, "Dedicated networks for IoT : PHY / MAC state of the art and challenges," *EAI endorsed transactions on Internet of Things*, October 2015.

[172] "LoRaWAN^{TM}, Specification v1.0, LoRa Alliance, Inc. 2400 Camino Ramon, Suite 375 San Ramon, CA 94583 (2015)," LoRa Alliance, Tech. Rep., 2015.

[173] T. Zheng, M. Gidlund, and J. Åkerberg, "WirArb: A New MAC Protocol for Time Critical Industrial Wireless Sensor Network Applications," *IEEE Sensors Journal*, vol. 16, no. 7, pp. 2127–2139, April 2016.

[174] M. Magno, F. Ait Aoudia, M. Gautier, O. Berder, and L. Benini, "WULoRa: An energy efficient IoT end-node for energy harvesting and heterogeneous communication," in *Design, Automation Test in Europe Conference Exhibition (DATE), 2017*, March 2017, pp. 1528–1533.

[175] F. Ait Aoudia, M. Magno, M. Gautier, O. Berder, and L. Benini, "A Low Latency and Energy Efficient Communication Architecture for Heterogeneous Long-Short Range Communication," in *2016 Euromicro Conference on Digital System Design (DSD)*, August 2016, pp. 200–206.

[176] R. Pozza, M. Nati, S. Georgoulas, K. Moessner, and A. Gluhak, "Neighbor Discovery for Opportunistic Networking in Internet of Things Scenarios: A Survey," *IEEE Access*, vol. 3, pp. 1101–1131, 2015.

[177] T. Pering, V. Raghunathan, and R. Want, "Exploiting radio hierarchies for power-efficient wireless device discovery and connection setup," in *18th International Conference on VLSI Design,*, January 2005, pp. 774–779.

[178] H. Qin and W. Zhang, "Zigbee-assisted power saving management for mobile devices," *IEEE Transactions on Mobile Computing*, vol. 13, no. 12, pp. 2933–2947, Dec 2014.

[179] R. Zhou, Y. Xiong, G. Xing, L. Sun, and J. Ma, "ZiFi: Wireless LAN Discovery via ZigBee Interference Signatures," in *Proceedings of the Sixteenth Annual International Conference on Mobile Computing and Networking*. ACM, 2010.

[180] P. Tuset-Peiró, X. Vilajosana, and T. Watteyne, "OpenMote+: a Range-Agile Multi-Radio Mote," in *Proceedings of the International Conference on Embedded Wireless Systems and Networks*, 2016, pp. 333–334.

[181] A. Springer, W. Gugler, M. Huemer, L. Reindl, C. C. W. Ruppel, and R. Weigel, "Spread spectrum communications using chirp signals," in *IEEE/AFCEA EUROCOMM*, 2000.